Global relative paleointensity and regional paleosecular variation: High resolution signals in New Zealand marine sediments

Jessie Louise Robbins

A thesis submitted for the degree of

Master of Science in Geology

at the University of Otago, Dunedin,

New Zealand.

March 5th 2008

Created 31/08/2015

WORDS OF INSPIRATION

"Civilization exists by geological consent, subject to change without notice."
(WILL DURRANT)

"If we knew what it was we were doing, it wouldn't be called research would it?"
(ALBERT EINSTEIN)

"One of the symptoms of an approaching nervous breakdown is the belief that one's work is terribly important"
(BERTRAND RUSSELL).

"Ooh, a graduate student huh? How come you guys can go to the moon but you can't make my shoes smell good"
(HOMER SIMPSON)

ACKNOWLEDGEMENTS

I am indebted to the following people and would like to acknowledge their valuable contributions to this project:

Alissa Quinn and Christian Ohneiser for their assistance with paleomagnetic sample preparation on board the Kilo Moana and Roger Revelle.

My supervisor, Gary Wilson, for ongoing constructive feedback and guidance in new disciplines and laboratory procedures.

Kirsty Tinto for her careful and thorough proof reading and assistance with UNIX program.

The Foundation for Research, Science and Technology, and the University of Otago for providing funding this project.

ABSTRACT

Advancement in understanding paleosecular variation and its driving mechanisms is hindered by the current paucity of paleomagnetic records from the Southern Hemisphere. To date, the record from New Zealand is limited, and dominated by data from volcanic rocks, with a distinct lack of continuous paleointensity data. Seven cores from the Waipaoa Basin, Bay of Plenty and northern Chatham Rise have been subjected to Alternating Field demagnetisation to derive records of paleosecular variation (PSV) and relative paleointensity (RPI) of Earth's magnetic field over historic and millennial timescales. Artificial remanence parameters saturation ARM and saturation IRM are used to assess the level of compliance with magnetic uniformity criteria of King et al. (1983), which is prerequisite for deriving relative paleointensity from sediments. Tephrochronology and ^{210}Pb isotope analyses have provided independent sedimentation rates for some cores.

The Laschamp (41 ka) and Mono Lake (34.6 ka) geomagnetic excursion events are identified in piston core JPC95, from the Bay of Plenty. The Laschamp excursion is manifest as the lowest (7% of maximum) intensity between ~ 47 ka and the present day, accompanied by an abrupt (~1ky) shallowing of inclination by 45°. The path of the dipole field during the Laschamp excursion is constrained longitudinally between 87.44°E and 99.77°E; and the magnitude of the latitudinal deviation from geographic north estimated to be 80°-110°. Both excursions and other millennial-scale features of the JPC95 RPI record are manifest in the GLOPIS-75 paleointensity stack of Laj et al. (2004); and in the numerous records compiled to produce the stack. Such correspondence lends testimony to the fidelity of the RPI records, and to the global and thus dipolar nature of the millennial scale RPI signal; whilst validating the use of sARM as a normalising parameter, and demonstrating the potential of New Zealand marine sediments to provide reliable records of RPI back to ~ 47 ka.

Identification and correlation of features with time constants similar to the shortest associated with the dipole field (600-700 years; Hulot & Le Mouel, 1994) suggests that the JPC95 record approaches the maximum resolution of the dipole RPI signal. Cores from the Waipaoa Basin provide higher resolution, recording continuous PSV and RPI variability on a decadal scale back to 300 yrs B.P. More records of comparable resolution, with independent age control, will constrain the spatial extent of this signal and assess its potential application as a high-resolution correlation tool.

Available records of paleosecular variation are not globally correlative over the period investigated (0-47 ka). Features of the JPC95 PSV record are identified in records from the South Atlantic, but not in Northern Hemisphere records of comparable temporal resolution. This implies manifestation of a regional, non-dipole signal that is hemispheric in extent, and persistent hemispheric asymmetry in conditions at the core-mantle boundary over the time frame explored here.

An inclination anomaly of -8.1° from core JPC95 is greater than previously estimated for New Zealand, but is consistent with the proposition of Elmelah et al. (2001), of a negative inclination anomaly characterising the southwest Pacific. Alternatively, the negative inclination anomaly, together with the far-sided virtual geomagnetic poles from core JPC95 constitute evidence for a northward displacement in the axial dipole, as modelled by Wilson (1971).

Table of Contents

LIST OF FIGURES

LIST OF TABLES

1. INTRODUCTION

1.1 Spatial form of the geomagnetic field

The earth's magnetic field is a potential field, which everywhere has direction and magnitude. The current nature of the field at the surface of the earth is best described using isomagnetic charts (Figs. 1.1, 1.2), in which magnetic vector components are plotted on a world map (Butler, 1992). Contour lines on these charts represent equal field direction (Fig. 1.1) or equal intensity (Fig. 1.2). By convention, the three dimensional direction at any point on Earth's surface is resolved into two vector components: one in the horizontal plane, the other in the vertical. Field direction is thus described in terms of azimuthal orientation from geographic north, or *declination*, and degree of deviation from horizontal, or *inclination.* Again by convention, inclinations in the Northern Hemisphere are positive (into the earth), whilst those in the Southern Hemisphere are negative (out of the earth; Fig. 1.3).

An *isoclinic* chart (e.g. Fig. 1.1) describes inclination of the magnetic field at the surface. The magnetic equator (where inclination $I = 0°$) wavers about the geographic equator and the *magnetic dipoles* where $I = \pm 90°$ are offset from the north and south geographic poles. Isogonic and isodynamic (e.g. Fig. 1.2) charts describe spatial variations in declination and intensity, respectively. Figure 1.2 illustrates that magnetic flux is highest ($\sim$ 60 μT) at the magnetic poles and lowest ($\sim$ 30 μT) in the equatorial vicinity (McElhinny, 1973).

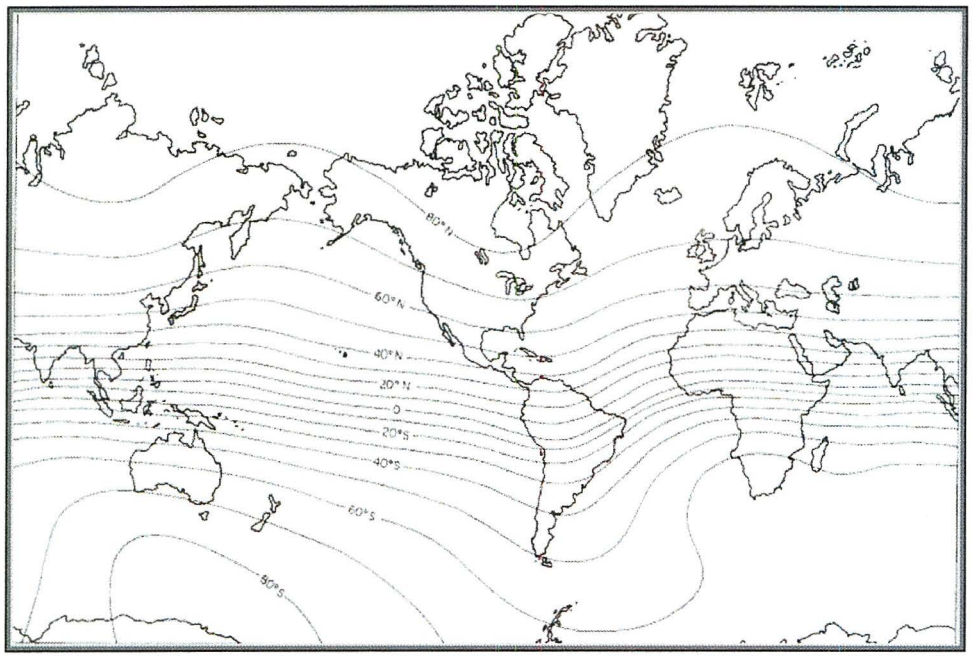

Figure 1.1: Isoclinic map illustrating global distribution of inclination of the earth's magnetic field at the surface in 1975. Contour interval = 10°. Note that contours of inclination are not symmetric about the geographic equator. Chart published by defence mapping agency hydrographic centre, Washington D.C.

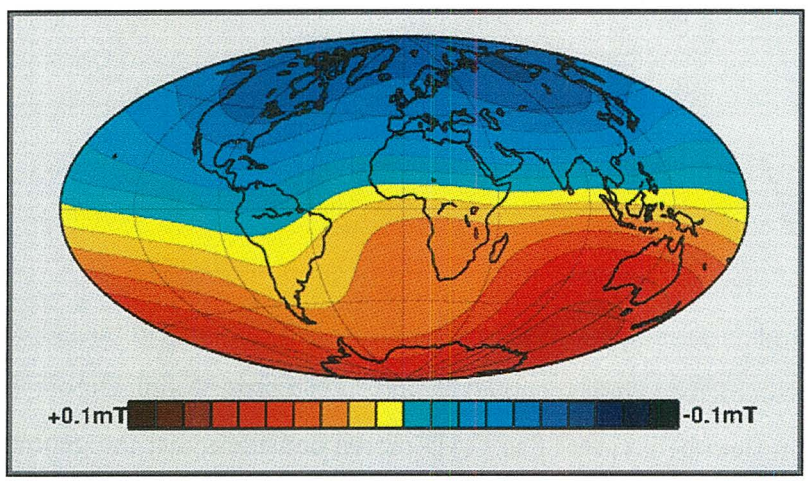

Figure 1.2: Isodynamic map illustrating variation in intensity of the radial field at the earth's surface. A general but irregular latitudinal gradient is apparent, with concentrations of intensity in the Polar Regions. The zero intensity contour (delineating the geomagnetic equator) wavers about the geographic equator. From Holme (2004).

1.1.1 The geocentric Axial Dipole Model (GAD)

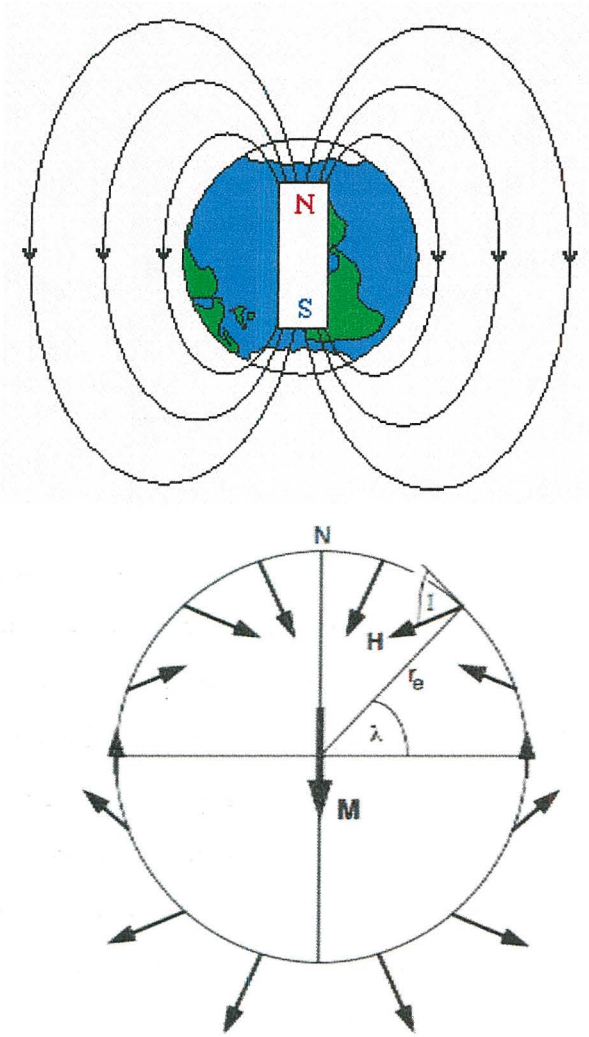

Figure 1.3: The magnetic field of the earth according to the geocentric axial dipole (GAD) model. Magnetic dipole M at the centre of the earth is aligned with the axis of rotation; N = north geographic pole; re = mean Earth's radius; H = magnetic field vector and I = inclination at geographic latitude λ; arrows schematically represent magnetic field directions at the Earth's surface produced by the geocentric axial dipole. For a GAD the geomagnetic equator and poles = geographic counterparts. From Butler (1992).

Of the numerous models developed to determine the origin of the field measured at the earth's surface, the most established and accepted is the Geocentric Axial Dipole (GAD) model, predicting long-term field behaviour. The GAD model considers that the geomagnetic field at the surface can be approximated by a single magnetic dipole at the centre of the earth, aligned with the axis of rotation (Fig. 1.3). For a GAD, the geomagnetic poles (where the axes of this centred dipole emerge at the earth's surface) coincide with the geographic poles. Lines of flux emanate from the south geomagnetic pole and converge at the north geomagnetic pole (as depicted in Figure 1.3). The geomagnetic equator, (defined by the great circle midway between the geomagnetic poles) for a GAD is also indistinct from the geographic equator (Opdyke & Channell, 1996). A GAD thus produces a field that is rotationally symmetric about its axis with declination = 0° everywhere. Contours of equal intensity form straight

about its axis with declination = 0° everywhere. Contours of equal intensity form straight lines parallel to latitude (as do contours of inclination), with intensity at the geographic poles being double that at the equator. Inclination for a GAD varies systematically from $I = 0°$ at the geographic equator to $\pm$ 90° at the geographic poles (Tauxe, 2005); and lines of equal inclination I are related by the dipole equation:

$$\tan I = \left(\frac{Hv}{Hh}\right) = \left(\frac{2\sin\lambda}{\cos\lambda}\right) = 2\tan\lambda \qquad [1.1]$$

Where Hv = H sin I = vertical component, Hh = H cos I = horizontal component of the geomagnetic field vector, and λ = geographic latitude.

Though the surface features of today's measured field approximate those of a GAD field, obvious departures from the simplest configuration include the lack of coincidence of magnetic poles ($I = \pm$ 90°) with the geographic poles, a wavering of the magnetic equator (I = 0°) about the geographic equator (Fig. 1.1), and spatial variation of magnetic declination. Thus the GAD model requires modification to accommodate the higher short-term complexity of earth's geomagnetic field. However, a fundamental hypothesis on which interpretation of paleomagnetic results depends, is that the *time-averaged* geomagnetic field *is* in fact that of a GAD (Merrill et al., 1998). This proposition constitutes the **Geocentric Axial Dipole hypothesis**, which is discussed further in subsequent sections.

1.1.2 Inclined Geocentric Axial Dipole Model

The present geomagnetic field is more closely approximated by an inclined GAD, angled 11.5° to the rotation axis (Fig. 1.4) such that the north geomagnetic pole (where extensions of the modelled dipole intersect the surface) lies at 79°N, 70.9°W (Opdyke & Channell, 1996). However, despite the closer approximation of the inclined model in reproducing general trends of the measured surface field, it cannot alone account for the considerable structure to contours of measured inclination (Fig. 1.1). Also, the inclined geomagnetic poles still stand apart from the (measured) magnetic poles (where $I = \pm$ 90°). This suggests that the geomagnetic field is yet more complicated than can be explained by a mere dipole at the

earth's centre (Butler, 1992). Although spherical harmonic analyses reveal that an inclined GAD accounts for 90% of the surface field, the residual remains significant (Butler, 1992).

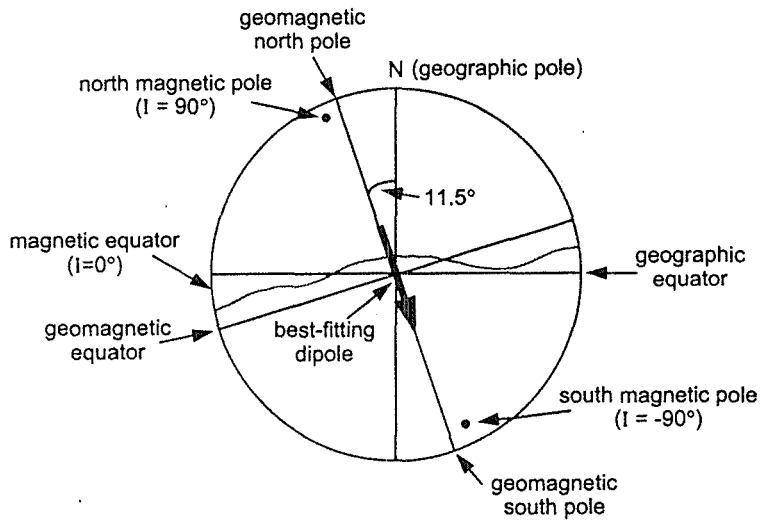

Figure 1.4: Diagram illustrating the distinction between magnetic (measured), geographic (in line with the rotation axis) and geomagnetic (for inclined GAD Model) poles and equators. The best fitting dipole is inclined at 11.5° to the axis of rotation. From Butler (1992).

An *eccentric dipole* describes the field only marginally better than the GAD, and its ability to do so is varies spatially. It is obtained by relaxing the geocentric constraint to further refine the fit of a single dipole to the geomagnetic field. The persistent discrepancy indicates the presence of a higher-order portion of the geomagnetic field: the *non-dipole field.*

1.1.3 The non-dipole field

Non-dipole sources of Earth's magnetic field are the reason that directions of the field vary substantially with location on Earth at any given time (Butler, 1992). McElhinny (1973) describes the instantaneous non-dipole field as the residual obtained by subtracting the best fitting dipole field (currently inclined at 11.5°) from that observed at the surface today. The term non-dipole encompasses fields of greater harmonic degree than the dipole field, e.g. quadrupole and octopole fields, which contribute to the complexity of the total field measured at the surface.

Yukutake & Tachinaka (1968) showed that whilst some features of the non-dipole field are temporally persistent, others change more rapidly (Fig. 1.5). Bullard et al. (1950) plotted six to seven continental-scale features dominating the non-dipole field, some displaying opposing field patterns. These can be modelled by an array of deep-seated, radially oriented dipoles (Lowes, 1955).

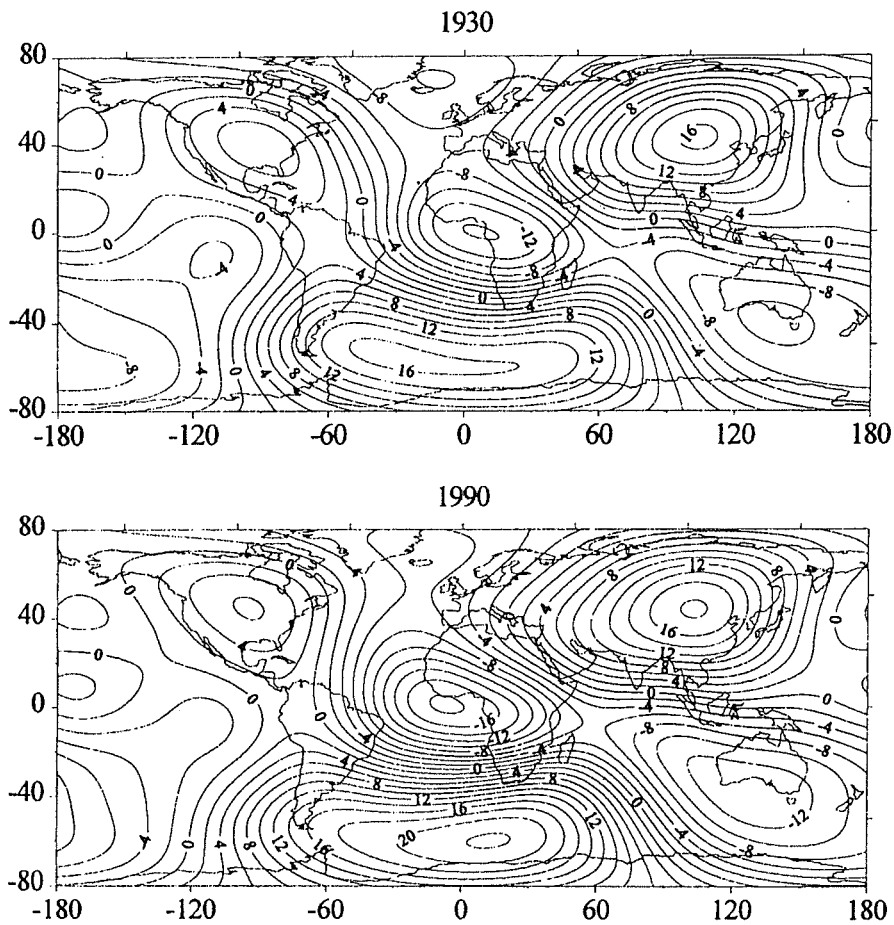

Figure 1.5: Isomagnetic charts illustrating the vertical component of the non-dipole field for 1930 and 1990. Contours are labelled in mT. Whilst some features appear to have changed or drifted westward over the 60-year period, others have remained relatively stationary. High intensity features are centred over East Asia, the South Atlantic and (to a lesser extent) North America; whilst negative intensities are evident over Africa. Little deviation from zero is apparent over the Pacific Ocean. From Merrill et al. (1998).

1.1.4 Geomagnetic Secular Variation

The contribution of non-dipole components to the complexity of earth's geomagnetic field (discussed above) is further exacerbated by the fact that both dipole and non-dipole components are changing substantially through time, with periodicities ranging from milliseconds to millions of years (Merrill & McElhinny, 1983). Generally, periods of less than a year are of external origin (atmospheric or ionospheric), since the electrically conducting mantle screens internal variations of such periods to the extent that they are not manifested at the earth's surface. Changes of internal origin are thus considered to be decadal or longer (Merrill et al., 1998).

The direction and intensity of the field vary in a sense that has been described as a wobbling dipole, or "random wander about the mean" (Butler, 1992). Such changes in the non-dipole and dipole components with periodicities on the order of $10^2 - 10^3$ years are described by the term *Geomagnetic Secular Variation* (Opdyke & Channell, 1996). Secular variation provides an explanation for discrepancy between the time-averaged field and the instantaneous field.

The largest changes in direction of the geomagnetic field during the past 150 years are associated with the non-dipole component of the field (Merrill & McElhinny, 1983). Some features of the non-dipole field have been noted to undergo a longitudinal shift of isoporic foci to the west at a rate of ~ 0.2°/year over historic times (Bullard et al., 1950). This sense of drift has dominated the past 7000 years (Turner & Thompson, 1981). Thompson & Oldfield (1986), however, found this to be preceded by a phase of eastward drift. *Westward drift* of the non-dipole component is not uniform over the earth's surface; confined primarily to the Atlantic hemisphere (Bloxham & Gubbins, 1986). Changes over the Pacific are less rapid, and strong concentrations of non-dipole anomalies at ± 90° of latitude appear to have remained stationary over time, varying only in magnitude (Holme, 2004). Yukutake (1993) presents evidence that low secular variation in the Pacific is a recent phenomenon, refuting hemispheric preference for drift of the non-dipole field. cf p 29

Models proposed to explain recent secular variation behaviour include westward drift of the non-dipole field; poleward drift of the non-dipole field, random changes in the non-dipole field and the standing and drifting models (Creer & Tucholka, 1982; Yukutake, 1979).

Westward drift is generally attributed to differential angular velocity of Earth's lithosphere and outer core, where the non-dipole components of the field are thought to originate (Opdyke & Channell, 1996). These authors also consider that lack of similarity between records from Argentina (Creer et al., 1983b), Australia (Barton & McElhinny, 1979), UK (Turner & Thompson, 1981) and the North American Great Lakes (Creer & Tucholka, 1982), together with the global inconsistency between inferred drift directions to confirm that secular variation *cannot* be attributed to wobble of the main dipole field axis, but to non-dipole components with different sources at different sites. This implies that patterns of secular variation are unlikely to be correlative over large distances (Opdyke & Channell, 1996).

Hide (1966) implicated the conducting fluid in the core, which is permeated by a magnetic field and able to support wave motion (Alfven, 1950), as a source for secular variation. The emerging explanation is that secular variation is driven by several contributing mechanisms in the outer core, exhibiting different characteristic time scales. Magnetohydrodynamic waves in the core have periods ranging from under a year (Alfven waves) to 100 years (Rossby waves), whilst changes associated with boundary conditions in the outer core exceed 10^8 years in period.

Merrill & McElhinny (1983) concluded that uncertainties regarding sources of secular variation are best resolved through analyses of paleomagnetic data to extend the time window of observation. Such studies of secular variation have been instrumental in developing an understanding of the spatial and temporal variations in Earth's magnetic field and in testing models of paleosecular variation (PSV) and dynamo processes (Herrero-Bervera et al., 2004).

The dynamic nature of the geomagnetic field is manifest not only in directional variation (secular variation), but also in intensity. Leaton & Malin (1967) showed the intensity of the dipole field to have decreased by ca. 5% per century since 1835, whilst the position of its axis (the north geomagnetic pole), in contrast, has remained relatively static since the same time (Bullard et al., 1950). Leaton & Malin (1967) also speculated on the demise of the main dipole by 3700-4000 AD should present trends continue.

1.1.5 Extracting the dipole component and testing the GAD hypothesis

Motion of the dipole axis since ~1600 AD has been calculated through spherical harmonic analyses (e.g. Fraser-Smith, 1987). Extending this knowledge of the dipole component back further in time requires spatial and temporal smoothing out of the effects of non-dipole secular variation. The position of the present geomagnetic pole is best estimated through examination of globally distributed field directions and determining the best fitting geocentric dipole (a spatial average). To distil the dipole signal from the paleomagnetic record at a single locality, a temporal mean must be calculated over an interval of time longer than the dominant periodicities of non-dipole variations. Spectral analysis of the non-dipole field indicates maximum energy with periods of 2500-3000 yrs (Butler, 1992). Ohno & Hamano (1992) determined temporal means for successive times at 100-yr intervals to approximate the position of the North Geomagnetic Pole (Fig. 1.6). Agreement of their data with dipole analyses for historical times implies that this interval may be sufficient to mask the effects of short-term (secular) variation of the non-dipole field. However, Barbetti (1977) recommends subsequently averaging these means (from a limited number of regions) at 500-year intervals and finding the spatial mean for the whole globe, in order to extract most accurately the gross movement of the dipole axis.

In applying this procedure to a compendium of paleomagnetic data averaged over a longer period of 10,000 years (Fig. 1.6), the position of the geomagnetic pole becomes indistinguishable from the present rotation axis (Ohno & Hamano, 1992). This observation implies that the time-averaged field is adequately described by the GAD model field (when averaged over at least 10,000 years); thus validating the GAD hypothesis. A customary practice in validating the GAD hypothesis has been to plot paleomagnetic poles spanning the past few million years to illustrate the coincidence of their mean with the geographic pole (Irving, 1964).

Using a 2000-yr interval, Ohno & Hamano (1992) failed to reproduce such coincidence of the geomagnetic and geographic poles. However, shorter records of several thousand years *have* shown clustering of virtual geomagnetic poles (VGPs) about the geographic pole (Hospers, 1954b). Further studies are required to constrain the length of time sufficient for motion of the dipole axis to average the axis of rotation.

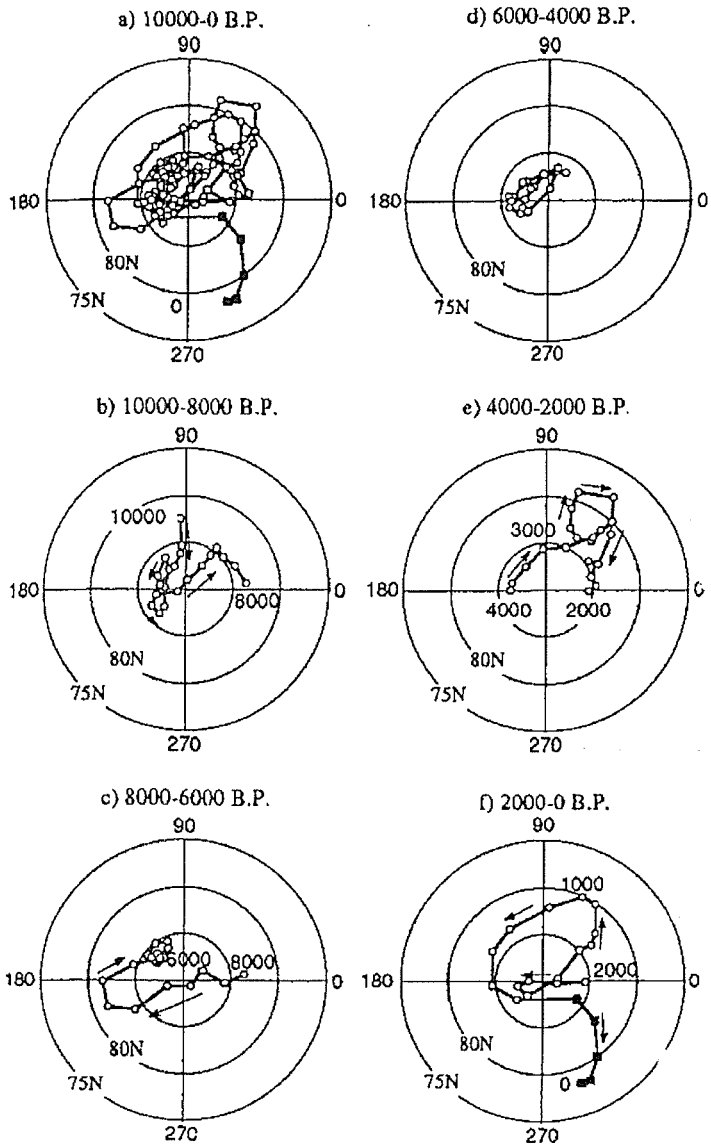

Figure 1.6: Locations of the North Geomagnetic Pole (dipole axis) at 100-yr intervals extending back to 10,000 years, as estimated by Ohno & Haamano (1992).

Another way in which the validity of the GAD hypothesis can be assessed is through testing the relationship of inclination (averaged over periods sufficient to smooth out secular variation of non-dipole *and* dipole fields) to site latitude (Opdyke & Channell, 1996). Opdyke & Henry (1969) and Schneider & Kent (1990a) analyzed paleomagnetic inclinations in marine sediment cores spanning a broad latitudinal range and ~ 10^5 to 10^6 years. Their results demonstrated that Pleistocene paleomagnetic inclinations plotted against latitudes are consistent with those predicted by the GAD model (Fig. 1.7). It has now become standard procedure in paleomagnetism to calculate time-averaged paleomagnetic poles, which, on the basis of the GAD hypothesis, are assumed to represent paleogeographic poles (Merrill et al., 1998).

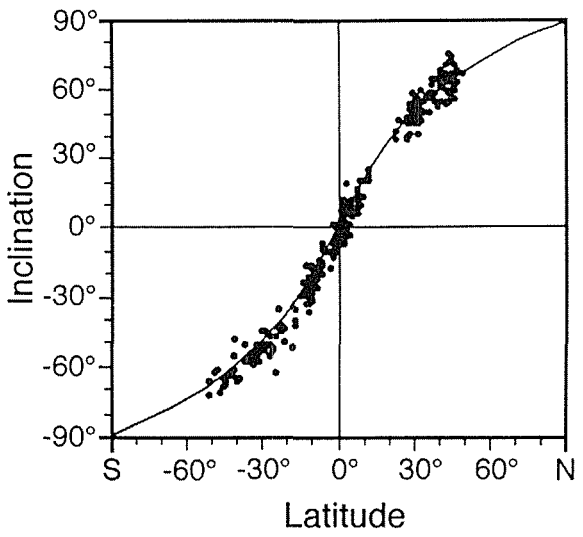

Figure 1.7: Inclination plotted versus latitude in widely spaced Pleistocene marine sediment cores. Line shows expected inclination derived from the dipole formula; thus data is consistent with the GAD hypothesis. After Schneider and Kent (1990a).

1.2 Origin of the Field

1.2.1 Geodynamo theory

Our ability to describe the geomagnetic field far exceeds our understanding of its origin (Butler, 1992). Harmonic analyses of Gauss (1839) revealed that the coefficients of external origin equal zero, thus confirming a dominant internal source for the geomagnetic field. McElhinny (1973) noted that in practice a small contribution from electrical currents in the ionosphere amounts to ca. 30 gammas (= 30 nT). Though the GAD is becoming an increasingly accepted model for describing long-term behaviour of the geomagnetic field, the underlying mechanisms have yet to be elucidated. Models of the non-dipole component of the field are still a matter of contention, and a detailed theory that can accurately predict the form of secular variation has yet to be devised.

Plausible established theories concerning the generation of Earth's magnetic field involve motions within Earth's liquid outer core. Primarily driven by thermal and compositional buoyancy sources at the inner core boundary, these are sufficient to produce electric currents necessary to generate a field (Buffett, 2000). However, paleomagnetic research suggests that Earth has possessed a magnetic field for at least 3.5 G.a. (McElhinny & Senanayake, 1980). In the absence of some compensatory regenerative process, ohmic loss of electric currents would destructively dissipate the field in ~10^4 years (Buffett, 2000).

Elsasser (1946) and Bullard (1949) made the first significant mathematical contributions to modelling Magnetohydrodynamic (MHD) dynamos. These authors demonstrated how a small stray field could be amplified into a much larger one, by magnetic induction of convection currents in a molten core; as well as the important role of the Coriolis force in generating a 3D toroidal field.

Systems of discs and feedback coils have been used to model geomagnetic field generation in the laboratory (Elsasser, 1958; Fig. 1.8). The essential elements of any MHD dynamo to be incorporated into theoretical models include:

1. A moving electrical conductor (represented by a rotating copper disc in Figure 1.8).
2. An initial magnetic field.
3. Interaction between the magnetic field and conductor to reinforce the original field through positive feedback (provided by the coil in figure 1.8).
4. A supply of energy to overcome electrical resistivity losses.

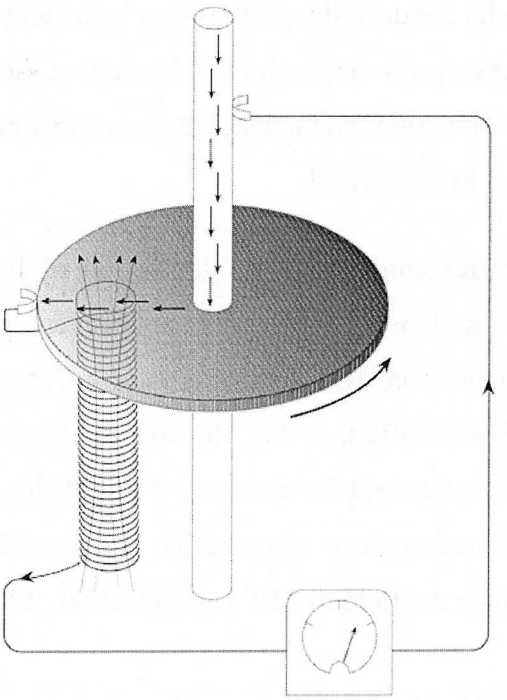

Figure 1.8: Self-exciting disk dynamo. Rotation of a copper disk rotates on an electrically conducting axle generates an electrical current (bold arrows). The coil under the disk generates a magnetic field (fine arrows). From Butler (1992): adapted from The Earth as a Dynamo, W. Elsasser, Copyright © 1958 by Scientific American, Inc. All rights reserved.

Lilley (1970) produced a flow pattern shown to act as a dynamo, in which the trajectories of fluid motions are twisted and sheared by the Coriolis force, resulting in toroidal field components completely contained within the core. Love (1999) defines this helical toroidal field (due to differential rotation) as the ω effect (Fig. 1.9). Modification of this through upwelling and downwelling (the α effect) produces turbulent, helical fluid motion and loops

of magnetic field, which coalesce (Love, 1999). Interaction between the electrically conductive Iron and Nickel alloy (comprising the outer core) and the magnetic field it passes through generates another associated field, to reinforce the original dipolar field. This positive feedback allows the core to operate as a self-exciting magnetohydrodynamic (MHD) dynamo (Glatzmaier & Roberts, 1995). Leakage through electrical resistivity that is not regenerated by fluid motions is thought to maintain the simple shape of the geomagnetic field (Butler, 1992).

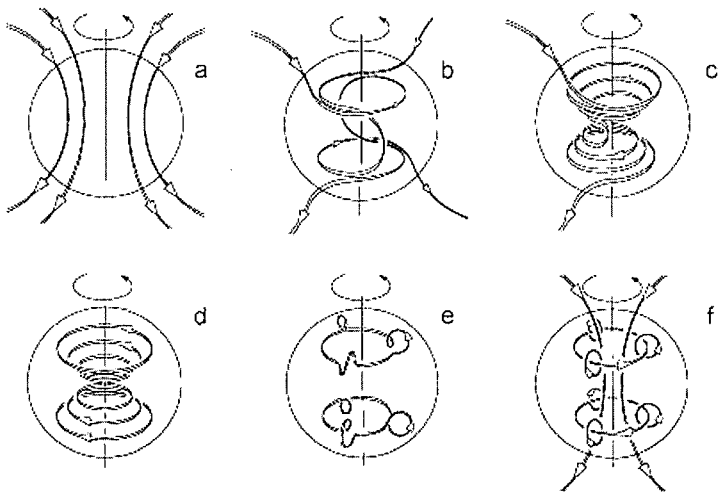

Figure 1.9: Schematic diagram illustrating the influence of the Coriolis force in the generation of the magnetic field. A poloidal field (a) subjected to Coriolis force is rotated to form a helical, toroidal, quadrupolar field, which is symmetric about the equator (b-d). This is known as the ω effect. Helical upwelling and downwelling results in development of twisted and sheared loops in the toroidal field (e), in the α effect. This provides positive feedback to reinforce the original dipolar field (f). From Love (1999).

Field reversals are endemic to geomagnetic dynamo behaviour, and the invariant operation of the MHD dynamo in either state of polarity lends further support to its validity (Krause & Roberts, 1980). A growing body of evidence also supports the additional influence of temperature anomalies in the lower mantle on the geomagnetic field, which has been compellingly proposed by authors such as Olsen & Glatzmaier (1996) and Bloxham (2000). Lilley (1970) suggested that deviation of the geomagnetic dipole axis from the geographic axis of rotation is an expression of asymmetric motions within the core. The increased

symmetry required for the geomagnetic and geographic poles to coincide would imply reduced dynamo action and consequent decay of the dipole field.

The energy input necessary to drive MHD fluid motions constitutes a substantial proportion of Earth's heat budget. The most plausible and accepted source of such energy is that derived from gradual cooling of Earth's core, with attendant expansion of the solid inner core at the expense of the liquid outer; which is freezing at the same rate (Buffett, 2000).

Modelling of the non-dipole field through radially pointing dipoles (Lowes, 1955), suggests an origin in fluid eddy currents within the liquid outer core, proximate to the interface with the overlying solid mantle (Butler, 1992). Non-dipole features are dynamic and exhibit growth, deformity and decay over time scales (10^1-10^3 yrs) similar to those of eddy currents in turbulent fluid flow (Yukutake & Tachinaka, 1968). Variations on this theme include models in which the radial dipoles are drifting (Aldredge & Hurwitz, 1964), or oscillating whilst fixed in position (Creer & Hogg, 1977).

The ongoing need to provide simultaneous solutions to the numerous non-linear equations governing physical properties of the earth, along with appropriate boundary and initial conditions defines the "earth dynamo problem" (Merrill et al., 1998). A wider distribution of paleomagnetic secular variation data will help distinguish between competing models and associated sources of secular variation in the non-dipole field (Creer, 1983).

The qualitative discussion of magnetohydrodynamics above provides an explanation for the time-averaged geocentric axial dipolar nature of the earth's magnetic field. Since Earth's rotation exerts dominant control on long-term fluid motions in the core, it follows that the geomagnetic field generated by these should be symmetric about the axis of rotation. The simplest such field is that defined by the GAD model.

1.2.2 Solving the geodynamo problem

To estimate the coefficients in a spherical harmonic analysis for higher degrees, a more global distribution of data is necessary. If enough high quality paleomagnetic data became available for successive times, then a spherical harmonic analysis could resolve changes in the non-

dipole field (Merrill et al., 1998). The spatial and temporal paleosecular variation (PSV) record will help elucidate the physics of the core, through providing additional constraints on the topographic characteristics of the core-mantle boundary and lateral properties of the lower mantle (Johnson & Constable, 1998). Observations of global distribution will also test the currently speculative suggestions of periodicity to the variation in Earth's dipole moment. Lanza & Zanella (2003) stress that high-quality PSV records require a sure identification and reliable dating of primary remanence, and should be as continuous as possible with high time resolution.

1.3 Significance of paleofield studies in New Zealand

Comparable patterns of secular variation over sub-continental regions are thought to reflect the size of non-dipole sources of geomagnetic field in Earth's outer core (Cox, 1969). Similarly, the longevity of secular variation patterns also reflects that of the core-mantle boundary conditions (thermal and compositional) and MHD processes responsible for producing them.

The historic non-dipole field and rate of geomagnetic secular variation are allegedly greater in the Southern Hemisphere (Cox, 1962). Whether or not such hemispherical asymmetry is a temporally persistent (on a millennial scale) or transient (century scale) feature of the geomagnetic field has significant implications for our understanding of the dynamo processes driving secular variation and field intensity. Permanent asymmetry in secular variation indicates long-term asymmetry in boundary conditions. Conversely, should the asymmetry prove an ephemeral feature upon long-term averaging, no persistent asymmetry in boundary conditions is implied.

Differences in secular variation between the Pacific and Atlantic hemispheres are also pertinent in the historical and archaeomagnetic fields, and that of the last 5 m.y. (Johnson & Constable, 1998). Doell & Cox, (1972); Shibuya et al. (1995) and Johnson & Constable (1998) reported anomalously low secular variation for the Pacific Basin region: extending north to the Aleutian Islands, east to Mexico, west to Pagan Island and south to New Zealand (Shibuya et al., 1995). Such observations imply persistent deviation from the axi-symmetric

PSV model (e.g. McFadden & McElhinny, 1997) and suggest different physical mechanisms for secular variation in the two hemispheres. The existence of the so called 'Pacific non-dipole low' has been contended, however, by investigations of secular variation at Easter Island (south-eastern Pacific; Brown, 2002), the Galapagos Islands (Cox, 1971) New Zealand (Cox 1969) and the Aleutian Islands (Bingham & Stone, 1972).

Long term mean inclinations in the Northern Hemisphere are often shallow, relative to the GAD, resulting in 'far-sided' VGPs. Wilson (1971) modelled this 'far-sided effect' using a northward shifted dipole; mathematically equivalent to a permanent quadrupole moment (Merrill & McElhinny, 1977). Both of these models require mean field at Southern Hemisphere sites to be steeper than the GAD; but more Southern Hemisphere data are required before their validity can be substantiated (Turner & Lyons, 1986).

Continuous records of PSV and relative paleointensity (RPI) are biased towards the Northern Hemisphere, with only recent contributions from the mid-high latitude Southern Hemisphere (e.g. Channell et al., 2000). The current paucity of paleomagnetic data precludes accurate discrimination between models of the non-dipole field, secular variation and their latitudinal variation. Longer, more widespread and accurate records of PSV and paleointensity from poorly sampled regions in the Southern Hemisphere are thus required to investigate regional variations in the short term, and time-averaged field in order to place constraints on global field models, and to test the axial dipole hypothesis (e.g. Brown, 2002; Carlut & Courtillot, 1998).

The term inclination anomaly is defined as the difference between mean inclination measured at a particular site and that expected at the same locality according to the GAD model (equation 1.1):

$$\Delta I = \text{mean } I - I_{\text{GAD}} \qquad [1.2]$$

New Zealand is situated at the south-western rim of the Pacific Ocean, a region characterised by a strong negative inclination anomaly of -10° throughout the Bruhnes Chron (Elmalah et al., 2001). This is based upon records from the Solomon Islands and north Fiji Basin, as well Northland volcanic records from New Zealand. However, the existing paleomagnetic database

for New Zealand and the South Pacific is temporally discontinuous and inadequate, and further data from New Zealand are desirable to corroborate the presence of a persistent anomaly.

Turner & Lillis (1994) obtained secular variation data back to 2500 years B.P. from lacustrine sediments of Lake Pounui. Their record is corroborated by spot readings of the archaeomagnetic field from Rangitoto Island lava flows dating back to 1100 AD (Robertson, 1986), as well as historic magnetic surveys and recordings (e.g. Cook, 1771; Farr, 1916). The consistent picture from these data is of westward drift, followed by a steady easterly change in declination from 1500 years B.P. to the present day. Cox (1969) used paleomagnetic directions (at irregular intervals) back to 0.68 Ma from North Island volcanic formations to discredit suggestions of long-term hemispheric asymmetry. Shibuya et al. (1992) documented geomagnetic excursions between 25 and 50 ka in lavas from the Auckland Volcanic Field, constituting the first igneous record of excursions from the Southern Hemisphere. Shibuya et al. (1995) extended the volcanic dataset and found angular standard deviations (ASD) lower than those predicted by secular variation models (e.g. McFadden & McElhinny, 1997), implying that the proposed Pacific 'non-dipole low' extends southwest to New Zealand. More continuous PSV records have been obtained by Turner & Lyons (1986) using cave sediments aged 120 - 130 k.y. and by Pillans & Wright (1990), who used a 500 k.y. secular variation record preserved in loess deposits (North Island), to identify the Mungo (35 ka) and Emperor (490 ka) excursion events. Aside from the aforementioned volcanic studies (Cox, 1969; Shibuya et al., 1992, 1995), paleointensity data from New Zealand is lacking.

New Zealand's location with respect to field slope is sufficiently proximal to the geomagnetic pole for inclination to be relatively steep in comparison to equatorial regions. This increases the potential for marine sediments to record accurately temporal fluctuations in inclination, alleviating the necessity for high quality declination records. Furthermore, the strong gradients in field direction and intensity that currently exist over New Zealand (Fig. 1.10) augment the amplitude of fluctuations in both (relative to low-gradient-regions) so that even subtle changes are likely to be detected in the paleomagnetic record. New Zealand is thus in a key position to carry out tests as to the spatial expression of secular variation and paleointensity signals. This can only be achieved if more continuous records become available to build upon the existing data set.

Specific hypotheses that this study endeavours to test include:

- That marine sediments in New Zealand can preserve accurate and reliable records of paleosecular variation and relative paleointensity of the geomagnetic field.
- That millennial to sub-millennial features of the purported 'global' signal of paleointensity are recorded in New Zealand marine sediments and can be used as a correlation tool on these time scales.
- That the negative inclination anomaly characterising the volcanic paleomagnetic record in New Zealand (and the southwest Pacific) is also manifested in New Zealand marine sediments during the last ~50 k.y.
- That the Pacific non-dipole low is manifest in New Zealand on a 50 k.y. time scale
- That mean field inclination in the Southern Hemisphere is steeper than that of a GAD, consistent with a northward-displaced axial dipole.
- That hemispheric asymmetry of secular variation is a persistent feature of the geomagnetic field back to ~50 ka.
- That millennial scale changes in inclination over the last ~50 k.y. are regional in nature, and can thus *not* be accounted for by a wobbling dipole, but by local field perturbations.

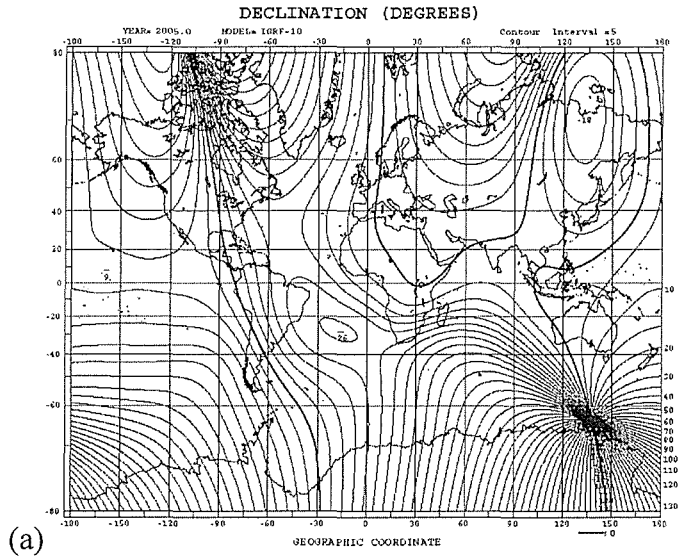

(a)

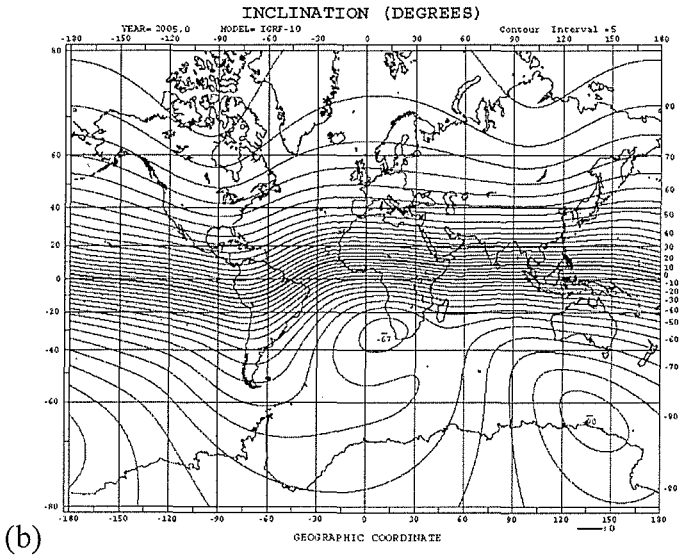

(b)

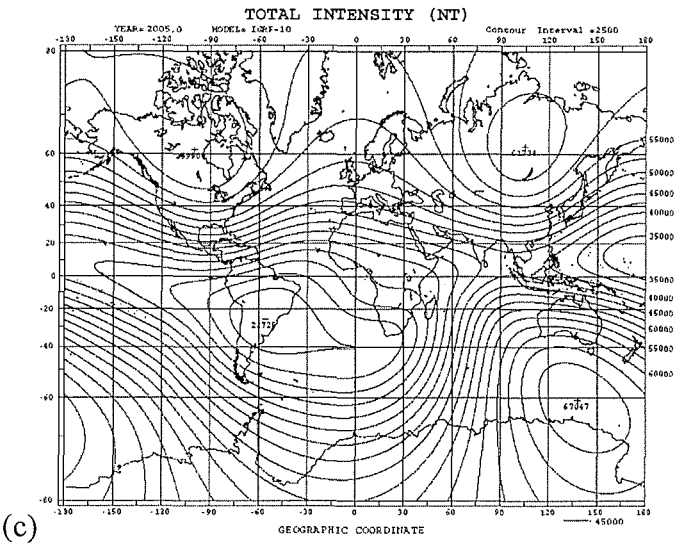

(c)

Figure 1.10: Isomagnetic maps showing contours of (a) inclination (b) declination, and (c) intensity of Earth's magnetic field at Earth's surface today. Taken from the IAGA V-MOD geomagnetic field modeling - International Geomagnetic Reference Field (World data centre for geomagnetism, 2006).

1.4 Using records of paleointensity and paleosecular variation as a dating tool

Temporal variation of Earth's magnetic field in both direction and intensity is recorded in a number of settings, potentially providing a high-resolution dating tool over a range of time-scales. Spot readings from volcanic rocks have traditionally been considered to provide a more reliable method of extracting paleo-orientations and intensities of the field, yielding absolute values of paleointensity (Tanaka et al., 1994).

Marine sediments potentially provide continuous records of changing geomagnetic parameters at a particular locality. Accurate chronologies may be derived from biostratigraphic, isotopic and tephrochronologic data. Owing to their proximity and high sediment input from rivers, continental margins have a far greater potential, (compared with the deep-sea), to preserve high-resolution continental records. They have long been recognized as important and rich reservoirs of information on Earth's history, and thus serve as excellent targets for paleomagnetic studies.

Paleomagnetic records from sedimentary rocks have been discredited on the basis of their time-averaged nature and uncertainties regarding the remanence acquisition process (Verosub, 1977). Fluctuations of paleodirection and paleointensity in records derived from marine sediments reflect the interaction of geomagnetic secular variations (of direction and strength), with depositional and post-depositional forces (Tarling, 1983). Magnetic grains settling at the sediment-water interface are subjected to inertial, viscous and magnetic aligning torques. Realignment also occurs (in water-saturated sediments) during post-depositional remanent magnetisation (pDRM) processes such as bioturbation and slumping (Irving, 1964). Lock-in of DRM occurs only once dewatering and consolidation restrain motion of sedimentary particles - a process that can take up to 10^3 years (Butler, 1992); resulting in a time lag between sediment and remanence ages. Paleomagnetic measurements from sediments are also inherently time- averaged, since the width (at half-height) of the response function of most magnetometer pick-up coils is such that adjacent measurements at 1 cm spacing are not independent. Such temporal smoothing of the record is compounded when sedimentation rates are low.

Palo-inclinations in marine sediments may be shallower than those of the paleofield as a consequence of compaction. Paleo-declinations often lack azimuthal orientation; and thus have been excluded from most paleomagnetic databases (Lanza & Zanella, 2003). Intensity of NRM is dependent on the grain size, concentration and mineralogy of magnetic constituents. This dependence must be compensated for through a normalisation parameter. Furthermore, sediments with low remanence intensities may require application of stacking techniques in order to amplify the signal.

Despite temporal smoothing and difficulties in obtaining a valid normalisation, records of relative paleointensity derived from sediment cores corroborate absolute paleointensities from volcanic rocks, and are considered to be accurate when certain rock magnetic criteria (see chapter four) are satisfied (Tanaka et al., 1994). Sedimentary records also provide high resolution and continuity, in contrast to the episodic spot readings of their igneous counterparts (Constable & Tauxe, 1987). The best approach to building a paleosecular variation (PSV) or relative paleointensity (RPI) curve is to integrate data from different lithologies, which provide independent constraints on the same phenomenon (Lanza & Zanella, 2003; Herrero-Bervera & Valet, 2002).

The potential of sediments as reliable recorders of relative variations of geomagnetic field intensity is ultimately demonstrated by the remarkable coherence between normalised relative paleointensity (RPI) records from geographically distinct areas, with different paleoenvironmental conditions (Tric et al., 1992). Emerging evidence supports the hypothesis of a globally coherent (i.e. predominantly dipolar) paleointensity signal (Guyodo & Valet, 1999; Roberts et al., 1997). Global synchronicity of both long and short wavelength features in the RPI signal is suggested from comparisons of RPI records from the North Atlantic (Laj et al., 2000), South Atlantic (Channell et al., 2000), Mediterranean Sea (Tric et al., 1992), Somali Basin (Meynadier et al., 1992), and Labrador Sea (Stoner et al., 2000). Such a signal can provide a means of high-resolution correlation over large distances, and an alternative temporal framework for areas where conventional chronologies are unreliable (Yamazaki, 2002). Laj et al (2004) demonstrated the potential of such correlations using globally coherent intensity fluctuations (Fig. 1.11), some with time constants close to the shortest associated with dipole variations (600-700 yrs; Hulot & Le Mouel, 1994). Unambiguous identification of

such features in records from widely separated sites facilitated compilation to produce the GLOPIS-75 global stack, extending from 10 k.a. to 75 k.a. Their study demonstrated that marine sediments can reliably record the geomagnetic dipole field with the maximum resolution theoretically possible on a global scale.

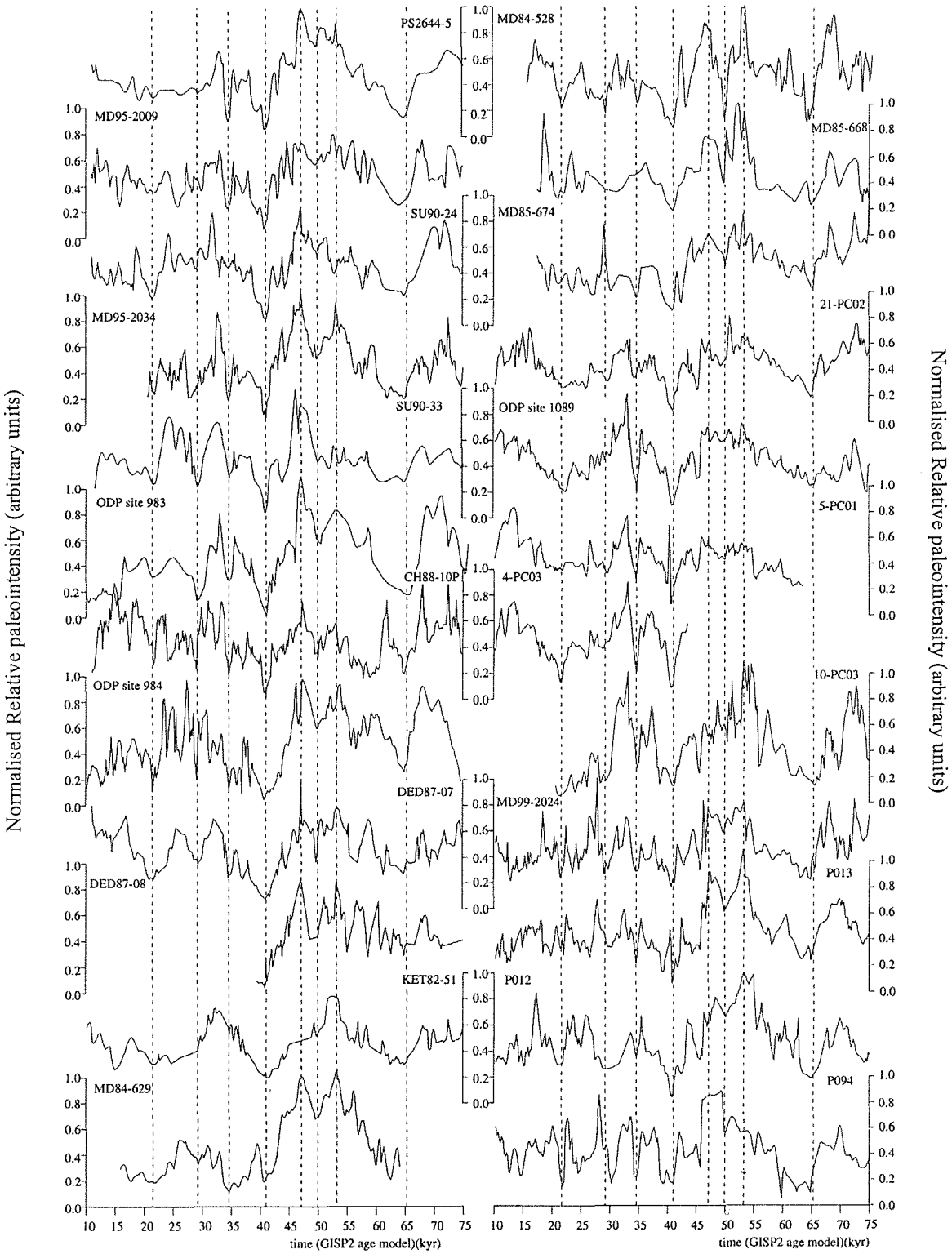

Figure 1.11: Individual paleointensity records used by Laj et al. (2004) to produce the GLOPIS-75 global paleointensity stack. All records are reported on the GISP2 age model after correlation with NAPIS-75. Broken lines mark the major tie points used for correlation. After Laj et al. (2004).

Development of a robust global paleointensity stratigraphy may serve as an independent, high-resolution time scale for comparison of sedimentary records (e.g. Peck et al., 1996). Applicability of the technique to New Zealand sediments has yet to be demonstrated.

Opdyke & Channell (1996) assert that the lack of coherency between records from Argentina, Australia, UK and North America disqualifies wobble of the main dipole as a source of secular variation. Such observations confirm the role of non-dipole components with different sources at different sites, with their relative size and distribution controlling regionality of the signal. Figure 1.12 illustrates the degree of similarity between records from the North American continent. Increasing the spatial distribution of PSV records will clarify the spatial extent of non-dipole signals, thus providing valuable constraints for models of the non-dipole field and constraining its applicability as a means of age control.

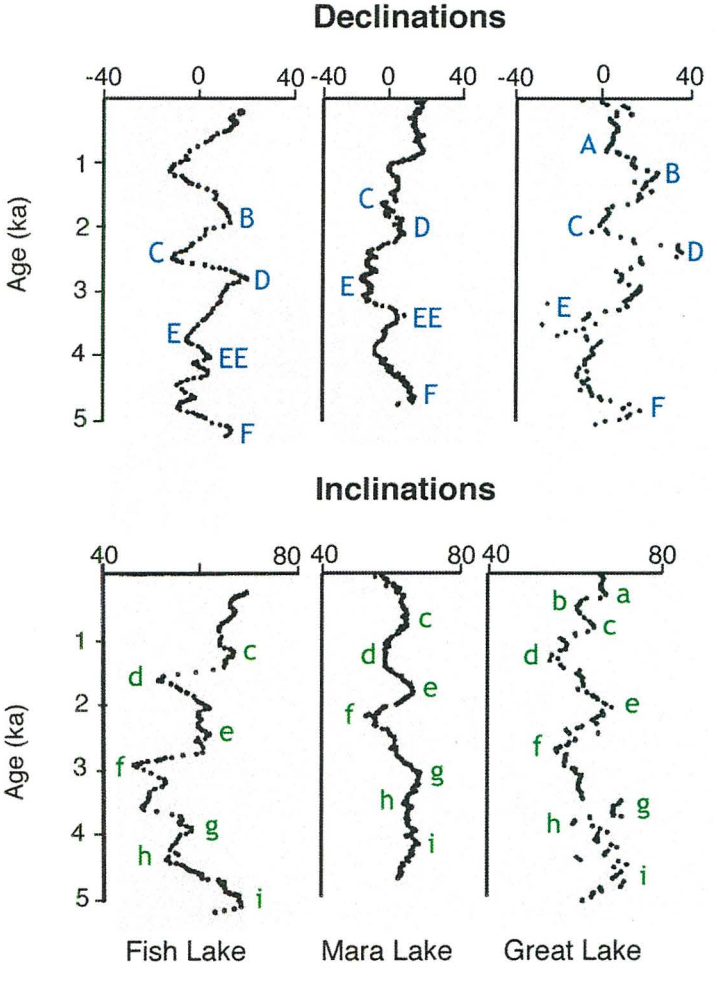

Figure 1.12: Comparison of inclination and declination records from Fish Lake, Oregon (Verosub et al., 1986); Mara Lake, British Columbia (Turner, 1987), and Great Lakes (Creer & Tucholka, 1982). Proposed correlations are indicated with letter codes at inflection points. After Opdyke & Channell (1996).

1.5 Regional setting

The continental margin to the east of the New Zealand's North Island is part of the tectonically active Hikurangi subduction system, marking the interface where oceanic crust of the Pacific plate is obliquely subducted beneath continental crust of the Indo-Australian plate (Fig. 1.13). This southern-most part of the Tonga-Kermadec-Hikurangi subduction system comprises an accretionary prism of anticlinal ridges, shelf and slope basins and the Hikurangi Trough structural trench (Lewis & Pettinga, 1993). For several million years, a succession of subducting seamounts and associated avalanche deposits (that collapse in their wake) has formed slope indentations and structural re-entrants in the deformation front (Orpin et al., 2002a). These represent the scars of tectonic erosion from seamount impacts, and have strongly affected basin sedimentation and regional structure along the northern margin (Lewis et al., 1998). Large volumes of fine terrigenous material have been delivered to the continental margin off the eastern North Island to form extensive postglacial sequences, inter-bedded with petrologically distinct tephras that occur throughout the Holocene. These sediments accumulate predominantly in tectonically subsiding mid-shelf basins (Lewis, 1973), which are often bordered on their seaward flanks by emergent anticlinal barriers (Orpin et al., 2002a). Structural complexity characterising the continental slope (e.g. the Poverty indentation) results from large-scale tectonic-sediment interactions in this region (Orpin et al., 2002a).

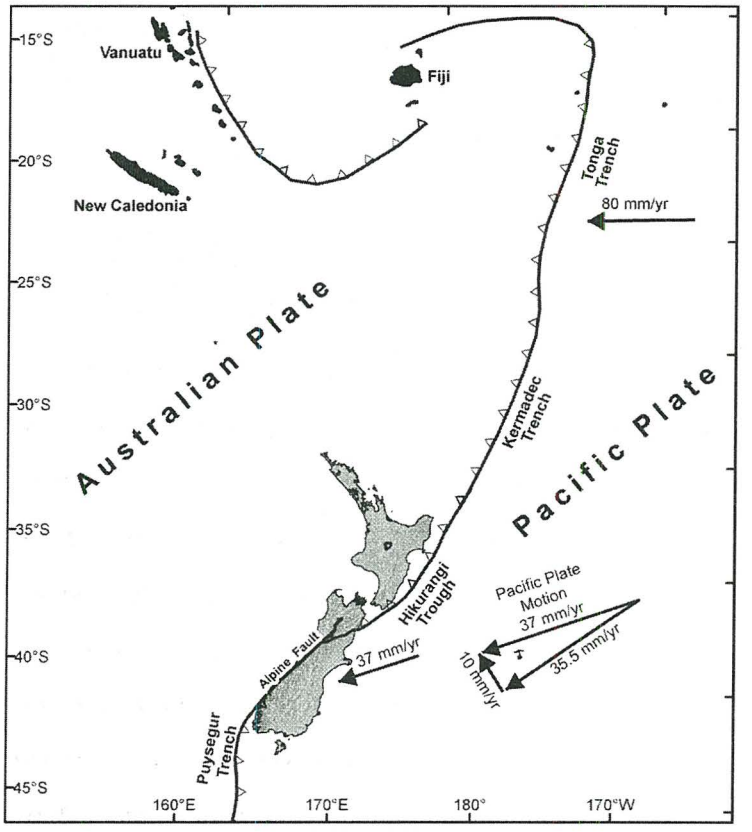

Figure 1.13: Tectonic setting of New Zealand, which sits astride the Pacific and Australian plates. The Hikurangi Trough marks the surface expression of a subduction zone beneath the North Island. The plate margin in the South Island is characterised by oblique continental collision, which has been accommodated on the surface through uplift of the Southern Alps and motion on the Alpine Fault.

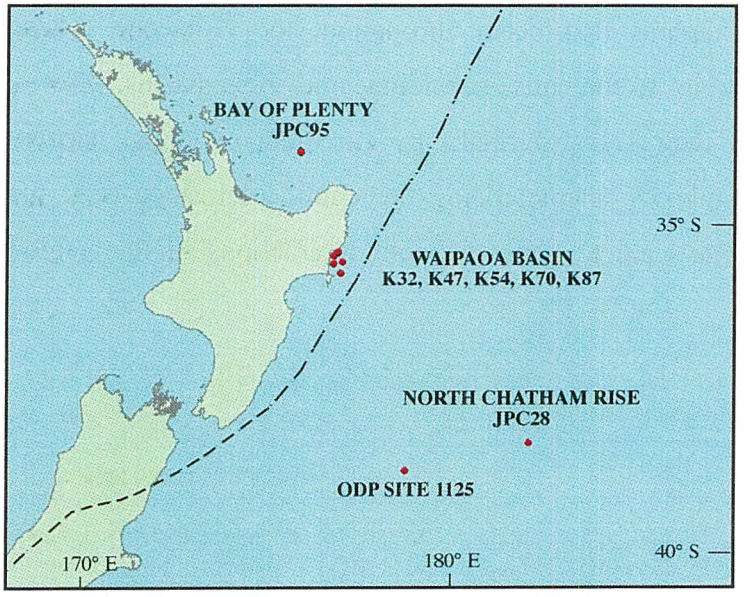

Figure 1.14: Core site locations for samples utilized in this study. Kasten cores were retrieved from the Waipaoa Basin (K32-K87). Jumbo piston cores from the Bay of Plenty (JPC95) and Northern Chatham Rise (JPC28) are also used to extend the record (temporally) and provide regional control.

1.5.1 The Waipaoa Basin

As part of the MARGINS 'Source to Sink' programme, the Waipaoa Basin to the east of Gisborne, New Zealand was selected for holistic studies investigating the generation, transfer and accumulation of sediments from terrestrial uplands to marine basins.

The Poverty Bay continental shelf (Fig. 1.15) extends 65 km between Mahia Peninsula and Monowai Rocks (Foster & Carter, 1997) and 22-26 km seaward to the shelf break (140-170 m depth). It straddles the top of the Neogene accretionary prism and forearc basin, which constitute a zone of active deformation associated with the offshore Hikurangi subduction margin (Lewis, 1980). The landward limit of imbricate thrust ridges on the outer continental shelf defines the periphery of the basin, (Lewis & Pettinga, 1993) which, during the Holocene, has served as a major repository for sediment discharged from the Waipaoa River. The annual load of suspended sediment delivered by the Waipaoa River, which drains the Raukumara Ranges, is ca. 15 x 10^6 t/yr. This is the fourth largest for any river in New Zealand, with yields per unit area among the highest on Earth (Walling & Webb, 1996). Owing to the prevalence of soft, fine-grained rocks in the catchment, 97% of this load is composed of mud and fine sand (Miller, 1981), which is dispersed through Poverty Bay in hypopycnal and hyperpycnal plumes. The high rate of basin subsidence (2 -4 mm/yr) and effective capture of sediment by the shelf edge Lachlan and Ariel anticlines have resulted in the accumulation of a thick, postglacial, mid-shelf mud deposit (Foster & Carter, 1997). The broad depositional syncline that constitutes the principle mud depocentre covers mainly the middle reaches of the Poverty Bay shelf, in water depths of 30-70 m (Foster & Carter, 1997). The synclinal axis extends 50 km southwest parallel to the shelf (Lewis, 1971), its landward flank marked by the coast, where Holocene uplift rates approach 4 mm/yr (Ota et al., 1987). Foster & Carter (1997) attributed a five-fold increase in accumulation rate in Poverty Bay since 8 ka to post-European deforestation.

Though the full internal structure of the basin is often masked by gaseous mud or gas-charged mud diapirs, it is characterised by thin, continuous reflectors dipping at shallow angles to the east above a prominent unconformity W1 (Lewis, 1973). This surface is considered to represent the last glacial regression 18 000 years ago (Carter et al., 1986). Upturning of layers against the flanks of the growing anticlines on the outer shelf suggests they act as

morphological barriers to progradation of the mid-shelf mud prism, except in the 13 km wide 'Poverty gap', where the prism has prograded to the shelf edge (Orpin, 2004).

Samples were collected from the Waipaoa Basin during a 6-week scientific cruise on board the Research Vessel Kilo Moana. In early 2005, the ship traced seismic survey lines throughout the basin in order to select suitable coring sites. Box and kasten cores were retrieved to investigate the manifestation of terrestrial signals in the marine record. Sub-samples of these cores were taken for paleomagnetic analyses.

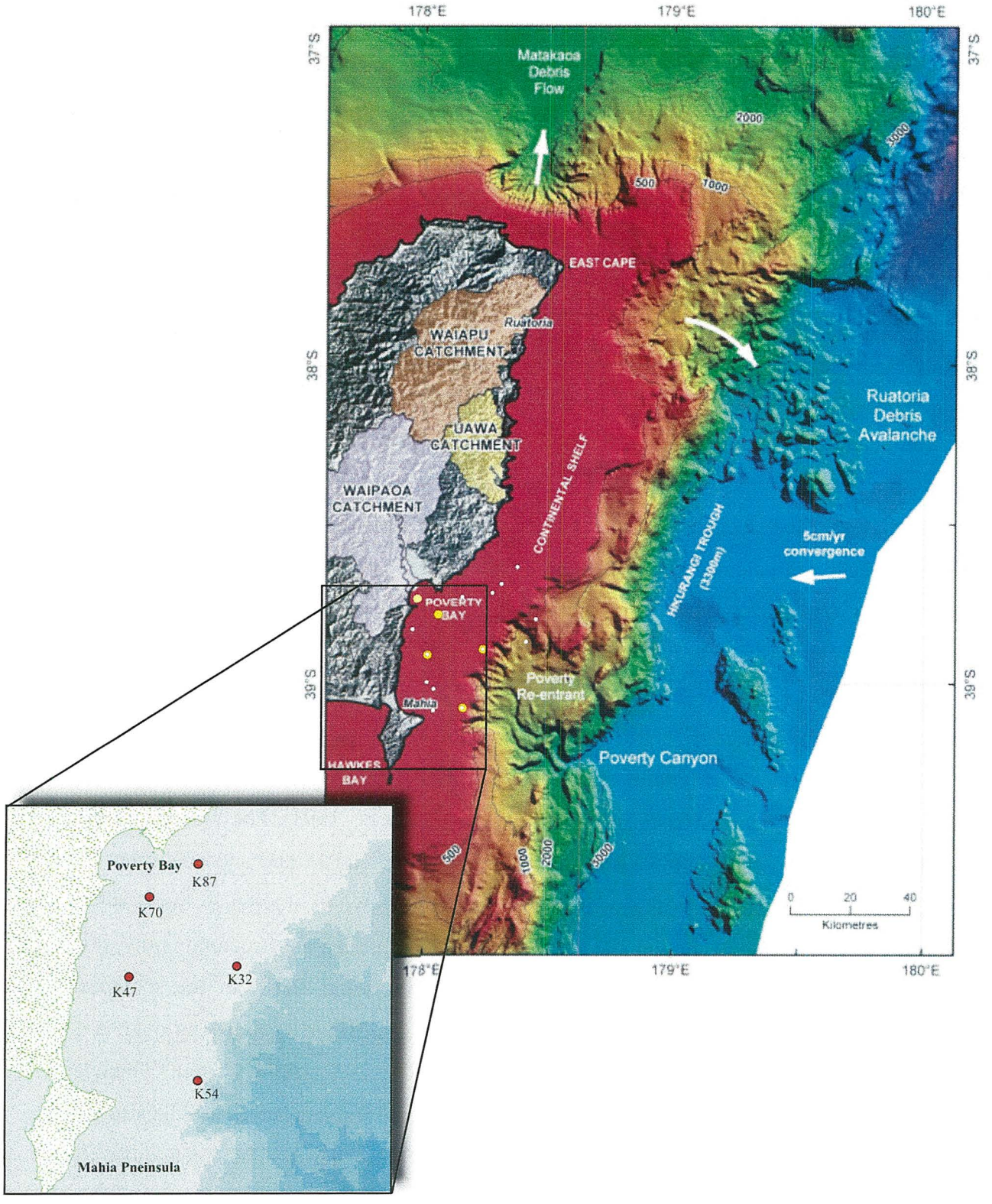

Figure 1.15: Three-dimensional representation of the continental shelf and slope offshore from Poverty Bay showing on and offshore dispersal parts of the Waipaoa dispersal system. Sampling sites from this study are marked as follows: white dots = sites of pilot samples, yellow dots = sites of kasten cores. Modified from Orpin et al. (2002).

1.5.2 Bay of Plenty: JPC 95

The Bay of Plenty marks the southern-most extremity of the Havre Trough, where it impinges on continental New Zealand (Fig. 1.16; Ballance, 1993). It lies within a NE-SW trending belt of active sub-marine tectonism and intense seismicity, associated with Quaternary back arc rifting and arc volcanism (Kohn & Glasby, 1978). Site JPC95 is situated in this central region near the base of the slope, within the seaward extension of the ensialic Taupo Volcanic Zone (TVZ). The offshore TVZ constitutes a NNE trending lineament of discontinuous spreading ridge systems, characterised by morphological complexity and irregular bathymetry. The interaction between the North Island shear belt, TVZ and Havre Trough in the Bay of Plenty has created a regional physiography that is dominated by a series of basement ridges and discrete sediment-filled troughs. On the continental shelf and upper slope the TVZ comprises a graben studded with volcanic knolls (Lewis & Pantin, 1984), whilst on the lower slope it is defined by the White Island and Tauranga troughs, and intervening Ngatoro and Wairaka Ridges and Wairaka Basin (Fig. 1.16).

Sedimentation in the southern Havre Trough – Bay of Plenty ridge and basin complex is highly variable and localized within structurally separate depocentres – rapidly subsiding grabens invariably bounded by basin-ward facing faults (Ballance, 1993). The Wairaka Basin, from which JPC95 was taken (Fig.1.16), is small (250 km^2), equant and sited between the Ngatoro and Wairaka Ridges to the west and east, respectively. Its margin to the north is marked by the Whakatane Seamount and although considered a separate structural entity, it is partially contiguous with the western shelf of the White Island Basin to the southeast (Ballance, 1993). A fault on the western flank of the Wairaka Ridge separates an older and more tilted sequence of forearc sediments along the basin's eastern periphery from a younger (down-thrown), horizontally bedded sedimentary sequence of volcaniclastic turbidites to the northwest, which occupy the central western part of the basin. The predominantly volcaniclastic sediment flux to the depocentres is principally derived from three sources: (1) from isolated eastern andesite massifs; (2) from submerged basement ridges flanking the depocentre; (3) from the New Zealand continental landmass to the southwest, supplied along three tectonically controlled conduits (Wright et al., 1990). Sediment from the first two sources is intimately related to the timing and periodicity of volcanism, whilst the flux of

terrigenous material varies between glacial-interglacial cycles. JPC 95 is located 4 km south of site H214, for which ages and rates of sedimentation have been calculated using volcanic ejecta and foraminiferal assemblages (Kohn & Glasby, 1978; Carter et al., 1995; Sikes et al., 2000).

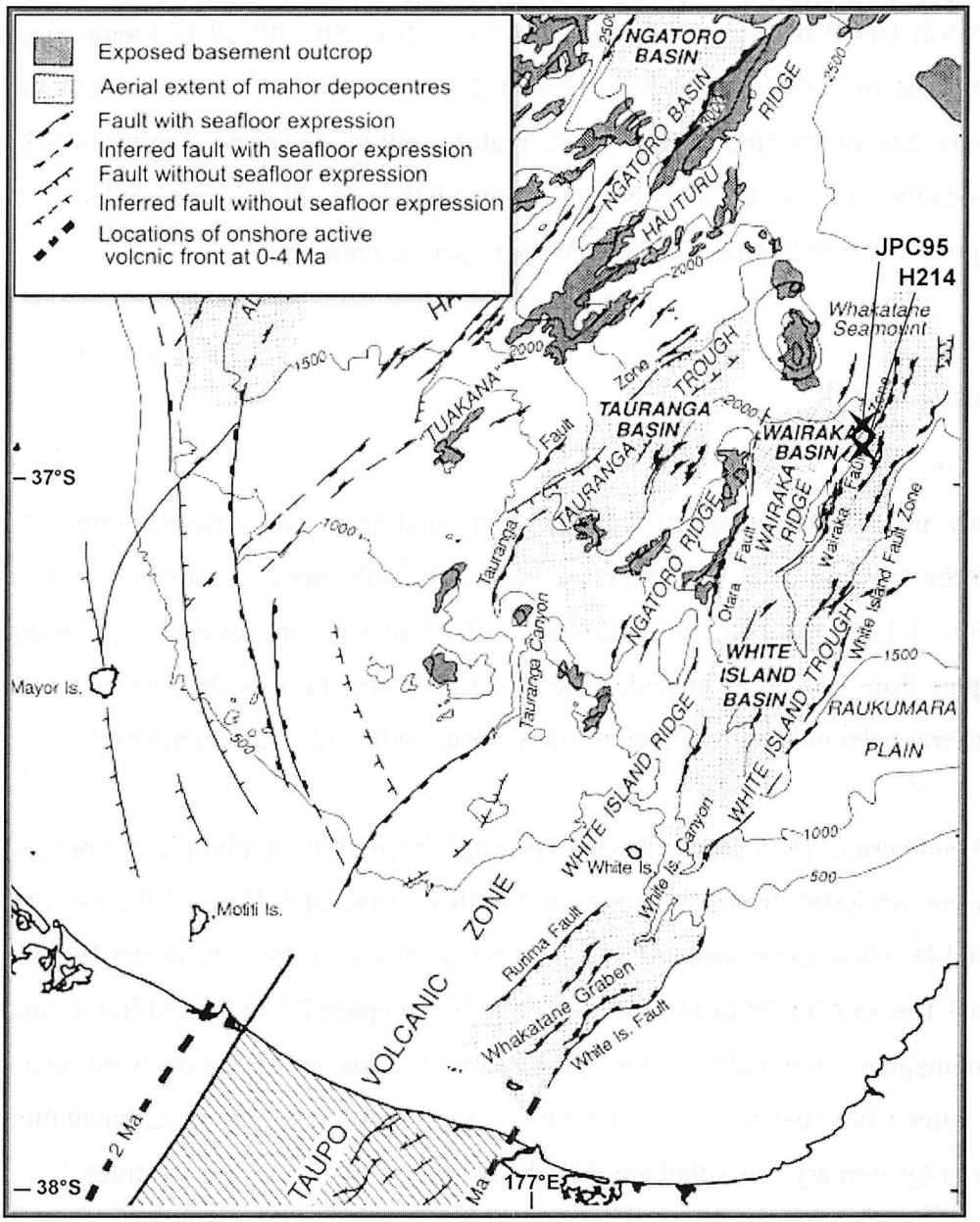

Figure 1.16: Synoptic structure and major sediment depocentres in the southern Havre Trough-Bay of Plenty. Marked are locations of sediment cores from sites JPC95 (this study) and H214 (Kohn & Glasby, 1978) within the Wairaka Basin. After Ballance (1993).

1.5.3 Northern Chatham Rise: JPC 28

JPC28 was retrieved from the northern slope of the Chatham Rise, a submerged continental plateau that extends eastward from central New Zealand over 1000 km. It is in the subtropical convergence zone (SCZ) and is swept by the East Cape current, which runs south along the eastern North Island before veering east along the Rise. Site JPC28 lies approximately 700 km to the east of New Zealand's South Island and east of the Hikurangi Channel, which occupies the axis of the Hikurangi Trough. Water depth at the coring locality is 2418 m. This coring locality is also 69 km northeast of ODP site 1125, from which no quality paleomagnetic data was retrieved (Gary Wilson, pers. comm.).

1.6 Field Work

This study utilizes paleomagnetic samples collected from two separate cruises. Box and kasten cores from the R/V Kilo Moana sampled the sub-surface sediments of the Waipaoa Basin (Figs. 1.14; 1.15), penetrating to depths of 0.5 m and 3 m, respectively. Discrete 2 cm^3 sub-samples from box cores provided the material for the pilot study (see section 2.5) from which general paleomagnetic behaviour of Waipaoa sediments was determined.

On the second cruise (R/V Roger Revelle) during March 2005, jumbo piston cores JPC28 and JPC95 were retrieved from the northern Chatham Rise and Bay of Plenty, respectively (Figure 1.14). These cores penetrated to greater depths than those from the Waipaoa Basin: JPC95 to 4.1 m and JPC28 to 11.5 m (though only the upper 2.6 m is used in this study owing to poor demagnetisation behaviour at greater depth). Sites on this cruise were selected to re-core localities where existing cores have proven to exhibit continuous sedimentation and the presence of Quaternary ashes that are well dated (Elisabeth Sikes, pers. comm.)

Continuous samples from both kasten (K32, K47, K54, K70, K87) and piston sediment cores (JPC28, JPC95) were collected in 1.5 m long U-channels. These were pushed into the split face of the core section, and material at the base of the U-channel cut away with fishing line, before extracting the sample and sealing it. All cores were azimuthally unoriented and assumed to penetrate the sediment vertically.

1.7 Project Aims and Objectives

This project aims to address the current lack of paleosecular variation (PSV) and relative paleointensity (RPI) curves for the New Zealand region; to test the suitability of marine sediments in this part of the world for paleomagnetic studies; to provide insight into regionality of dipole and non-dipole elements of the geomagnetic field; and to substantiate the validity of paleointensity records as a means of high resolution dating and magneto-stratigraphic correlation for young (0-50 ka) marine sediments.

PSV and RPI records from this study, combined with the few existing PSV curves established for New Zealand contribute to gaining a complete appreciation of the spatial and temporal nature of geomagnetic secular variation and fluctuations in intensity on a millennial (past ~50 k.yrs.) to sub-millennial (past few hundred years). Appending the available paleomagnetic database is important to refine understanding of non-dipole elements of the geomagnetic field, and to discern which of the several end-member models for secular variation (section 1.1.4) most effectively describes the observed changes in field direction preserved in such records. Ongoing assessment of these models will in turn contribute to resolving uncertainties regarding the source, processes and three-dimensional controls on dynamo processes governing secular variation of the non-dipole field.

Development of an age model using millennial to sub-millennial scale variability of Earth's geomagnetic field has potential to provide higher resolution than is currently available from traditional reversal polarity, oxygen isotope and radiocarbon stratigraphies. Such a refined method of paleomagnetic dating, based on changing geomagnetic paleointensity and/or paleosecular variation, could be applied to paleoclimatic records on a regional, if not global scale. This study aims to test the applicability of such methods, through ascertaining the regionality of the PSV and RPI signals recorded in New Zealand marine sediments. Correlation of prominent features and excursion events contained in records obtained in this study with those in the few established PSV and RPI curves with similar temporal coverage from the Southern Hemisphere (e.g. Channell et al., 2000) and around the globe (e.g. Laj et

al., 2004) should place constraints on the spatial extent of millennial-scale PSV and RPI signals, and their respective sources.

Records from this study also contribute to elucidating the extent of the purported Pacific non-dipole low, and magnitude of the negative inclination anomaly dominating the southwest Pacific (Elmelah et al., 2000). Inter-hemispheric comparisons will facilitate assessment of the permanent versus transient nature of hemispheric asymmetry of non-dipole features and secular variation, and associated boundary conditions that produce them.

The above aims are addressed through paleomagnetic analysis of five continuous samples collected in early 2005 from offshore East Cape in the Waipaoa Basin; and of two jumbo piston cores from the Chatham Rise (JPC 28) and the Bay of Plenty (JPC 95), New Zealand. The latter two cores are analyzed to determine the reproducibility of results from the Waipaoa Basin and to extend the record (back further in time).

Alternating Field (AF) demagnetisation techniques are performed on all seven cores in order to provide continuous measurements (at a sampling resolution of 1 cm) of paleo-inclination, declination and intensity of NRM. Principle Component Analysis (PCA) is applied to remove coring-induced overprints and isolate a characteristic component of NRM (interpreted as primary DRM). Variation in paleofield direction of the ChRM through time provides secular variation curves; and intensity of ChRM is used to derive relative paleointensity (RPI) records for each core. Tephra horizons within cores JPC28, JPC95 and K54, and ^{210}Pb isotopic data from cores K47, K54 are used to develop a chronology for the respective PSV and RPI records from these cores.

Analysis of all magnetic parameters is undertaken to interpret the extent to which grain size and concentration of the magnetic constituents have affected the normalised paleointensity record. This is used to establish whether sediments from these cores exhibit the degree of uniformity and homogeneity that is pre-requisite for paleointensity studies (King et al., 1983). Cores (and portions of cores) that conform to uniformity criteria (in accordance with King et al., 1983, Tauxe, 1993) are used to derive RPI curves through normalising ChRM against saturation ARM. This compensates for variations in NRM that do not reflect changing intensity of the paleofield. The validity of the most continuous and reliable RPI curves is then

tested by confirming lack of correlation between the normalised paleointensity record and bulk magnetic parameters, and reinforced (for one core) by establishing concordance with the global RPI stack GLOPIS-75 (Laj et al., 2004).

1.8 Layout of Thesis

This thesis is divided into seven major chapters, each of which represents an independent step towards fulfilling the main objectives of this project as laid out above. Chapter one introduces the concepts of the geomagnetic field and its components, the Geocentric Axial Dipole (GAD) model and, its derivative, the inclined GAD. It then identifies inadequacies in these models, primarily their failure in the short term to account for non-dipole sources of the field and secular variation. Section 1.2 outlines the basics of geodynamo theory and identifies the need for more paleomagnetic data to refine models of geodynamo processes driving Earth's geomagnetic field. Section 1.3 outlines why paleomagnetic studies in New Zealand are implicated in providing resolution to the geodynamo problem, through records of the dipole/ non-dipole elements of Earth's paleofield. The key application of relative paleointensity as a new means of high-resolution dating in marine sediments is then explored in section 1.4.

Chapter two outlines the requisite data sets that will be extracted from kasten and piston cores, and laboratory methods employed to obtain them, in order to ultimately construct records of paleofield direction and relative paleointensity. Establishing antiquity of the remanence is accomplished through Alternating Field demagnetisation; described in section 2.2. This is followed by a discussion (section 2.3) of the various magnetic parameters that provide a crude approximation of the *magnetic activity* of core samples (see appendix 9.2 for definition) and constrain their capability to preserve a primary remanence. The procedures involved in imparting and measuring artificial remanence parameters; anhysteretic remanent magnetisation (ARM) and isothermal remanent magnetisation (IRM) on kasten and piston cores are described. Information derived from laboratory-induced bulk remanence parameters is complimented by magnetic susceptibility (κ) and median destructive field (MDF), whose measurement and applications are also discussed. Techniques employed to analyze and manipulate the datasets (to extract remanent direction and intensity) are presented in section 2.4. Section 2.5 describes the pilot study, which was undertaken in order to provide

preliminary information on the behaviour of Waipaoa sediments in response to AF and thermal demagnetisation treatments. Kasten cores were selected partly on the basis of the results from this study.

Results are presented in chapter 3, which begins with a generalized summary of sample demagnetisation behaviour, and describes attempts to orient cores azimuthally to derive true declination. Down core measurements of magnetic parameters are then presented in log form for each core and described (section 3.3). The means of assigning chronology to cores JPC95, JPC28, K47 and K54 are described in section 3.4.

Chapter 4 addresses the possible contributions from magnetic mineralogy, granulometry and concentration to the trends observed in chapter 3. Criteria recommended for paleointensity studies using sediments are tabulated. Tests are then applied to all cores in order to assess the level of compliance with rock magnetic criteria. Bivariate scatter plots of magnetic parameters (κ, κARM, sIRM) and constructed parameters (S ratios, Hard IRM, κARM/κ and sIRM/κ) are used to characterise the magnetic fraction in terms of magnetic grain size, mineralogy and concentration and the degree to which these properties vary with depth throughout each core. At the end of chapter 4, the compliance of each core to the aforementioned rock magnetic criteria is summarized. Finally, all information presented in chapters 2 and 3 is collated and discussed for each individual core in turn. Depth intervals over which a ChRM is considered to have been isolated are identified, as are intervals over which the secular variation and relative paleointensity records are considered unreliable.

Chapter 5 is concerned with deriving an accurate record of relative paleointensity through normalisation of ChRM by sARM, whilst ensuring that uniformity criteria and additional recommendations for paleointensity studies are complied with. The validity of the normalisation is confirmed through a series of tests. Records of relative paleointensity and paleosecular variation (PSV) attached to their respective chronologies (where available) are described in section 5.4.

Chapter 6 constitutes the discussion, by which the major hypotheses laid out in section 1.3 are addressed using the most continuous and reliable records of PSV and RPI. Identification of two geomagnetic excursions in the PSV and RPI records from core JPC95 is discussed in

section 6.1. Reliability of the RPI record is established through comparison with the GLOPIS-75 global stack (Laj et al., 2004). Comparison of both RPI (section 6.2) and PSV (section 6.3) with existing records from the Northern and Southern Hemispheres facilitates assessment of the regionality and potential of millennial-scale magnetic signals as a high-resolution correlation tool back to ~ 50 ka. JPC95 records are then used to comment on contentious topics including temporal persistence of hemispheric asymmetry, the Pacific non-dipole low and the negative inclination anomaly of the southwest Pacific.

Chapter 7 summarizes the main conclusions that can be drawn from this investigation, stating their respective implications and significance; and identifies potential directions for future research. All definitions and additional information relating to the cryogenic magnetometer are included in the appendices, along with calculations and core descriptions.

2. LABORATORY METHODS & DATA ANALYSIS

2.1 Requisite Data Sets

For a complete description of the magnetic field through time it is necessary to obtain both paleodirectional data, which (together with an age-depth function) will ultimately constitute a record of secular variation and paleointensity data. It is essential to establish the antiquity of both data sets to ensure the record is representative of the ambient geomagnetic field at the time of deposition and not of spurious components acquired thereafter. The capacity of the sediments to preserve paleointensity signals must also be ascertained to provide a measure of confidence in the final record of relative paleointensity.

2.2 Antiquity of NRM

2.2.1 Alternating Field Demagnetisation

Natural Remanent Magnetisation (NRM) was initially measured every cm prior to any laboratory treatment of the sample. NRM intensity represents the vector sum of primary and secondary components of magnetisation and is measured along three orthogonal axes: x, y and z. Its magnitude is strongly dependent on magnetic concentration and grain size.

Paleomagnetic stability and antiquity of the measured data sets was established through Alternating Field (AF) demagnetisation (see appendix 9.2). This procedure was employed to preferentially erase any secondary, spurious components of NRM, and isolate the highest stability component of remanence: the Characteristic Remanent magnetisation (ChRM). The ChRM, where isolated in magnetically homogeneous sediments (chapter 4), was logically inferred to be a Detrital Remanent Magnetisation (DRM; see appendix 9.2). The intensity and direction of the ChRM were then used to construct records of paleosecular variation (PSV) and relative paleointensity (RPI). Separating components of NRM also provides critical information regarding the coercivity of samples. Discrete pilot samples (from box cores) and U channels (from kasten and piston cores) were subjected to step-wise Alternating Field (AF) demagnetisation on the three orthogonal axes x, y and z, at intervals of 5 mT from 5 to 40

mT, and in 10 mT steps from 40 to 100 mT. Magnetic moment was measured following each stage of treatment at 1 cm intervals and all measurements saved to a network folder.

2.2.2 Demagnetisation characteristics and Median destructive field

Demagnetisation plots of magnetisation intensity vs. peak alternating field provide information on coercivity, and its variation with depth. Median destructive field (MDF; see appendix 9.2) was estimated (for each cm) through examination of such plots to determine the level at which 50% of remanence had been erased. The MDF is thus a proxy for bulk coercivity, which in turn is mineralogy and/or grain-size dependent. Curves with convex-up geometry indicate high coercivity magnetic minerals, fine grain size (SD-PSD), or both. Concave-up curvature (low MDF) in contrast, implies soft, ephemeral behaviour and low-stability, arising from lower coercivity (e.g. Fig. 2.1).

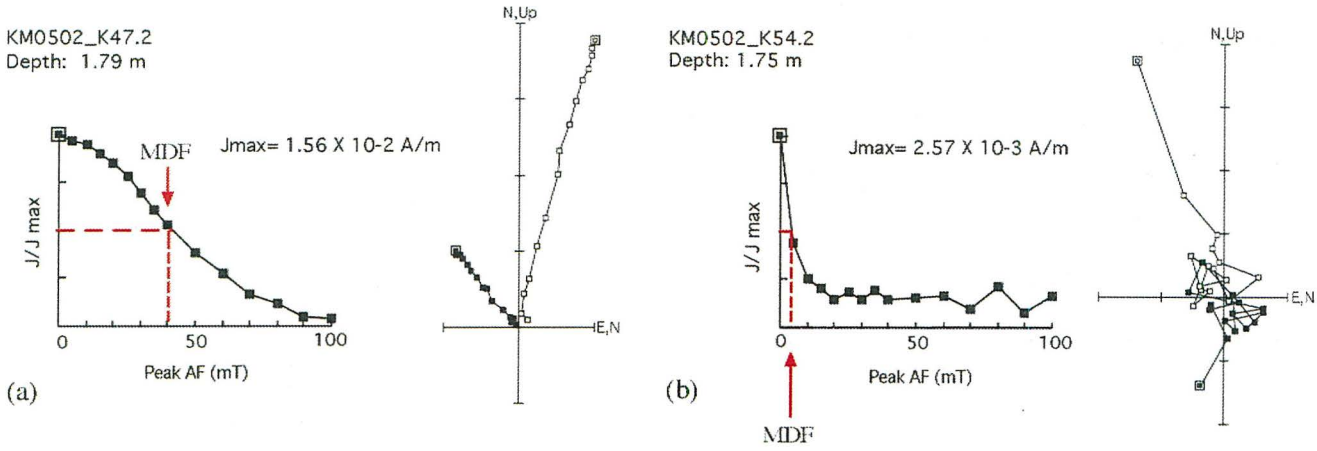

Figure 2.1: Comparison of demagnetisation plots (left) and median destructive fields (MDF) for sampling depths exhibiting (a) high and (b) moderate coercivity. Orthogonal component projections for these sampling depths are also illustrated (right). In (a) MDF is ~ 40 mT, indicating moderate coercivity; in (b) MDF is much lower (< 10 mT), which reflects low coercivity behaviour. Removal of remanence at low peak fields in (b) may be due to grains in the multi-domain (MD) state that are magnetically 'soft'.

2.3 Establishing capacity of sediments to retain primary remanence

The capacity of sediments to retain a primary remanence is assessed from their rock magnetic characteristics. More specifically, magnetic mineralogy, grain size and concentration should all be uniform according to criteria for paleointensity studies (see sections 4.1; 5.2) proposed by King et al. (1983). Magnetic parameters that are dependent on such properties are used to quantify their level of variation in each core. Key information is derived particularly from laboratory-induced bulk remanence parameters saturation anhysteretic remanent magnetisation (sARM) and isothermal remanent magnetisation (sIRM). ARM was imparted on all seven cores, whilst measurements of IRM were carried out only on a single core (K47), selected on the basis of its model response to AF demagnetisation (see section 3.1).

2.3.1 Laboratory-induced Anhysteretic Remanent Magnetisation (ARM)

Saturation ARM primarily provides a measure of ferrimagnetic mineral concentration, though it also exhibits the greatest grain size dependence of all the concentration dependent parameters (Peters & Dekkers, 2003). The sensitivity of sARM to changes in grain size enables constraints on magnetic granulometry to be estimated for each core. This data compliments information derived from magnetic susceptibility (grain size-independent; see section 2.3.3, appendix 9.2) and Median Destructive Field (MDF), which is strongly grain-size dependent, to provide a crude approximation of the *magnetic activity* of core samples (see appendix 9.2).

ARM was imparted on demagnetised cores by exposing them to a steady inducing bias field (DC field) superimposed onto a larger, smoothly decreasing alternating field. Past studies into paleointensity e.g. King et al. (1981, 1982); Cisowski & Hall (1997); Roberts et al. (1997) used bias fields of 0.05 - 0.1 mT and peak alternating fields of 99 - 100 mT, since acquisition of ARM is essentially linear and proportional with the bias field up to 0.1 mT for magnetite (King et al., 1982). However, the field at which non-linearity becomes apparent is dependent on magnetic concentration; higher concentrations being linear over larger field ranges (Peters

& Dekkers, 2003). Many studies lack justification for the chosen bias field, and assume that saturation is complete by 100 mT.

In this study, the alternating field was initially increased progressively in increments of 10 mT up to 100 mT (using a 0.1 mT DC field) to confirm that the saturation ARM had in fact been achieved. Asymptotic curves of ARM acquisition in this trial confirmed that sARM was reached between 90 and 100 mT in core K47. ARM was then imparted on remaining cores at higher alternating fields of 80, 90 and 100 mT. In cases where ARM declined between 90 and 100 mT, the maximum value (at 90 mT) was used to represent saturation. The saturation ARM was measured every cm along the core length, and subsequently removed from each core (completely) by AF demagnetisation using the same peak fields as applied to demagnetise the NRM.

Another experiment was performed in order to verify whether the level of the DC field being adopted was appropriate. This involved growing an ARM by increasing the peak alternating field as described above (from 10 to 100 mT) under a particular DC field, then demagnetising the core and repeating the process under a different DC field. This procedure was followed for DC fields of 0.05 mT, 0.1 mT, and 0.5 mT. Results of this experiment are illustrated in Figure 2.2. Saturation is reached between 90 and 100 mT regardless of the DC field used, and varies from a mean of 0.026 A/m (DC = 0.05 mT) to 0.051 A/m (DC = 0.1 mT) to 0.21 A/m (DC = 0.5 mT). ARM values used in subsequent calculations are those acquired using a direct field of 0.1 mT (the bias field recommended by King et al., 1982).

Existence of anisotropy in a sediment core renders the NRM less efficient in providing reliable estimates of paleointensity. Anisotropy of anhysteretic remanence was tested for by inducing an ARM at 100 mT in two directions, and comparing the resultant saturation intensities. This was carried out on several cores, none of which were found to show any directional dependence of anhysteretic remanence (Fig. 2.3).

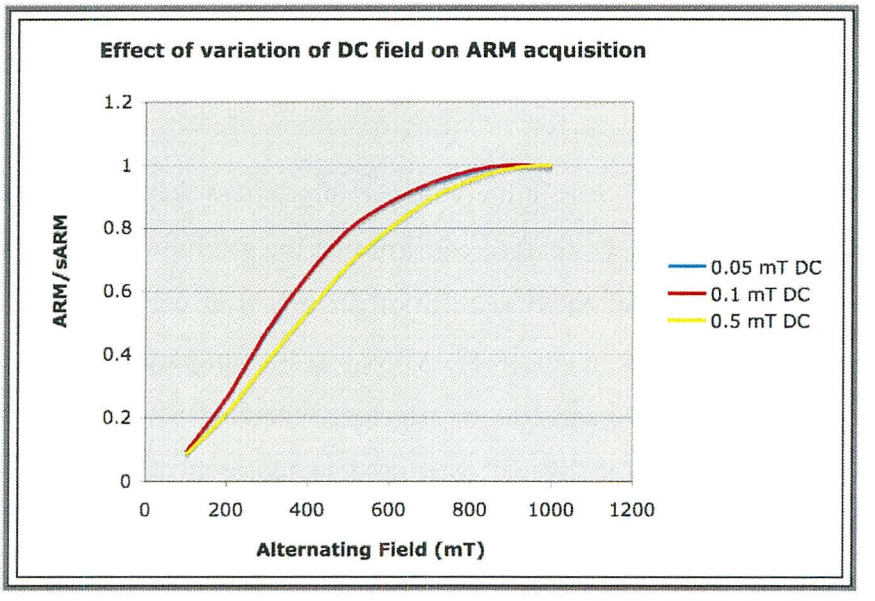

Figure 2.2: Effect of varying the DC field in ARM acquisition experiments for core K47. Saturation ARM is reached by 100 mT regardless of the DC field used.

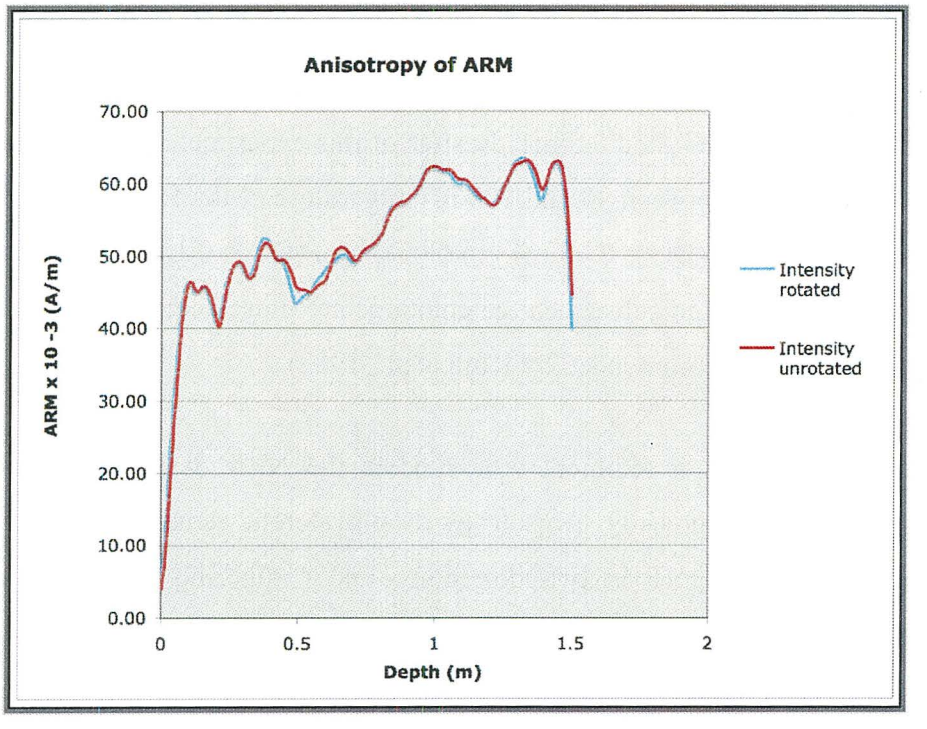

Figure 2.3: Acquisition of ARM for core K47 in two directions: one in which the core was rotated 90° about the z-axis of the U-channel (blue line). Coincidence of these curves confirms the lack of anisotropy of ARM.

2.3.2 Laboratory-induced Isothermal Remanent Magnetisation (IRM)

Saturation IRM (sIRM), like sARM, is dependent on the concentration of ferrimagnetic material and is generally inversely proportional to grain size, exhibiting greatest sensitivity to magnetic particles in the 10-20 μm size range. The field at which saturation is reached and the coercivity of remanence (the back-field required to reduce the IRM from saturation to zero) provide constraints on the mineralogy of ferromagnetic constituents, whilst saturation IRM compliments κ and saturation ARM in determining variations in magnetic concentration (see chapter 4).

Core K47 was demagnetised at 100 mT and dissected into 2 cm lengths in order to ensure consistent magnetisation of the entire length of core. The sub-samples were then impulse magnetised in incremental steps of 10 mT up to 200 mT; steps of 50 mT from 200 to 500 mT; and steps of 100 mT from 500 to 1000 mT, in order to identify the saturation field along the core. Following each IRM step, the sample was reassembled in the long core tray so that the remanent magnetisation acquired at each step could be measured every cm using the cryogenic magnetometer. Once saturated, samples were reversed (rotated 180° in the pulse magnetizer) and impulse magnetised using identical field steps; thus demagnetising them and progressively bringing to saturation in the backfield direction (-z) to determine the remanent coercivity B_{cr} (Fig. 2.4).

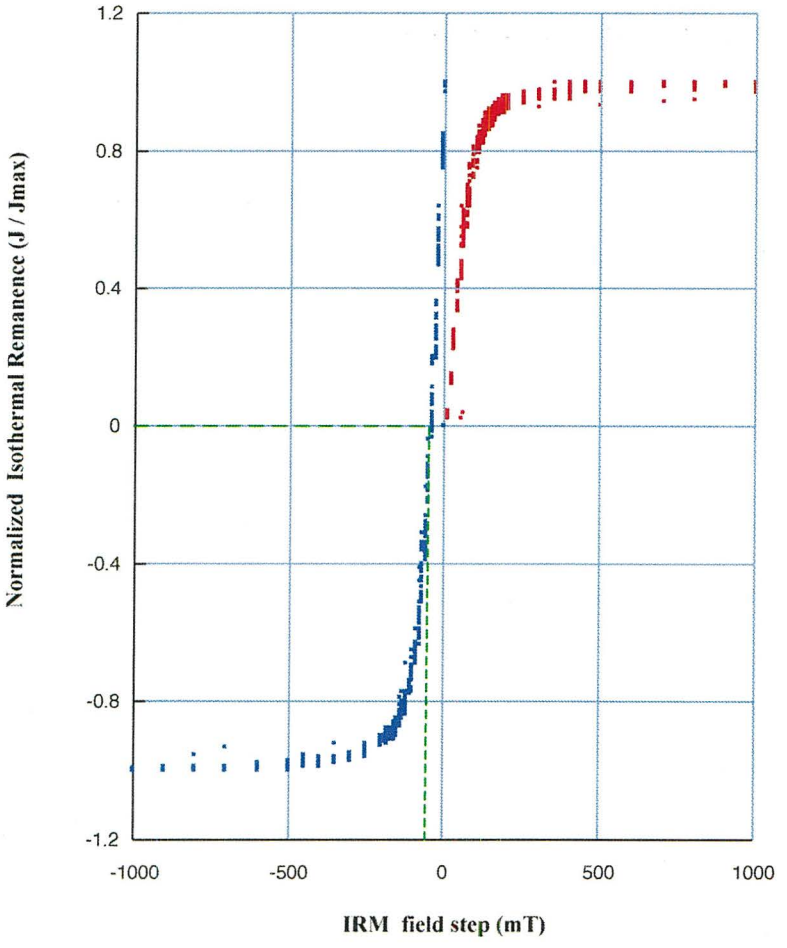

Figure 2.4: Acquisition of Isothermal Remanent Magnetisation (IRM) in K47 (data from 10 cm intervals). The sample was impulse magnetised normally to 1 T (red line), and then reverse impulse magnetised to 1T (blue line). Leveling out of the asymptotic curves at a mean saturation IRM of 37.4 A/m occurs at fields of approximately 450 mT. Green broken line marks mean *Bcr* = -45 mT (the level at which magnetisation is reduced to zero).

2.3.3 Volumetric Magnetic susceptibility (κ)

Volumetric magnetic susceptibility (κ, see appendix 9.2) provides a first order measure of the concentration of ferrimagnetic material. Susceptibility κ is often enhanced in tephra horizons, and features in the κ record units can aid in core correlation. The Bartington in-line magnetic susceptibility bridge was used to measure κ down-core at 1 cm intervals prior to any laboratory treatment of samples.

2.4 Data Analysis

2.4.1 Data Manipulation

Data files of all long core measurements were copied from the network folder RAID <PUYSEGUR> to a workbook in Microsoft Excel for manipulation. Data retained included sample ID, depth, treatment type, demagnetisation level (AFZ), total intensity, magnetic susceptibility (κ), x intensity, y intensity, and z intensity. Declination and inclination were calculated through application of the following formulae:

$$\text{Declination} = A\cos\left(\frac{-x}{\sqrt{-x^2+y^2}}\right) \qquad [2.1]$$

$$\text{Inclination} = A\tan\left(\frac{-z}{\sqrt{-x^2+y^2}}\right) \qquad [2.2]$$

(where x, y and z represent orthogonal directions within the cryogenic magnetometer).

2.4.2 Deconvolution of Intensity

Since magnetic intensity is volume dependent, deconvolution is required to adjust for volume reduction against the measurement profile. An intensity reading is taken by the SQUID sensor over a span of ~10 cm according to x, y and z response functions, such that no measurement is completely independent of the next. Towards each end of a U-channel, where that 10 cm

range includes sample plus air, a deconvolution adjustment is required to account for the decrease in sample volume and consequent decrease in intensity. See appendix 9.4 for calculation of deconvolution functions.

2.4.3 Orthogonal component projections

Orthogonal component diagrams aid significantly in identification of the various components of NRM isolated by demagnetisation (Tauxe, 2002). Data was sorted and saved in a text tab-delimited file format compatible with 'Z Plot' (the program used for analysis of directional paleomagnetic data). Once opened in 'Z Plot' the data is displayed on three separate orthogonal component projections, enabling 3-D visualization of direction as well as changes in intensity. Declination is invariably projected onto the northeast (horizontal) plane, whilst inclination is projected onto the north-up (N-Up) vertical plane, east-up vertical plane (E-Up), or in the vertical plane defined by the declination measured for a particular point (H-Up). This latter projection, although providing true inclination angles, shows misleading angles between consecutive points, since each point is plotted in a slightly different plane dependant on its declination. Generally, therefore, the north-up or east-up plots were used for picking paleodirections through PCA.

2.4.4 Principle Component Analysis

Principle component analysis (PCA) was performed on the demagnetisation data from every cm throughout the length of each core using orthogonal component projections in 'Z plot'. The sequence of progressive demagnetisation data points for a given depth was used to identify the linear component of NRM of greatest stability (termed ChRM; appendix 9.2). The least squares regression line defining the component was mathematically determined; the orientation of which is taken to represent inclination and declination for a given depth. The mean angular deviation (MAD) value was also calculated for the trajectory of points defining the ChRM to provide a quantitative estimate of the precision with which the line of best fit was determined (Butler, 1992).

It is favourable in PCA to use as much of the data as possible to depict the ChRM direction. However, in many samples, the lowest coercivity grains had clearly acquired a spurious

component of viscous remanent magnetisation (VRM; appendix 9.2) during the coring process. The persistence of the VRM varied between cores, and only data collected following demagnetisation of the VRM was used for PCA. Intervals over which MAD $\geq 10°$ are considered ill defined and thus were not used in construction of PSV records. Wherever possible, points farthest from the origin were used to maximize the signal to noise ratio (Butler, 1992). Points closest to the origin were often ignored (e.g. Fig. 2.5) if NRM intensity had dropped below 10% of the original value. At such intensities the magnetometer is unlikely to distinguish signal from noise.

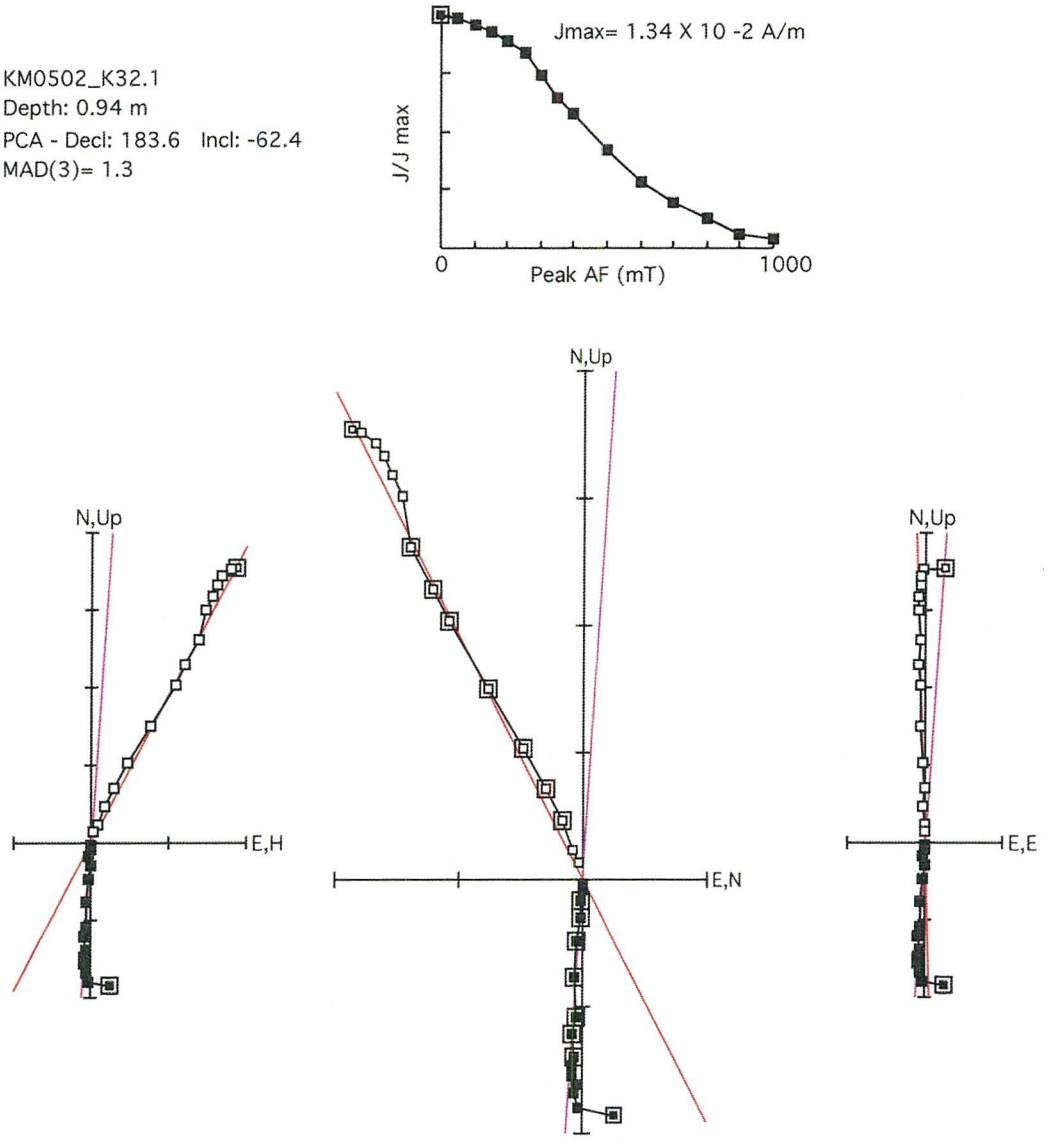

Figure 2.5: Illustration of the procedure for determining direction of a ChRM (characteristic component of NRM) through PCA, using orthogonal component projections. The points selected to represent the linear, highest stability component of NRM are highlighted in the north-up projection (centre). Projections onto the H-up plane (plane of declination) and east-up plane are shown to the left and right, respectively. White squares = inclination; black squares = declination. Coloured lines define the 3-D orientation of the isolated ChRM: red in the vertical plane (inclination), pink in the horizontal plane (declination).

2.5 Pilot Study

A pilot study into demagnetisation properties of discrete samples was undertaken to provide preliminary information that would ensure appropriate treatment of continuous samples. The main objective of the pilot study was to ascertain how the magnetic component of sediments in the Waipaoa Basin behave in response to Alternating Field (AF) demagnetization; more specifically to determine the directional stability and coercivity distribution characteristics of their natural remanent magnetisations.

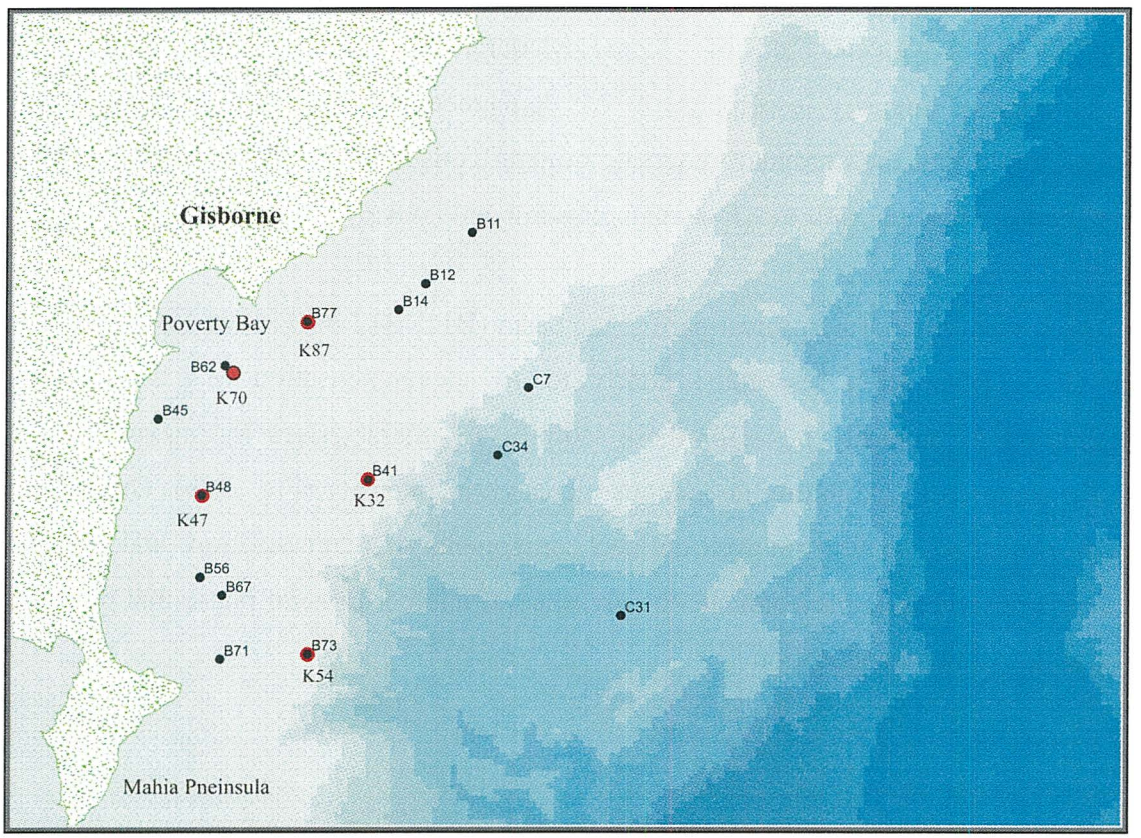

Figure 2.6: Locations of pilot samples (small symbols) from box cores collected from Poverty Bay continental shelf and slope. Larger red dots depict locations of kasten cores selected for paleomagnetic analyses (labelled).

Fifteen discrete samples from the Waipaoa shelf and slope (Fig. 2.6) were initially selected, from which to conduct the pilot study into the properties and magnetic minerals comprising the samples. Samples were selected to attain a wide distribution throughout the basin, and wherever possible, to coincide with the locations of kasten cores that could potentially be

analyzed; though only box cores (discrete samples) were retrieved from the continental slope. Each 2 cm^3 sample was subjected to AF demagnetisation in the following steps: 10, 15, 20, 25, 30, 35, 40, 45, 50, 55, 60, 70, 80, 90 and 100 mT. Lack of discrete specimens from the Roger Revelle cruise precluded the possibility of a pilot study at core sites JPC28 and JPC95.

Most favourable responses were obtained from the central part of the shelf (B41, B48, B62, B73 and B77) and the continental slope (C7, C31, C34). Demagnetisation vs. intensity plots for these samples are characterised by convex-up curvature, and orthogonal component projections by linearity of NRM components (Fig. 2.7a). Consistency in direction of inclination and declination for these samples allowed successful isolation of a well-constrained ChRM above peak fields of ~ 15 mT. Moderate coercivities are inferred from the gradual reduction of intensity in response to AF demagnetisation (MDF ~ 40 mT). These observations imply that the dominant magnetic mineral constituent of these samples retains stable remanence, responds well to AF demagnetisation and is likely to be (titano)magnetite.

Samples taken from the northern-most part of the basin (B11, B12 & B14) and several close to shore (B45, B56, B67) responded poorly to AF demagnetisation (e.g. Fig. 2.7b). Demagnetisation vs. intensity plots for these samples are characterised by uneven loss of intensity; in some cases exhibiting anomalous increases in intensity (Fig. 2.7b). Orthogonal component projections exhibit no well-defined components of magnetization, and thus no ChRM. These observations may indicate the presence of another mineral phase that does not respond well to AF demagnetisation.

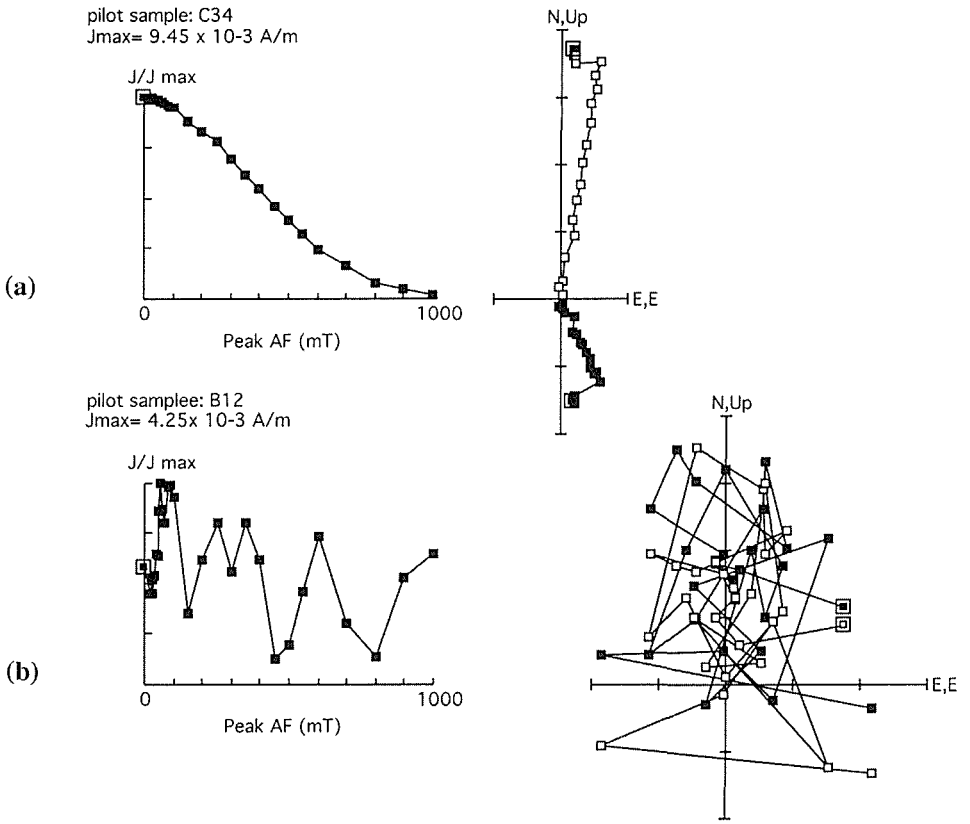

Figure 2.7: Plots of demagnetisation level vs. intensity (left) and orthogonal component plots (right) illustrating three-dimensional direction of the NRM at each demagnetisation step. Pilot sample C34 (a) behaves well in response to AF demagnetisation, as observed from the convex-up shape to the intensity loss curve and consistent direction exhibited in the orthogonal component plot. In contrast, no consistent direction of remanence was obtained from AF treatment of sample B12 (b). Several peaks on the intensity plot (left) indicate that the minerals contained in this sample may be better suited to thermal demagnetisation.

A property common to grains carrying secondary NRM in hematite or goethite bearing rocks is a short relaxation time (τ) resulting from low product $v.h_c$ (volume x coercive force) (Butler, 1992). Hence grains with high coercive force *hc* but small volume can still carry secondary NRM, which will not be effectively be removed by AF demagnetisation because their coercive force can easily exceed the maximum intensity of the applied alternating field. In rocks with hematite as the dominant ferromagnetic mineral, removal of VRM invariably requires thermal demagnetisation.

The second stage of the pilot study involved subjecting a further eight samples to thermal demagnetisation in the following increments of heating: 40°C, 60°C, 80°C, 100°C, 140°C, 180°C, 220°C, 240°C, 300°C, 350°C, 400°C, 450°C, 500°C, 600°C, 700°C. Unfortunately,

the samples in which we were most interested (i.e. those closest to the samples that hadn't demagnetised under AF treatment) broke apart during the early stages of the heating process. Thus kasten cores from these sites have not been used in the main study.

Kasten core samples from sites adjacent to the best-behaved pilot samples on the shelf were selected to undergo AF demagnetisation and detailed paleomagnetic analyses to form the basis of this study. These samples and corresponding adjacent kasten core samples include B41 (K32), B48 (K47), B73 (K54), B62 (K70) and B77 (K87).

3. RESULTS

3.1 Sample Demagnetisation Behaviour

The quality of demagnetisation data varies as a function of remanence intensity. In general, sediments with lower NRM intensities (generally $\leq 10^{-4}$A/m) exhibit uneven and soft demagnetisation behaviour e.g. Fig. 3.1 (l), with greater persistence of viscous remanent components and scatter in directional data. This is most likely due to less effective alignment of the coarse-grained minerals. Median destructive fields (MDF) of NRM, ARM and IRM in samples with high remanence intensity ($\geq 10^{-3}$ A/m) are similar and centred around 40 mT. This implies that all types of remanence are carried by the same fine-grained ferromagnetic mineral. Maximum angular deviation (MAD) values are generally less than 10° for all samples, indicating that the magnetisation components are well defined.

The NRM of all cores contains a viscous overprint, which is easily removed by peak fields of 5-20 mT (Fig. 3.1). This is likely to be an ephemeral remanence imparted from the core barrel during the coring process. The extent to which the VRM persists is generally consistent throughout a particular core. However, the magnetic core barrel is more intensely magnetised at each end (of the dipole), where in addition, greater surface area is in contact with the barrel (due to end plates). Together these factors result in greater VRM extent in the upper- and lower-most ~5 cm of core. VRM is also imparted at boundaries between core sections during cutting. Reorientation of magnetic grains in the upper- and lower-most ca. 10 cm, and at core section boundaries can render data over these intervals ambiguous. Hence they are often excluded from interpretation.

Scatter and VRM extent also appear to worsen with proximity to core section boundaries where greater surface area of sediment within the core has been exposed to potential field sources. Figure 3.1 (l) for JPC 28 is taken from 2 cm above the section boundary. The extent of this effect is generally confined to within 5 cm of the cut surface.

Removal of the viscous component generally reveals a (uni-vectorial) single component persisting to peak alternating fields of 90 - 100 mT e.g. Fig. 3.1 (a)-(h). The residual

magnetisation at peak alternating fields of 90 mT generally represents less than 10% of the original intensity. Increased scatter at such high fields results from magnetisations close to the noise level (10^{-6}-10^{-8} A/m) of the cryogenic magnetometer. In discussion of the four demagnetisation behaviour categories identified below, letters refer to Figure 3.1.

Type 1: Single component behaviour

Type 1 behaviour is characterised by intense, stable remanences that are directed linearly toward the origin of orthogonal component plots (Fig. 3.1 (a) - (c)), which generally exhibit little/no scatter, and no pronounced overprint. This behaviour is characteristic of the majority of measurements for core K47 (below 0.56 m), lower JPC 95 (below 2.4 m), and parts of K70 (0.3-0.47 m). The half-parabolic shape to the intensity curve for K47 implies demagnetisation of a single phase with approximately normally distributed grain size to create the observed coercivity spectrum.

Type 2: Persistent VRM

The first 6 points in vector component plots (d), (e) and (f) define a trajectory that deviates in direction from that of points following. The intensity plot for (e) exhibits marked concavity of intensity loss at fields up to 30 mT, indicating lower resistance to demagnetisation and soft behaviour, characteristic of a VRM overprint. This is followed by an increase in intensity as a component of higher stability is removed. The orthogonal component plot shows inclination following two similar but separate trajectories (before and after the increase in intensity). In (d) and (f) in contrast, the first six points on orthogonal component plots define a broad curve toward points thereafter, representing overlapping coercivity spectra of the two components: a VRM and higher stability ChRM. On intensity plots the curvature defined by these points at low fields is more *convex-up* than at higher fields, unlike that in (e).

In the upper 1.5 m of core K32, The behaviour defined by the first 6 points (to 25 mT) varies between that characterised by (e) and that typical of (f). This alternation between initial convexity and concavity in intensity plots is interpreted as a VRM of consistent extent but varying direction, imparted from the core barrel. The angle between the two vector components of magnetisation (VRM and ChRM) controls the resultant trajectories of

direction and intensity in (e) and (f). Erasure of antipodal VRM may enforce the remaining ChRM. VRM is consistently erased by the 30 mT step in both K87 (d) and K32 (e & f), above which demagnetisation of the ChRM continues toward the origin with relatively consistent direction and often some scatter.

Type 2': Weak VRM

Cores that demagnetise linearly exhibit varying degrees of scatter. In type 2' cores, the severity of scatter is insufficient to inhibit determination of paleodirection through principle component analysis. Upper (0.21-0.8 m) K54 (g) is characterised by uneven loss of intensity and some scatter in direction. Somewhat greater scatter is evident in K32 below 1.45 m (h), associated with lower initial NRM. Loss of intensity is more irregular and more concave-up (softer) than for type-1 behaviour, suggesting lower coercivity. Less parabolic (more linear) loss of intensity (than for that of type-1 behaviour) implies a more even grain size distribution e.g. (i) for JPC95. Figure 3.1 (g), (h) & (i) show removal of a low-coercivity VRM by ~ 5 mT, followed by subsequent progressive removal of a higher-coercivity ChRM that is slightly less well defined than for type 1 behaviour.

The majority of cores measured in this study fall under this category for at least part if not all of their length, including K47 (0-0.56 m), K54 (0.21-0.8 m), all of K87, JPC28 (0-0.45 m; 1.05-1.9 m), and much of upper JPC95 (0.22-0.9 m; 1.58-1.98 m; 2.17-2.4 m).

Type 3: GRM

Figure 3.1 (j) shows behaviour due to a Gyro-Remanent Magnetisation (GRM) imparted at higher peak fields during AF demagnetisation, which is often associated with the presence of Greigite (Hu et al., 1998). Remanent magnetisation first decreases and then increases after demagnetisation in successively higher fields. This phenomenon appears in vector component plots for K70 as linear decay of consistent direction (type 1 or type 2 behaviour) followed by a veering of paleomagnetic direction at peak fields above 70-80 mT to follow a different trajectory - away from the origin. A GRM is evident throughout core K70 to varying extents.

Type 4: Incomplete demagnetisation

Highly irregular and uneven decay of intensity with numerous peaks generally occurs in weakly magnetised cores, in which NRM intensity is on the order of 10^{-4} A/m. The high degree of scatter in orthogonal component projections often hinders definition of any NRM components through PCA. Intervals characterised by this behaviour include parts of core JPC28 (0.45-1.05 m; 1.9-2.6 m), JPC95 (0.9-1.57 m; 1.99-2.17 m), K54 (0.8 m to base), and parts of lower K32. In the latter two cores transition to this behaviour is associated with increasing grain size/domain state such that remanence is poorly preserved (see section 4.3). Figure 3.1 (k) for JPC28 exhibits linear decay up to fields of 30 mT, above which loss of intensity becomes erratic, and directions of inclination and declination scatter without cleaning to the origin. This may occur as the NRM intensity approaches the precision level of the magnetometer (10^{-6}-10^{-8} A/m).

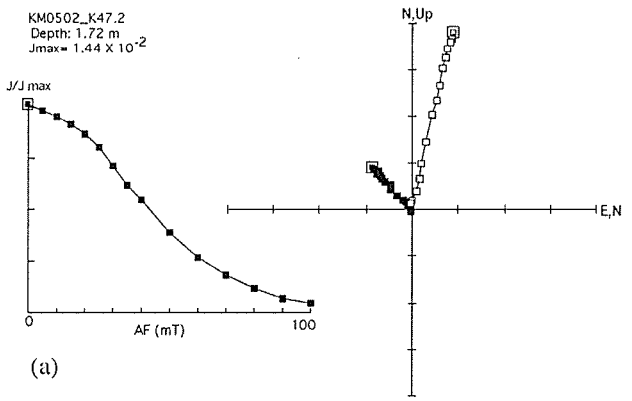
KM0502_K47.2
Depth: 1.72 m
Jmax= 1.44 X 10-2
J/J max
0
AF (mT)
100
N,Up
E,N

(a)

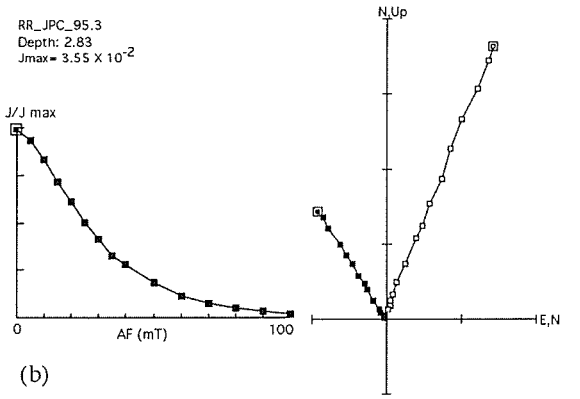
RR_JPC_95.3
Depth: 2.83
Jmax= 3.55 X 10-2
J/J max
0
AF (mT)
100
N,Up
E,N

(b)

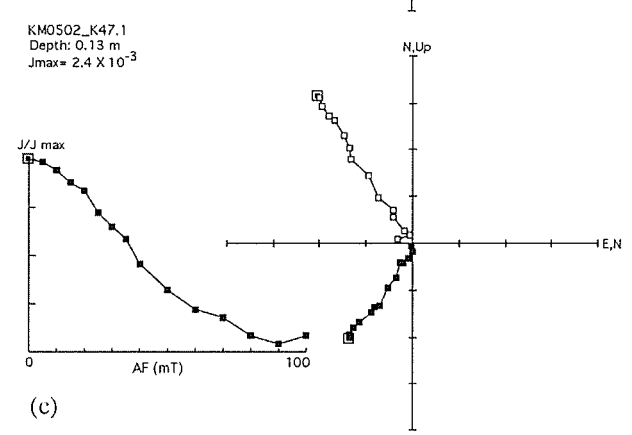
KM0502_K47.1
Depth: 0.13 m
Jmax= 2.4 X 10-3
J/J max
0
AF (mT)
100
N,Up
E,N

(c)

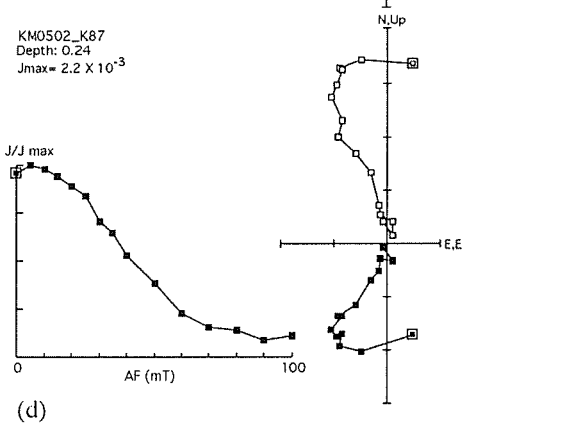
KM0502_K87
Depth: 0.24
Jmax= 2.2 X 10-3
J/J max
0
AF (mT)
100
N,Up
E,E

(d)

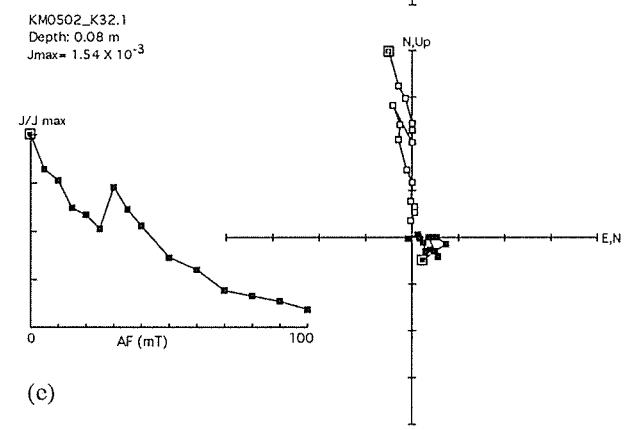
KM0502_K32.1
Depth: 0.08 m
Jmax= 1.54 X 10-3
J/J max
0
AF (mT)
100
N,Up
E,N

(e)

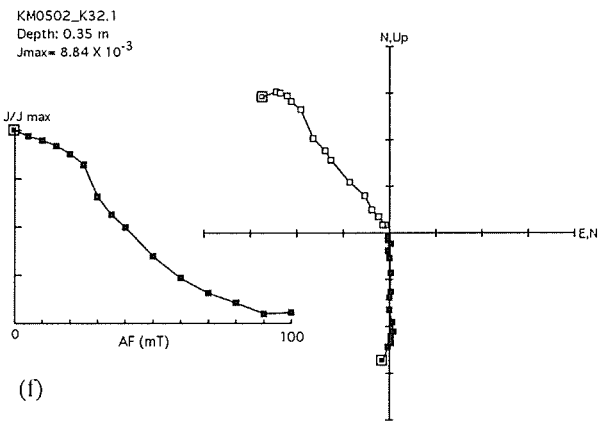
KM0502_K32.1
Depth: 0.35 m
Jmax= 8.84 X 10-3
J/J max
0
AF (mT)
100
N,Up
E,N

(f)

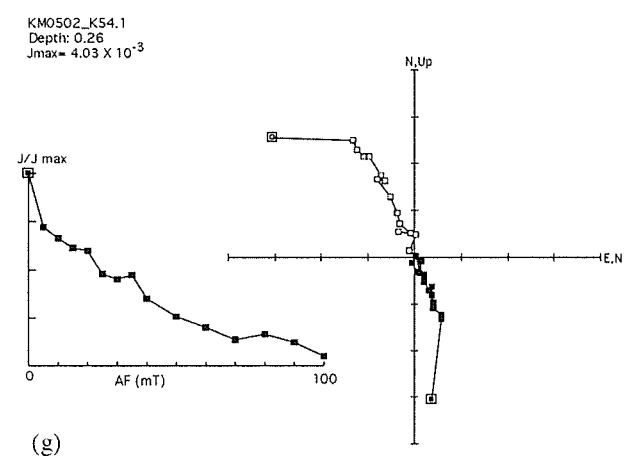
KM0502_K54.1
Depth: 0.26
Jmax= 4.03 X 10-3
J/J max
0
AF (mT)
100
N,Up
E,N

(g)

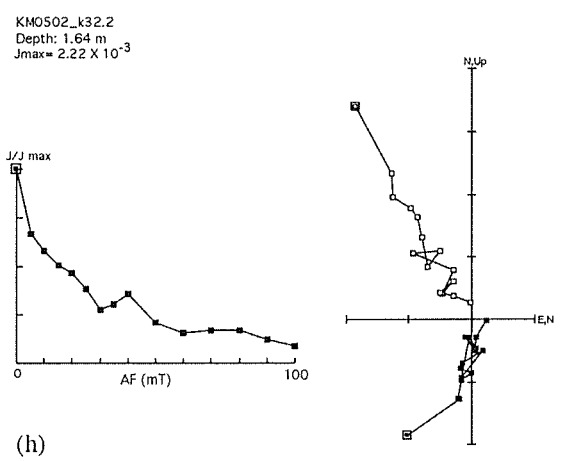
KM0502_k32.2
Depth: 1.64 m
Jmax= 2.22 X 10-3
J/J max
0
AF (mT)
100
N,Up
E,N

(h)

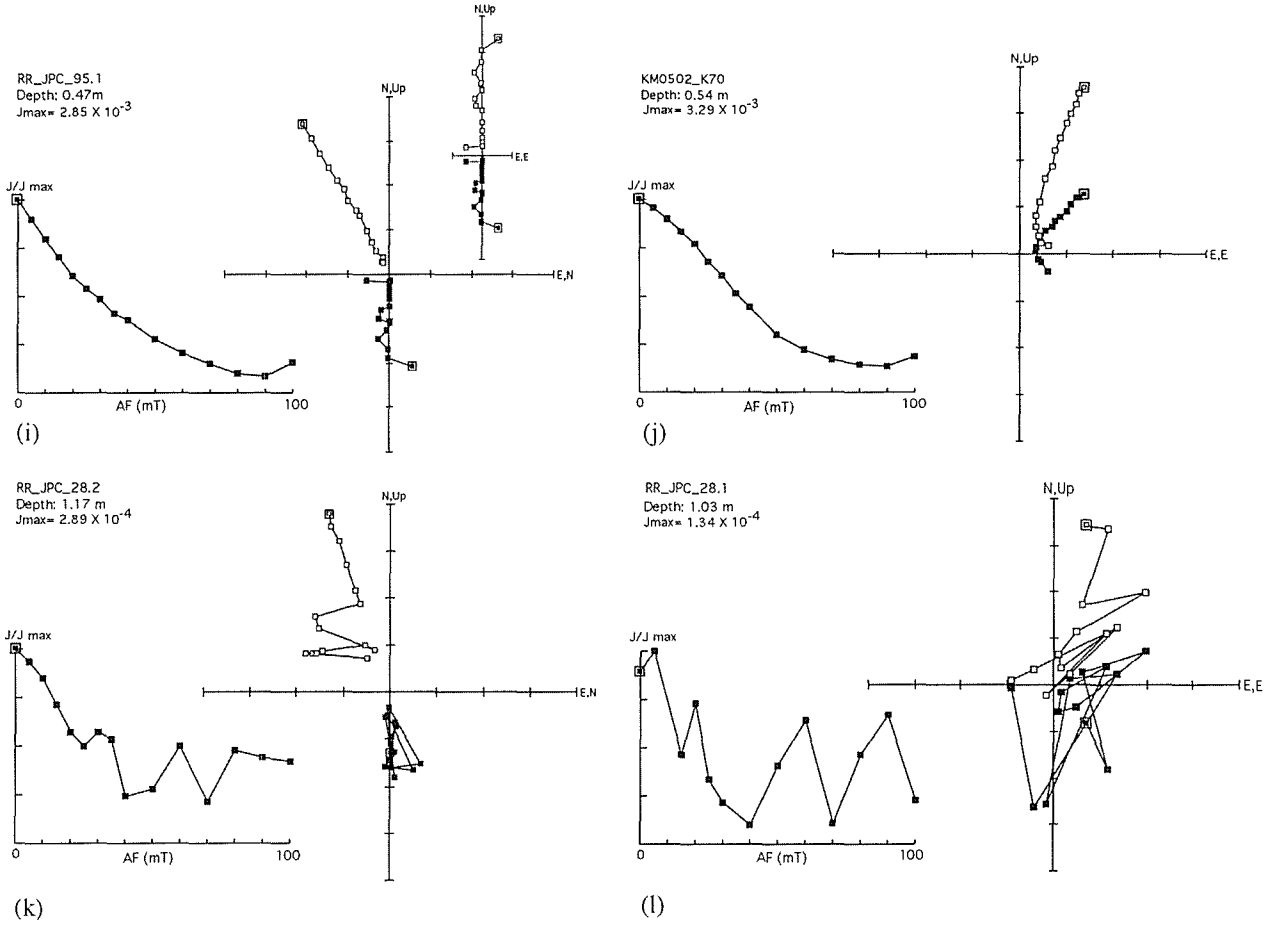

Figure 3.1: Two-dimensional plots of intensity vs. demagnetisation level (left) and 3-D orthogonal component projections (right) from various samples to illustrate the demagnetisation behaviour categories (refer to text): single component behaviour (a-c); persistent VRM (d-f); weak VRM (g-i); Gyroremanent magnetisation (j) and incomplete demagnetisation (k, l). Depth of measurement is noted for each diagram; Maximum intensity Jmax (usually = NRM) is in units of A/m.

3.2 Declination

Since samples were not azimuthally oriented when collected, it was necessary to adjust measurements of declination to represent the true paleofield. Unfortunately, the surface of most cores used in this study was soft and unconsolidated, and material was either disturbed during sampling or lost altogether. Thus declination cannot be obtained by adjusting the uppermost (and therefore most recent) sample to the present day declination.

Alternatively, if the record is sufficiently long for the time-averaged field to be representative of the GAD model, then directional data may be adjusted by some increment that shifts the Fisherian mean to $d = 0°$. Figure 3.2 shows all directional data for each kasten core along with the Fisherian means, represented three dimensionally in stereographic projections. Directions of the paleofield exhibit clustering about the Fisherian mean value in all cores. Assuming the clustering to represent a 'random wander' about the mean enables true declination to be obtained through scaling all data to produce a zero mean declination. Greater scatter in JPC95 is associated with the longer record (4.5 m ~ 49 ka; see section 3.4) obtained for this core, in which the tighter cluster comprises predominantly measurements in the upper 2 m. Relatively high variability is also evident in paleodirections for JPC28 (1.98 m), which, based on the (limited) available tephrochronology, represents ~ 33 k.y. Sedimentation rates on this part of the Chatham Rise (JPC28) are thus lower than those in JPC95. The fact that means for these cores lie outside of the clusters may suggest that means for the shorter records are unlikely to represent the GAD. Considering this, and that the interval of time sufficient to average out secular variation is contentious, declinations in this study are rotated to a zero mean for comparative purposes, but presented as relative only, thus avoiding speculative assumptions relating to secular variation averaging.

The only core for which the surface remained intact and relatively undisturbed is JPC28. Inclination calculated from PCA at 0 m in this core ($I = -66°$) matches the value expected at this locality today according to the International Geomagnetic Reference Field. Thus for JPC28 only, values of declination may also be fixed so that the surface value equals that of today given by the IGRF (~ 23°). This independent method of adjusting the declination record provides a useful comparison to the method using Fisherian means, which relies on the

inherent assumption that records are sufficiently long for the time-averaged field measurements to represent that of the GAD. Good agreement between corrected declinations obtained from both of the above methods lends support to their validity, and implies that the ~ 33 k.y. represented in core JPC28 is sufficiently long for the mean direction to approximate that of a GAD ($d = 0°$).

Yet another method involves comparing trends in the declination and inclination record with those obtained from other studies, and rotating the declination for each core. This proved a difficult task for cores from the Waipaoa Basin, since they lack chronology and records from the Southern Hemisphere are limited.

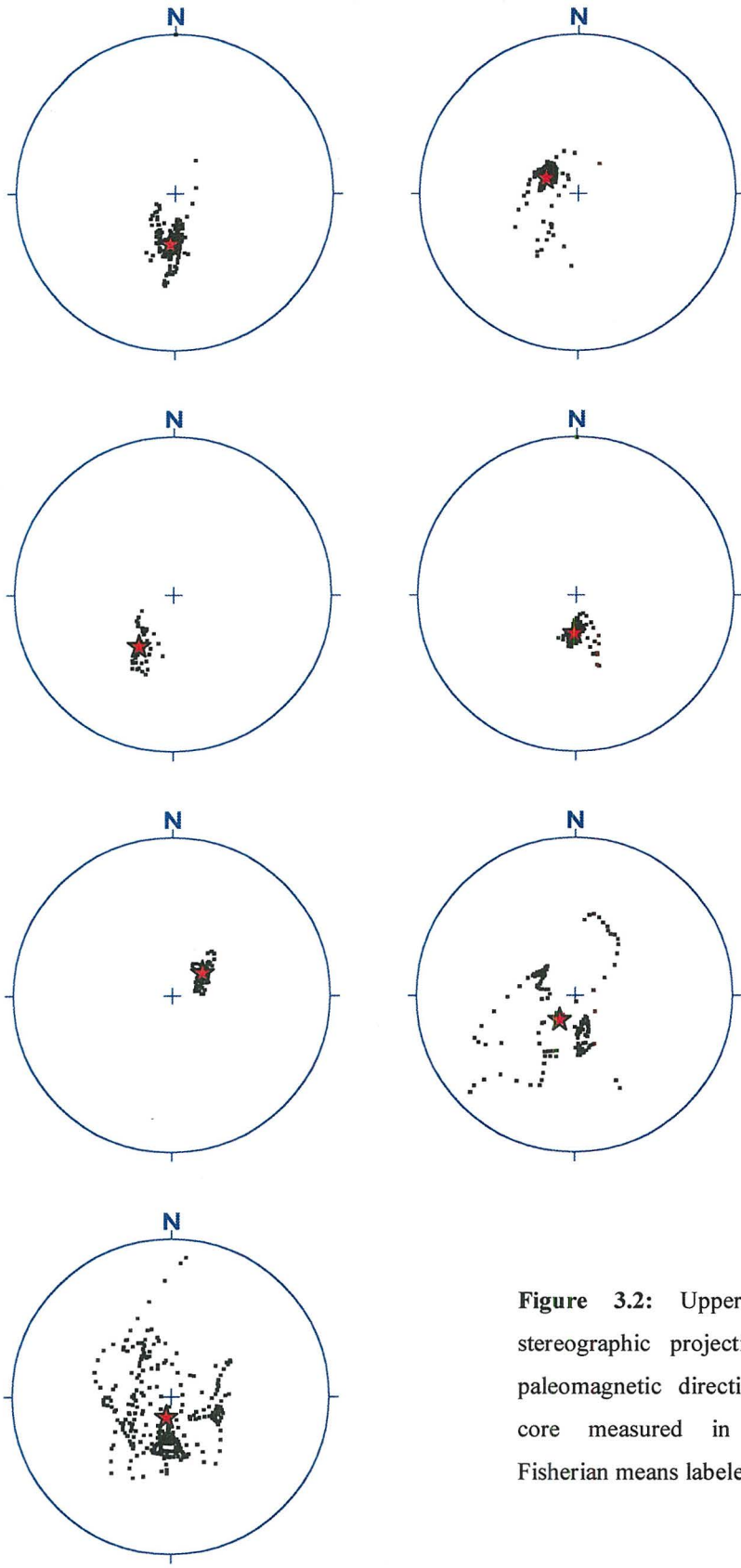

Figure 3.2: Upper hemisphere stereographic projections showing paleomagnetic directions for each core measured in this study. Fisherian means labeled as red stars.

3.3 Down-core measurements of magnetic parameters

Core K32

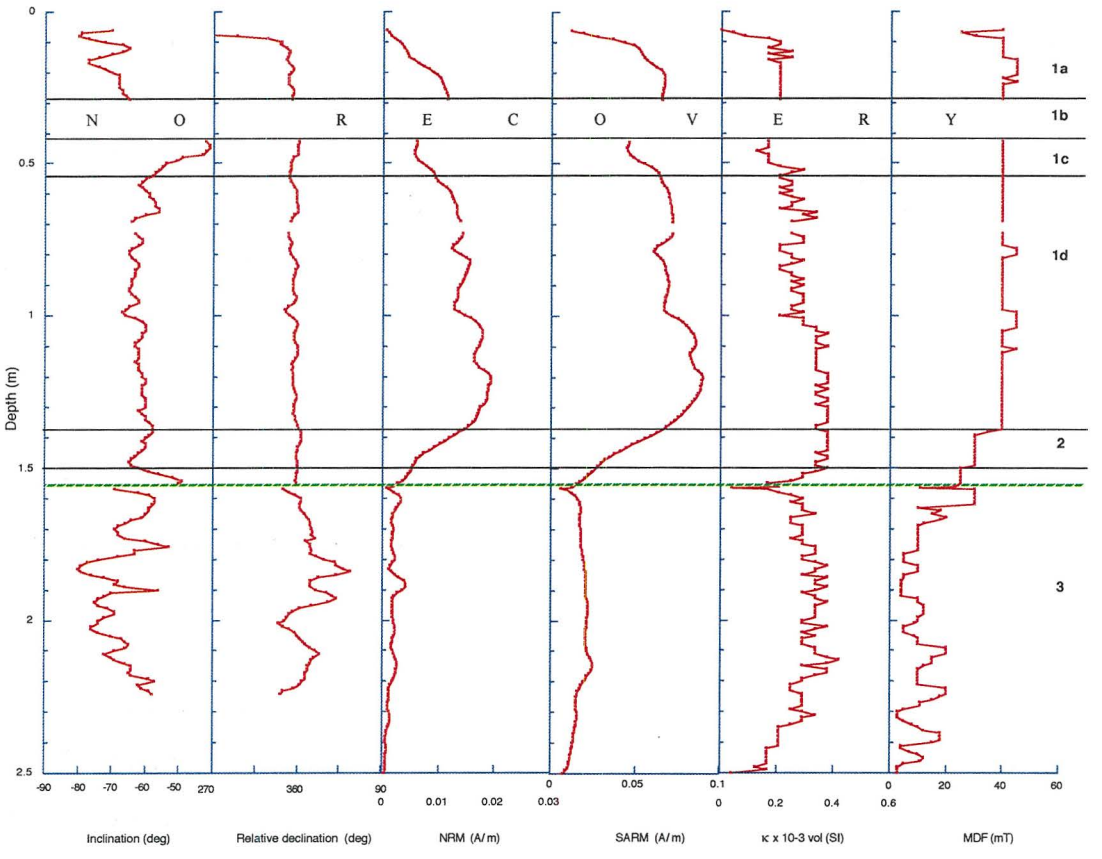

Figure 3.3: Down-core log of magnetic properties for core K32. Divisions (based on magnetic behaviour) are labelled on the right hand side; black lines mark division boundaries. Broken green line marks core section boundary (1.56 m).

The upper 6 cm of core K32 was unfortunately not recovered. Inclination varies between -41° and -80° about a mean value of -63°, becoming more variable in division 3. Intensities of NRM and sARM exhibit a punctuated down-core increase in division 1 and remain relatively low over division 3, the transition occurring in division 2. Magnetic susceptibility (κ) is concentrated between 0.2 and 0.4 $x10^{-3}$ SI units, exhibiting two step-wise increases in division 1 (around ~ 0.5 m and ~ 1.0 m); and a step-wise decline in division 3 below ~ 2.24 m towards the core base. Intensities of NRM and sARM, κ and MDF all exhibit a decline at the section boundary (1.56 m). Division 1 is characterised by higher MDF, which varies about a mean of 39 mT, compared to a mean of 13 mT in division 3, in which MDF is also more

variable. The transition from high and consistent to low and variable MDF occurs over division 2.

Division 1a (0.06 – 0.29 m):

Sediment in the top 0.16 m of this core was poorly consolidated, with material lost from the upper 2 cm and lower 1 cm due to core expansion. Inclination varies between –65° and -80° about a mean of -72°. Intensity of NRM steadily increases in the upper 29 cm of core from 6.72 $x10^{-4}$ to 1.15 $x10^{-2}$ A/m. A rise in κ also occurs from 0 to 0.2 $x10^{-3}$ SI in the upper 5 cm. High frequency fluctuations about 0.2 $x10^{-3}$ SI persist down to 0.16 m, below which it settles at this level. MDF varies about a mean of 40 mT.

Division 1b (0.3 – 0.42 m):

No material was recovered over this interval. Orthogonal component plots covering the gap exhibit progressively shallower angles of inclination, which does not return to angles observed above until 0.54 m.

Division 1c (0.43 – 0.54 m):

Inclination below the break in recovery is 23° shallower than that measured above, reaching a minimum of -41° at 0.46 m, below which inclination steepens again to approach the mean value for the interval below. Intensity at 0.43 m measures 5.99 $x10^{-3}$ A/m (lower than that measured above); increasing to 9.28 $x10^{-3}$ A/m by 0.54 m. Greater variability in κ is evident below the break; whilst MDF is stable, reaching 40 mT.

Division 1d (0.55 – 1.37 m):

Intensity continues to increase irregularly to a maximum value of 1.94 $x10^{-2}$ A/m at a depth of 1.22 m, below which it decreases by several orders of magnitude to a minimum at the boundary between the two core sections at 1.5 m. Inclination varies about a mean of - 61°. Changes in κ generally parallel those of NRM, with high frequency, low amplitude fluctuations about a mean of 0.25 $x10^{-3}$ SI from 0.54 –1 m, and 0.34 $x10^{-3}$ SI from 1-1.37 m. MDF barely deviates from the mean (40 mT) for this division.

Division 2 (1.38 m – 1.5 m):

Inclination and declination continue to vary as in division 1d. Intensity of NRM and sARM exhibit a progressive decline towards predominantly low values relative to

division 1, whilst κ shows no change. Division 3 marks a transition from high and stable MDF (division 1) to lower and more variable MDF (division 3).

Division 3 (1.5 m – 2.5 m):

Inclination fluctuates with higher amplitude than in the above division, and shallows by 16° within 5 cm of the section boundary (1.56 m), below which declination is also more variable. Paleofield directions could not be determined below 2.24 m owing to poorly defined magnetisation components. Excluding the section boundary, κ is relatively stable with a mean of 0.31 $x10^{-3}$ SI down to 2.24 m. Below 1.5 m MDF exhibits greater variability relative to division 1, fluctuating between 3 and 20 mT about a mean of 2 mT (considerably lower than the division 1 mean). The section boundary is marked by a decline in intensity, κ, and MDF. Directional measurements 5 cm either side of the join are disregarded owing to observed core expansion at section ends. Levels of NRM, sARM, κ and MDF decline from ~2.24 m with proximity to the core base.

Core K47

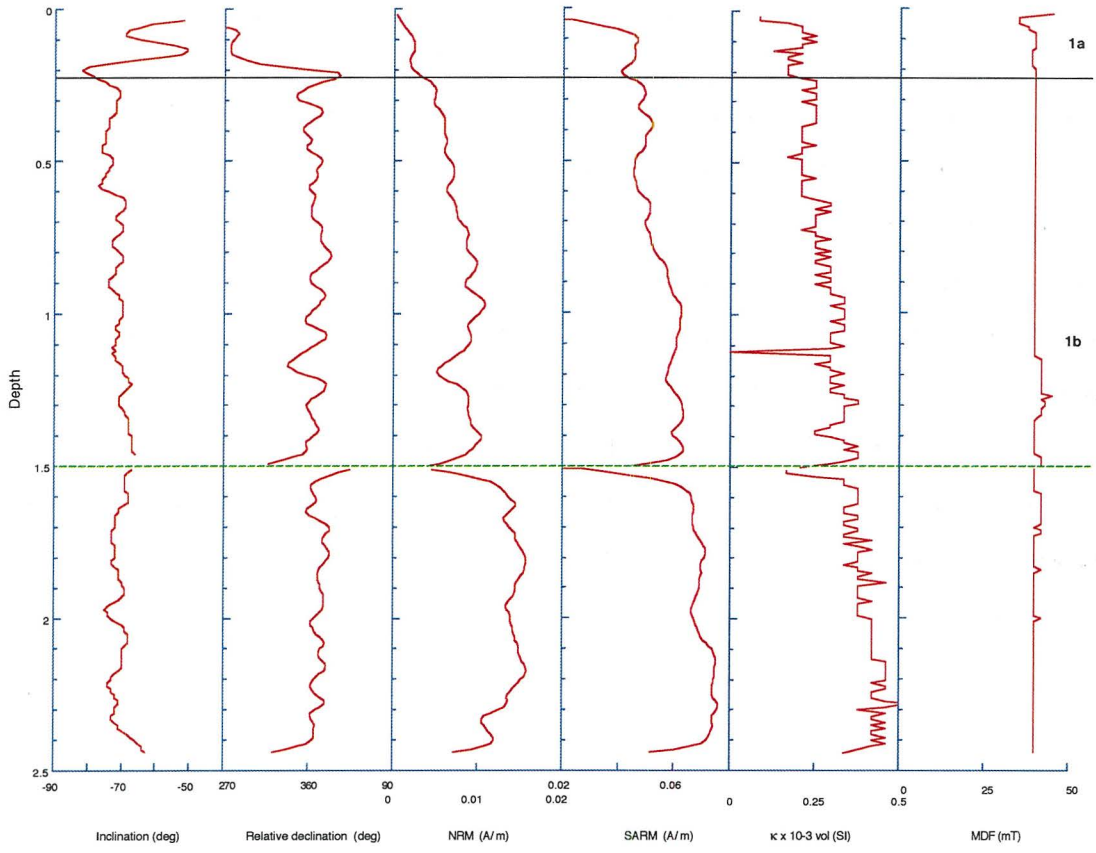

Figure 3.4: Down-core log of magnetic properties for core K47. Divisions (based on magnetic behaviour) are labelled on the right hand side; black lines mark division boundaries. The broken green line indicates the position of the core section boundary (at 1.5 m).

Of all cores used in this study, K47 provides one of the most complete and continuous records of magnetic field orientation; PCA was possible between 0.04 m and the core base (2.44 m). Inclination oscillates between -51° and -82°, about an overall mean of -72° (excluding the top, base and section boundary). At 0.05 m inclination is similar to that of today's field; though above this orientations were difficult to pick using PCA. Intensity of NRM, sARM and κ exhibit an overall trend of steady increase down-core. This trend is disrupted by a drop in intensity at the core section boundary (1.5 m). Intensities and κ also decline at the core base. Below the variability in the upper 0.2 m, MDF consistently measures 40-45 mT.

Division 1a (0 – 0.23 m):

Relatively high amplitude variations in inclination and declination between 0 and 0.23 m may be related to observed poor consolidation and/or acquisition of remanence from the core barrel, completely overprinting the NRM over this interval. The top of the core section is characterised by lower values of NRM than for the rest of the core, with NRM, sARM and κ increasing in the upper 0.1 m.

Division 1b (0.24 m – 2.44 m):

After an initial 8° shallowing of inclination down-core, values fluctuate about a mean of -72°. Both inclination and declination fluctuate with generally higher frequencies and lower amplitude than observed in the upper 0.2 m. NRM increases by an order of magnitude over the upper 1 m of core and sARM and κ parallel this trend; κ gradually increasing from 0.17 $x10^{-3}$ to 0.34 $x10^{-3}$ SI units. Intensities (NRM & sARM) and κ decrease from ~1 to ~1.2 m, below which all three parameters continue to rise. A spike in κ values at 1.12 m is not paralleled in other parameters. Below this, κ values vary between 0.29 $x10^{-3}$ and 0.38 $x10^{-3}$ SI units down to the core section boundary (1.5 m). Disturbance at the section boundary (1.5 m) is evident in all parameters, and measurements within 5 cm of this break are disregarded. Below the section boundary all parameters return to levels up to or exceeding those above. Between 1.56 m and 2.4 m, NRM has a mean value 0.014 A/m, attaining its maximum level of 1.58 $x10^{-2}$ A/m at both 1.82 m and 2.18 m. Maximum $\kappa = 0.5 \times 10^{-3}$, attained at 2.28 m. A stable MDF of 40-45 mT persists from 0.24 m down to the core base. Intensities and κ decline in the lower 5 cm; and shifts in inclination (~10°) and declination (~40°) are considered unreliable.

Core K54

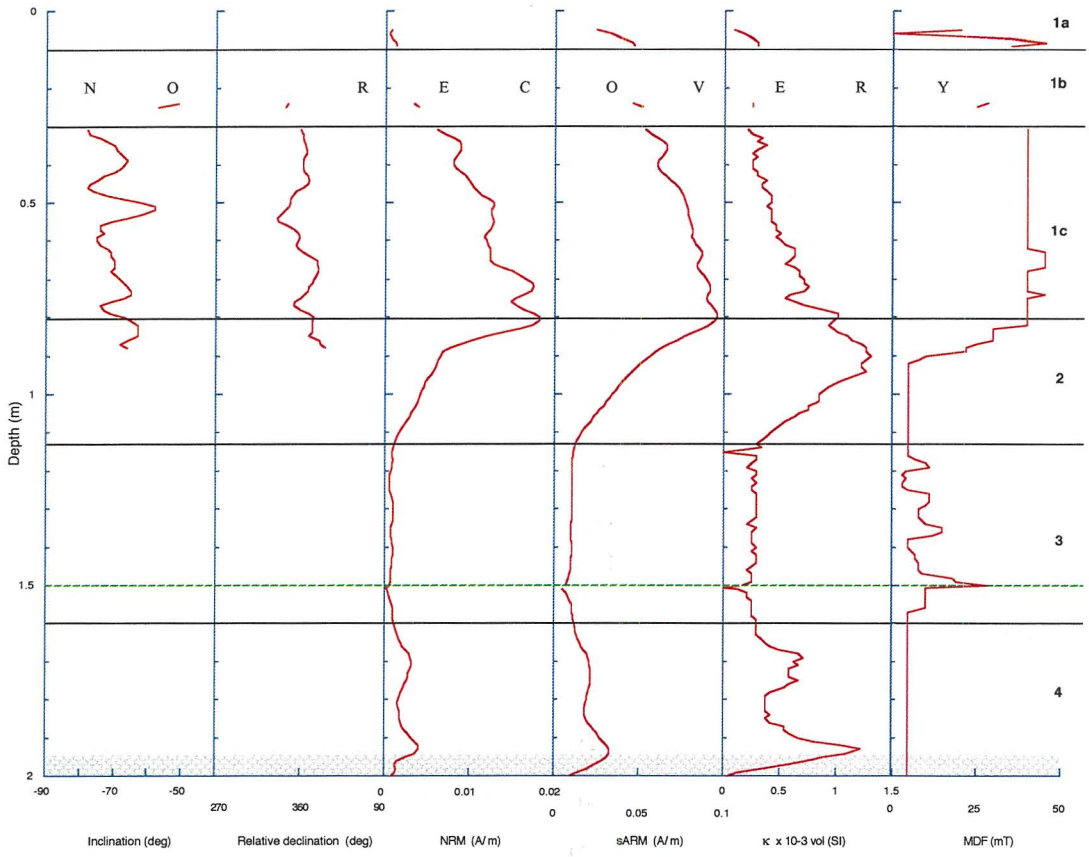

Figure 3.5: Down-core log of magnetic properties for core K54. Divisions (based on magnetic behaviour) are labelled on the right hand side; black lines mark division boundaries. The broken green line indicates the position of the core section boundary (at 1.5 m).

Although a total length of 201.5 cm of core was collected from this site, PCA could not be performed below a depth of 0.88 m, due to poor sample response to AF demagnetisation. There was no recovery over the intervals 0-4 cm, 10-23 cm and 26-30 cm. Tephra was observed from 1.95 m to the core base. Inclination ranges overall between -51° and -80° with no apparent cyclicity to the oscillations about a mean value of -70°. For the portion of core in which paleodirections were most accurately determined, MDF measures ~ 40 mT.

Division 1a (0.05 – 0.09 m):

Levels of NRM and κ and MDF are relatively low: κ rising to 0.29 $x10^{-3}$ SI and NRM to 1.29 $x10^{-3}$ A/m by 0.09 m. as intensity and κ increase, MDF increases

abruptly from 0 to 45 mT. Components of NRM were insufficiently defined to extract reliable paleodirections from PCA.

Division 1b (0.1 – 0.3m):

Material was only recovered between 24 and 25 cm. Relatively shallow inclination over this 2 cm suggests disturbance and casts doubt on the reliability of paleodirection. Levels of NRM, sARM and κ are intermediate between those of divisions 1a and 1c.

Division 1c: (0.31 –0.8 m):

Directional parameters show cyclicity, inclination varying between –58° and -78° about a mean of -69° (0.31-0.88 m). Determination of paleomagnetic direction is possible for this interval owing to relatively high NRM, sARM and κ. These parameters increase in parallel, gradually and unevenly, whilst MDF consistently reaches at least 40 mT.

Division 2 (0.81 –1.13 m):

After reaching a maximum of 1.82 $x10^{-2}$ A/m at 0.81 m, NRM intensity declines to 7.66 $x10^{-3}$ A/m by 0.88 m, below which PCA is not possible. Intensity of sARM parallels this trend, and MDF declines step-wise from 40 mT to 20 mT between 0.8 m and 0.92 m. Magnetic susceptibility (κ), in contrast, continues to increase to its maximum of 1.3 $x10^{-3}$ SI units at 0.9 m. (below maxima of NRM & sARM). Below this depth κ declines with NRM, sARM and MDF; NRM dropping by an order of magnitude to 8.9 $x10^{-4}$ A/m and κ to 0 by 1.13 m.

Division 3 (1.14 – 1.59 m):

Paleodirections of NRM were indeterminable over this division. Intensities of NRM & sARM remain relatively low, as does κ, whilst MDF varies between 3 and 15 mT (excluding the section boundary). At the section boundary (1.5 m) NRM drops to its minimum value of 5.1 $x10^{-4}$ A/m and κ to 0 SI, though MDF increases here.

Division 4: (1.6 m – 2.02 m):

Two peaks centred around 1.71 and 1.93 m are evident in NRM, sARM and κ (the lower of which are potentially related to the presence of tephra below 1.95 m); whilst MDF is consistently low (5 mT) throughout this basal division.

Core K70

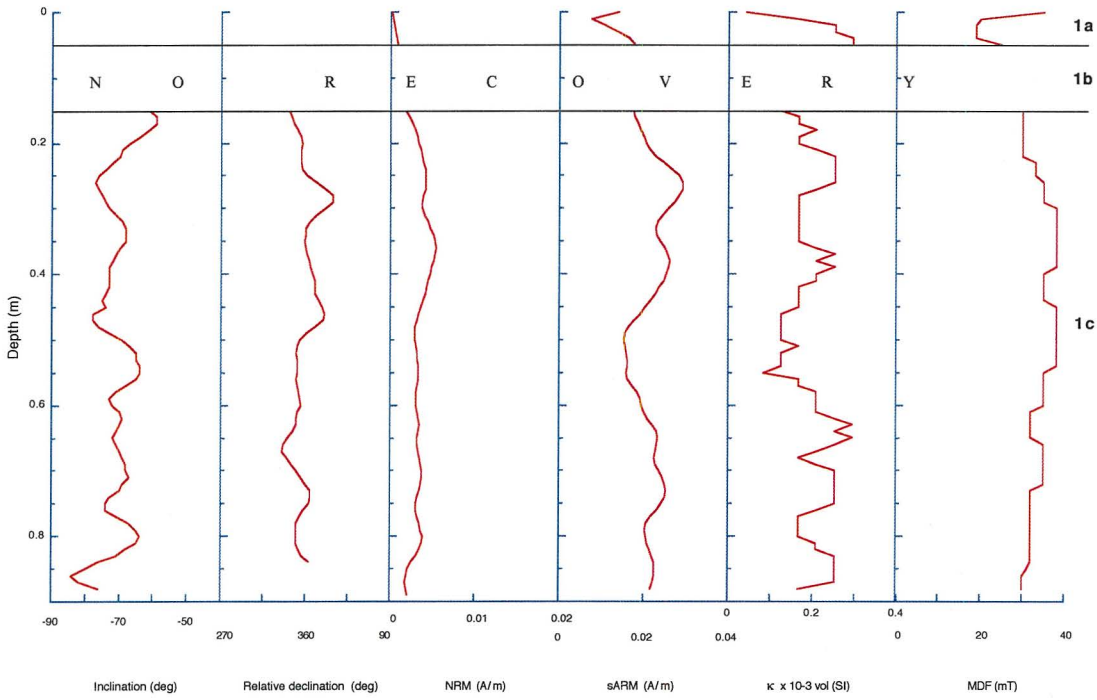

Figure 3.6: Down-core log of magnetic properties for core K70. Divisions (based on magnetic behaviour) are labelled on the right hand side; black lines mark division boundaries. Only a single U-channel was obtained for this core.

Division 1a (0 - 0.05 m):

Intensity of NRM begins to rise (to 8.0 $x10^{-4}$ A/m), as does sARM (below a decline in the upper 2 cm) and κ increases from 0 to its maximum of 0.29 $x10^{-3}$ SI units. These increases are concurrent with a decline in MDF from 35 mT to 20 mT, followed by a return to 25 mT. Determination of reliable paleodirection of NRM through PCA was not possible.

Division 1b (0.06-0.14 m): No recovery.

Division 1c (0.15 – 0.46 m):

Inclination ranges between -57° and -82°, oscillating about a mean value of -71°. A viscous component of NRM is evident in orthogonal plots, persisting to 15 mT throughout. Above this step, components demagnetise linearly toward the origin up to peak fields of 70-80 mT, above which increases in intensity are associated with a GRM (see section 3.1). Intensities of NRM and sARM are generally low throughout K70 in comparison with other cores. Below the break in recovery,

NRM climbs to a maximum of 5.36 $x10^{-3}$ A/m at 0.36 m, and sARM to a maximum of 0.029 A/m (at 0.26 m). Intensity of NRM fluctuates about a mean of 3.14 x 10^{-3} A/m, and κ about a mean of 0.19 $x10^{-3}$ SI units, ranging between 0.04 $x10^{-3}$ and 0.25 $x10^{-3}$ SI. An incremental increase in MDF from 30 mT to 38 mT occurs down to 0.3 m, below which MDF is more consistent, attaining maximum overall values between 0.3 m and 0.54 m (though not continuously).

Core K87

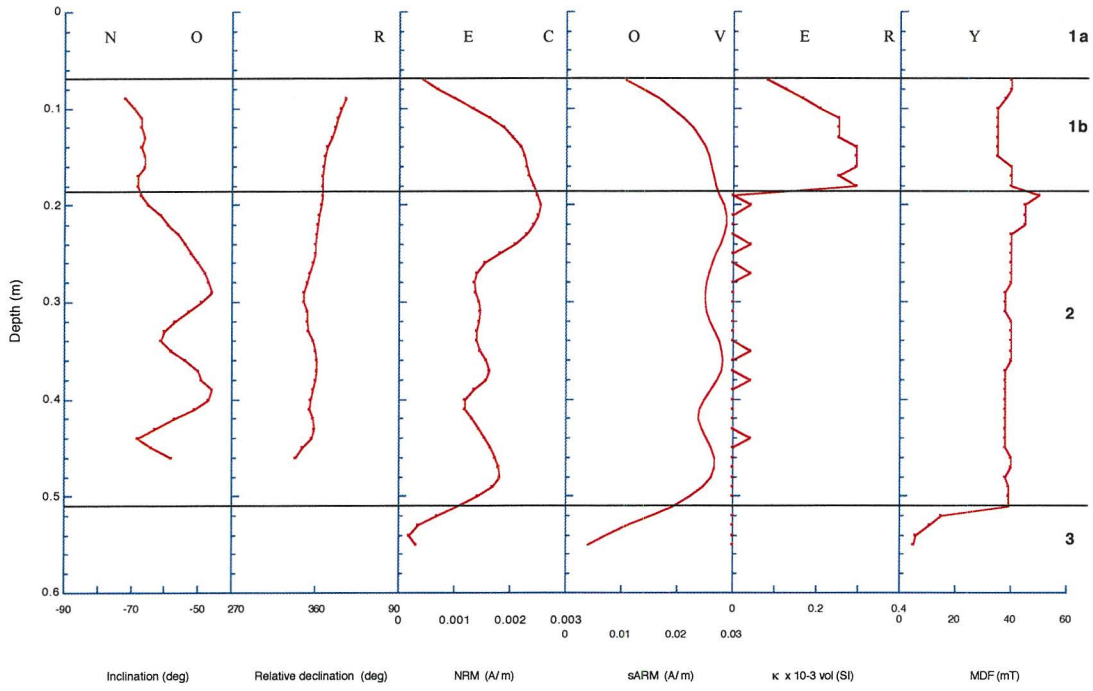

Figure 3.7: Down-core log of magnetic properties for core K87. Divisions (based on magnetic behaviour) are labelled on the right hand side; black lines mark division boundaries. Only a single U-channel was obtained for this core.

For the sections of core K87 above 0.09 m and below 0.47 m, PCA was unable to be performed. Hence the PSV record for this core is the shortest of the entire study. Inclination ranges between -46° and -86°. As with K70, intensity of NRM is relatively low for the entire length of core K87, with a peak of 2.54x10 $^{-3}$ A/m (at 0.2 m). Relatively high MDF was observed down to 0.5 m.

Division 1a (0 – 0.17 m):

No recovery

Division 1b (0.07 – 0.18 m):

Directions of NRM were obtained from PCA below 0.09 m. Angles of inclination appear anomalously steep (-72° to -68°) down to 0.18 m. Intensities of NRM and sARM increase in parallel throughout this division; the rate of increase lessening below ca. 0.15 m. Magnetic susceptibility (κ) also increases to a maximum of 0.29 $x10^{-3}$ SI at 0.14 m, which is approximately sustained down to 0.18 m, and MDF ranges between 35 an 40 mT.

Division 2 (0.19 – 0.5 m):

Inclination shallows by 18° from -69° at 0.19 m to -46° at 0.29 m, below which it fluctuates between -52° and -69°. Declination varies by 28° throughout division 2. Intensity of NRM continues to increase to its maximum value of 2.41 $x10^{-3}$ A/m (at 0.22 m), where sARM also attains its maximum value of 0.028 A/m. Below 0.22 m NRM declines to 1.35 $x10^{-3}$ A/m (by 0.28 m) and then fluctuates between 1.18 $x10^{-3}$ A/m and 1.8 $x10^{-3}$ A/m about a mean of 1.46 $x10^{-3}$ A/m down to 0.5 m. A dramatic decline in κ between 0.18 and 0.19 m from 0.29 $x10^{-3}$ SI to zero occurs over just 1 cm between divisions 1 and 2. Relatively low values of κ (0 - 0.04 $x10^{-3}$ SI) persist below this to the core base. Maximum MDF of 50 mT was recorded at 0.19 m, returning below this to ~ 38-45 mT, which is sustained for the remainder of division 2. Despite moderate coercivity (inferred from MDF) directional measurements were not obtainable below 0.47 m.

Division 4 (0.51 m – 0.55 m):

Intensities of NRM and sARM continue their decline (initiated in division 2) towards the core base to minimum values of 1.99 $x10^{-4}$A/m and 0.004 A/m, respectively. Zero magnetic susceptibility (κ) was recorded below 0.45 m. A relatively dramatic decline (from 40 mT to 5 mT over 4 cm) in MDF occurs below 0.5 m.

Core JPC28

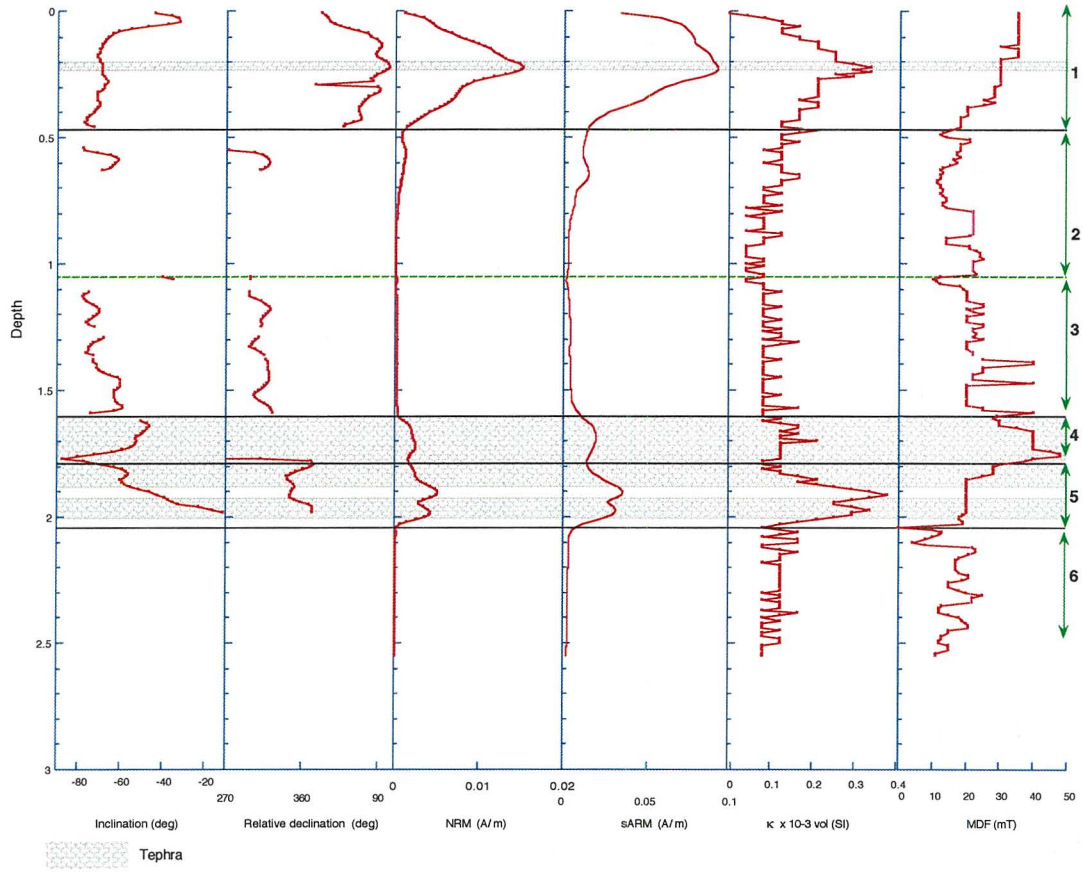

Figure 3.8: Down-core log of magnetic properties for core JPC28. Divisions (based on magnetic behaviour) are labelled on the right hand side of the diagram; black lines mark division boundaries. The broken green line indicates the position of the core section boundary (at 1.05 m).

Significant gaps in the magnetic measurements for this core are the result of large sections for which accurate paleodirections were indeterminable. Intensities of NRM and sARM are generally low except in the proximity of tephra horizons, which occur at 0.2-0.22 m, 1.6-1.87 m and 1.92-2.0 m. Magnetic susceptibility (κ) is concentrated between 0.04 and 0.17 $x10^{-3}$ SI units throughout the core, though values range from 0 to 0.38 $x10^{-3}$ SI units; the maximum being reached at 1.91 m within the lower tephra unit.

Division 1 (0.01 – 0.46 m):

The upper 1 cm of core was not recovered. Excluding measurements in the upper 10 cm, which was disturbed during sampling, angles of inclination are concentrated about a mean of –70.5° and declination about a mean of 78°, shifting westward by

~40°. Concentration dependent parameters NRM, sARM and κ increase from the surface to reach maximum values at 0.22 - 0.24 m of 1.51 $x10^{-2}$ A/m, 0.091 A/m and 0.34 $x10^{-3}$ SI, respectively (coincident with the upper tephra horizon); declining below this depth. No parallel increase in MDF is evident, though it declines gradually below the peaks in concentration dependent parameters, from 39 mT to 18 mT.

Division 2 (0.47 – 1.05 m):

Relatively low NRM, sARM and κ are associated with poor definition of directional components of NRM. Paleodirection was thus only determined between 0.54 and 0.63 m, where all three parameters exhibit a slight increase. All three concentration dependent parameters exhibit a progressive step-wise decrease over this division, though high frequency variations with amplitude of ca. 0.04 $x10^{-3}$ SI persist throughout the κ record. Coercivity-proxy MDF is generally lower than in division 1 but variable between 10 and 25 mT.

Division 3 (1.06 – 1.6 m):

Inclination determined immediately below the section boundary (1.05 m) is anomalously shallow and is thus disregarded. Below 1.1 m, however, inclination (where determinable) wavers about a mean of –72.5°. Concentration-dependent parameters are relatively low over this division, though means are slightly higher than values in lower division 2. Mean NRM = 2.49 $x10^{-4}$ A/m, mean κ = 0.11 $x10^{-3}$ SI. Direction of NRM was determinable with the exception of a few intervals. Variation in MDF is comparable to that of division 2 (above).

Division 4 (1.61 m – 1.79 m):

An increase in intensity values at 1.6 m is concurrent with a step in inclination angle from –74° at 1.59 m to -50° at 1.61 m. This depth coincides with observation of tephra that extends between 1.6 m and 1.87 m and resumes between 1.92 and 2 m. Inclination steepens from -59° (at 1.61 m) to -87° (at 1.77 m), below which it shallows to -69°. Declination was not determinable over this division. A slight increase in mean κ is also apparent from 0.11 $x10^{-3}$ SI above 1.6 m to 0.17 $x10^{-3}$ SI (1.6 m to 1.79 m). This is coeval with an increase in MDF (at 1.6 m), which attains its maximum of 48 mT at 1.76 m. Intensity of NRM decreases to at 1.77 m 1.62 $x10^{-3}$ A/m. Below this depth demagnetisation vs. intensity plots become increasingly

concave-up as MDF decreases towards values characteristic of the lower tephra (~ 20 mT).

Division 5 (1.8 – 2.04 m):

Inclination shallows from -63° to -11°. Another tephra horizon between 1.92 m and 2 m is approximately coeval with spikes in concentration dependent parameters NRM, sARM and κ at ~ 1.92 m, which are more pronounced than those associated with the upper tephra. Maximum κ of 0.38 $x10^{-3}$ SI occurs at 1.91 m. Despite heightened intensity and susceptibility, MDF (in contrast to the increase observed within the upper tephra) is relatively low (18-20 mT). This is reflected in increasingly concave-up demagnetisation vs. intensity plots, implying comparatively low coercivity and soft behaviour characterising the lower tephra unit. Inclination is only discernable down to 1.99 m. Below the lower tephra, NRM intensity approaches zero, as κ also declines to 0.13 $x10^{-3}$ SI by 2.04 m. From 2.05 (div. 5) to 2.05 m (div. 6) MDF drops from 19 mT to 0 mT.

Division 6 (2.05 m – 2.55 m):

Below the lower tephra horizon, demagnetisation behaviour further deteriorates as NRM (and sARM) intensities diminish to levels insufficient for PCA to yield reliable paleodirections of NRM. Intensity of NRM varies between 7.0 $x10^{-5}$ and 6.7 $x10^{-4}$ A/m, κ between 0.08 and 0.16 $x10^{-3}$ SI units, and MDF between 0 and 25 mT. More variable MDF with irregular increases is attributable to highly uneven and incomplete loss of intensity, with several spikes throughout demagnetisation. They are thus not considered to provide a reliable proxy for coercivity here.

Core JPC95

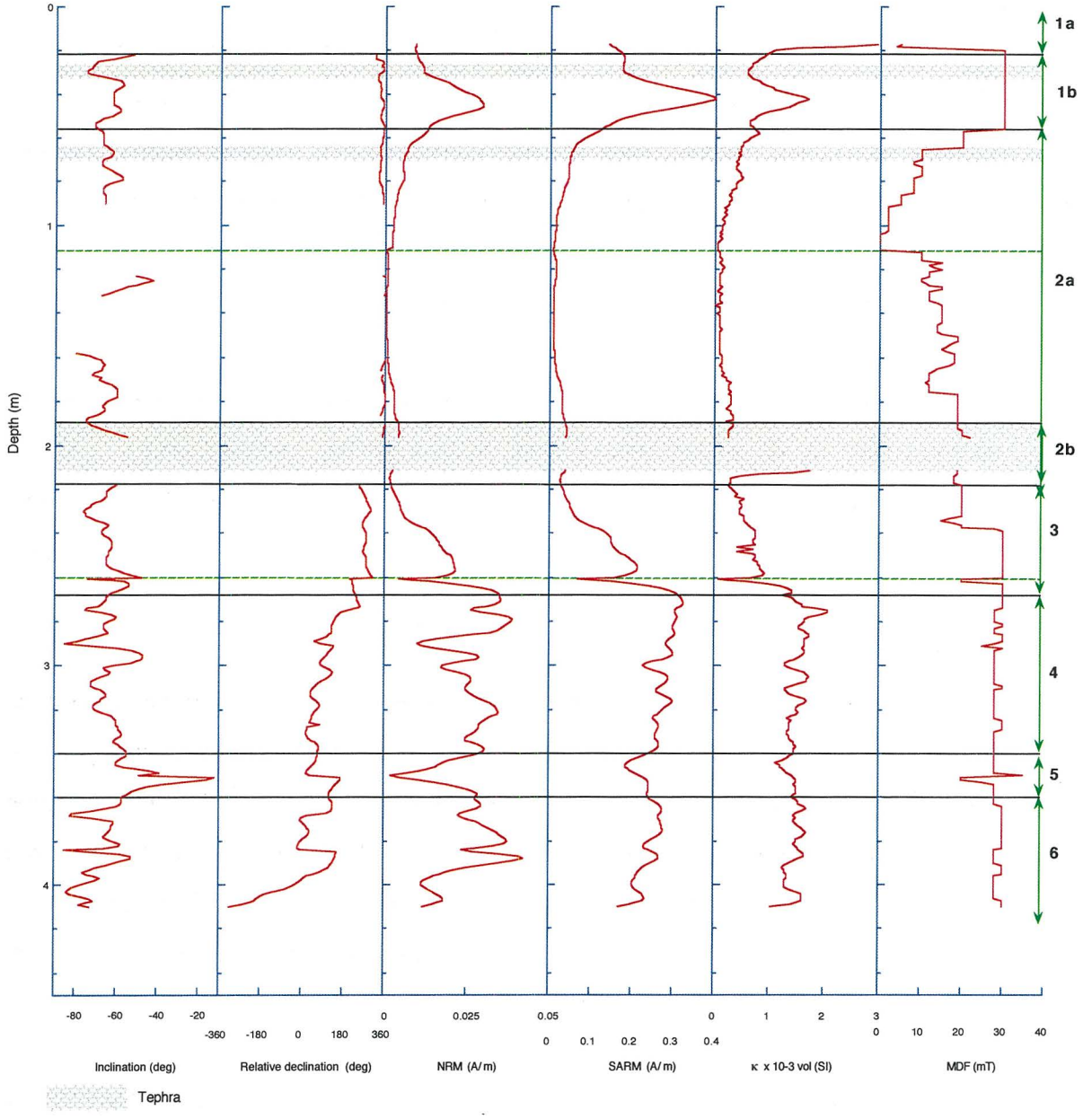

Figure 3.9: Down-core log of magnetic properties for core JPC95. Divisions (based on magnetic behaviour) are labelled on the right hand side of the diagram; black lines mark division boundaries. The broken green lines indicate the position of core section boundaries (at 1.1 m & 2.6 m).

The upper 16 cm of this core was not recovered. Declination and inclination could also not be discerned over the following intervals: 0.9-1.23 m, 1.33-1.57 m and 1.99-2.17 m. Inclination oscillates about a mean value of -64°, between a maximum of -12° and minimum of -85°. The

overall down-core drift in magnetic declination may indicate rotation of the core barrel during penetration; thus little confidence is placed in the relative paleo-declination curve. Tephra horizons were observed from 0.27-0.31 m, 0.64-0.68 m and 1.91-2.09 m. Magnetic Susceptibility (κ) reaches higher values in JPC 95 than in all other cores, reaching a maximum value of 3.23 $x10^{-3}$ SI units at 0.16 m. Concentration dependent parameters exhibit similar overall trends. Though no significant perturbation is evident at the upper section boundary (where levels approach minima), a decline in intensity by one order of magnitude, and of κ by 0.6 $x10^{-3}$ SI units occur at the lower section boundary (2.6 m).

Division 1 (0.16 – 0.21 m):

Observation of material in the upper 16 cm that was possibly tephra could explain the high κ, starting at its maximum value of 3.23 $x10^{-3}$ SI units at 0.17 m and declining rapidly to 0.92 $x10^{-3}$ SI units by 0.21 m. At this depth, NRM intensity measures 9.25 $x10^{-4}$ A/m. In contrast to MDF, κ increases from 5 to 30 mT over 3 cm.

Division 1b (0.22 – 0.55 m):

Inclination and relative declination were obtained from 0.22 m down to 0.9 m, varying about means of –64° and 1.5°, respectively. Concentration-dependent parameters NRM, sARM and κ exhibit parallel behaviour over this interval. All three rise towards a peak: NRM reaching its maximum of 2.95 $x10^{-2}$ A/m at 0.46 m and κ 1.68 $x10^{-3}$ SI at 0.42 m (following a brief decline above the rise). These parameters then decline concurrently toward minimum values. Coercivity is relatively high, MDF measuring 30 mT down to 0.56 m.

Division 2a (0.56 m – 1.9 m):

Isolation of the ChRM component of NRM becomes increasingly difficult below 0.56 m. The step-wise decline in MDF towards the section boundary (1.1 m; where MDF = 0 mT) reflects increased scatter in orthogonal component plots, and paleodirections that are less constrained than those above. Minima in NRM, sARM and κ occur between 1.1 m and 1.6 m, where loss of NRM with AF demagnetisation is uneven and concave-up. NRM intensity reaches a minimum of 7.74 $x10^{-4}$ A/m at 1.16 m, at which depth κ measures 0.1 $x10^{-3}$ SI. However, κ reaches its minimum value of 0.04 $x10^{-3}$ SI at 1.4 m. Below the upper section boundary (1.1 m), MDF varies between 10 and 22 mT. Determination of reliable paleodirections of NRM

(from PCA) was only possible over parts of this division, which throughout is affected by a high degree of scatter, and VRM proximate to the section boundary.

Division 2b: (1.91m – 2.18 m):

Tephric material between 1.97 m and 2.1 m was not recovered. Intensities of NRM and sARM below the break in recovery resume at levels comparable to those above it. (NRM = 2.4 $x10^{-3}$ A/m), as does MDF. Below the break in recovery κ resumes at a higher level of 1.7 $x10^{-3}$ SI and drops to 0.3 $x10^{-3}$ SI over 1 cm, which coincides with the base of the tephra unit. No paleodirection was determined over most of this interval.

Division 3: (2.19 m –2.7 m):

Inclination varies about a mean of -65° and relative declination about -92°. This division is characterised by a gradual rise in concentration-dependent parameters NRM, sARM and κ. Intensity increases by an order of magnitude and κ by 1.2 $x10^{-3}$ SI units to 1.5 $x10^{-3}$ SI. An abrupt increase in MDF from 19 to 30 mT occurs at ~2.4 m. Perturbation in all parameters is evident at the section boundary (2.6 m). Though inclination was determinable from 2.18 m, reliable paleodirections were only obtained below 2.35 m (NRM = 8.4 $x10^{-3}$ A/m and κ = 0.6 $x10^{-3}$ SI) where a transition occurs from soft, uneven and incomplete demagnetisation behaviour to harder, 'type 2 and type 1' behaviour (see section 3.1). Demagnetisation vs. intensity plots are smoother and more convex-up below 2.35 m, with generally complete decay of intensity to the origin.

Division 4: (2.7 m – 3.4 m):

Mean inclination = -62°: not significantly different to that of division 4. Inclination over both of these divisions (from 2.19 to 3.4 m) varies about an overall mean of -64°. The rise in concentration-dependent parameters to 2.7 m is underlain by fluctuations about moderate levels, of relatively high frequency (and amplitude in the case of NRM). MDF consistently attains levels of ~ 30 mT.

Division 5: (3.4 m – 3.6 m):

Intensity of NRM declines suddenly approaching zero at 3.5 m. This drop is paralleled by a less pronounced decrease in the sARM and κ records between 3.4 and 3.5 m, a marked shallowing of inclination values and an eastward step in relative declination. Levels of MDF are relatively stable and high to 3.5 m, where two

anomalous spikes occur – one an increase, the other a decrease. Between 3.5 and 3.6 m values of all parameters recover to approximate those above this excursion.

Division 6: (3.61 m – 4.1 m):

Mean inclination is slightly more negative below 3.6 m with a mean of -68° but varies widely between -53° and -85°. The magnitude and proximity to the core base of the westward drift in relative declination (in the basal 25 cm of core) casts doubt on its reliability. The basal 10 cm of the declination record are therefore excluded from further interpretation. Levels of, and variability in NRM, sARM, κ and MDF approximate those above the 3.5 m perturbation (division 5). Excluding values within 10 cm of both perturbations (at 2.6 m and 3.5 m), the mean inclination below 2.7 m = -65°, mean NRM = 2.7 $x10^{-2}$ A/m, mean κ = 1.7 $x10^{-3}$ SI units and mean MDF = 28 mT.

3.4 Establishing an independent time scale

Identification of several tephra horizons in cores JPC28 and JPC95 and sedimentation rates derived from ^{210}Pb analyses in cores K47, K54 provide a limited chronostratigraphic framework for these cores, which facilitates comparison between records of paleosecular variation (PSV) and relative paleointensity (RPI) derived from them.

The offshore dispersal of late Quaternary air fall material from the four major volcanic centres in the North Island has been enhanced by strong winds and proximity to the Pacific Ocean, as well as voluminous rhyolitic eruptions (Pillans & Wright, 1992). The Bay of Plenty contains deposits of five deglacial and Holocene ashes as well as four glacial ashes (Carter et al., 1995).

Using ferromagnesian mineralogy, Kohn & Glasby (1978) identified in core H214 (Fig. 1.16) the Rerewhakaaitu Ash, Waiohau Ash, Rotomo Ash and Whakatane Ash (later re-interpreted by Sikes et al. (2000) as being Mamaku Ash through Radiocarbon dating of benthic foraminifera). Kohn & Glasby (1978) used the burial depth of identified tephras to estimate late Pleistocene and Holocene sedimentation rates at site H214. Sikes et al. (2000) used tephra horizons and radiocarbon ages from foraminifera to place additional constraints on the chronology for this site. Core JPC95 (4 km south of site H214) contains both the Mamaku Ash (8.2 $\pm$ 20 cal. ka) and Oruanui Formation (26.5 $\pm$ 230 cal. ka; Wilson, 2001), which provide constraints on sedimentation rates within this core (Fig. 3.10). In order to convert depth to calendar years it is assumed that sedimentation rates between dated events are constant. Sedimentation rate below the oldest known date is assumed to be similar to that above the marker.

The Chatham Rise and Bounty Trough, to the east of the North Island are, in contrast to the east coast, devoid of deglacial and Holocene tephras. Owing to changes in the prevailing wind direction since the glaciation, only the largest of the glacial tephras (Oruanui Formation) is present (Sikes et al., 2000). It is thus not surprising that only one tephra is contained in core JPC28 (from the northern Chatham Rise) and that it is identified as the Oruanui Formation (Paul Shane, pers. comm.). This tephra bed constitutes the only dated marker within core

JPC28 upon which to base a chronology. The records from this core have been tentatively placed on a time scale derived using only this tephra, assuming sedimentation rate above the tephra to be constant, and that below to be identical. The age model derived for cores JPC28 and JPC95 using tephra beds is presented in Figure 3.10.

Core	Depth (cm)	Tephra Identification	Centre	Age (^{14}C) B.P.	Age cal. B.P.
JPC28	160--200	Oruanui Formation (Kawakawa tephra)	Taupo	22 590 ± 230	26 500 [a, c]
H214	77-78	Mamaku	Okataina	7 250 ± 20	8 200 [a]
	96-97	Rotoma	Okataina	8 530 ± 10	9 500 [b]
	153-159	Waiohau	Okataina	11 850 ± 60	13 800 [b]
	205-206	Rerewhakaaitu	Okataina	14 700 ± 110	17 700 [b]
JPC95	27-31	Mamaku	Okataina	7 250 ± 20	8 200 [a]
	64-68	To be determined			
	191-209	Oruanui Formation	Taupo	22 590 ± 230	26 500 [a, c]
K54	195-229	To be determined	Taupo		

Table 3.4: Ages of volcanic material identified in cores used in this study and from site H214 (Kohn & Glasby, 1978). Radiocarbon ages are from (Frogatt & Lowe, 1990). Converted calendar ages marked [a] are from the radiocarbon age calibration of Stuiver et al. (1999); ages marked [b] are from Lowes et al. (1999); ages marked [c] are from Wilson (2001).

Tephra observed in kasten core K54 from 1.95 m to the depth of the original core base at 2.3 m has been identified as originating from a Taupo source (Alan Palmer, pers. comm.). This constrains the age at the core base to be less than or equal to 3400 cal. years B.P. (age of the Waimahia ash). However, sedimentation rates from ^{210}Pb analyses in cores K47 and K54 of 0.86 cm/yr and 1.19 cm/yr, respectively (Steve Kuehl, pers. comm.), reveal that cores from the Waipaoa Basin are much younger than those from outside of the basin (JPC95 and JPC28) both of which contain the Oruanui Formation (26.5 ± 230 ka; Wilson, 2001). The ^{210}Pb sedimentation rate for core K54 indicates an age of ~ 164 ± 33 years (1842 AD) for the tephra at 1.95 m. Further analyses have yet to be undertaken to constrain the identity of this tephra horizon. Assuming the sedimentation rates to be accurate within ~20% potential error (Steve Kuehl, pers. comm.), the basal tephra in core K54 is preliminarily considered to be the

Tarawera Ash/Lapilli, ejected during the 1886 AD Tarawera Basalt eruptive episode (Nairn, 2002).

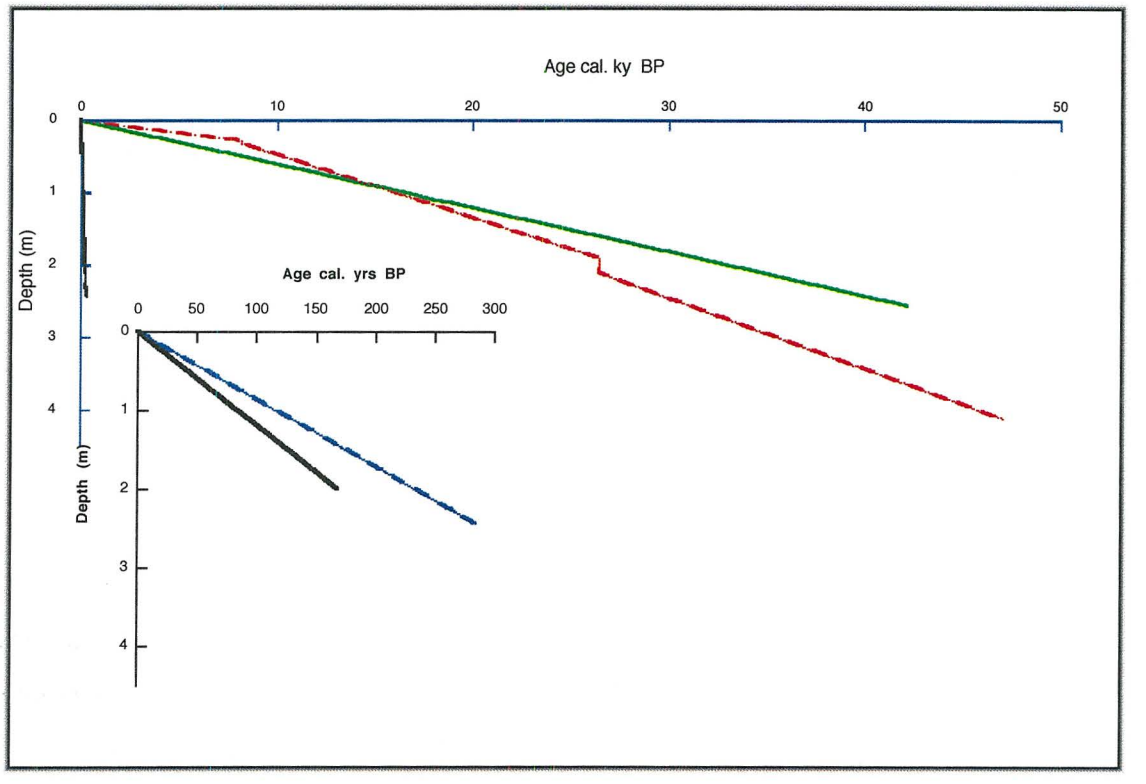

Figure 3.10: Age vs. depth plot for piston cores JPC28 (green line: based on identification of the Oruanui Formation only) and JPC95 (broken red line: based on identification of Oruanui Formation and Mamaku Ash horizons); and kasten cores K47 and K54 (black lines; based on preliminary sedimentation rates calculated using ^{210}Pb). Based upon this chronology, rate of sedimentation is greater in JPC95 (Bay of Plenty) than in JPC28 (north Chatham Rise), and kasten cores from the Waipaoa Basin exhibit sedimentation rates that exceed those in the piston cores by at least two orders of magnitude.

4. ROCK MAGNETISM

Remanences produced in different laboratory fields and the ratios between them may be profitably used in the rock magnetic characterization of sediment samples (Thompson & Oldfield, 1986). In this chapter, various techniques are applied to constrain magnetic granulometry, concentration and mineralogy for the core samples described in preceding chapters. The degree of variability in such properties determines the potential for derivation of high-fidelity relative paleointensity (RPI) records from these cores.

4.1 Rock magnetic criteria for paleointensity studies

For sedimentary records of relative paleointensity to be deemed reliable, it is imperative to separate geomagnetic field from environmental contributions to the signal. This is achieved through (i) normalising the NRM intensity (see 5.1) and (ii) ensuring magnetic homogeneity – an implicit assumption in relative paleointensity studies. King et al. (1983) defined magnetic uniformity with a set of criteria that were used to construct a selection process, by which to identify sediments (Table 4.1) that are magnetically homogenous. The rock magnetic criteria defined by King et al. (1983), and modified by Tauxe (1993), provide an empirical test of suitability for relative paleointensity studies. The degree to which cores in this study comply with the uniformity criteria is assessed throughout the course of this chapter through an extensive rock magnetic examination.

Rock Magnetic Criteria	TESTS
Mineralogy For mineralogy to be uniform natural remanence must be carried by stable magnetite (Fe_3O_4), or a mineral of similar composition.	- Reflected light microscopy and electron diffraction, or IRM and thermo-magnetic experiments. - Median Destructive Field (MDF) - Mineralogy dependent IRM parameters (B_{cr} and sIRM) and parametric ratios (S ratio, HIRM). - Bivariate scatter plots of magnetic parameters
Grain Size Grain size within the range of 1-15 μm (medium - coarse PSD to fine MD) is required for the DRM/sARM ratio to be unaffected by grain size variations (King et al., 1983).	- Hysteresis experiments of Day et al. (1977) or Lowrie-Fuller test indicate domain state. - MDF, B_{cr} - Ratios κARM/κ, sIRM/κ and sIRM/κARM give relative changes in particle size. - Variation in κARM/κ should not exceed a factor of ± 2.5 with respect to the mean (Meynadier et al., 1992).
Concentration Variations in magnetite content should not exceed 20-30 times the minimum concentration (King et al., 1983); or should not vary by more than an order of magnitude (Tauxe, 1993), since ARM is affected by particle interaction.	- Determination of range in κ values. - Comparison of sIRM values.

Table 4.1: Rock magnetic criteria and respective tests to establish uniformity of magnetic constituents, developed by King et al. (1983) and modified by Tauxe (1993).

4.2 Mineralogy

Saturation of IRM in core K47 occurred at fields of approximately 450 mT in both directions (Fig. 2.4). The coercivity of remanence B_{cr} ranges from 38.5 mT to 52.5 mT (Fig. 4.1), with a mean of 43.2 mT, and MDF for all cores generally lies between 25 and 40 mT (Fig. 3.3-g) with exceptions attributable to changes in magnetic granulometry - discussed in the subsequent section of this chapter. The above results are consistent with magnetite being the major carrier of NRM (Dunlop, 1972). The mean B_{cr} and sIRM indicate a lack of hematite, suggesting that NRM is predominantly a detrital remanence rather than a chemical remanence.

Parametric ratios reflect variations in the coercivity spectrum of the magnetic mineral assemblage and therefore the mineralogy. Without mineral separation techniques, (thermomagnetic analyses and X-ray diffraction), the common magnetic minerals can be distinguished using combinations of simple room temperature magnetic parameters, of which the S ratio is considered the most useful (Evans & Heller, 2003). The **S ratio** provides a measure of the proportion of saturation at the applied backfield. This constructed parameter is derived by normalising the remanence acquired in a backfield (BIRM) of 0.1T (or 0.3T) by the sIRM (Bloemendal, 1983):

$$S = IRM_{-0.1T\,(or\ -0.3T)} / sIRM \qquad [4.1]$$

Ferrimagnetic minerals generally approach saturation in backfields of ≤ 0.1 T (Thompson & Oldfield, 1986). $S_{-0.3}$ is utilized as a proxy for recognizing mineralogical changes, particularly the proportion of magnetite relative to hematite. Ratios approaching 1 indicate lower coercivity and a higher proportion of ferrimagnetic minerals (e.g. magnetite), whereas values closer to zero indicate higher coercivities and canted antiferrimagnetic mineralogy (e.g. Hematite; Bloemendal, 1983). In core K47, $S_{-0.3}$ varies between 0.84 and 0.99 about a mean of 0.96 (Fig. 4.1), indicative of a magnetic mineralogy dominated by (titano)magnetite, with little/no hematite. $S_{-0.1}$ exhibits a strong secondary response to variations in grain size, providing a convenient measure of the fraction of low coercivity, coarse grains (Bloemendal,

1983). $S_{-0.1}$ ranges between 0.61 and 0.78, with a mean of 0.72 (Fig. 4.1), reflecting the presence of fine magnetite.

Hard IRM (**HIRM)** compliments the S ratio and B_{cr} as a means of monitoring changes in magnetic mineralogy. HIRM (Fig. 4.1) provides a measure of the concentration of antiferrimagnetic minerals e.g. Hematite (or very fine grained magnetite) that have *higher* coercivity than the back field of –0.3 T (Robinson, 1986):

$$HIRM_{-0.3} = (sIRM + IRM_{-0.3}) / 2 \qquad [4.2]$$

where $IRM_{-0.3}$ is negative. Mean HIRM in K47 = 0.78 A/m, suggesting a lack of Hematite. The inversely related parameters S ratio and B_{cr} together summarize magnetic hardness in core K47; which is characteristic of ferrimagnetic mineralogy.

High ratios of sIRM/κ (> 100 kA/m) are indicative of pyrrhotite or hematite, since magnetisation per unit volume in antiferrimagnets is an order of magnitude lower than for ferrimagnetics such as (titano)magnetite, which is typified by low sIRM/κ ratios (< 4 kA/m; Peters & Thompson, 1998). In core K47 sIRM/κ fluctuates about a mean of 0.12 A/m (Fig. 4.1); implying preponderance of magnetite.

Graphical representation of combined room-temperature magnetic parameters is useful in assessing magnetic mineralogy. Peters & Thompson (1998) developed biplots using simple susceptibility and remanence ratios to qualitatively identify magnetic minerals present within samples. In combination, the biplots provide a means for distinguishing between pyrrhotite, greigite and (titano)magnetite. Data from core K47 lie within the fields defined for magnetite/titanomagnetite in both bivariate scatter plots (Fig. 4.2); thus complimenting sIRM, S ratios, HIRM and B_{cr}, and corroborating that magnetic mineralogy is relatively uniform and dominated by magnetite or titanomagnetite.

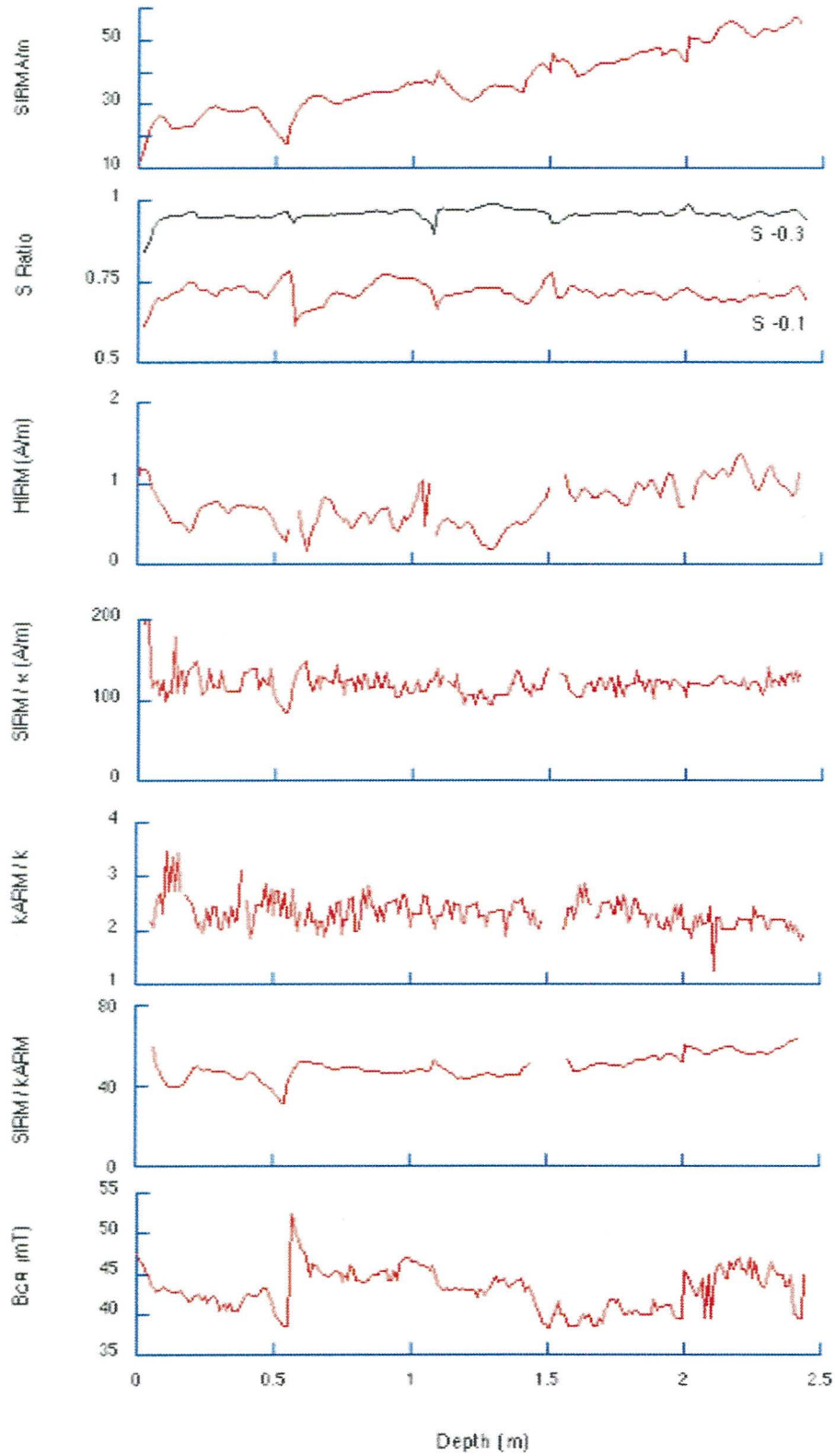

Figure 4.1: Rock magnetic stratigraphy for core K47 showing interparametric ratios: κARM/κ, κARM/sIRM (SI units); S ratio (dimensionless); sIRM/κ; sIRM/κARM (mT) and coercivity of remanence B_{cr} (mT) plotted against depth below sea floor.

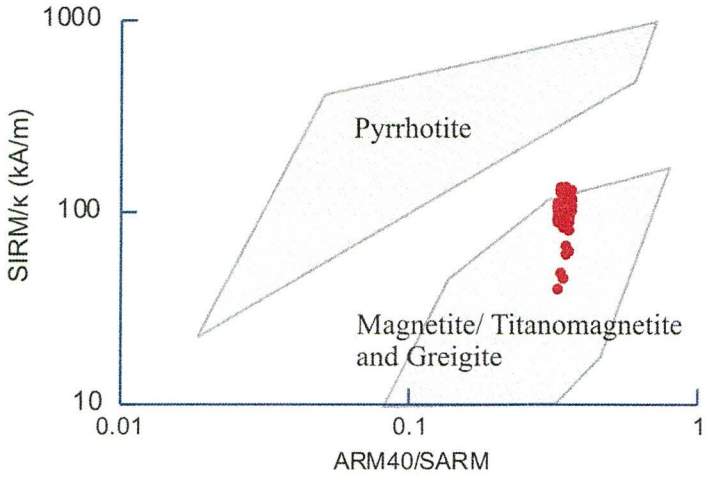

(a)

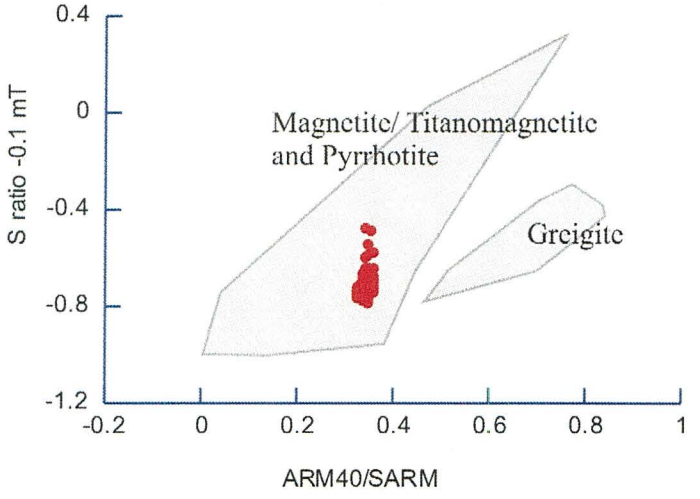

(b)

Figure 4.2: Interparametric ratios ARM 40 mT / SARM vs. (a) SIRM/κ and (b) $S_{-0.1}$ for K47 (red) illustrated on biplots used for the qualitative identification of magnetic minerals. Field boundaries taken from Peters & Thompson (1998).

4.3 Magnetic Granulometry

4.3.1 The modified Lowrie-Fuller test

Consistently high (~ 40 mT) MDF values (Fig. 3.4) in core K47 and lack of VRM indicate moderate coercivity, suggestive of magnetite grains in the SD-PSD state. The modified Lowrie Fuller test (Johnson et al., 1975) based on the relative stability of ARM and IRM, is useful in distinguishing whether very fine or coarse magnetic particles comprise the dominant remanence carriers. This test relies on the observation that stability of NRM against demagnetisation declines with increasing strength of the biasing field for SD particles, whilst the converse is true for MD grains (Lowrie & Fuller, 1971). Thus greater stability of a weak field remanence (ARM) than a remanence acquired in a strong field (IRM) during AF demagnetisation implies preponderance of SD grains in the sample. If IRM exhibits greater stability than ARM, however, magnetite is considered to be predominantly in the MD size range. Johnson et al. (1975) stressed that application of the test to grains of intermediate condition or to a spectrum of particle size may result in confusing overlap of IRM and ARM demagnetisation curves.

Normalised AF demagnetisation curves for K47 are presented in Figure 4.3 for a range of depths. Stability of ARM is consistently similar to and slightly greater than that of IRM, with MDFs centred on ca. 30 mT and 20 mT, respectively. However, overlap of demagnetisation curves is evident at all depths, which indicates either that particles are of intermediate (PSD) size (for which the test is not as discriminatory) or that a range exists.

Cisowski (1981) showed that the test is not valid for non-interacting SD grains and also proposed a test for the degree of interaction based on the point of intersection of IRM acquisition and demagnetisation curves on the normalised moment axis. The intersection point of IRM curves (Fig. 4.3) lies close to 50%, consistent with non-interacting, SD magnetite (Cisowski, 1981).

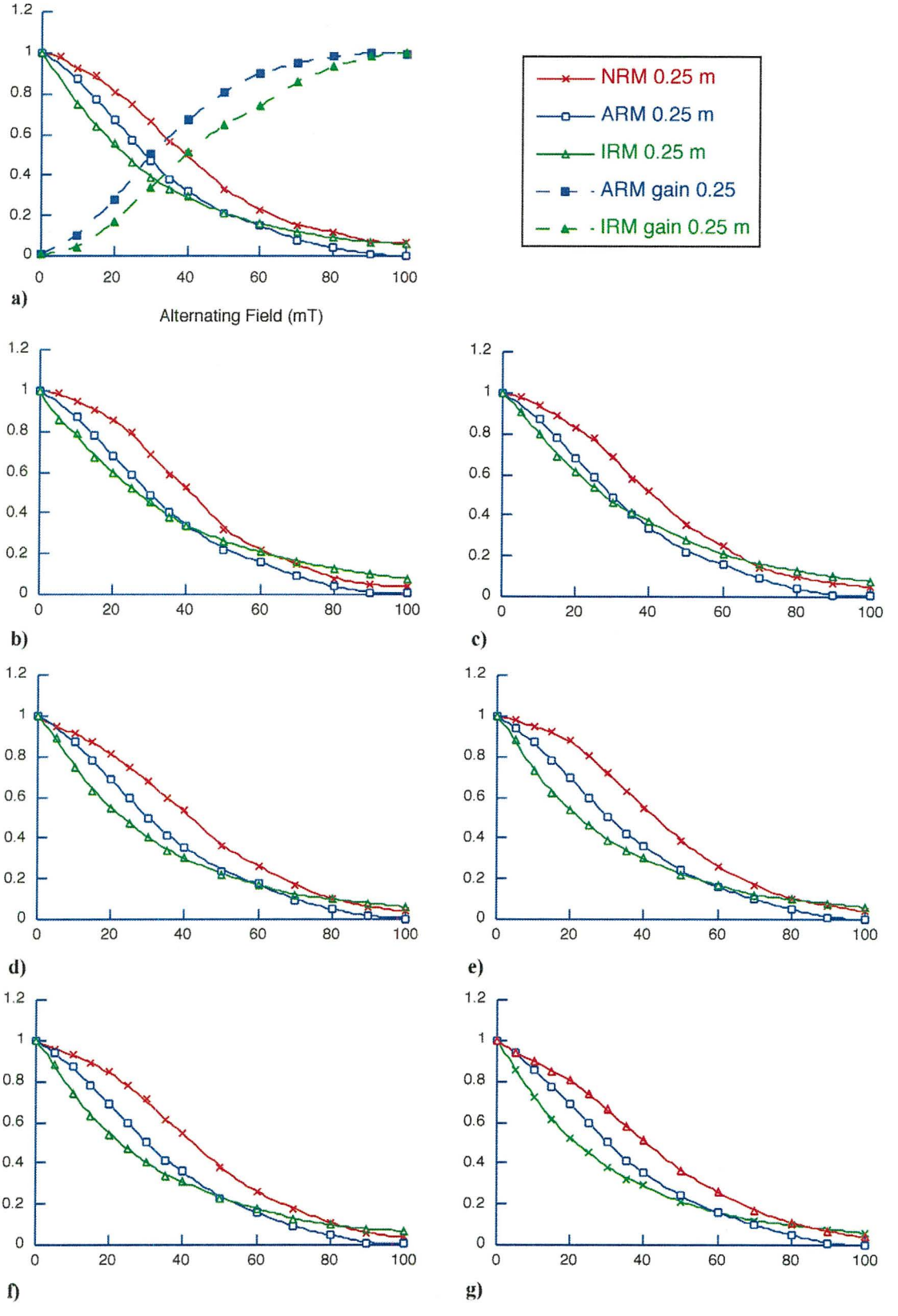

Figure 4.3: Comparison of AF demagnetisation curves for NRM (red crosses), ARM (blue open squares) and IRM (green open triangles) and remanence acquisition for ARM and IRM (closed symbols) in core K47 at depths of (a) 0.25 m, (b) 0.5 m, (c) 0.8m, (d) 1.2 m, (e) 1.6 m, (f) 2 m & (g) 2.4 m.

4.3.2 Models of grain size using induced remanence parameters

Assuming uniform mineralogy dominated by magnetite in core K47 (established in section 4.1), B_{cr} provides a sensitive indicator of relative grain size, varying from < 10 mT for MD grains and grains < 1μm to ~ 100 mT for small, elongate PSD or SD grains (Thompson & Oldfield, 1986). In core K47, remanence is completely erased by reverse fields of 40-60 mT (Figs. 2.4, 4.1), which is consistent with the relatively low coercivity of remanence that is characteristic of magnetite in the size range < 1-10 μm (Peters & Dekkers, 2003).

The granulometric dependences of IRM at a given backfield, and of sIRM (for particular values of κ) are illustrated in Figures 4.4 and 4.5, respectively (Thompson & Oldfield, 1986). However, since both models were developed using pure magnetite samples; their application to bulk mineralogies (e.g. sediments in core K47) may compromise their ability to predict accurately absolute magnetic grain size.

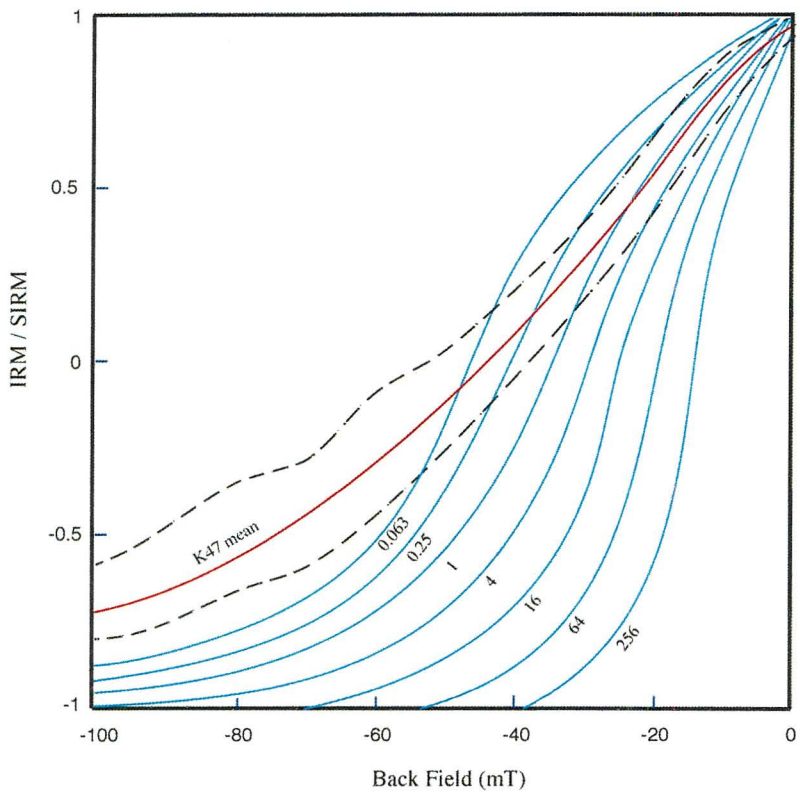

Figure 4.4: Variation of grain size with IRM at specific back-fields for sized magnetite (boundaries from Thompson & Oldfield, 1986). Red line marks mean values for K47; dotted lines define upper and lower data.

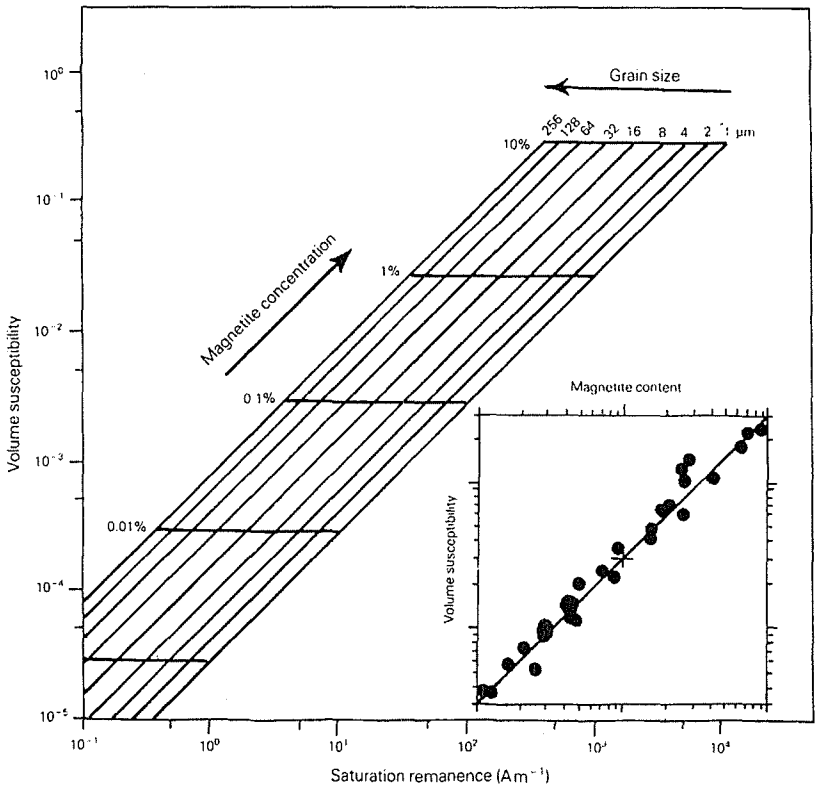

Figure 4.5: Bilogarithmic sIRM vs. susceptibility (κ) plot for pure magnetite, illustrating relationship of both parameters to magnetic grain size and concentration. Inset shows the relationship between κ and concentration that is commonly observed in natural samples. After Thompson & Oldfield (1986).

4.3.3 Grain size dependent parametric ratios

Dividing two concentration dependent parameters results in ratios that are (at least at first order) concentration independent. These ratios can thus be interpreted in terms of grain size trends or composition, provided that mineralogy is consistently dominated by magnetite (Peters & Dekkers, 2003). Selected interparametric ratios reputed to provide an indication of domain state of the magnetic assemblage include sIRM/κ, sIRM/κARM and κARM/κ (King et al., 1982; Peters & Dekkers, 2003).

The ratio of sIRM to κARM (Fig. 4.1) increases with magnetic grains size and is particularly useful for detecting grains slightly larger than SP (low sIRM/κARM; Thompson & Oldfield, 1986). This ratio only responds to remanence carrying magnetic material and thus has the major advantage of being unaffected by SP or paramagnetic material. However, it is less

sensitive and more difficult to interpret than κARM/κ and sIRM/κ (Opdyke & Channell, 1996).

Observed size dependence of the numerator for both sIRM/κ (Fig. 4.6) and κARM/κ (Fig. 4.7b) in magnetite, coupled with relative size independence of the denominator, results in higher ratios where smaller particles are abundant. The sIRM/κ ratio is more sensitive to changes in the proportion of large (>10 μm) grains; whilst κARM/κ, is more sensitive to fine SD grains (Bloemendal, 1983). However, grains < 0.1μm are characterised by similar ratios to those of very large magnetite, which can complicate interpretation grains (Peters & Dekkers, 2003). In core K47, sIRM/k varies between 0.08 and 0.18 kA/m about a mean of 0.12 kA/m. The lack of any overall down-core trend (Fig. 4.1) indicates little variation in magnetic grain size.

Of all magnetic parameters, sARM exhibits greatest grain size dependence in assemblages dominated by magnetite (Fig. 4.7a), following two separate power laws as an inverse function of grain diameter (that above and below 1 μm). The gradient is steepest for smaller grains (Evans & Heller, 2003). Magnetic susceptibility (κ) in contrast, is enhanced by superparamagnetic (SP) magnetite (d < 0.3 μm) and by large MD grains (d > 10 μm), super-imposed on a grain-size independent baseline (Dearing, 1999). Changes in the ARM/susceptibility ratio with depth thus provide an indication of relative changes in grain size within the magnetically stable (SD-MD) fraction (Fig. 4.7b; Peters & Dekkers, 2003). In core K47, κARM/κ varies at most by a factor of 1.8 with respect to the mean value of 2.3, exhibiting no apparent down-core trend (Fig. 4.1). This corroborates interpretation of the sIRM/k record, implying only minor variations in magnetic grain size.

The model in Figure 4.4 (Thompson & Oldfield, 1986), illustrates that core K47 contains both pseudo-single domain (PSD) and super-paramagnetic (SPM) magnetic grains (Fig. 4.3). In another model (Fig. 4.4) relating the proportion of magnetisation with increasing backfield to grain size for magnetite (Thompson & Oldfield, 1986), K47 data appears to contain a spectrum of magnetic grain sizes, including PSD and super-paramagnetic (< 0.05 μm) grains. However, this model was developed for characterization of pure magnetite samples; and thus may be of limited application to data from a bulk mineral assemblage (e.g. core K47).

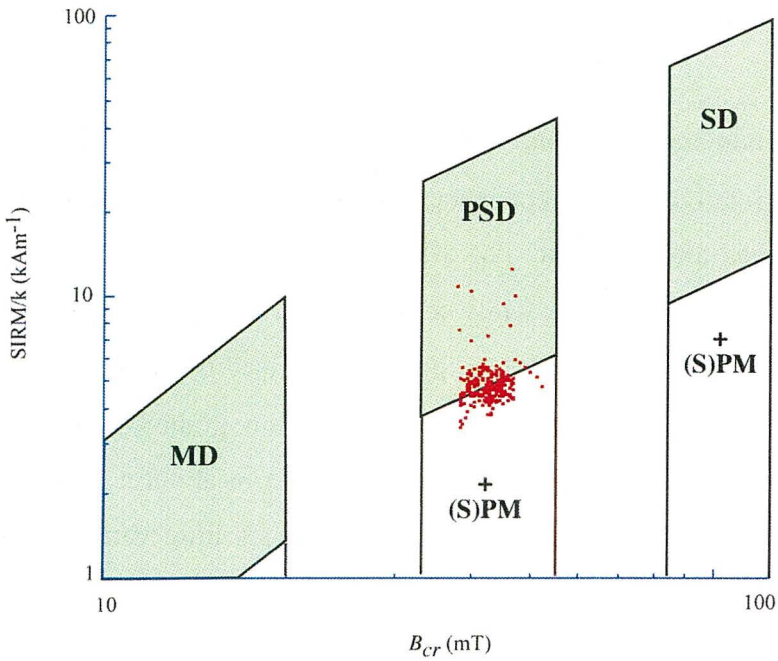

Figure 4.6: Dependence of coercivity of remanence B_{cr} on domain state for magnetite grains. MD = Multidomain; PSD = Pseudo-single domain; SD = Single domain; (S)PM = Super-paramagnetic. Data from K47 (red) plots in both PSD and (S)PM fields. Field boundaries taken from Thompson & Oldfield (1986).

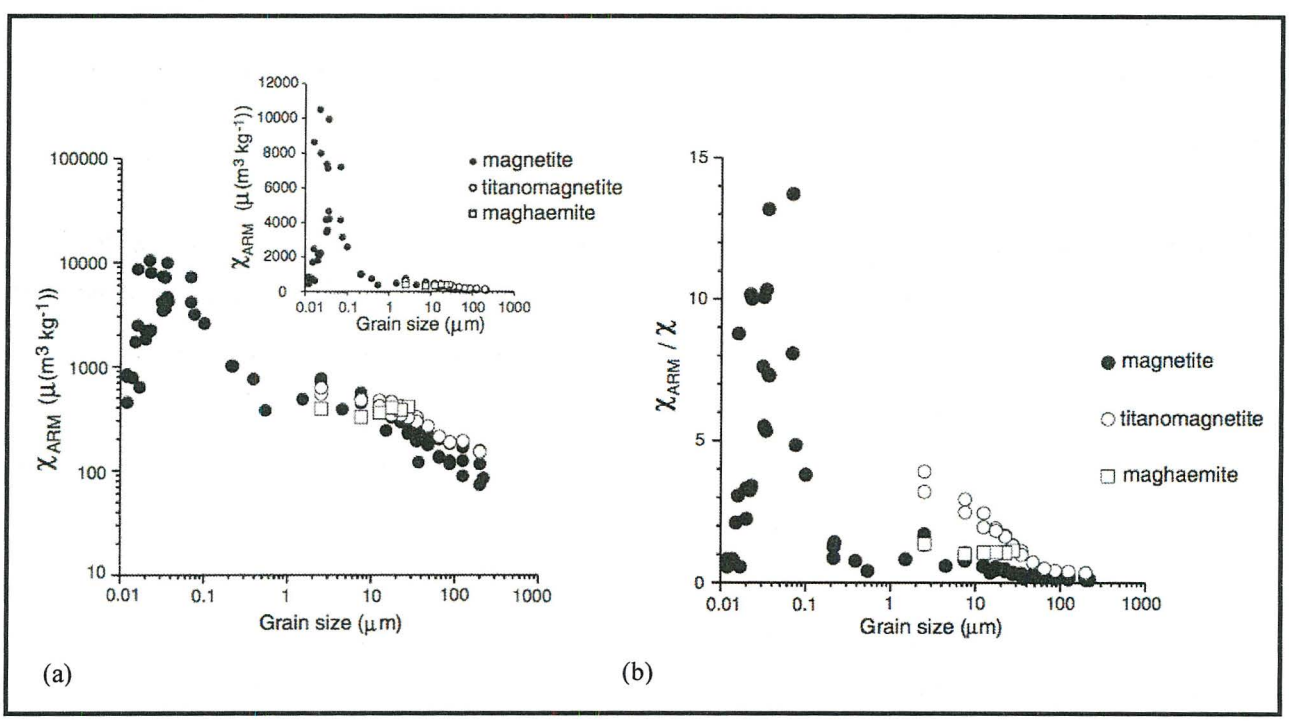

Figure 4.7: Variation of (a) mass-dependent anhysteretic susceptibility (χARM) and (b) the ratio χARM/χ, with particle size for magnetite, titanomagnetite and maghemite. Inset in (a) shows variation of χARM on a linear scale. After Peters & Dekkers (2003).

4.3.4 Granulometric constraints from κARM vs. κ model

Dankers (1978) measured rock magnetic parameters for carefully sized magnetite. Observing that ARM is enhanced in fine grains, whilst κ is enhanced in large grains, Banerjee et al. (1981) produced an empirical model relating specific values of anhysteretic susceptibility κARM (sARM normalised by the strength of the DC field) and κ, to specific grain sizes and concentrations of dispersed magnetite (Fig. 4.8). This phenomenological model may be utilized as a crude guide to relative variations for large numbers of samples (King et al. 1982). Slopes of greater magnitude reflect the bias of κARM toward fine-grained magnetite; conversely, shallower slopes reflect the bias of κ towards coarse-grained magnetite. Evans & Heller (2003) stressed that the resolving power of Banerjee plots is much greater for SD-PSD distributions than for samples dominated by MD assemblages.

Banerjee plots of κARM vs. κ (Fig. 4.8) for cores K47, K70 and K87 generally define a linear trend, representative of consistency in grain size (accompanied by variations in concentration, represented by distance from the origin).

Banerjee plots for cores K47, K70 and K87 are exhibit a single dominant mode of grain size. In core K47, this is relatively confined to the lower 1-5 μm field (Fig. 4.8b); and is centred about a mean of ~ 5 μm in cores K70 (Fig. 4.8d) and K87 (Fig. 4.8e). The magnitude of grain size variation in these cores is comparable to that of upper K54, ranging between ~ 1 and 10 μm. No obvious correlation between grain size and depth is apparent. Deviations from the modal grain size occur in the upper 5 cm of all cores.

Two distinct linear trends are apparent in cores K32 and K54, corresponding to different depth intervals (divisions 1 and 3 in Figs. 3.3 & 3.5). They represent a bi-modal grain size distribution, separated by a transitional zone (division 2). The steeper gradient for these cores represents relatively fine-grained magnetite (division 1), whilst the shallower gradient depicts coarser-grained magnetite characterising the lower part of the core (division 3). In core K32, the finer grains above 1.38 m plot within the 0.1-1 μm field. Coarsening from ~1 μm to ~5 μm occurs between 1.39 and 1.45 m, below which the coarser magnetic fraction ranges from 5 μm up to 25 μm. In core K54, magnetic grains ≤ 1 μm dominate above ~ 0.5 m, whereas

from 0.5 - 0.77 m data plot in the field corresponding to 1 - 5 μm. The greater transition from fine to coarser magnetic material occurs from 0.78 - 0.9 m, below which, magnetic grain size plots consistently close to the 20-25 μm field boundary.

Ratios from the upper 23 cm of core JPC28 indicate relatively fine grain size, < 1 μm, coarsening to ~ 10 μm between 0.23 and 0.46 m. Grain size ranges from ~ 5 to 25 μm between 0.47 and 1.6 m, and fines from 5 μm to 0.1 μm between 1.6 m and 1.85 m, coincident with the observation of normal grading in the upper tephra unit. The presence of coarser material from 1.85 – 2.02 m is consistent with the description of coarser tephra over this interval.

Depth dependence of the κARM/κ ratio is evident throughout core JPC95 (Fig. 4.8g; Fig. 4.9). Material is finer than 0.1 μm in the upper 0.54 m, below which it is centred at 5 μm to a depth of 2.34 m. The apparent coarseness from 2.1m to 2.15 m, in which grain size increases to above the 20-25 μm field, is likely to be due to the high κ associated with tephra (1.91-2.09 m). From 2.35 m to the base of the core (4.1 m) grain size varies from < 1 to 5 μm. In summary, application of the phenomenological model of King et al. (1982) to JPC95 data shows that grain size below 0.55 m is relatively restricted to between 1 and 5 μm. Outliers that deviate substantially from the main trends include the uppermost core interval (0.17 - 0.21 m) and measurements proximal to the core section boundary at 2.6 m.

Figure 4.8: Data from all cores are plotted on the modified phenomenological model of King et al. (1982), which relates anhysteretic susceptibility κA and κ with magnetic grain size and concentration. Where not specified concentration is < 0.25% magnetite.

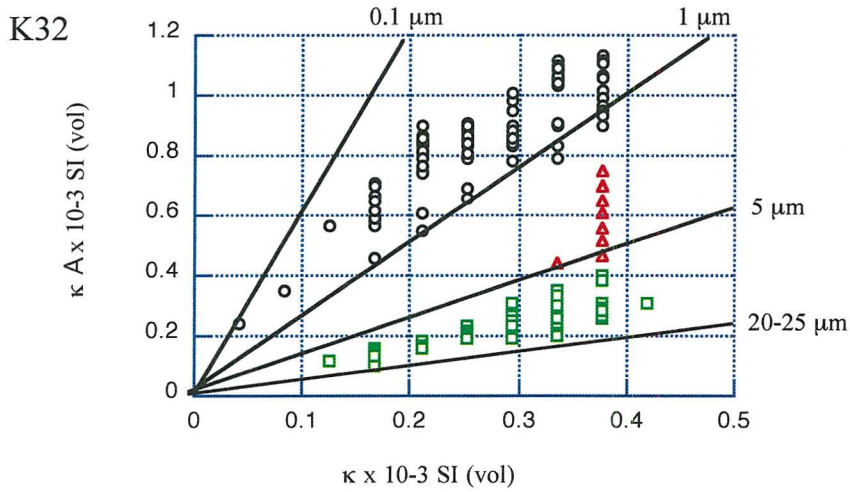

(a) Plot of κ vs. κA for K32 with fields defined by King et al. (1982). Open circles = 0.06 – 1.38 m; triangles = 1.39 – 1.45 m; squares = 1.46 – 2.5 m.

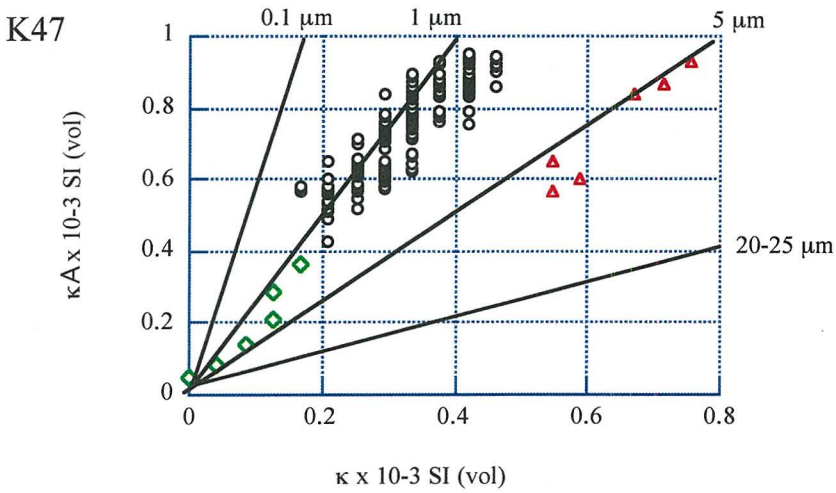

(b) Plot of κ vs. κA for K47 with fields defined by King et al. (1982). Diamonds = upper 5 cm; triangles = outliers; all remaining data are represented by open circles.

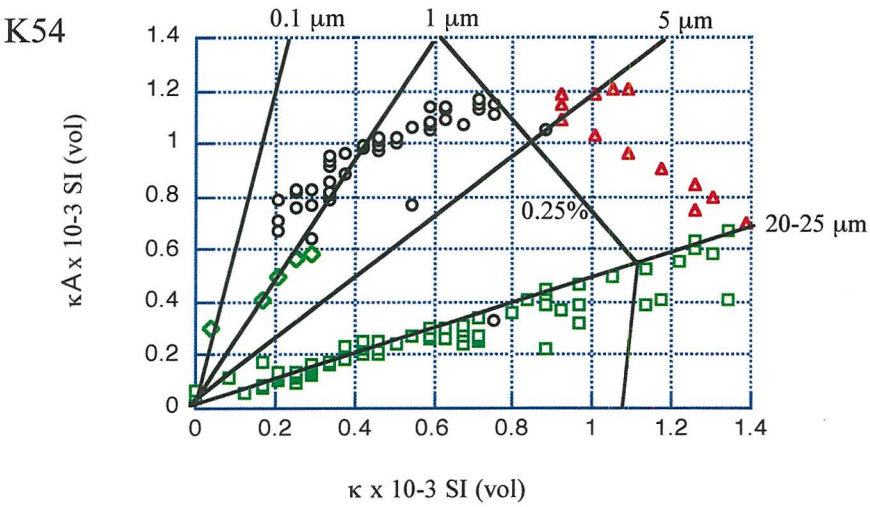

(c) Plot of κ vs. κA for K54 with fields defined by King et al. (1982). Diamonds = upper 5 cm; open circles = 0.05 – 0.77 m; triangles = 0.78 – 0.9 m; squares = 0.91 – 2.01 m.

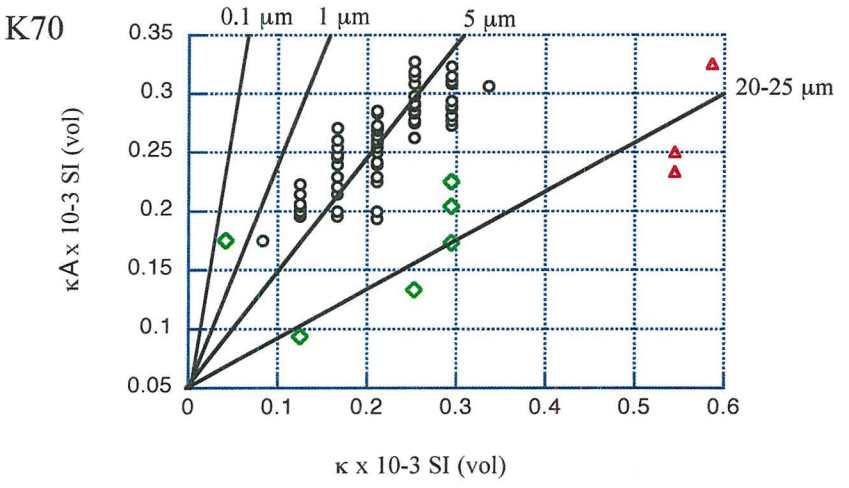

(d) Plot of κ vs. κA for K70 with fields defined by King et al. (1982). Diamonds = upper 5 cm; triangles = outliers at depths of 0.17 m, 0.39 m & 0.61 m; open circles = all remaining data.

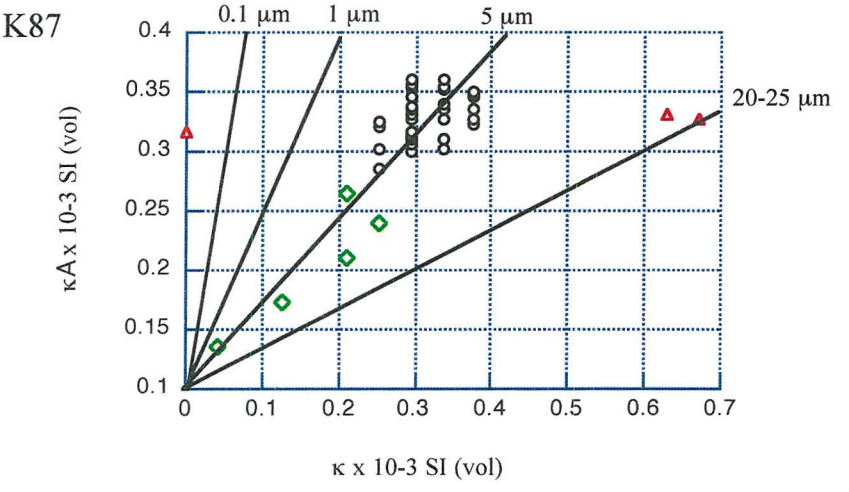

(e) Plot of κ vs. κA for K87 with fields defined by King et al. (1982). Diamonds = upper 5 cm; triangles = outliers at depths of 0.17 m, 0.28 m and 0.39 m; circles = all remaining data.

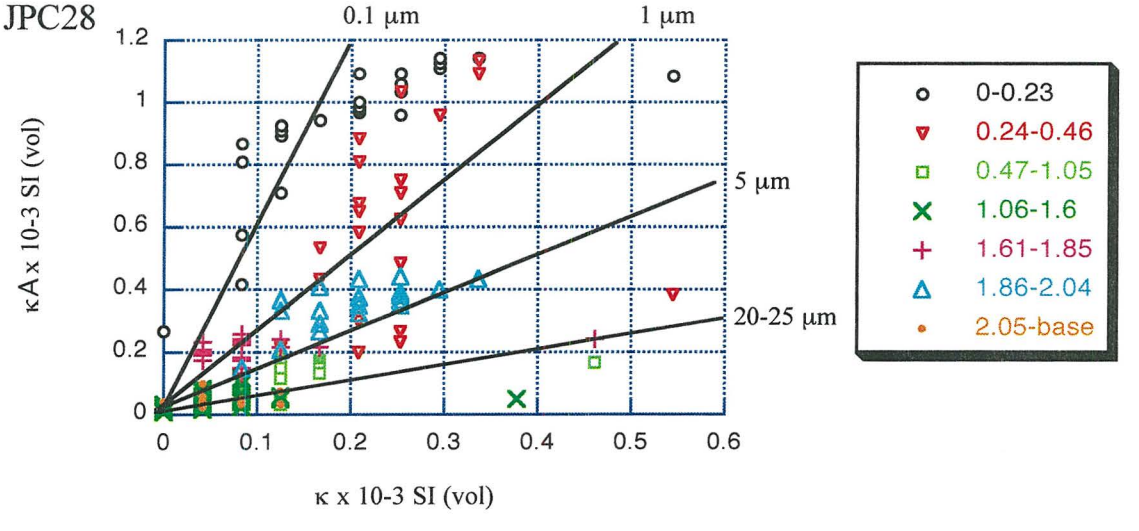

(f) Plot of κ vs. κA for JPC28 with fields defined by King et al. (1982). Variation in concentration and grain size with depth is illustrated through symbols representative of different depth intervals (refer to key).

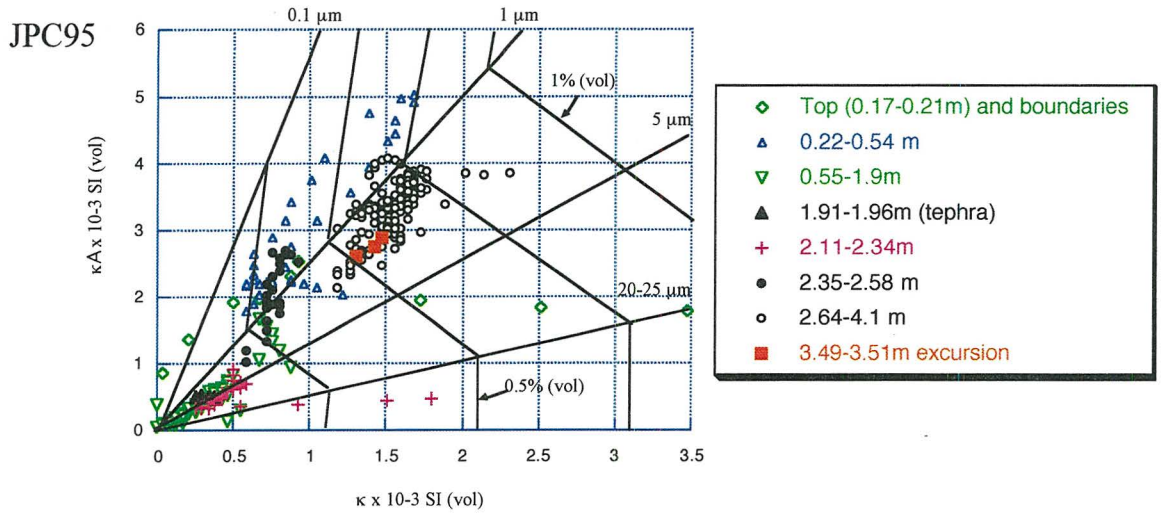

(g) Plot of κ vs. κA for JPC95 with fields defined by King et al. (1982). Variation in concentration and grain size with depth is illustrated through symbols representative of different depth intervals (refer to key).

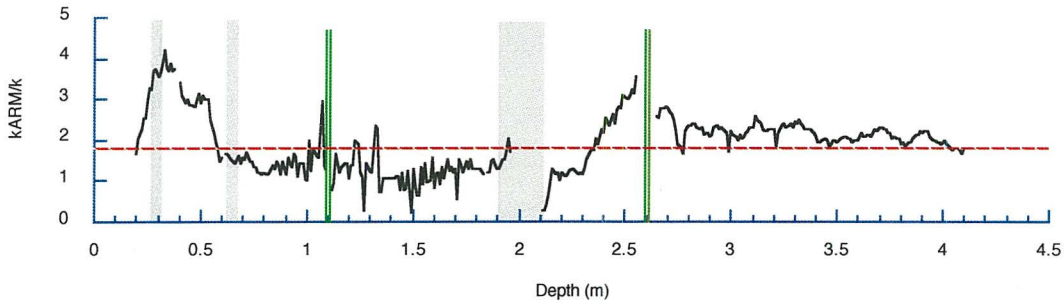

Figure 4.9: Variation in the κARM/κ ratio throughout core JPC95. Higher ratios reflect finer magnetic grain size. Variation never exceeds a factor of 2.5 with respect to the mean (red broken line = 1.94). Green, broken lines indicate section boundaries; grey shading indicates tephra horizons.

Meynadier et al. (1992) considered that for reliable determination of paleointensity, κARM/κ should not vary of more than a factor of ± 2.5 with respect to the mean value. This is because statistical alignment of magnetic grains is largely dependant upon their volume, such that different grain sizes can yield differing responses to variations in field intensity. This condition is satisfied for cores K32, K47 (Fig. 4.1), K70 and K87 from the Waipaoa Basin and core JPC95; omitting the upper-most, basal and core break intervals over which dubious ratios likely reflect sediment disturbance. Only ratios from the upper 0.88 m of K54 are within the acceptable range, below which grain size appears to coarsen. Variation of the ratio

in core JPC28 often exceeds these limits; exhibiting multi-domain behaviour over the intervals 0.47 m- 1.6 m, and 2.02 m – 2.55 m that is not associated with tephra horizons.

The paramagnetic and diamagnetic contributions to κ can constitute up to ≥ 50% of the measured κ in marine sediments (Peters & Dekkers, 2003). Since SP and MD grains have similar properties, high concentrations of SP material may compromise grain size interpretation of parametric ratios sIRM/κ and κARM/κ. Distinguishing between them requires measurement of frequency dependent susceptibility, to detect the presence of grains near the SD-SP threshold (Opdyke & Channell, 1996).

4.4 Indicators of magnetic concentration

4.4.1 Constraints on magnetic concentration from κARM vs. κ model

Concentration dependent magnetic parameters include NRM, sARM sIRM and κ, of which sARM and κ are often selected as the most reliable indicators of magnetic concentration. In the Banerjee model (Fig. 4.8), changes in concentration of the magnetic fraction are represented by distance from the origin. The linearity of the κARM vs. κ data (Fig. 4.8) in most cores indicates that change in κ is mainly due to variations in concentration. All cores from the Waipaoa Basin, and core JPC28 (i - vi) are generally characterised by concentrations of less than 0.25% magnetite, whilst JPC95 values approach 1% vol. magnetite.

On the grounds that the tops of cores and section boundaries often yield low concentrations (K47, K54, K87, JPC95), and/or anomalous grain size (K70, JPC28, JPC95), data within 5 cm of a boundary are disregarded. The consistent recurrence of outliers at depths of 0.17, 0.39, 0.61 and 1.67 m in *all* cores are due to anomalously high magnetic susceptibilities at these depths. These are interpreted to result from contamination of the measuring tray, and are thus excluded from analysis.

In cores K47, K54, K70 and K87, variation in magnetic concentration exhibits little depth dependence, varying throughout up to ~ 0.25% magnetite. In cores K32 and K54 (Fig. 4.8 a & c), magnetic content shows depth dependence, increasing down to 1.38 m (K32) and 0.77 m

(K54), respectively. Concentration remains relatively stable over the grain size transition, and progressively declines from 1.45 m and 0.9 m, respectively, to the core bases. In core JPC28, the highest magnetic concentrations occur in the upper 0.46 m, and within the lower tephra horizon (1.85-2.02 m; Fig. 4.8f). Magnetic content is lowest in divisions 2, 3, and 6 (Figs. 3.8, 4.8f), between 0.47 and 1.6 m, and below 2.02 m. The tephra horizon at 1.61 m -1.87 m exhibits concentrations that are intermediate between those of the lower tephra and overlying material.

Overall concentration in JPC95 is variable up to ~ 1 % magnetite. Concentration increases from the surface down to 0.42 m, below which it decreases to 0.54 m. Lowest concentrations (< 0.25 % magnetite) characterise division 2a (Figs. 3.9, 4.8g): the interval from 0.55 to 1.9 m and the upper part of the Oruanui Formation (1.91-1.96 m). Although the lower part of this tephra was not recovered, high κ at 2.11 m (Fig. 3.9) suggests that its magnetic content is relatively high. From 2.1 m (below the break in recovery) to 2.58 m, concentration increases to approach maximum values that are characteristic of the lower core (below 2.64 m) where concentration ranges between ~ 0.5 and 1 % vol. magnetite (Fig. 4.8g).

Magnetic parameters sARM, sIRM and κ increase monotonically with the amount of magnetic material. Volumetric magnetic susceptibility (κ) provides the best first order measure of bulk magnetic content (Heider et al., 1996); though interpretation is complicated when concentration of ferrimagnetic material is low and κ may respond to antiferrimagnetic (e.g. Hematite), paramagnetic, or diamagnetic material (e.g. CaCO3). Variability in κ never exceeds a factor of thirty for cores used in this study (e.g. Fig. 4.10), which is the proposed limit of concentration variability acceptable for paleointensity studies (King et al., 1983).

NRM is considered the least reliable indicator of concentration, being largely controlled by mineralogy, grain size and mode of remanence acquisition as well as intensity of the geomagnetic field. However, since NRM, sARM and sIRM and κ are all to some extent dependent upon magnetic concentration, synchronous down-hole fluctuations in these parameters would indicate that intensity is controlled by magnetic content, rather than geomagnetic field intensity (Bloemendal, 1983). Though variations in the above parameters follow broadly similar trends in core K47 (Fig. 4.10), subtle differences are apparent

throughout, implying that the observed variation in NRM cannot be attributed to concentration alone.

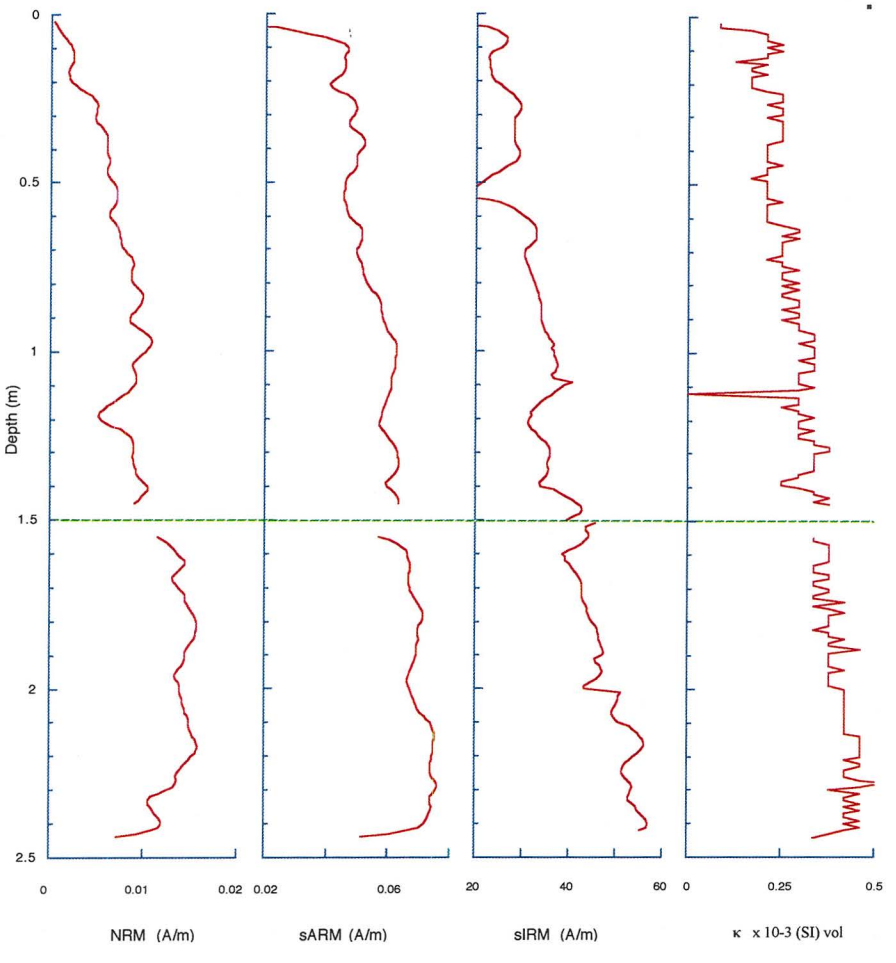

Figure 4.10: Down-core plots of concentration dependent magnetic parameters in core K47: NRM, sARM, sIRM and κ. Green broken line defines section boundary at 1.5 m.b.s.f.

4.4.2 Concentration from sIRM

Saturation magnetisation of magnetite at room temperature is reported as js = 480 G (Pullaiah et al., 1975). The mean saturation magnetisation observed in core K47 is sIRM = 37.4 A/m. Assuming uniform mineralogy and grain size (established in sections 4.2, 4.3), and random distribution of long axes, the concentration of magnetite can be estimated using equation 4.3:

$$\text{sIRM} = \text{js} \times (\text{volume fraction magnetite}) \qquad [4.3]$$

$$\therefore \quad \text{Concentration magnetite} = \text{sIRM} / \text{js}$$

$$= 37.4 \times 10^{-3}\ \text{G} / 480\text{G}$$

$$= 7.7 \times 10^{-5}$$

$$\approx 0.008\ \%\ \text{magnetite}$$

Validity of these assumptions is supported by consistency in values of *Js* and B_{cr} throughout core K47. The concentration calculated from equation 4.3 is also consistent with that estimated from the Banerjee model (Fig. 4.8b).

4.5 Compliance with rock magnetic criteria for evaluating Relative Paleointensity

Cores K32, K47, K70, K87 and JPC95 conform to all rock magnetic criteria specified in table 4.1. The mineralogical assessments employed in this study involve IRM parameters, and are thus only applicable to K47. For this core it was established that magnetite is the dominant carrier of remanence. Since demagnetisation characteristics of all other cores were generally similar to those of K47 (over the portions that satisfy granulometric and concentration requirements), it is assumed that magnetite is also the principle carrier in cores for which IRM experiments could not be performed. The only core in which evidence suggests otherwise is K70, which, over some intervals acquired a GRM (see section 3.1), associated with the presence of sedimentary Greigite (Hu et al., 1998).

Concentration variability in core JPC95 (maximum κ / minimum κ = 27.5) lies within the acceptable range (not exceeding a factor of 20-30) defined by King et al. (1983) for paleointensity applications. Excluding the interval of low concentrations, over which paleodirections are indeterminate (0.9 m-1.6 m; Figs. 3.9, 4.8g) reduces the concentration variation in core JPC95 significantly, to a factor of 13.8.

Criteria regarding grain size (see table 4.1) are violated in K54 and JPC 28 only. In K54 this is due to coarser magnetite below 0.88 m. Division 1 (above 0.88 m., Fig. 3.5) exhibits

granulometric uniformity within the recommended range of 1-15 μm. In core JPC28, coarser, multi-domain magnetic material > 15 μm from 0.47 m to-1.6 m and 1.85 m to 2.02 m is excluded from relative paleointensity derivations in the following chapter.

4.6 Relating rock magnetism to trends in magnetic parameters

Core K32

Measurements of paleomagnetic direction in the upper 0.16 m (Fig. 4.11) are disregarded owing to the poor consolidation of sediments and core expansion in this upper interval. However, relatively high MDF values indicate high coercivities, and the likely presence of magnetite grains within the SD–PSD range. Data collected 5 cm either side of the core section boundary appears to have been affected by reorientation of magnetic grains from core expansion or sediment disruption. Shallow inclinations below the break in recovery (0.3 - 0.42 m) and persisting down to 0.54 m are also classed as unreliable.

The gradual but punctuated rise in all concentration dependent parameters (NRM, sARM and κ) from 0.54 m to 1.38 m (Fig. 4.11) is interpreted to reflect increasing concentration of magnetite. This is supported by increasing distance from the origin evident in the Banerjee plot (Fig. 4.8a) and by an observed darkening of lithology below 0.9 m, as NRM, sARM and κ increase to their respective maximum values at 1.38 m. Together with stability of directional measurements (MDF consistently reaching 40 mT) over the majority of this interval (from 0.54 m to 1.50 m), these data imply that cyclicity evident in the directional record represents a true paleo-signal.

Throughout the upper section of core, VRM persists to peak alternating fields of 30 mT. Poor definition of magnetic components below ~ 1.5 m, and declining values of NRM, sARM κ, and MDF between 1.38m and 1.5 m are attributed to the coarsening of magnetic grain size evident in Figure 4.8a. This coarser size mode (up to 25 μm) persists to the core base (2.5 m), and is likely to be responsible for lower NRM and ARM intensities as well as lower MDF (and thus coercivity). The marked increase in variability of inclination and relative declination below 1.5 m is therefore considered dubious. Since κ is enhanced in MD grains, this parameter shows little decline until 2.3 m. Attenuation of intensities and κ below this depth may be controlled by falling concentration (as implied by Figure. 4.8a). ChRM is considered a reliable and true record of paleofield direction over the following intervals: 0.16 – 0.29 m, 0.54 – 1.50 m, and 1.62 - 2.29 m.

Figure 4.11: Down-core measurements of magnetic properties for core K32; also showing relative variations in magnetic grain size and concentration as determined from the Banerjee plot for this core (Fig. 4.8a). Divisions are labeled to the right of the figure; green broken line depicts the position of the section boundary (1.56 m). Block arrows indicate increasing or decreasing parameters, respectively.

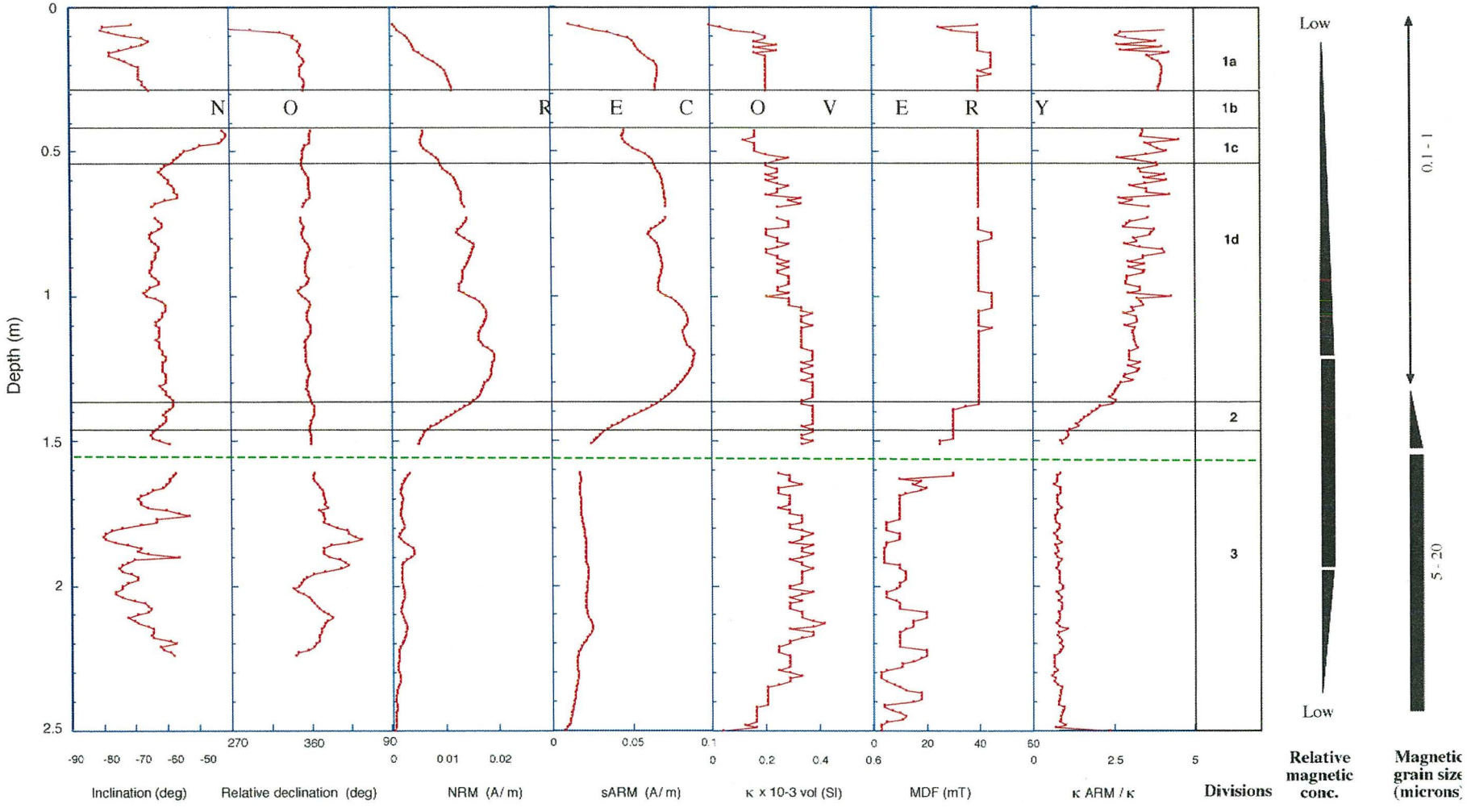

Core K47

Widely variable values of inclination in the upper 0.23 m are considered to represent a viscous secondary overprint or coring-induced disturbance of the poorly consolidated sediment; and not a reliable ChRM. Intensities measured over this interval are the lowest for core K47, and the anomalously high amplitude of variability in inclination and declination suggests modification of any pre-existing ChRM direction through sediment disturbance or preferential VRM acquisition at the ends of the core, where magnetisation of the core barrel is most intense. Similarly, measurements in the basal 4 cm of core are also disregarded owing to uncertainty of the signal's origin and validity. Measurements within 5 cm of the section boundary (1.5 m) are disregarded, with the exception of sIRM and B_{cr}, which have been corrected for reduced sample volume at the ends of core sections (see appendix 9.4)

A predominantly stable and relatively high MDF from 0.2 m to the base of the core (Fig. 4.12) suggests relatively high coercivity, and that the cyclicity evident in inclination and declination curves represents a reliable ChRM and true secular variation of the paleofield; with the exception of the interval 5 cm either side of the section boundary (11.45-1.55 m), where lower κ, intensities (NRM, ARM) and anomalous shallowing of inclination indicate disturbance associated with core cutting procedures. The overall down-core increases in NRM, sARM and sIRM intensities, as well, Since variability in B_{cr} is not paralleled in the κARM/κ ratio, the variability in as κ, indicate an increase in magnetic concentration, a range in which is indicated in Figure 4.8b. B_{cr} is interpreted to reflect minor variations in mineralogy throughout the core; though the range in B_{cr} indicates a preponderance of magnetite. ChRM is considered a reliable and true record of paleofield direction over the following intervals: 0.24 m– 1.45 m and 1.55 m – 2.40 m, respectively.

Figure 4.12: Down-core measurements of magnetic properties for core K47; block arrow showing an overall down-core increase in magnetic concentration as determined from the Banerjee plot for this core (Fig. 4.8a). Magnetic grain size is relatively homogeneous throughout this core (1-5μm). Core is not sub-divided due to homogeneity; green broken line depicts the position of the section boundary (1.5 m).

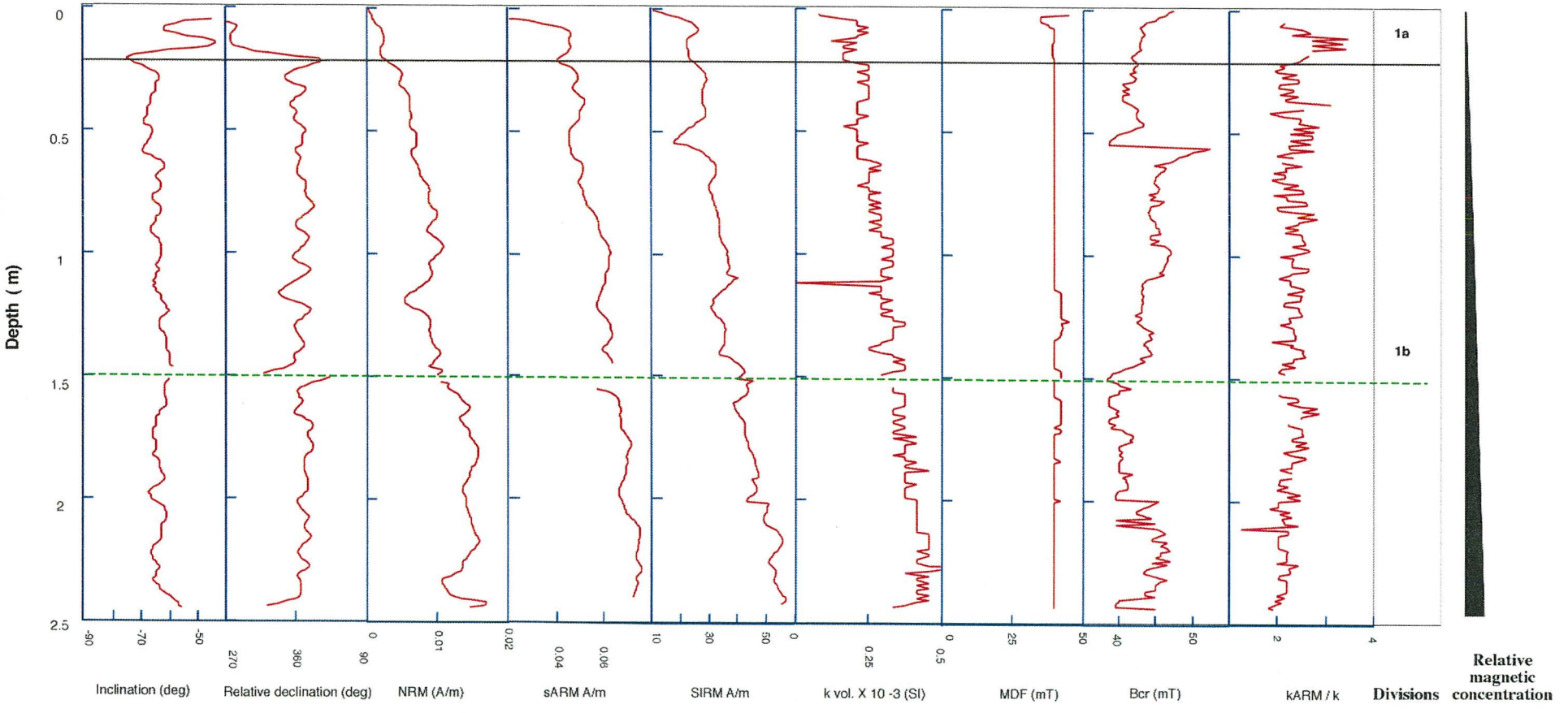

Core K54

Inclination and declination are only considered reliable between 0.3m and 0.88 m (Fig. 4.13). Intensity of NRM, κ and MDF are all relatively high over this interval, providing confidence in the ChRM picked. The Banerjee plot for core K54 (Fig. 4.8c) exhibits an irregular increase in the fraction of magnetic material from 0.3 m to 0.78 m (as concentration dependent parameters increase), and a coarsening from 0.78 m to 0.9 m as intensities of NRM & sARM decline. The remainder of core (below 0.9 m) is characterised by coarse (~20-25μm) magnetite. Magnetic susceptibility (κ) continues to rise down to 0.9 m, most likely because κ is enhanced in MD grains (in contrast to sARM). The subsequent decline in κ is likely to be associated with falling magnetic concentration from 0.9 m to 1.12 m, below which it remains relatively low. Outside of the 0.3-0.88 m interval, low magnetic concentration and/or coarseness render data inadequate to obtain reliable paleodirections from PCA. Inclination measured from 0.24 m to 0.25 m is disregarded; anomalously shallow angles interpreted as an effect from lack of material above and below. As with all other cores, measurements within 5 cm of the section boundary are excluded from further interpretation. ChRM is considered a reliable and true record of paleofield direction from 0.31 to 0.88 m.

Figure 4.13: Down-core measurements of magnetic properties for core K54; also showing relative variations in magnetic grain size and concentration as determined from the Banerjee plot for this core (Fig. 4.8c). Divisions are labeled to the right of the figure; green broken line depicts the position of the section boundary (1.5 m). Block arrows indicate a relative increase or decrease in parameters, respectively.

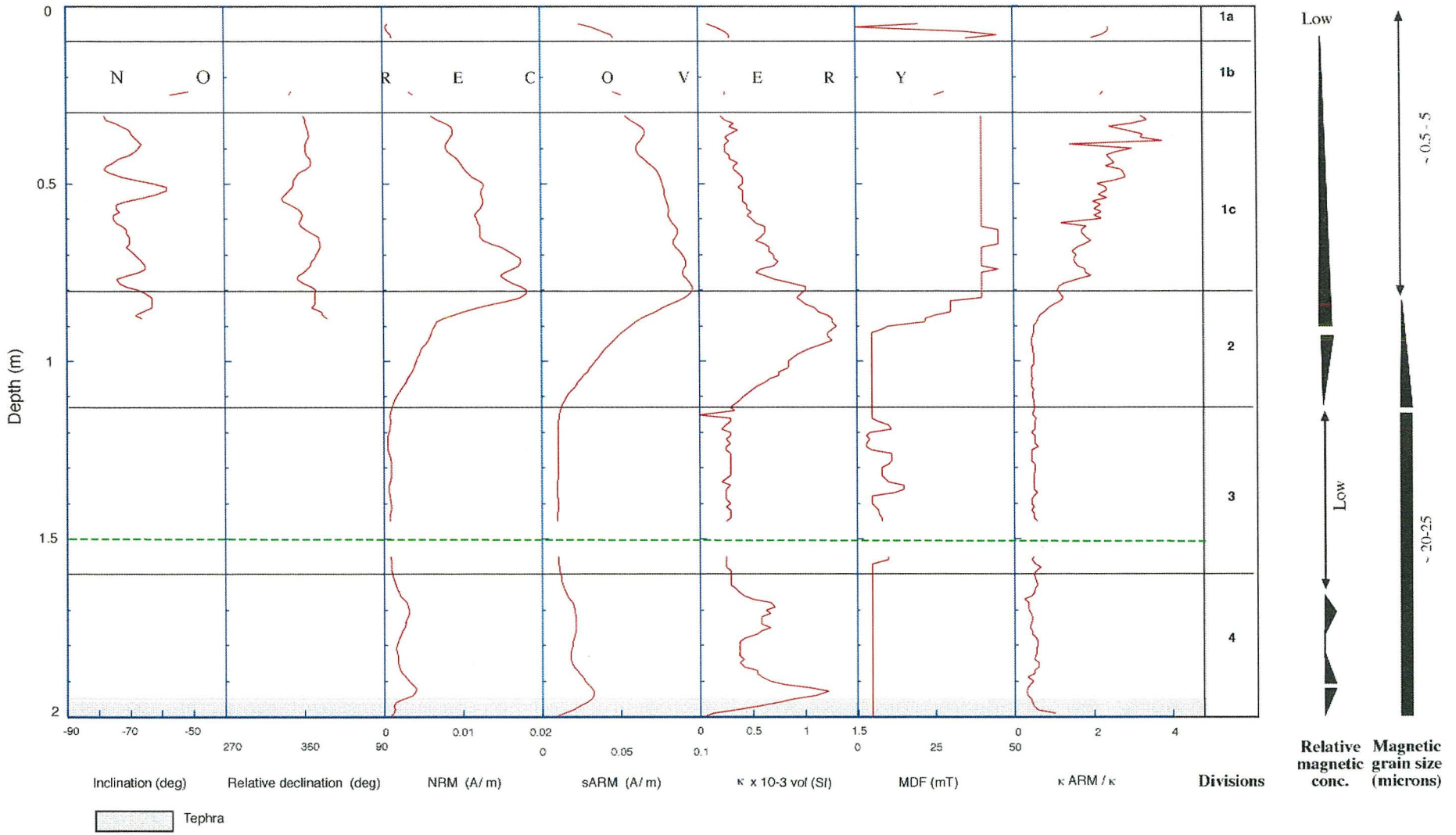

Core K70

In the recovered portion of core K70, inclination and declination of the ChRM are well-constrained (Fig. 4.14); orthogonal component projections exhibiting predominantly linear and complete demagnetisation above peak alternating fields of 15 mT. Moderate coercivities are implied by consistency in MDF values > 24 mT, despite relatively low intensities and variable κ (0.04-0.29 $x10^{-3}$ SI) recorded throughout this core. Grain size is relatively consistent throughout according to Figure 4.8d, which also shows concentration increasing irregularly down to 0.26 m, and varying below this depth. ChRM is considered a reliable and true record of paleofield direction from 0.14 m to the base of the core (0.88 m).

Figure 4.14: Down-core measurements of magnetic properties for core K70. Negliable variation in magnetic concentration or grain size is evident from the Banerjee plot for this core (Fig. 4.8d). Magnetic grains size varies throughout between 1 and ~ 10 μm; magnetic concentration is consistently < 0.25 % magnetite (Fig. 4.8d).

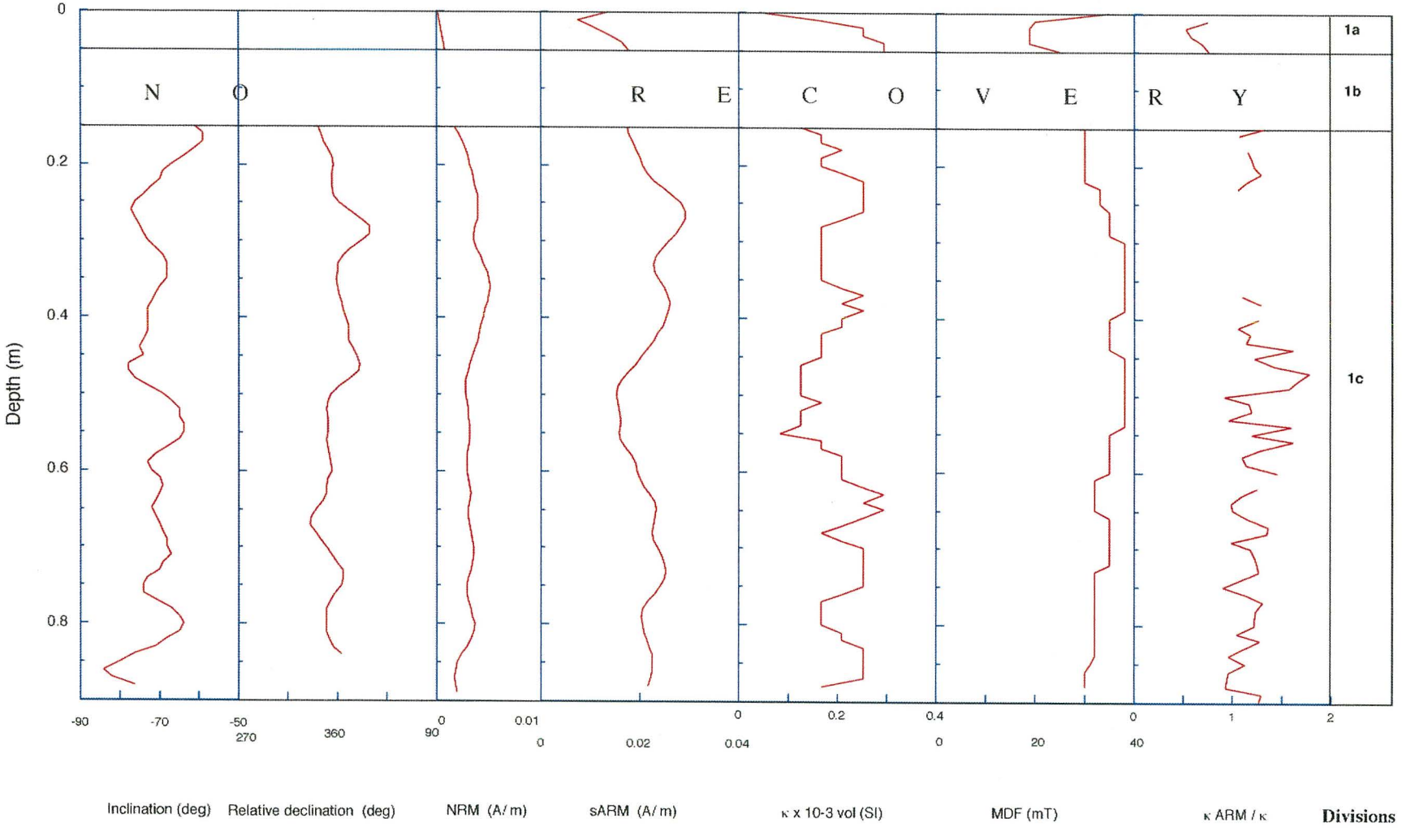

Core K87

Increases in NRM and κ from 0.07 m to 0.18 m are interpreted (using Figure 4.8e) to reflect increasing concentration of magnetic material. The marked decrease in κ below 0.18 m (Fig. 4.15) is interpreted to represent a drop in the magnetic fraction at 0.18 m. Concentration remains low to the core base (0.55 m). Attenuation of intensities and MDF in division 3 (in the basal 5 cm) is likely to reflect convolution at the end of the U-channel and is thus disregarded. Directional fluctuations of ChRM are considered to represent a reliable and true record of paleofield direction from 0.09 m to 0.55 m.

Figure 4.15: Down-core measurements of magnetic properties for core K87. Negliable variation in magnetic concentration or grain size is evident from the Banerjee plot for this core (Fig. 4.8e). Magnetic grains size varies about a mean of ~ 5 μm; magnetic concentration is consistently < 0.25 % magnetite (Fig. 4.8e). A single U-channel section only was obtained from this core.

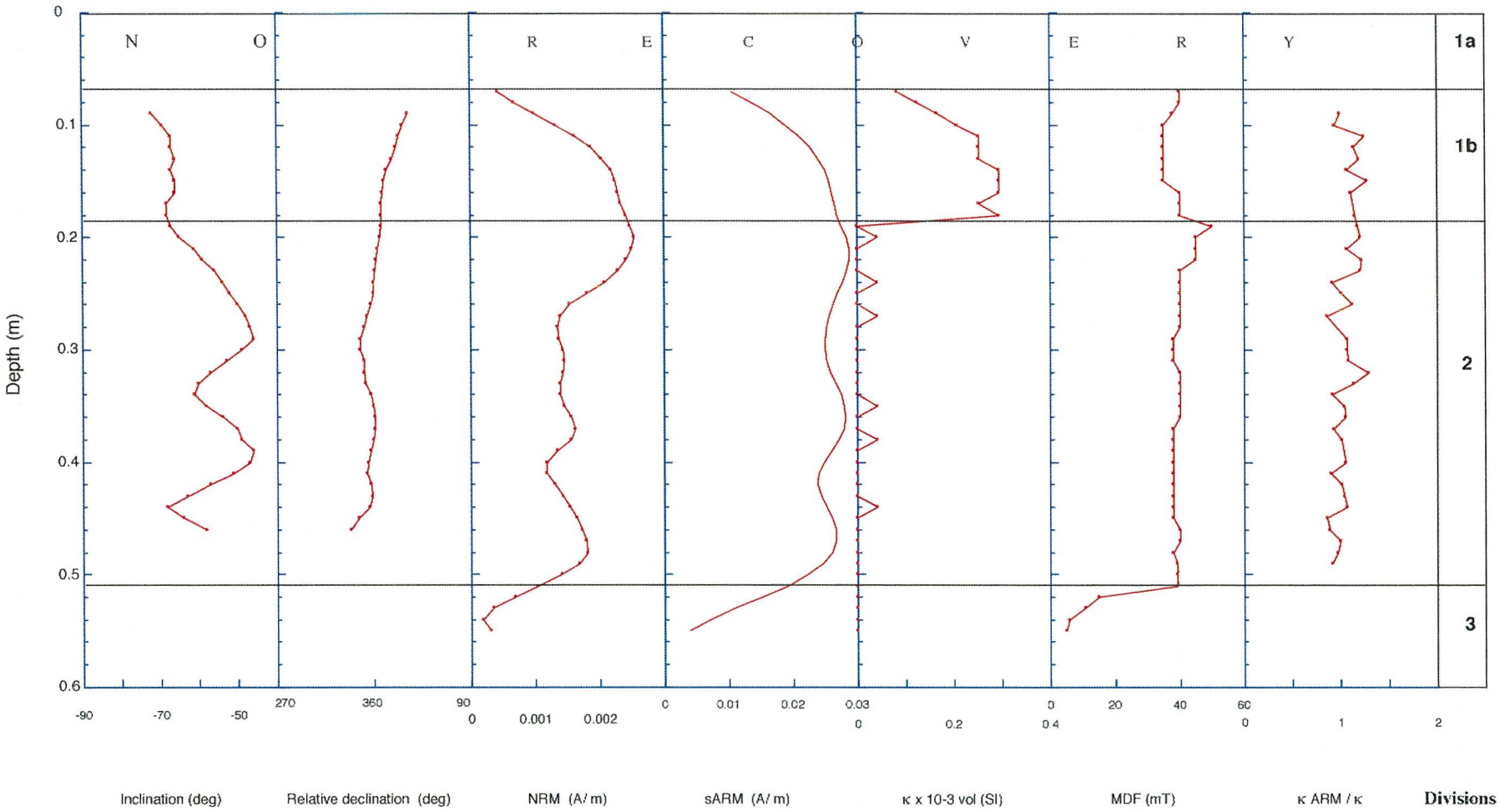

Core JPC28

The large portion of this core for which paleodirections were undefined are due to variations in character of the sediment, with lower concentrations of ferrimagnetic minerals rendering many intervals either unsuited to AF demagnetisation or incapable of retaining a NRM.

ChRM directions measured from ~10 cm (below disturbed sediment) down to 0.46 m are likely to represent a true paleofield signal, since MDF as well as intensity and κ are relatively high (Fig. 4.16). Lower coercivities and incomplete, poor demagnetisation behaviour in divisions 2 and 3 (0.47-1.6 m) is likely to be due to relatively coarse magnetic material in lower concentrations (Fig. 4.8f). Tephra layers at 1.6-1.87 m, and 1.92-2.0 m explain increases in concentration-dependent parameters (NRM, sARM intensities and κ) over these intervals, particularly in the lower tephra. The upper of these tephras, the Oruanui Formation (see section 3.4) is finer (see appendix 9.3) and exhibits normal grading, which is apparent also in the Banerjee plot (Fig. 4.8f). The coarser nature of the lower tephra, which also appears richer in ferrimagnetic material (Fig. 4.8f), is reflected in lower coercivities, as indicated by MDF (Fig. 3.8). The apparent differences in magnetic content and granulometry between the two tephras may imply independent origins. The 5 cm of sediment that has accumulated in between the two horizons also supports this hypothesis, this thickness representing some time separating the two events (dependant on sedimentation rate).

The change in inclination at 1.77 m is not interpreted to represent behaviour of the paleofield, considering it's occurrence within a tephra unit that is normally graded (see appendix 9.3). Rotation of magnetic grains within the tephra may be controlled to a greater degree by gravitational influences; unlike in silt, in which magnetic grains freely align with the ambient paleofield. The step in inclination at 1.6 m (across the tephra-mud contact) also casts doubt on the reliability of paleofield estimates obtained from within the tephra unit. Relative paleointensity estimates (from within the tephra unit), which are independent of gravitational influences, may be reliable.

Relatively low NRM, sARM & κ below 2.02 m suggests reduced magnetic concentration below the tephra horizons in addition to coarsening implied by complete loss of coercivity. This is corroborated by the Banerjee plot (Fig. 4.8f), which exhibits an abrupt decrease in

concentration below 2 m, returning to levels approximating those above the tephra. ChRM is considered to represent a reliable and true record of paleofield direction from 0.05 m to 0.46 m and 1.11 m to 1.59 m.

Figure 4.16: Down-core measurements of magnetic properties for core JPC28; also showing relative variations in magnetic grain size and concentration as determined from the Banerjee plot for this core (Fig. 4.8f). Divisions are labeled to the right of the figure; green broken line depicts the position of the section boundary (1.05 m). Blocks of varying width indicate relative changes in parameters.

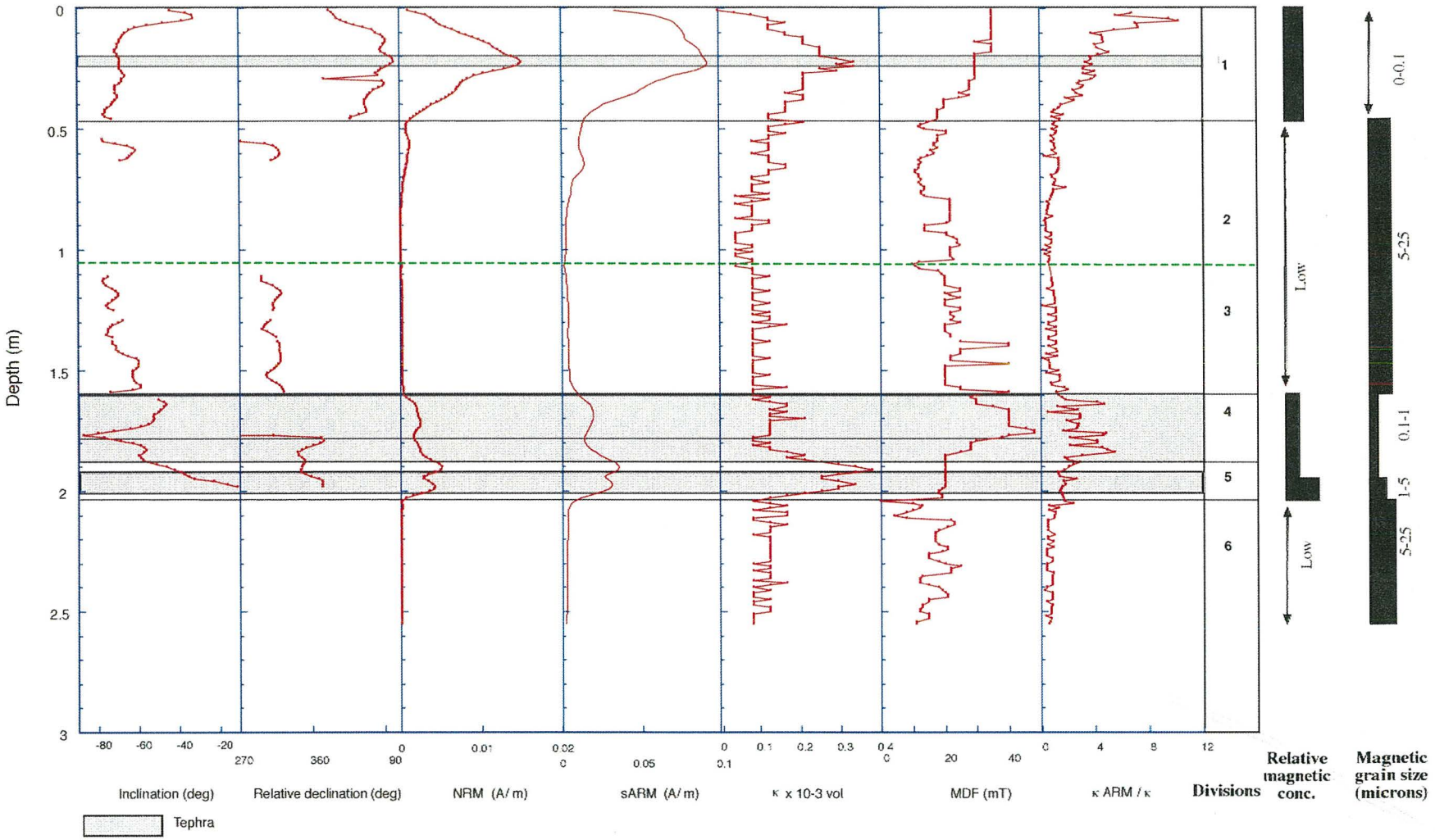

Core JPC95

From 0.22 m to 0.9 m magnetic concentration dependent parameters and MDF are sufficient to obtain well-constrained paleodirections from PCA; concentration attaining relatively high levels (maximum in the case of sARM) at ~ 0.4 m, and decreasing below this (Fig. 4.17). Coercivity also declines from 0.55 m toward the section boundary (1.1 m). Consistently low concentrations (minima in NRM, sARM intensities and κ) persist from 1.15 m to 1.6 m. Demagnetisation vs. intensity plots over this interval are characterised by concave-up curvature and uneven loss of intensity. ChRM determinations from 1.23 m-1.32 m are interpreted to be less accurate owing to consequent directional data scatter. A slight increase in magnetic concentration is evident from 1.6 m to 2.18 m. Directions of ChRM determined from 1.6 to 1.96 m and 2.18 m to 2.35 m are considered reliable, though good (type 1) demagnetisation behaviour is observed only below 2.35 m; where coercivity increases to ~ 30 mT in response to fining of magnetic grain size (as indicated by the rising κARM/κ ratio in Fig. 4.17). The marked increase in MDF at 2.35 m may indicate the crossing of a threshold magnetic grain size, below which the capability of grains to preserve remanence increases dramatically. The gradual increases in NRM and sARM intensities, and (to a lesser extent) κ, suggest gradually increasing magnetic concentrations from 2.18 m to 2.7 m accompanied by fining down to 2.55 m. From 2.35 m to base, comparatively good demagnetisation behaviour is explained by higher magnetic concentrations and grain size centred around 1 μm (2.35-2.6 m); and in the range 1-5 μm (2.6 m - 4.1 m; Fig. 4.8g).

The step in declination across the lower boundary at 2.6 m and concurrent shift in inclination from - 48° to -74° (Fig. 3.9) rouses suspicions of a change in the angle of core penetration, thus rendering one section inaccurate. The shift may be attributable to disturbance of the interface during sampling. Furthermore, the 720° (overall) down-section change in declination indicates significant rotation of the core barrel during penetration. This is most obvious in the basal 10 cm of the declination record, where ~ 360° of rotation is apparent. This portion of the declination record is thus disregarded (not presented in subsequent figures); and reliability of the entire declination record is dubious.

Temporary inclination shallowing and relatively dramatic decline in NRM intensity (and not in sARM intensity) at 2.9 m and at 3.5 m (mid-section) are interpreted to represent geomagnetic excursions. Consistency in sARM, κ and the κARM/κ ratio over these perturbations attest to a geomagnetic origin.

Lack of correspondence between tephra layers and levels of concentration dependent parameters indicates no enhancement of magnetic concentrations within these horizons; with the exception of high κ at the base of the Oruanui Formation (2.18 m).

The isolated ChRM is considered to represent a reliable and true record of paleofield direction over the following intervals: 0.22 m – 0.9 m; 1.6 m – 1.96 m; 2.18 m – 2.55 m; and 2.65 m – 4.1 m.

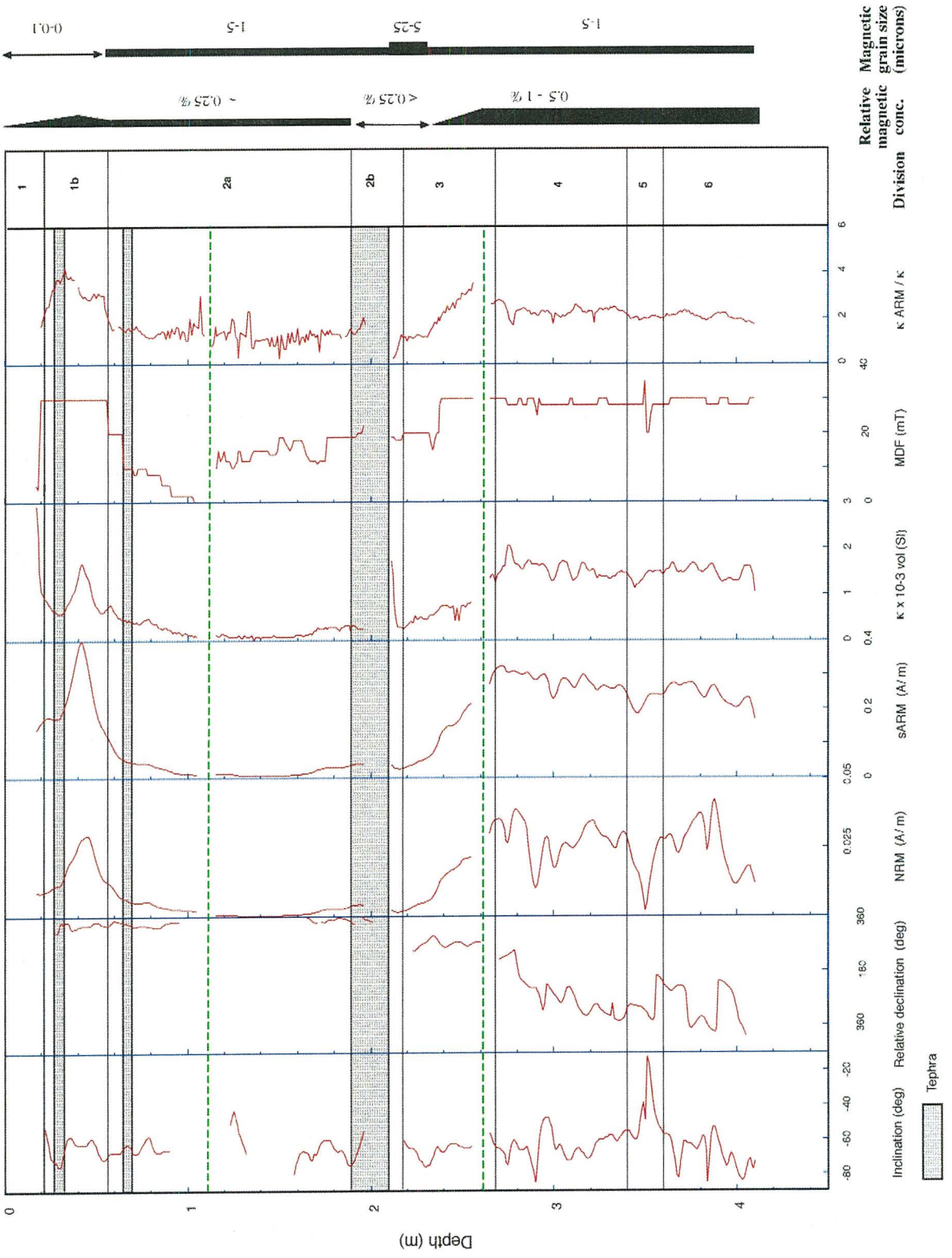

Figure 4.17: Down-core measurements of magnetic properties for core JPC95; also showing relative variations in magnetic grain size and concentration as determined from the Banerjee plot for this core (Fig. 4.8g). Divisions are labeled to the right of the figure; green broken line depicts the position of section boundaries (1.1 m & 2.6 m). Blocks of varying width indicate relative down-core changes in parameters; and block arrows indicate an increase or decrease, respectively.

5. RELATIVE PALEOINTENSITY (RPI)

The method for determination of relative paleointensities in marine sediments relies on the proposition that the intensity of DRM is a linear function of ambient field over the range of geomagnetic field intensity (Tucker, 1980). This is generally not the case; intensity of the geomagnetic field at the time of remanence acquisition is not a simple function of the DRM intensity of the sediment (Tauxe, 1993). The record of NRM intensity displayed in Figs. 3.3-3.9 cannot alone provide reliable estimates of paleointensity, owing to the myriad of factors affecting the intensity of NRM and thus the paleointensity proxy. These include variations in the concentration and type of magnetic mineral phases within the sediment, as well as sedimentation rate, environment of deposition, degree of bioturbation, diagenesis, compaction and sampling-induced disturbance. Separation of geomagnetic from environmental controls is maximised when samples demonstrate adherence to criteria defining magnetic homogeneity (King et al., 1983, Tauxe, 1993; table 4.1). Changes relating to the concentration of remanence carrying grains (in magnetically homogenous samples) are routinely compensated for through normalising NRM intensity by some form of artificial remanence parameter (e.g. saturation ARM or saturation IRM).

5.1 Selection of parameter for normalisation of NRM

Levi & Banerjee (1976) emphasized the importance of judicious selection of normalising procedure in paleointensity determinations, and the necessity for the chosen procedure to "activate the same spectrum of magnetic particles which are also responsible for the NRM." (Levi & Banerjee, 1976). These authors found that the demagnetisation curve most closely approximating that of NRM (and therefore with most similar coercivity spectra) was that of saturation ARM, rather than saturation IRM. They further discredited sIRM (for normalisation purposes) due to the instability of the NRM/sIRM ratio during demagnetisation, as well as the relative differences in magnitude: sARM typically exceeds NRM by a few tens to hundreds of times, whereas sIRM is thousands of times larger (Levi & Banerjee, 1976). Johnson et al. (1975) advocated the use of sARM, considering its particular sensitivity to particles in the SD-PSD range (whereas sIRM and κ respond more to MD magnetite), and its similarity to thermal remanence. Since detrital grains originally acquire their magnetic

moments as a thermal remanence, DRM is essentially a reconstituted TRM (Johnson et al. 1975). King et al. (1983) also favoured sARM over other parameters. Tauxe (1993) recommended ideally using several methods of normalisation, which should all yield consistent results.

Levi & Banerjee (1976) recommended comparing demagnetisation curves of NRM and ARM (or IRM); identical magnetisation behaviours providing a good indication that a similar range of grains are involved in both types of remanence. Figure 4.3 shows demagnetisation curves of NRM, ARM and IRM. The MDF for ARM demagnetisation is generally 10-15 mT lower than for NRM, with similar curvature and a relatively consistent difference (throughout demagnetisation) of ~ 0.2 in normalised remanence. Lack of overlap between these curves suggests that ARM is carried on lower coercivity grains than NRM. In contrast, IRM curves exhibit a dissimilar shape, mimicking ARM at lower and NRM at higher levels. Data from all depths show a crossing of ARM acquisition and demagnetisation curves at around 50% and a crossing for IRM data at ~ 40%, implying that ARM is more stable against demagnetisation than IRM. This greater stability and symmetry renders sARM a more appropriate normalising parameter than sIRM.

5.2 Fidelity of Relative Paleointensity (RPI) records

5.2.1 Compliance with rock magnetic criteria for studies of RPI

A problem inherent to using sARM as a surrogate for field intensity is that variations in ARM do not always accurately reflect changes associated with varying concentration of magnetic material; they can also reflect changes in domain state/grain size. King et al. (1983) demonstrated that the DRM/sARM ratio is dramatically affected by changing particle size for magnetite smaller than 1 μm; and in the coarse multi-domain state (> 15 μm) grains are too 'soft' to retain a stable primary remanence (Parry, 1965). Thus only magnetite in the size range 1-15 μm is considered relatively unaffected by minor variations in particle size. Particle interactions also play a major role in the process of ARM acquisition (Cisowski, 1981), such that variation in magnetite concentration of > 20-30 times the minimum would adversely affect the accuracy of the DRM/sARM ratio as a measure of relative paleointensity (King et al., 1983). Thus for valid normalisation sediments must first conform to rock magnetic criteria

(summarised in table 4.1) to ensure consistency in magnetic domain state, concentration and mineralogy (Merrill et al., 1998).

In addition to the rock magnetic criteria discussed in chapter four, desirable attributes for relative paleointensity studies recommended by Tauxe (1993) include:

- No inclination error (bioturbated sediments preferable to laminated).
- Normalisation carried out using several methods should yield consistent results.
- A stable, well-defined single component of magnetisation at level used for normalisation.
- Coherence between RPI and bulk rock magnetic parameters used in normalisation should be minimal.
- Records from a given region should agree within the limits of a common time scale.

Franke et al. (2004), discovering that matrix lithology can account for more than 50% of observed RPI dynamics, proposed that another criterion of lithological homogeneity should be considered.

Although adherence to the above quality criteria may increase the reliability and accuracy of relative paleointensity (RPI) determinations, Haag (2000) stressed that the general trend of Earth's changing magnetic field intensity can be preserved even in sediments with strong ferrimagnetic mineral variations.

5.2.2 Effects of Viscous Remanence (VRM) on RPI determination

NRM intensity of cores in this study is normalised by the saturation ARM (sARM). Since the NRM intensity represents the vector sum of secondary and characteristic components, relative variations in paleofield intensity can only be derived after demagnetisation of spurious (secondary) components. In general, all secondary components appear to have been removed by fields of 30 mT, although some cores show no evidence for any overprint beyond the 5 mT step. Hence NRM is normalised at a different demagnetisation level appropriate to each individual core (the ChRM), depending on the extent to which the viscous remanence persists. Normalisation was also performed using NRM (prior to AF demagnetisation treatment) for comparison (Fig. 5.1).

Cores exhibiting close coincidence between (sARM) normalisations using NRM and ChRM (cores K47, K70, K87, and JPC28) are those in which any viscous component has little or no effect on the relative paleointensity estimate. Grains in the MD state are too magnetically 'soft' to retain a stable primary remanence and are more susceptible to acquisition of VRM (King et al., 1983). Significant difference between NRM and ChRM normalisations in the lower portions of K32 and K54 (Fig. 5.1), is consistent with lower intensity, deterioration of coercivity, and lower MDF values below ~ 1.38 m in K32 and ~ 0.78 m in K54. Granulometry bi-plots suggest that this is attributable to a coarsening of grain-size in both cases (see Fig. 4.8a & c), to sizes beyond the acceptable limits defining uniformity for paleointensity studies (Tauxe, 1993). Data over these intervals are therefore excluded from RPI determinations.

Normalisations for JPC95 also show evidence for a viscous component, contributing to the variable down-core difference between NRM and ChRM normalisations. Maximum RPI using NRM occurs at the upper core section boundary (1.1 m). Low coercivity and poor demagnetisation behaviour proximal to the boundary are likely to be a consequence of enhanced acquisition of VRM. This results in the two normalisations having different maxima at widely separated depths. The curves presented in Figure 5.1 are thus both normalised to their respective values at 3.8 m (the ChRM/sARM maximum). Relative Paleointensity estimates normalised using ChRM are less affected by viscous remanence, and therefore considered more reliable. The explanation for enhanced VRM from 0.55 m to 1.1 m (where coercivity deteriorates on approach of the boundary) relative to the interval below (1.1 m - 2.35 m) is not immediately obvious, considering that Figure 4.8g indicates *higher* concentration over the upper interval and granulometry is comparable (Fig. 4.9). Concurrence of the RPI estimates above 0.54 m and below 2.35 m, however, coincides with finer magnetic grain size and higher magnetic concentrations (as interpreted from Figures 4.8g, 4.9).

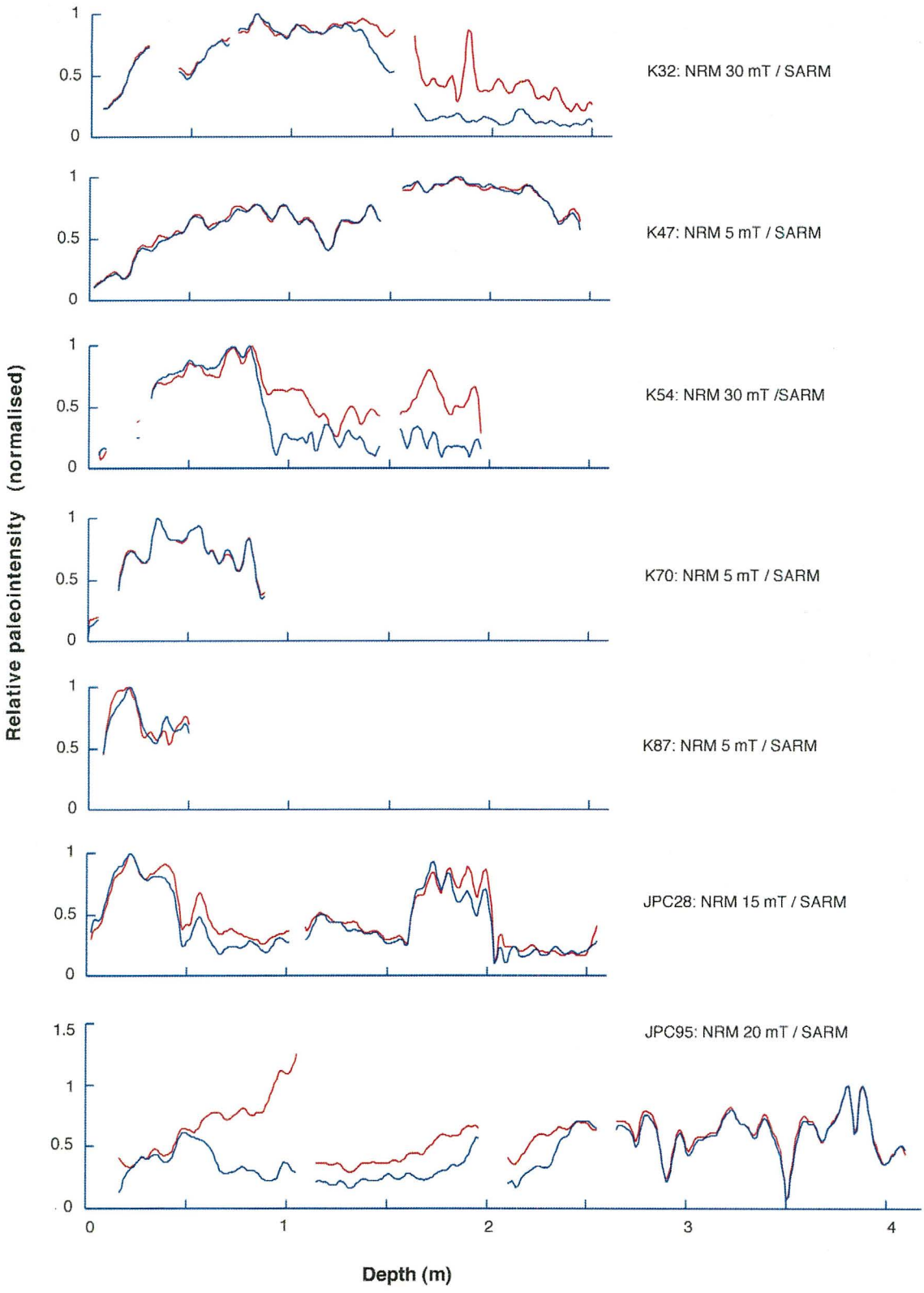

Figure 5.1: Comparison of RPI estimates for all cores used in this study, obtained by normalising the NRM intensity (red) by sARM, and normalising the ChRM value (blue) by sARM. The ChRM is the magnetisation remaining after removal of viscous components. Good agreement between the two curves implies little or no dependence of RPI on the level chosen for normalisation.

Tauxe et al. (1995) claimed that flawed calculations of RPI arise from using *any* of the above-mentioned magnetic parameters (sARM, sIRM or κ) to normalize NRM, since none of these 'brute force methods' take into account the possible contribution of viscous remanence. Because during the Bruhnes Chron (last 780 000 years) VRM is likely to be sub-parallel to the primary DRM, it may go undetected and thus result in inaccurate paleointensity estimates. Tauxe et al. (1995) suggests that normalisation by the 'pseudo-Thellier method' conveniently separates unwanted VRM, whilst also assessing uncertainty of the RPI estimate. This method involves the use of Arai plots to calculate the best-fit slope relating NRM and ARM between two field steps, considering the uncertainty in both.

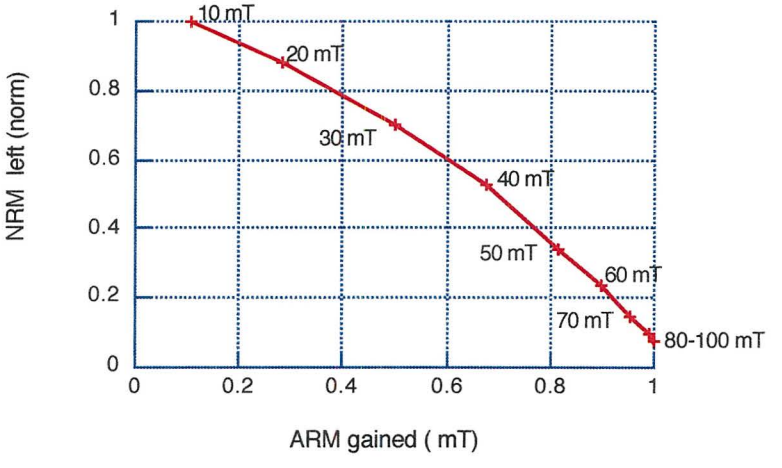

Figure 5.2: Arai plot showing normalised NRM left vs. ARM gained at the same peak fields, from 10 mT (top right) to 100 mT (bottom left) in field steps of 10 mT, for core K47.

The only core for which ARM acquisition data is available from low to high field steps in this study is K47. Tauxe et al. (1995) interpreted a pronounced concave-up curvature between 5 and 30 mT on an Arai plot for data from the Ontong-Java plateau as reflecting the removal of a viscous component. Data from core K47 (Fig. 5.2), however, shows no evidence of enhanced curvature at low field steps; in contrast being characterised by broad convexity. This observation, together with coincidence of RPI estimates using NRM and (those using) ChRM (30 mT) in cores K47, K70, K87 and JPC28 (Fig. 5.1) implies negligible effect of VRM components on RPI estimates. Thus the pseudo-Thellier method using partial ARM is

deemed unnecessary for these cores; and its application to remaining cores is precluded by lack of adequate ARM acquisition data.

5.3 Testing the normalising parameter

5.3.1 NRM/ARM ratio

Tauxe (1993) suggested that a constant ratio of NRM to ARM throughout demagnetisation would confirm suitability of ARM as a normalising parameter. Cores used in this study consistently show that the ratio remains relatively constant up to ~ 80 mT (Fig. 5.3). Above this level, the ratio increases, implying higher coercivity of NRM, and thus violation of the requirement for similar coercivity spectra at such high fields.

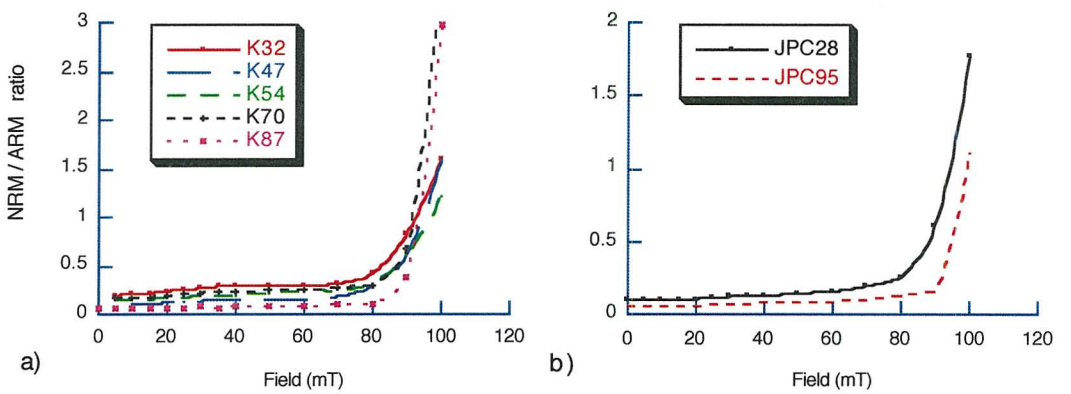

Figure 5.3: Plots illustrating variation in the NRM/ARM ratio with increasing alternating field in cores from (a) the Waipaoa Basin, and (b) northern Chatham Rise (JPC28) and Bay of Plenty (JPC95), at depths that exhibit results representative of each core. Ratios remain relatively stable to 800-900 Gauss for all cores.

5.3.2 Arai plots

Linearity of Arai plots showing ARM left vs. ARM gained is also favourable when using ARM for normalisation. Tauxe et al. (1995) used the slope of the most linear portion of the NRM left vs. ARM gained plot to estimate paleointensity using the pseudo-Thellier method (Fig. 5.2). Arai plots for the cores in this study are fairly linear (e.g. Fig.5.4).

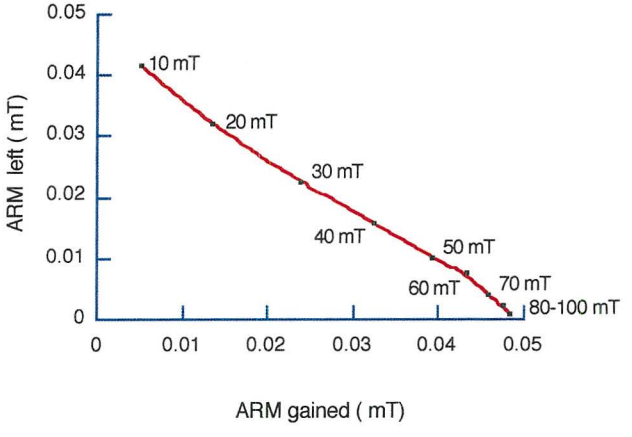

Figure 5.4: Plot of ARM gained vs. ARM remaining at the same peak alternating field for core K47 at 0.3 m. Lack of curvature at low field steps may imply the lack of viscous components (VRM).

5.3.3 Grain size and concentration dependence of RPI

For normalisation to be considered successful and representative of changes in intensity of the geomagnetic field, influence of environmental factors must be removed (Weeks et al., 1995). Changes in rock magnetic parameters are linked to paleoceanographic conditions prevailing at the time of deposition and may largely reflect depositional conditions (Meynadier et al., 1992). Thus correlation between normalised intensity and concentration dependent parameters κ or sARM, indicates that climatically controlled factors have not been removed from NRM (Tauxe & Wu, 1990). There should also be no correlation between the normalised record and the grain-size dependent ratio κARM/κ (King et al., 1983). The validity of normalisation by sARM in this study is substantiated by the absence of correlation between the above parameters and the evolution of the NRM/sARM ratio (Fig. 5.5); confirming that normalised intensity is not affected by magnetic granulometry, or concentration.

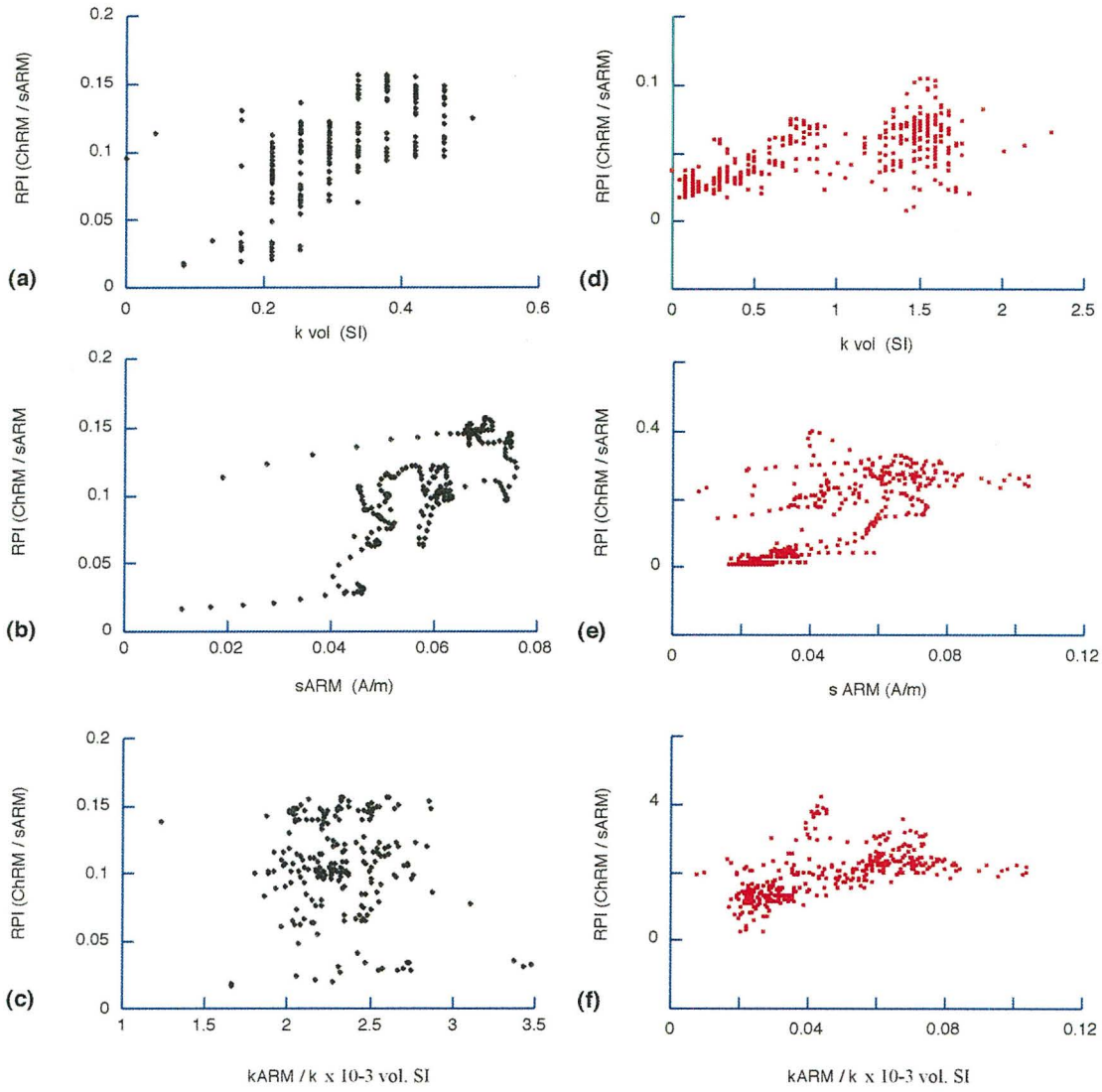

Figure 5.5: RPI vs. κ, sARM and κARM/κ for cores K47 (a-c) and JPC95 (d-f). Lack of correlation in any plot implies that RPI is not controlled by variations in concentration *or* grain size or concentration; thus confirming the appropriateness of saturation ARM as a normalising parameter.

Yamazake (2002) stressed that sARM should *not* be used for normalisation purposes if κ_{ARM}/κ is inversely correlated to κ, since this implies that ARM acquisition is controlled by interactions due to changing mineral concentrations. Figure 5.6 exhibits only a weak inverse correlation for core K47, and no apparent correlation for JPC95; thus providing little evidence for controlling influence of particle interaction over ARM.

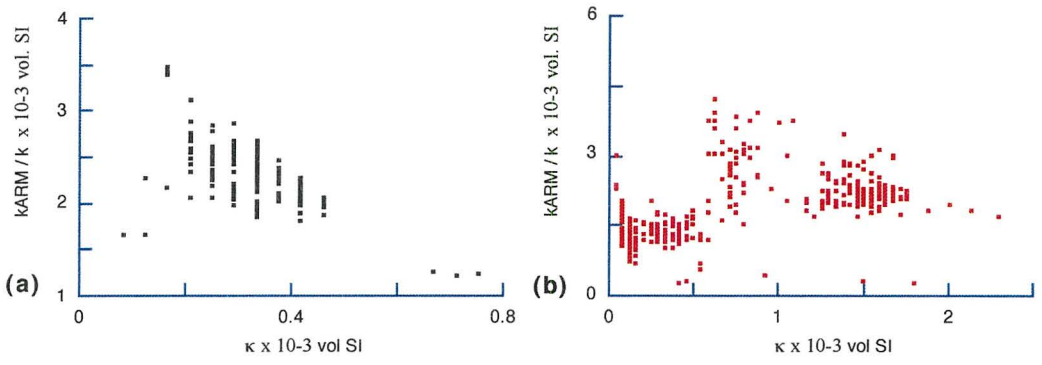

Figure 5.6: Graph of κ_{ARM}/κ vs. κ for cores (a) K47 and (b) JPC95; both plots exhibiting no strong correlation and thus implying negligible influence of particle interaction on magnetisation intensity for this core.

5.3.4 Comparison of RPI from different normalising parameters

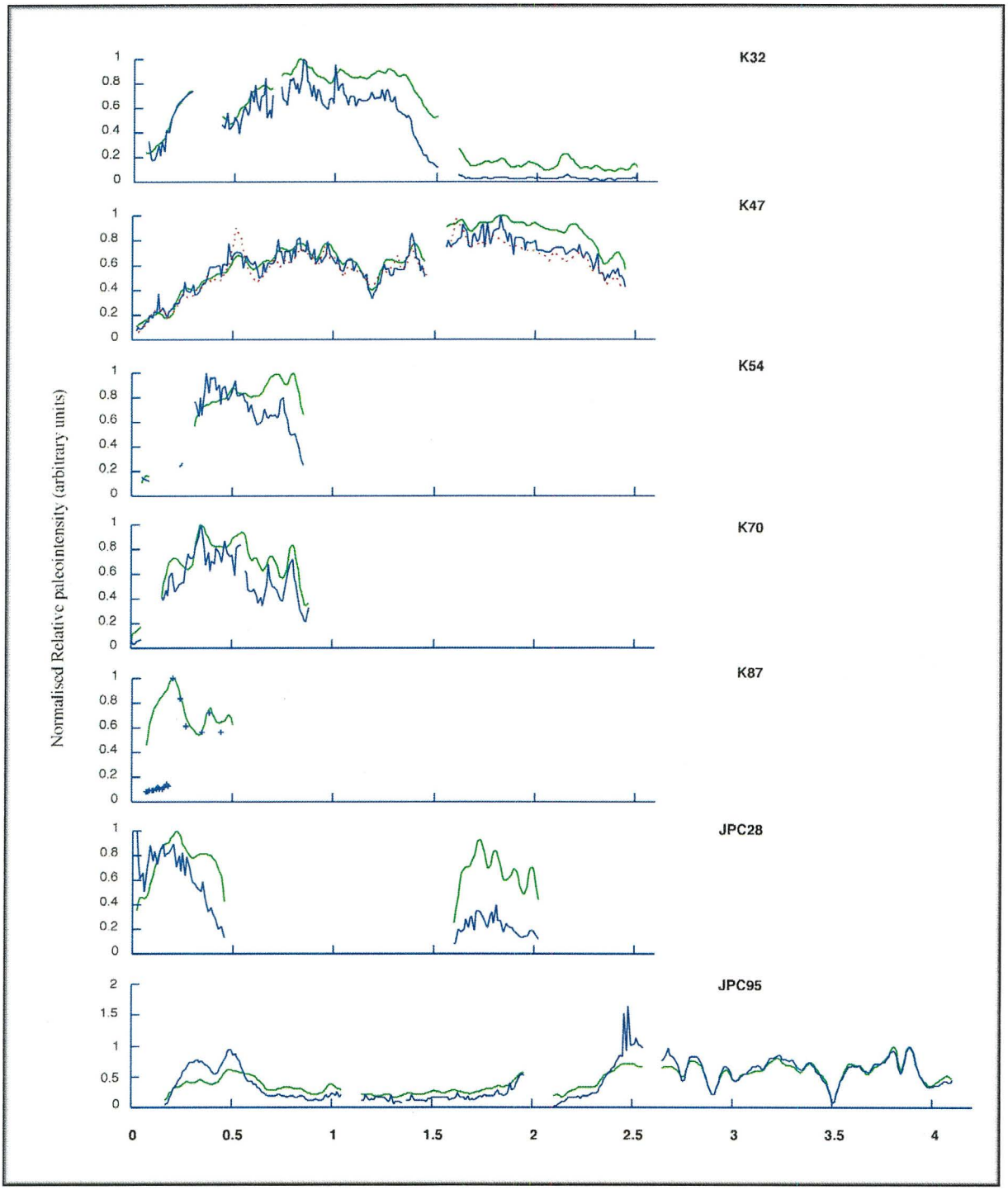

Figure 5.7: Comparison between relative paleointensity (RPI) estimates obtained though normalising ChRM (NRM after removal of viscous components of magnetisation) by saturation ARM (green) and by low-field susceptibility (blue) for all cores used in this study. For core K47 NRM normalised by saturation IRM is also plotted (red dotted line). Agreement of results using different parameters validates the resultant normalisations. Sections of K54 and JPC28 for which uniformity criteria are not met may produce spurious estimates of relative paleointensity, and are thus omitted.

The high level of concordance between RPI estimates for core K47 (Fig. 5.7) derived using multiple normalisation parameters (saturation ARM, κ and saturation IRM) corroborates the validity of this record. Such agreement provides confidence that estimates of RPI obtained from this core are reliable. RPI estimates using κ and sARM are also relatively concordant for cores K70, JPC95 and upper K32. Deviation between sARM and κ normalisations is greatest in cores K54, and JPC28. These are interpreted to be a consequence of non-uniform rock magnetic properties and are thus excluded from further interpretation.

5.4 Description of relative paleointensity records

5.4.1 Identification of unreliable RPI data

In core K32, a distinctive decline in RPI is evident below ~ 1.38 m (Figs. 5.1, 5.7). Although criteria pertaining to uniformity (King et al., 1983) are met for this core, rock magnetic analyses reveal coarsening below this depth from magnetic grain sizes of ~1 μm above 1.38 m to ~20-25 μm below (Fig. 4.8a). Thus in the interests of maximizing reliability of the relative paleointensity record, only the record above 1.38 m (only) is considered further. Relative paleointensity in core K47 exhibits a gradual increase from the surface to a broad high between ~ 0.5 and 1 m. An RPI low of 0.4 RPI units at 1.19 m is underlain by a broad high, with maximum RPI occurring at 1.83 m; below this depth, RPI declines to mid-range values (~ 0.6 RPI units) towards the core base (2.44 m).

Estimates of RPI for core K54 using sARM and those using κ are inconsistent even for the upper part of this core (Fig. 5.7), for which uniformity criteria are satisfied. The normalisation using sARM is considered more reliable (see section 5.1 for justification). Relative paleointensity using sARM exhibits a rise from moderate (~ 0.6 RPI units) to maximum values (1 RPI unit) between 0.31 and 0.8 m, and a return to moderate values (0.6 RPI units) from 0.8 m to 0.85 m. In core K70, RPI appears highly variable between 0.15 and 0.88 m. The amplitude of variation, however, may be exaggerated compared with longer records that have maxima at greater depths (e.g. cores K47, JPC95). The two intervals of core JPC28 for which relative paleointensities are considered reliable consist of two highs: the upper culminating at 0.22 m; the lower at 1.73 m.

The relative paleointensity record for core JPC95 is the longest obtained from this study, both physically and temporally (see section 3.4). A broad high in the upper core down to ~ 0.5 m is underlain by a low (< 0.1 RPI units) that extends from 0.55 m to ~ 2.35 m. Magnetic grain size is coarser over this interval of low RPI (Fig. 4.9), and magnetic concentration relatively low (Fig. 4.8g). Coincidence of relatively low RPI with magnetic coarseness and low magnetic concentration, together with poor definition of directional components of magnetization, insinuate that this interval of the RPI record should be regarded with caution (though it is still presented).

5.4.2 Description of Paleosecular Variation (PSV) and Relative Paleointensity (RPI) records with available chronology

Records of paleosecular variation (inclination and declination) and relative paleointensity (ChRM/sARM) derived from Waipaoa Basin cores are presented in Figure 5.8. Average sedimentation rates (see section 3.4) are available only for cores K47 (0.86 cm/yr) and K54 (1.19 cm/yr). These rates are used to place the respective records of PSV and RPI on a common time scale (Fig. 5.9). The time interval recorded by both K47 *and* K54 (26-71 yrs B.P.) is characterised by a gradual increase in both RPI records; the general trend being apparently consistent. In contrast, fluctuations in inclination and declination signals in core K47 are inconsistent with those in core K54 over the same period. In particular, paleo-inclination derived from core K54 exhibits variations with higher amplitude (than those in K47) over this time interval (Fig. 5.9). A potential correlation with core K70, based on similarity of inclination features, is dashed in Figure 5.8. Aside from this potential match, Waipaoa records of PSV and RPI are insufficiently continuous, and contain too few prominent features, to serve as an accurate means of correlation.

Longer records of PSV and RPI from cores JPC28 and JPC95 (from outside the Waipaoa Basin) are also presented on a common time scale in Figure 5.9, based upon available tephrochronology (see section 3.4). The RPI for core JPC95 exhibits an increase from 5 to ~10 ka; inconsistent with the JPC28 RPI record, which exhibits a rise from the present to ~ 4 ka, and a decline from 4 ka to 8 ka. Generally low RPI from ~11 to ~ 29 ka is not interpreted here to represent a low in the paleofield (owing to variation in concentration and grain size – see section 5.4.1). Despite discontinuity in the two records and limited chronology in core

JPC28 (based on identification of a single tephra), the comparable timing of a broad relative paleointensity high in the relative paleointensity records from ~29 ka to ~ 32 ka supports the provisional chronology for core JPC28.

The RPI record for core JPC95 exhibits a low (of 0.21 RPI units) at 2.9 m, or ~ 35,707 $\pm$ 250 cal. yrs B.P. of ~ 1ky duration, which is concurrent with steep inclination. This is preceded by a minor peak at ~ 36.5 ka; concurrent with a shallow inflection point in the inclination record. Another RPI peak at ~ 39 ka is not accompanied by any significant inflection in inclination. A prominent feature of the RPI record from JPC95 is the distinct minimum at ~ 42,600 $\pm$ 250 cal. k.y. B.P. (3.5 m), which coincides with a shallowing of inclination (Fig. 5.9). This event exhibits the lowest RPI values and inclination angles for the period explored here. Inclination shallows from -57° to -12° over ~1 ka as declination swings by ~ 40° to the west. Inclination then steepens abruptly from -12° to -49° over ~ 100 years as declination executes a ~150° swing to the east, after which it swings back west more gradually by ~ 60° over ~1400 yrs. The excursion is preceded by two well-defined peaks in RPI at ~ 46.2 ka and ~ 47.0 ka, representing maxima in relative paleointensity for the ~50 k.y. duration of the JPC95 record; and a trough (0.35 RPI units) at ~ 48.3 ka. The PSV record from core JPC95 between 42 and 50 ka consists of several fluctuations in inclination (-53° to -83°) and declination (with amplitude ~180°).

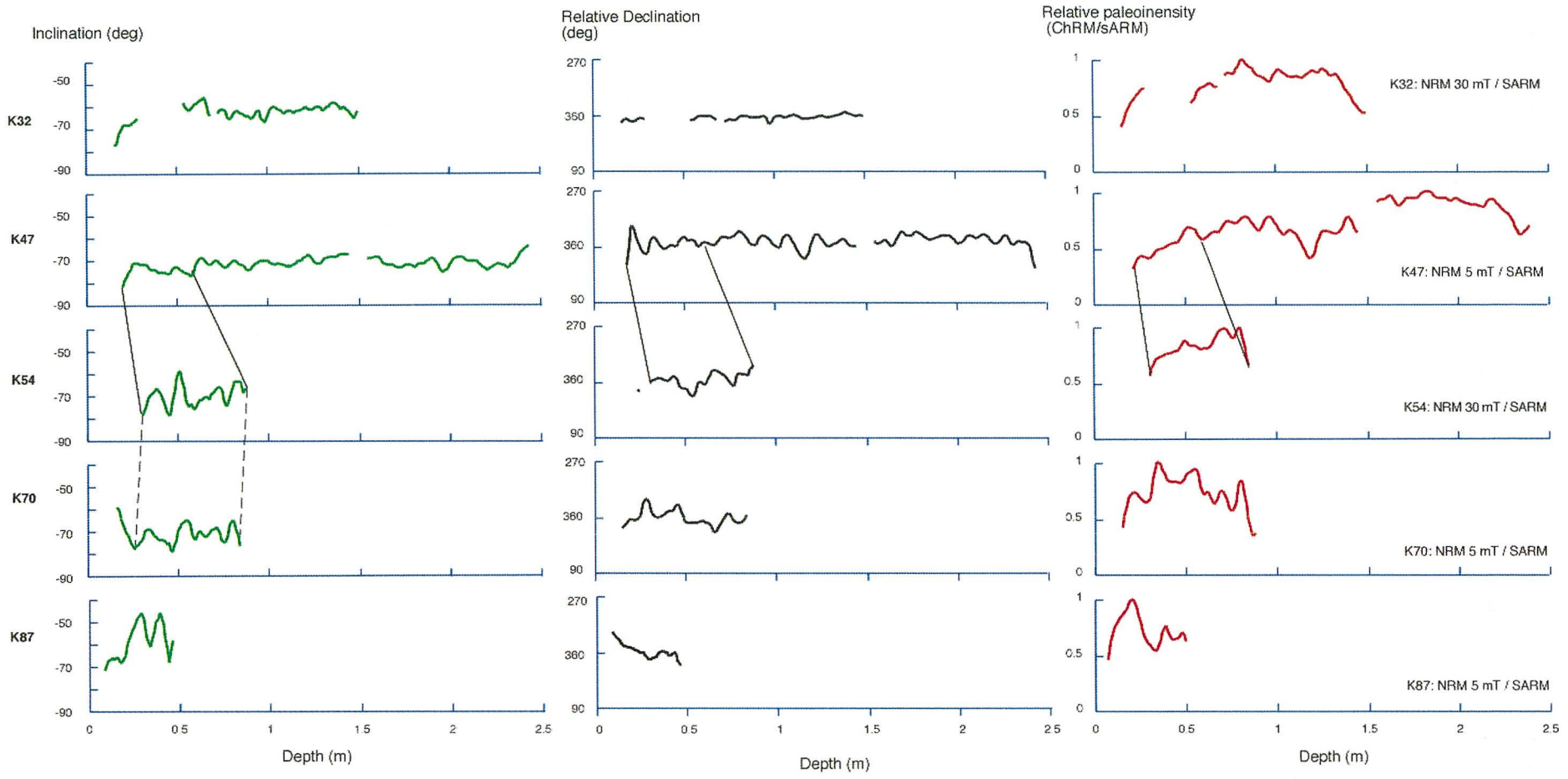
Inclination (deg)
Relative Declination (deg)
Relative paleoinensity (ChRM/sARM)
K32
K47
K54
K70
K87
-50
-70
-90
270
360
90
1
0.5
0
K32: NRM 30 mT / SARM
K47: NRM 5 mT / SARM
K54: NRM 30 mT / SARM
K70: NRM 5 mT / SARM
K87: NRM 5 mT / SARM
0
0.5
1
1.5
2
2.5
Depth (m)

Figure 5.8: Records of paleosecular variation (paleo-inclination, paleo-declination) and relative paleointensity (RPI) derived from Waipaoa Basin sediment cores. Solid lines linking the records derived from K47 and K54 define the time interval 26-71 years B.P. based on available sedimentation rates (Paul Shane, pers. comm.). Broken lines indicate potential correlation of these records (K47, K54) with that from core K70, based on similarity of inclination features.

Figure 5.9: Records of paleo-inclination, paleo-declination and relative paleointensity (RPI) from cores with independent chronological information placed on common time scales. Kasten cores from the Waipaoa Basin (K47, K54) are hundreds of years old based on sedimentation rates (Paul Shane, pers. comm.); whilst piston cores JPC95 and JPC28 extend thousands of years based upon identification of the Oruanui Formation (26.5 ka cal. B.P.) in both cores and the Mamaku tephra (8200 ka cal. B.P.) in core JPC95. Sedimentation rate for JPC28 is assumed to be uniform over the length of the entire core (as with cores K47, K54); whilst rates for core JPC95 were calculated for each interval bounded by tephra.

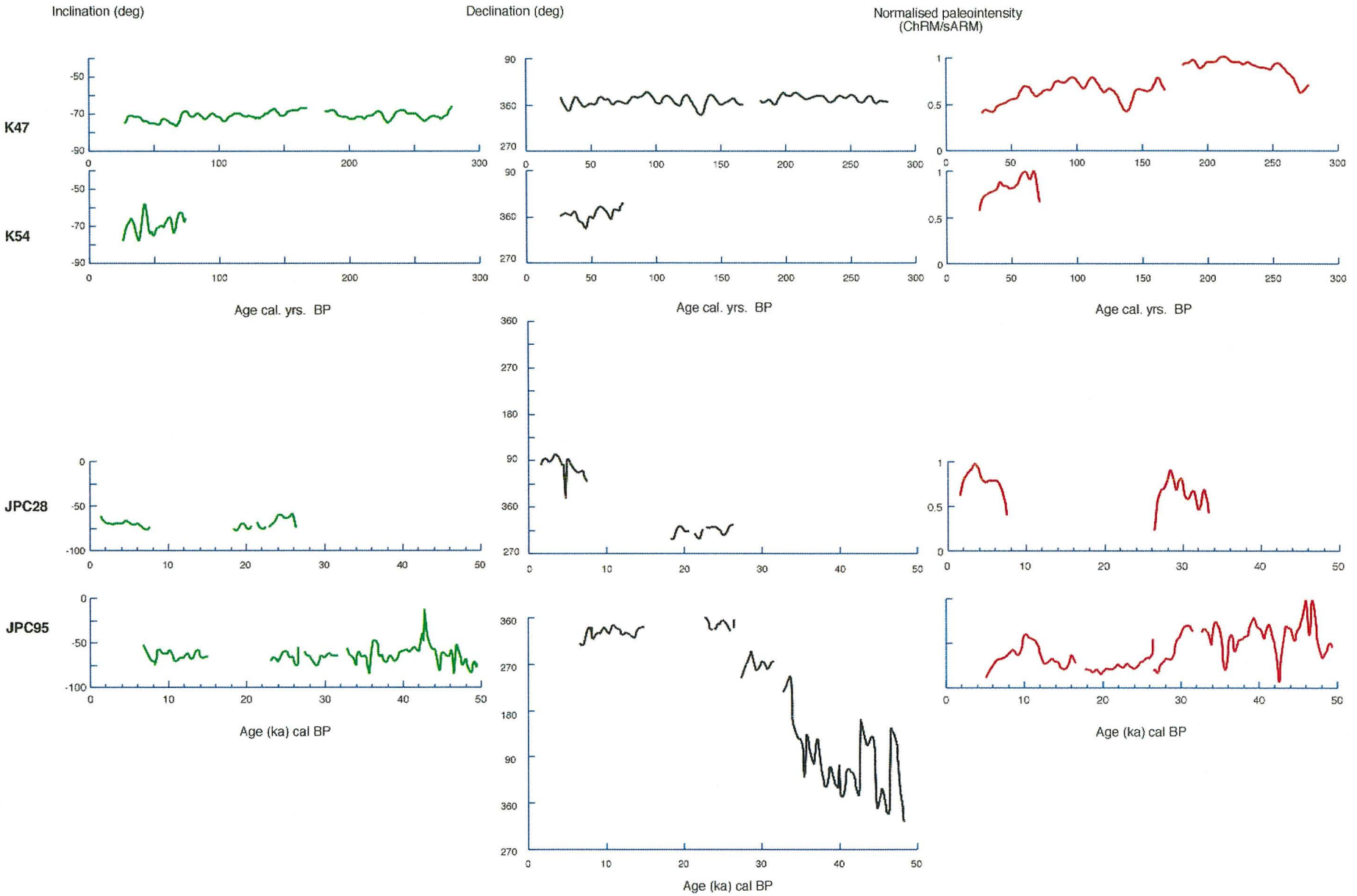
Inclination (deg)
Declination (deg)
Normalised paleointensity (ChRM/sARM)
K47
K54
JPC28
JPC95
Age cal. yrs. BP
Age cal. yrs. BP
Age cal. yrs. BP
Age (ka) cal BP
Age (ka) cal BP
Age (ka) cal BP

6. DISCUSSION

6.1 Geomagnetic Excursion Events

Geomagnetic secular variations include VGPs up to 40° removed from the geomagnetic pole; whilst VGPs exceeding this angle are classified as a geomagnetic excursion (Barbetti & McElhinny, 1976). Such excursions (as recorded in marine sediments) have the potential to provide a valuable method of stratigraphic correlation. The local, regional or global extent of recent unstable geomagnetic behaviour might also aid in constraining field reversal models and in understanding the full spectrum of geomagnetic field behaviour (Levi & Karlin, 1989).

6.1.1 Geomagnetic excursions reported for the past 50 ka

Evidence for the existence of geomagnetic excursions has been controversial (Opdyke & Channell, 1996) owing, primarily, to difficulty in detecting such features. However, several excursions from the Bruhnes Chron are now confirmed through their documentation at numerous localities, and are considered to represent perturbations in the geomagnetic field. Among those detected in the most recent 50 ka are the Mono Lake (27-28 cal. ka; Liddicoat & Coe (1979) or 31.5-33.3 GISP2 ka; Benson et al., 2003); Lake Mungo (30-32 ka; Barbetti & McElhinny, 1972); and Laschamp (46.6 $\pm$ 2.4 ka: Levi et al., 1990; 41$\pm$ 2 ka: Schramm et al., 2000) excursions.

Bonhommet & Babkine (1967) first documented the Laschamp excursion in the Laschamp and Olby flows of the Chaine des Puys lavas, Massif Central, France. The Skalamaelifell excursion, recorded in Icelandic lavas, has also been correlated with the Laschamp excursion (Levi et al., 1990). Though events of such short duration are less likely to be recorded in sediments (owing to the time-averaging of remanence acquisition), the Laschamp excursion has been identified in sedimentary records of relative paleointensity from the Mediterranean Sea and South Indian Ocean (Tric et al., 1992); Gulf of California (Levi & Karlin, 1989), Somali Basin (Meynadier et al., 1992); South Atlantic (Channell et al., 2000); Labrador Sea (Stoner et al., 2000); Amazon Fan (Cisowski & Hall, 1997); sub-polar North Atlantic and the Blake outer Ridge (Laj et al., 2000). Such widespread documentation of the event has

confirmed its association with the dipole field. Laj et al. (2004) utilized the above-listed records (Fig. 1.11) to obtain a high-resolution global paleointensity stack dating back to 75 ka (Fig. 6.2), in which the Laschamp event is unambiguously identified, as is the Mono Lake excursion.

In RPI records from the above localities, the Laschamp excursion is manifest as the lowest intensity of (at least) the past 140 k.y. (Meynadier et al., 1992). Its duration is somewhat ambiguous, owing to the "shoulders" either side of the trough in paleointensity, which complicate estimation of a baseline. However, Laj et al. (2004) constrained the duration (defined as "full width at half maximum" of intensity lows) of the Laschamp excursion to between 1000 and 1900 years.

Directions of the paleofield in the Laschamp and Olby flows deviate ~ 140 ° from the axial dipole direction (Bonhommet & Babkine, 1967), and virtual geomagnetic poles (VGPs) are 40° different to those from the excursion unit in Iceland. At both localities, however, the event is characterised by rapid inclination shallowing, and a westerly swing in declination. Absolute paleointensities covering the excursion in the Laschamp, Olby and Skalamaelifell flows are less than 15% of the field's present strength (Levi et al., 1990), whilst those of the period following are approximately two thirds the archaeomagnetic field (Salis et al., 1987).

Such abnormally low paleointensity at the time of the excursion suggests that the reversed polarity state was not fully established. A period of diminished geomagnetic moment is consistent with those obtained in the initial stages of polarity transitions (Prevot et al., 1985), during which, interferences from the non-dipole field become enhanced (Roperch et al., 1988). These may produce regional transitional directions while the main field is still dipolar, with normal polarity but reduced strength. Thus, the paleomagnetic directions of the Laschamp excursion have been interpreted to represent an aborted reversal rather than a stable reversed polarity interval (Harrison, 1980). Excursions in paleofield direction may not be observed ubiquitously if the reversal failed prior to complete destruction of the main field. Geomagnetic expression and age of the excursion may, therefore, vary for widely separated sites owing to the regional nature of the non-dipole field, and to the time-averaged versus instantaneous nature of remanence acquisition processes (Levi & Karlin, 1989).

The Mono Lake excursion is also recorded as a low in paleointensity and anomalous paleodirection. A swing in declination to the west of ~ 60° is followed by a swing to the east of ~ 40°, whilst inclination swings towards negative values (Liddicoat & Coe, 1979). The elusive nature of this excursion implies a short duration of $\leq 10^3$ years (Opdyke & Channell, 1996).

The Lake Mungo excursion, identified in aboriginal fireplaces, is accompanied by extremely high field strengths (Barbetti & McElhinny, 1972). Coe (1977) invoked various sources in Earth's outer core to account for such high intensities. More records constraining the spatial extent of the Lake Mungo excursion are required to elucidate whether dipole or non-dipole sources are responsible, as well as the shape, number and configuration of potential non-dipole sources (Coe, 1977).

The Auckland volcanic field, New Zealand, is the only other locality on Earth (besides the Laschamp, Olby and Skalamaelifell flows) where the Laschamp excursion is recorded in lavas (as well as the Mono Lake and Lake Mungo events). The excursions are manifest as intermediate paleodirections between 25 and 50 ka (Shibuya et al., 1992). The only *continuous* paleomagnetic record from New Zealand of sufficient length to record these excursions is the secular variation curve of Pillans & Wright (1990) obtained from North Island loess. From this (500 k.y.) PSV record, the authors correlated a period of anomalously low inclination with the Lake Mungo Event (30-32 ka). Though no reference was made to the Laschamp excursion, the Mungo Event is immediately preceded in the record (at ~ 40 ka according to their time scale) by extreme negative inclinations, and the lowest NRM intensities of the record. Despite lack of a normalised paleointensity record, Pillans & Wright (1990) believed that their NRM record faithfully reflects changes in strength of the paleofield.

6.1.2 Geomagnetic excursions recorded in core JPC95

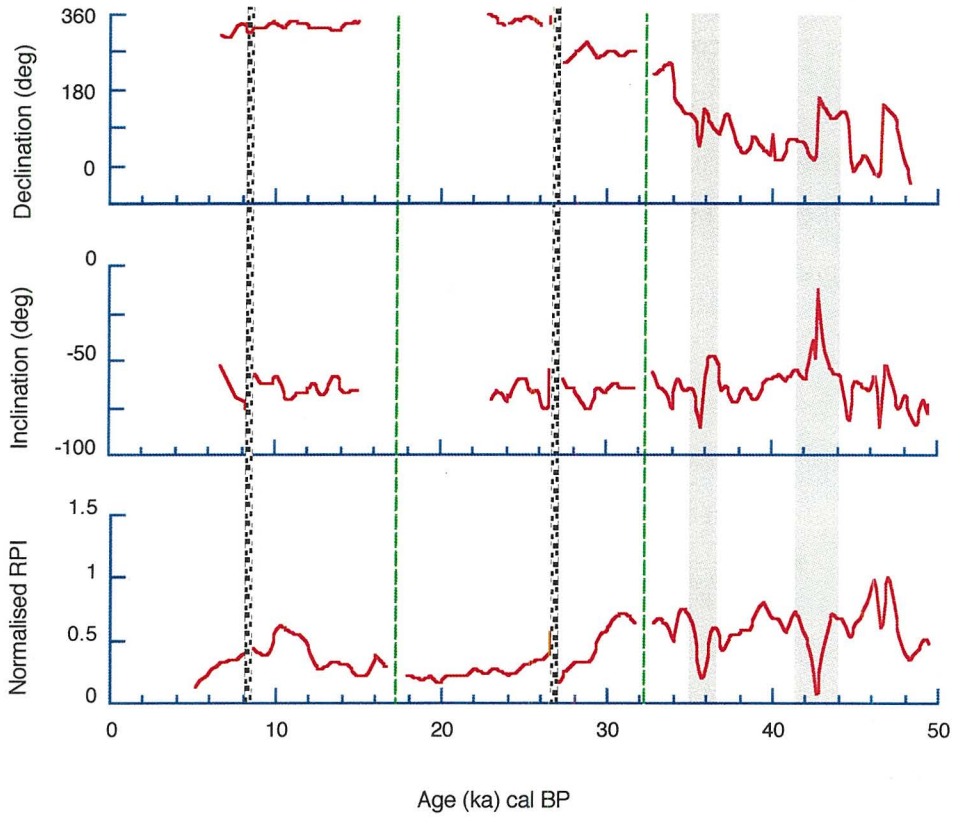

Figure 6.1: Records of paleo-declination (potentially affected by rotation during core penetration), paleo-inclination and relative paleointensity of Earth's geomagnetic field extracted from core JPC95. Broken green lines mark core section boundaries (1.1 & 2.6 m). Grey area defines anomalous lows at 42,600 ± 250 cal. yrs B.P., and 35,707 ± 250 cal. yrs B.P. The former age lies within the potential error limits defined for the Laschamp excursion (41 ± 2 ka; Schramm et al., 2000).

A chronology based solely upon ages of the Mamaku Ash (8,200 ± 10 cal. yrs B.P.) and Oruanui Formation (26,500 ± 240 cal. yrs B.P.) identified within this core, places the minimum in core JPC95 RPI record at ~ 42,600 ± 250 cal. yrs B.P. (Fig. 6.1); consistent with the reported age of the Laschamp excursion (Bonhommet & Babkine, 1967; Levi et al., 1990; Roperch et al., 1988). Grain size and magnetic concentration do not vary across the excursion, nor do they differ from those characterising sediment above and below (Fig. 4.8g). Magnetic susceptibility (κ) exhibits no substantial perturbation over the low, though coercivity (inferred from MDF) is more variable between 42.7 and 43.2 ka (± 240 yrs) than before or after. On the

basis of the age coincidence, anomalous inclination behaviour and relative paleointensity determinations, the feature at 42,600 ± 250 cal. yrs B.P. is correlated with the Laschamp excursion. The duration of the excursion in core JPC95 (based on the available tephrochronology) is ≤ 2 k.y., consistent with that estimated by Laj et al. (2004). Several prominent features of the GLOPIS-75 stack of Laj et al. (2004) are also evident in the JPC95 RPI record; which justifies the use of the excursion as a tie point, to better constrain the chronology for core JPC95. The resulting attuned RPI record is presented against the GLOPIS-75 stack in Figure 6.2.

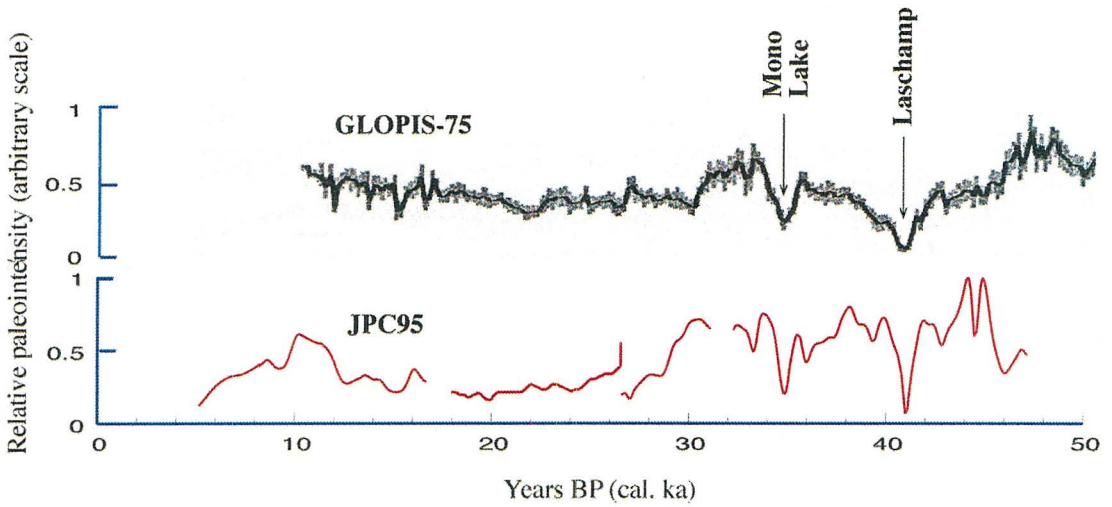

Figure 6.2: Comparison of the RPI record derived from JPC95 (lower curve) with the GLOPIS-75 paleointensity stack (upper curve; Laj et al., 2004). Note that the age of the Laschamp excursion in the stack (~41 ka) has been used to fine-tune the tephra-based chronology of JPC95.

The available tephrochronology places the marked low in the JPC95 RPI record following recovery from the Laschamp excursion, and accompanied by more negative inclination at 35,707 ± 250 cal. yrs B.P. (and constrains its duration to ~ 1 k.yrs.). This trough in RPI is also apparent (at 34.6 ka) in the paleointensity stack (Fig. 6.2) of Laj et al. (2004), who correlates it with the Mono Lake excursion, based on the most recent estimate for its age (31,500 – 33,300 GISP2 yrs B.P.; Benson at al., 2003). Using the Laj et al. (2004) stack to fix the Laschamp excursion in core JPC95 at 41 k.y., the position of the later intensity low shifts to 34,786 ± 250 cal. yrs B.P. This age, together with similar trends in inclination to those

recorded by Liddicoat & Coe (1979), and comparable durations, provide justification for correlating this feature in core JPC95 with the Mono Lake excursion.

Relative paleointensity is high at ~ 31 ka in the JPC95 record; close to the documented time of the Lake Mungo excursion (~30 ka). However, lack of a pronounced peak in RPI or anomalous paleodirections preclude correlation with the Lake Mungo Event.

6.1.3 Path of the dipole field during the Laschamp Excursion

Figure 6.3 illustrates the behaviour of paleo-inclination during the Laschamp and Mono Lake excursion events as recorded in cores from the South Atlantic, southwest Pacific and lake Baikal, Siberia. Both of the Southern Hemisphere records exhibit shallowing and a shift to less negative values during the Laschamp excursion.

Core JPC95 was retrieved from longitude 177.44°E; and cores 5PC01, 4PC03 (South Atlantic) from longitudes of 9.66°E and 9.93°E, respectively. Assuming that the Laschamp event constitutes an excursion of the dipole field, the observation that inclination shallows at both of these sites, separated by ~168° of longitude, provides significant constraints on the path of the dipole during the Laschamp excursion. The consistent sense of change at these sites indicates that they both lie on the same side of the axial plane of no net change (Fig. 6.4); which strikes perpendicular to the direction of polar shift, and dips at an angle bisecting the pole's angular displacement. This plane must strike between 357.44° and 9.66°E; thus the excursion of the north geomagnetic pole took place along a longitudinal path of 87.44°E-99.66°E.

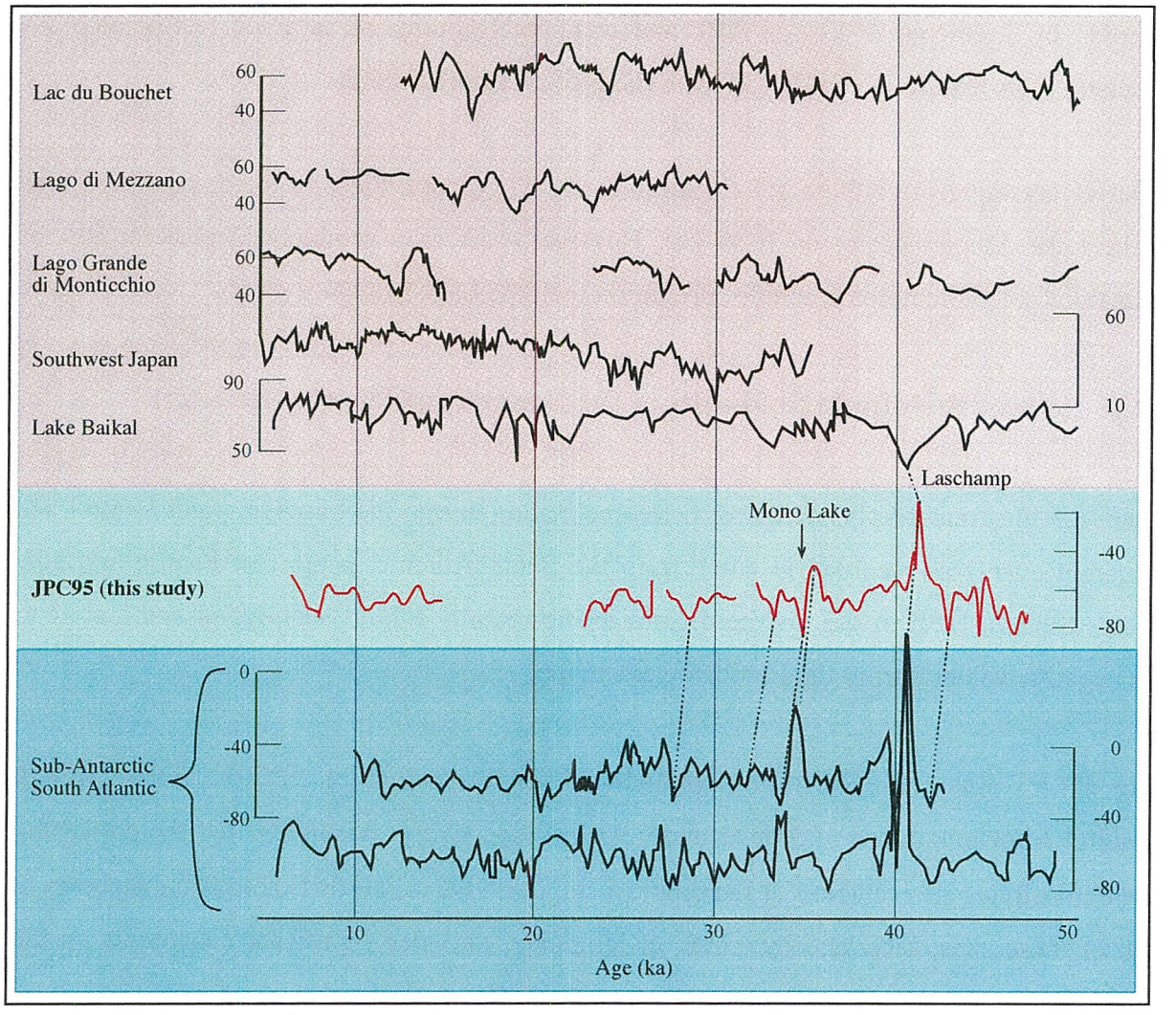

Figure 6.3: Comparison of inclination record preserved in core JPC95 with various records from the Northern Hemisphere (upper zone) from Lac du Bouchet (Thouveny et al., 1990); Lago di Mezzano and Lago Grande di Mizzano (Brandt et al., 1999); southwest Japan (Ohno et al., 1993) and Lake Baikal (Peck et al., 1996); and two records from the Southern Hemisphere (lower zone): sites 5PC01 (lower) and 4PCO3 (upper) from the sub-Antarctic South Atlantic (Channell et al., 2000). Broken lines mark inferred tie points of correlation.

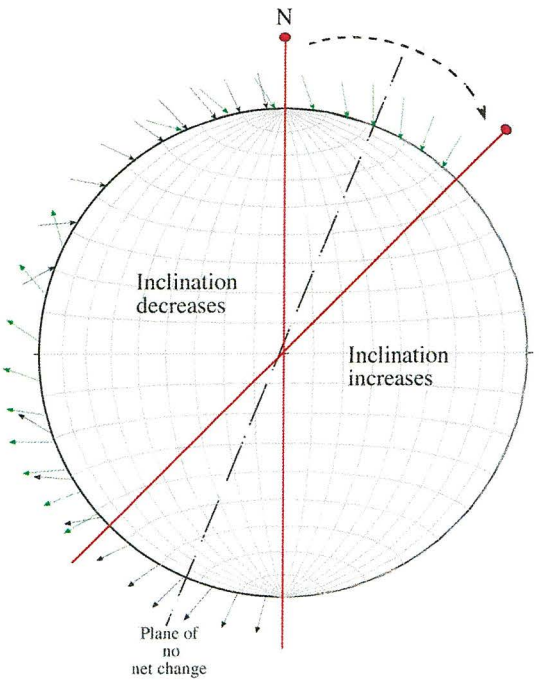

Figure 6.4: schematic illustration showing effect of meridional displacement of the north geomagnetic pole on field direction around the globe. In this example the pole is displaced by 45° of longitude from the north geographic pole. This results in an increase in magnetic inclination in half of the world and a decrease in inclination in the other half, separated by the plane of no net change (dashed). Black arrows show field inclination at Earth's surface for a GAD; green arrows show field inclination at the surface after tilting the dipole by 45°. Sites showing the same sense of change must therefore lie on the same side of the plane of no net change.

Inclination at Lake Baikal also shallows (decreases) during the Laschamp excursion event to I ~ 40° (GAD I = 68.94° at latitude 52.4°N). The angular deviation of the pole from geographic north necessary to approximate the observed inclination changes at all three sites was investigated through the following derivations of the dipole equation:

$$\cos p = \sin(\lambda_p) \sin(\lambda_s) + \cos(\lambda_p) \cos(\lambda_s) \cos(\phi_p - \phi_s) \quad [6.1]$$

and

$$I_x = \tan^{-1}(2 \cot p) \quad [6.2]$$

where p represents the angular distance from site to pole; λ_p and λ_s represent latitude of pole and site, respectively; ϕ_p and ϕ_s represent longitude of pole and site, respectively; I_x represents expected inclination based on the dipole equation (equation 1.1).

Various values of λ_p were substituted using 87.44°E < ϕ_p < 99.66°E, to yield values of I_x that most closely approximate those observed at all three sites during the Laschamp excursion. No single VGP can account for the observed paleofield directions at Lake Baikal, Bay of Plenty (JPC95) *and* the South Atlantic. However, all are accounted for by a deviation of between 80° and 110° from the geographic pole, along the meridian 87.44°E (Fig. 6.5). This displacement is that which yields inclinations most closely approximating those observed at all four sites. The inability of a single VGP to explain all of the observed inclination changes (at all sites) during the Laschamp excursion is attributable to the enhanced interference from (regional) non-dipole signals during the period of reduced dipole intensity.

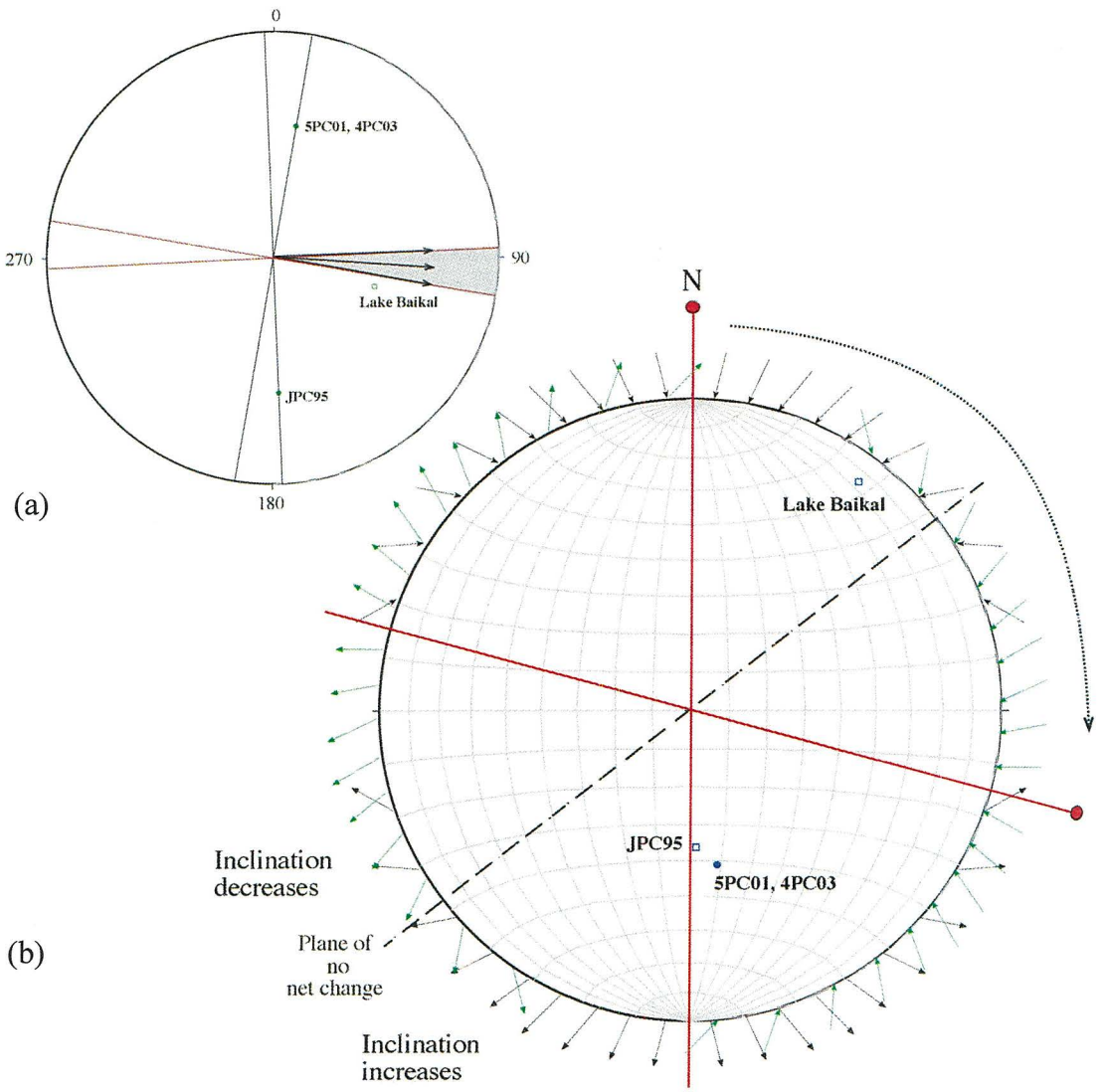

Figure 6.5: **(a)** View from north geographic pole, showing sites mentioned in text and potential range for the plane of no net inclination change (black). Perpendicular to these are the potential directions of longitudinal pole displacement (shaded region defines the range). By convention filled circles are in the (lower) Southern Hemisphere; hollow circles in the (upper) Northern Hemisphere. **(b)** Schematic illustration of Earth (as viewed from 0°E) showing effects of an excursion (of 105° in the dipole field along longitude ϕ = 90°E), on inclination. Black arrows show field inclination at Earth's surface for a GAD; green arrows show field inclination at the surface after tilting the (geocentric axial) dipole by 105°. Inclination increases (becomes less negative) at sites JPC95, 5PC01, 4PC03 and decreases at Lake Baikal (as observed in Fig. 6.3). By convention hollow circles lie in the upper hemisphere (270-90°E); filled circles are in the lower hemisphere (90-270°E).

6.2 Interhemispheric correlation of RPI

The global manifestation of the Laschamp and Mono Lake geomagnetic excursion and some other millennial scale RPI features is established in Figure 6.2. However, a greater number of tie points are identified when comparing the JPC95 RPI (this study) to the various individual records used to compile the Laj et al. (2004) stack (GLOPIS-75), of which a sample are presented in Figure 6.6. The manifestation and exact timing of some (subordinate) pre- and post- Laschamp features varies between studies. Major features, however, are broadly consistent back to ~ 75 ka (Laj et al., 2004). Not all millennial-scale features in the JPC95 RPI record are apparent in all other records of RPI. However, a number of features in this record from the South Pacific (with time constants of < 1 k.y.) are also manifest in some records from the sub-polar North Atlantic (core PS2644-5), South Atlantic (ODP site 1089; 4-PCO3, 5-PC01) and Blake Outer Ridge-Bermuda Rise (cores MD95-2034; CH88-10P), which implies that a dipole signal is recorded in each case. A high degree of similarity is evident particularly when comparing the JPC95 RPI record to those from the South-Atlantic Ocean (Channell et al., 2000; Stoner et al., 2002); some of which are separated from core JPC95 by only 4° of latitude. In addition to the Laschamp and Mono Lake excursions, several peaks preceding the Laschamp and a peak immediately post-dating the Mono Lake excursion are common to records from both Northern and Southern Hemispheres.

Time constants shorter than 600-700 yrs are not associated with dipole field variations; but with non-dipole terms (Hulot & Le Mouel, 1994), and thus do not necessarily correlate worldwide. Comparison of data from this study with other sedimentary records supports the notion that geomagnetic excursions *and* millennial-scale features of paleointensity (some with time constants of < 1 k.y.) are globally correlative. This implies that the RPI record from core JPC95 is driven by fluctuations of a dipolar nature and attains a resolution comparable to the shortest time constants associated with dipole field variations, according to Hulot & Le Mouel, (1994).

Features with time constants < 600-700 years are apparent in the RPI record from core K47. Ascertaining the spatial extent of these signals will require comparison with other records that achieve similar resolution and continuity. Considering that sediment influxes in the Waipaoa

Basin are among the highest on Earth, localities with the potential to provide such records may be limited. The Gulf of Papua, Papua New Guinea and coastal areas of the East Indies and Philippines are potential candidates. Such a comparison would test the potential application of relative paleointensity as a high-resolution correlation tool on sub-millennial, or human time scales; as has been established here down to ~ 600-700 yr. time scales using core JPC95. Though sub-millennial variations in the RPI signal may not be globally correlative, consistency of RPI features even on a regional scale (should this be established) may aid significantly in constraining the timing of paleoclimatic events.

Figure 6.6: Comparative presentation of relative paleointensity records from this study (JPC95) and others from the north and South Atlantic used (among others) to produce the GLOPIS-75 global stack (Laj et al., 2004). All records are reported on the GISP2 age model after correlation with NAPIS-75. All records are presented on a common scale of normalised RPI units. Broken lines depict identified points of correlation between the records: black tie lines are those identified by Laj et al. (2004) and used for correlation; red tie lines link core JPC95 to the other records.

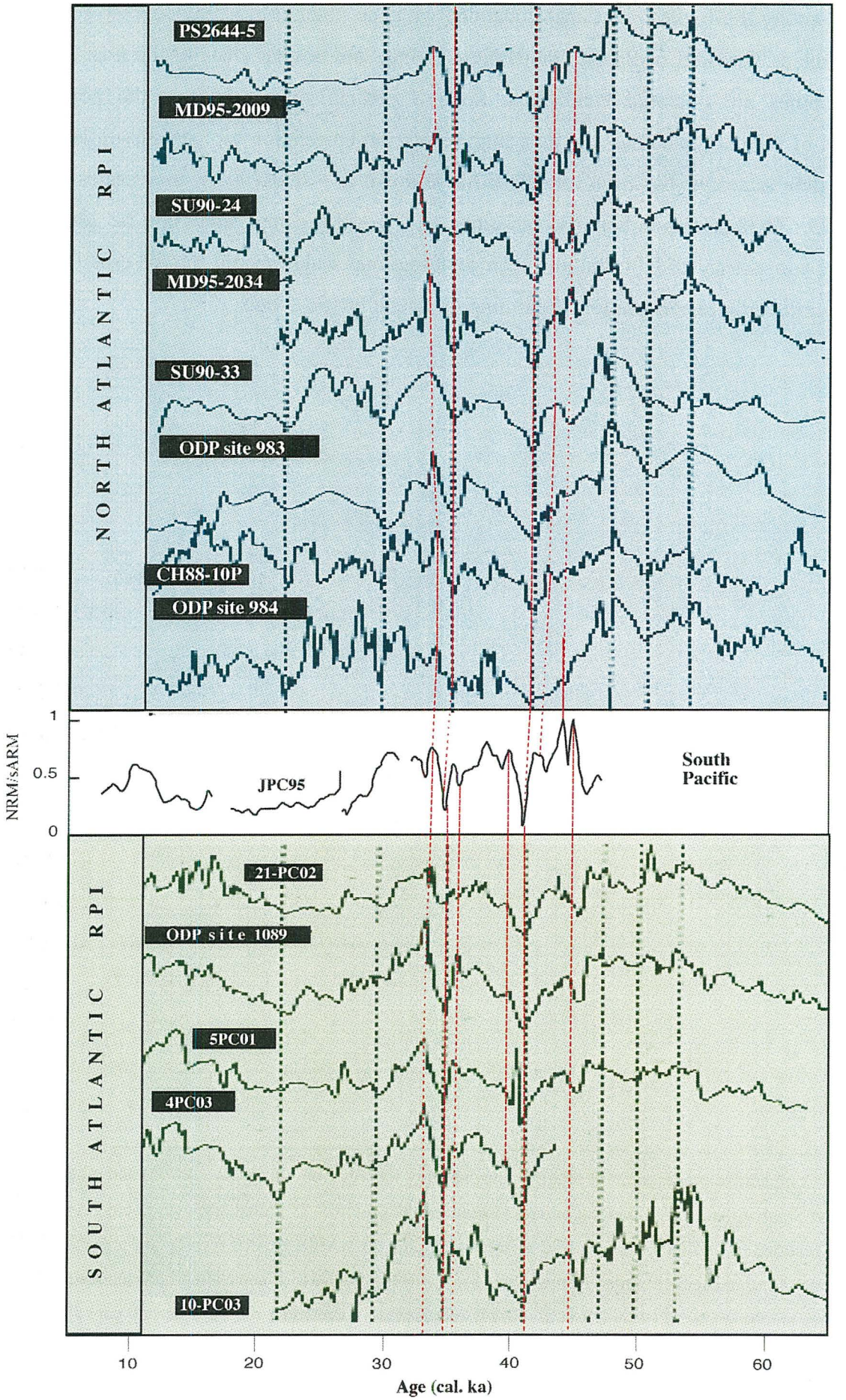
NORTH ATLANTIC RPI
PS2644-5
MD95-2009
SU90-24
MD95-2034
SU90-33
ODP site 983
CH88-10P
ODP site 984
NRM/sARM
1
0.5
0
JPC95
South Pacific
SOUTH ATLANTIC RPI
21-PC02
ODP site 1089
5PC01
4PC03
10-PC03
10
20
30
40
50
60
Age (cal. ka)

6.3 Regionality of Paleosecular Variation (PSV)

Despite a lack of published secular variation records, particularly from the Southern Hemisphere, covering a comparable time frame to core JPC95 (~ 50 ka), it is evident in Figure 6.3 that the JPC95 inclination record exhibits greater coherence with records from the Southern Hemisphere than it does with various Northern Hemisphere curves. In particular, both records from the Southern Hemisphere exhibit similar perturbations at the times of the Laschamp (~ 41 ka) and Mono Lake (~ 35-36 ka) excursions. Amplitudes of these excursions are much more pronounced in the Southern Hemisphere inclination records than in their northern equivalents. Such inter-hemispheric differences are interpreted to reflect the greater manifestation of non-dipole signals in their respective source regions, as the intensity of the dipole field became reduced during each geomagnetic excursion event.

Features in the JPC95 PSV record occur ~ 1 k.y. earlier than their equivalents in the South Atlantic cores (Fig. 6.3), which is also apparent when comparing the respective RPI records from each region; though only prior to correlation with NAPIS-75 by Laj et al. (2004). The time lag is therefore most likely due to errors in chronology in cores 4-PCO3 and 5-PC01, given that core JPC95 is attuned to the GLOPIS-75 relative paleointensity stack. The lag does not constitute evidence for longitudinal drift of the non-dipole field.

Aside from the excursion events, several less definitive tie points are apparent between the South Pacific and South Atlantic records (Fig. 6.3), suggesting that higher frequency (~1 k.y.) millennial-scale inclination features are correlative on a hemispheric scale. No such correspondence is evident when comparing records from the Northern Hemisphere, implying that the millennial-scale PSV signal in the Southern Hemisphere extends from the South Pacific to South Atlantic - potentially hemispheric in extent; but not global. Asymmetry in the PSV signal inherently implies temporally persistent (~ 30 k.y.) asymmetry in the boundary conditions responsible for such variability. This may be attributable to a single, hemispheric-scale non-dipole source; or some property of the dipole field that produces directional variability that is hemisphere-dependent. Consistency in PSV over an angular distance of almost 180° may, alternatively, reflect enhanced manifestation of the (global) dipole signal in

both sets of Southern Hemisphere records; possibly due to relative weakness of non-dipolar features at both localities on this time scale.

Excluding the Laschamp and Mono Lake excursions (of dipolar origin), the fluctuations in core JPC95 inclination are of comparable amplitude to those in the South Atlantic, at least from ~ 22 ka to 47 ka (the most continuous portion of the JPC95 record; Fig. 6.3). This observation suggests that the Pacific non-dipole low is not manifest in New Zealand on this time scale; though longer and more continuous records are necessary to confirm this implication.

6.4 Inclination anomaly characterising the south-west Pacific

Elmelah et al. (2001) used data from New Zealand Northland Volcanics, integrated with data from the Solomon's region and north Fiji Basin, to propose that a negative inclination anomaly (equation 1.2) of at least 10° characterises the southwestern Pacific during the Bruhnes Chron (Fig. 6.7). No significant departure from the GAD value is evident from 1.5 to 2.5 ka in the New Zealand composite curve (Turner & Lillis, 1994); nor in lacustrine records from southeastern Australia back to 3 ka (Barton & Barbetti, 1982); nor in cave sediments from New Zealand, dated ~120-130 ka (Turner & Lyons, 1986).

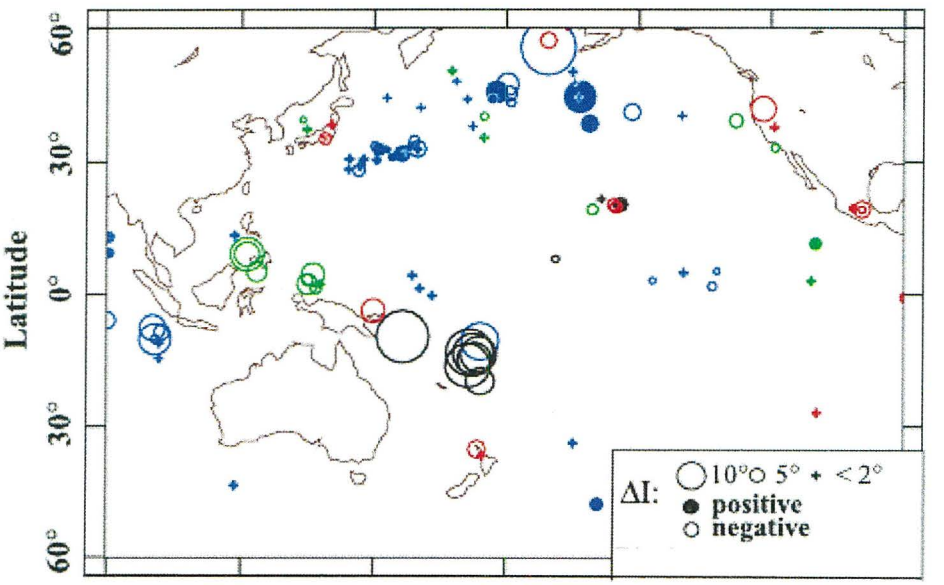

Figure 6.7: Map of inclination anomalies for the Bruhnes Chron using sedimentary and volcanic data (after Elmelah et al., 2001). Sizes of circles are proportional to the amplitude of the anomaly; colours indicate source of paleomagnetic data: Black = marine sediments (Elmelah et al., 2001); Red = volcanics; Blue = Lamont database; Green = other sediments.

Inclinations derived from the longest core in this study, JPC95, yield an overall mean of -64.5°. The value for this region predicted from the Geocentric Axial Dipole formula (equation 1.1) = -56.4°. Thus the inclination anomaly obtained from sediment core JPC95 is ΔI = -8.1°; which is greater than that reported for the Northland volcanics (~ 5° according to Elmelah et al., 2001); and implies that the mean field in this region (over the time span of these data) is steeper than that predicted from the GAD model. A non-zonal structure with such longevity may be explained by mechanisms such as thermal core-mantle coupling and/or the influence of core-mantle boundary topography on core convection, as suggested by Elmelah (2001) and Gubbins & Gibbons (2004).

The negative inclination anomaly calculated from core JPC95 results in a far-sided virtual geomagnetic pole (VGP) for the past ~ 47 ka. This result is also consistent with the model of Wilson (1971), which accounts for far-sidedness of VGPs with a northward shift of the main axial dipole; and with that of Merrill & McElhinny (1977), which implies a mathematically equivalent permanent quadrupole moment. Both of these authors model an axi-symmetric response that requires mean field at *all* Southern Hemisphere sites to be steeper than the GAD value; not just those from the southwestern Pacific.

Elmelah et al. (2001) report a large inclination anomaly in the southwestern Pacific; but the data set includes few sites elsewhere in the Southern Hemisphere. Brown (2002) reported an inclination anomaly of only -0.5° at Easter Island (southeastern Pacific). More data from the southern central and eastern Pacific, and South Atlantic are required before the models of Wilson (1971) and Merrill & McElhinny (1977), can be validated or refuted; and to constrain further the spatial extent and longevity of the proposed anomaly.

6.5 Extent of the Pacific non-dipole Low

The degree of VGP dispersion for a population of directions provides an estimate of secular variation, commonly quantified by the parameter Angular Standard Deviation (ASD); or the circle containing 66% of the data. Cox (1969) reported an ASD of 19.6° from paleomagnetic measurements on 22 volcanic formations spanning the last 0.68 m.y. This value is higher than that predicted from PSV models F (Merrill & McElhinny, 1983; Fig. 6.8) and G (McFadden & McElhinny, 1997), which is ~ 14.5° - 16°. Shibuya et al. (1995) calculated an ASD of 11.5° for northern New Zealand, using virtual geomagnetic poles (VGPs) obtained from monogenic volcanoes. In contrast to the findings of Cox (1969), this value is much lower than predicted by PSV models. From this result, Shibuya et al. (1995) inferred that the Pacific non-dipole low is as large as the Pacific Ocean, and thus should be regarded as a global feature of non-axisymmetry; rather than a local feature in an axisymmetric PSV distribution.

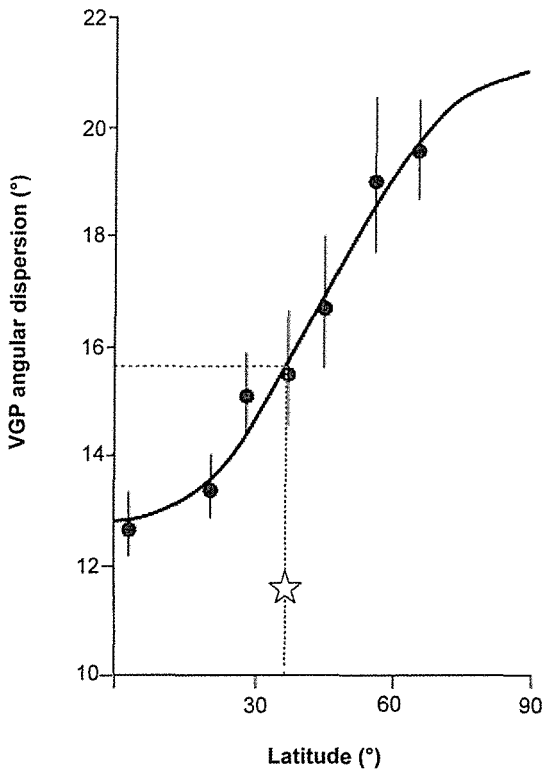

Figure 6.8: Least squares fit to paleosecular variation (PSV) data spanning the last 5 my. Error bands are 95% confidence limits; star marks estimate of ASD from this core JPC95 (11.6°) at latitude λ of ~37°S, which closely approximates that of Shibuya et al., (1995) of 11.5° for a latitude λ of ~ 35°S. Modified after Merrill & McElhinny (1983).

The lack of inter-hemispheric tie points in PSV records presented in Figure 6.3 implies that the inclination signal cannot be solely due to a dipole field. Though a greater degree of similarity is evident when comparing Southern Hemisphere records, amplitudes of some inclination features correlated between New Zealand (JPC95) and South Atlantic (5PC03, 4PC01; Channell et al., 2000) records, appear enhanced in the South Atlantic. Assuming that such variability in paleodirection (Fig. 6.6) represents a non-dipole field signal, the amplitude difference may be interpreted as evidence for the alleged 'Pacific non-dipole low' (Merrill et al., 1998). However, other features e.g. the variability in inclination preceding the Laschamp excursion, appear more pronounced in the JPC95 record. A more continuous PSV record from the Pacific, and a greater number of tie points are required to resolve this issue.

The ASD of virtual geomagnetic poles derived from the JPC95 PSV record was calculated in order to provide a statistical comparison to the results of Shibuya et al. (1995). Each reliable measurement of paleodirection from core JPC95 has been used to calculate a virtual geomagnetic pole (Fig. 6.9; see appendix 9.5 for calculations). Measurements were made every centimetre down-core, which, using the available chronology, represents ~ 100-300 years (though each is temporally smoothed according to response functions for the SQUIDS). Intermediate directions characterising the Mono Lake and Laschamp geomagnetic excursions, each with a duration of ~ 1ky (Laj et al., 2000; Liddicoat & Coe, 1979), were excluded from these calculations. These field directions are not considered representative of normal geomagnetic behaviour, nor of secular variation. The ASD for core JPC95 was approximated through the following relationship to the precision parameter k (equation 6.1), which measures 6.1 for calculated VGPs from core JPC95 (Fig. 6.9). Measurements used to construct the VGP distribution and ASD statistic presented here do not represent evenly distributed sampling intervals from the present day back to ~ 47 ka (age at core base). Although a total of 4.11 m of core was measured, 185 measurements of paleofield direction were classified either as unreliable, or as being associated with geomagnetic excursion events.

$$ASD = \left[\frac{81}{\sqrt{k}}\right] = 32.8° \qquad [6.1]$$

This value of ASD (for VGPs from core JPC95) is significantly higher than the estimate of Shibuya et al. (1995) of 11.5°, and thus cannot be interpreted to support their interpretation that the Pacific non-dipole low *is* manifest in New Zealand over this time scale (~ 50 ka).

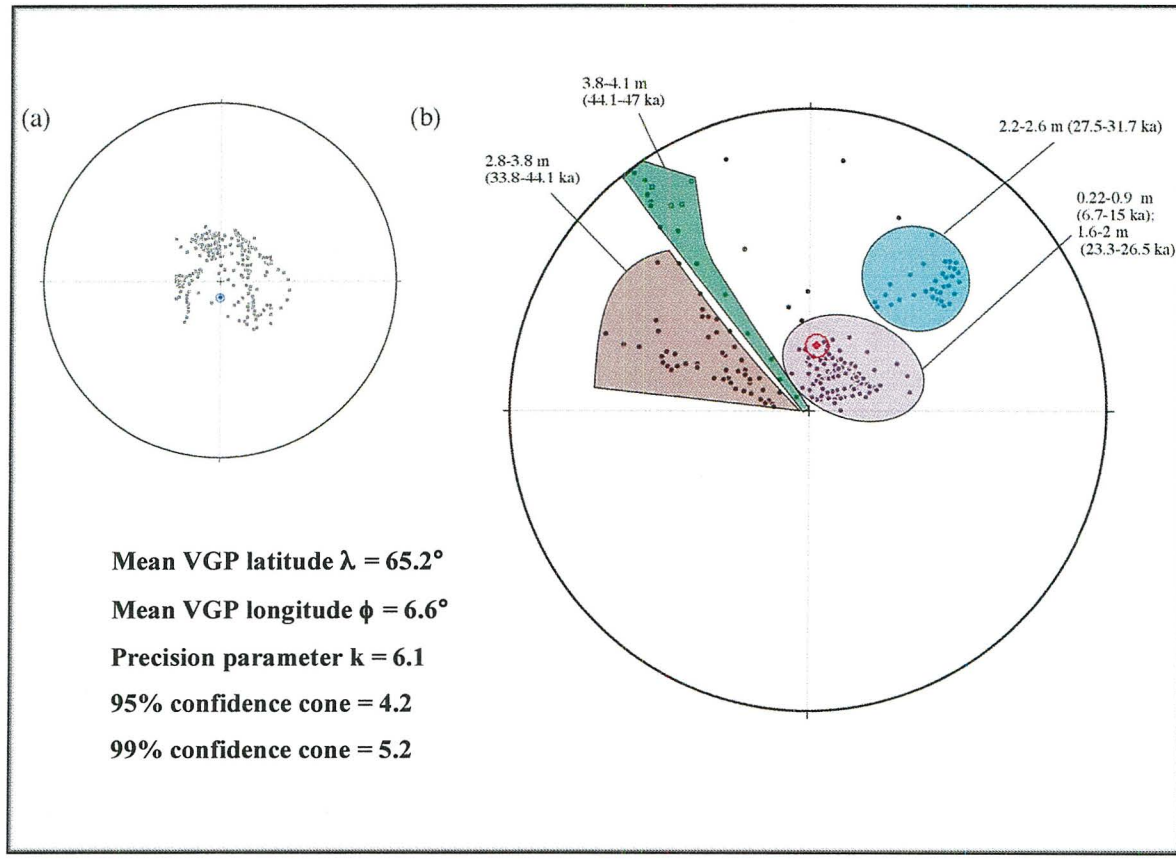

Figure 6.9: Equal angle projections of (a) Plaeo-field directions from core JPC95, and (b) virtual geomagnetic poles (VGPs) calculated from paleofield directions measured in core JPC95 (both plots excluding unreliable measurements and intermediate directions associated with geomagnetic excursions). Blue diamond in (a) and red diamond in (b) mark positions of the Fisherian mean, encircled by the 95% confidence cone. Open and closed circles indicate Southern and Northern Hemispheres, respectively. Groupings define specified depth intervals in core JPC95.

The VGP distribution for core JPC95 varies with depth interval (Fig. 6.9). Estimates of VGPs for the basal 0.2 m of core (~ 44 ka to ~ 47 ka) plot furthest from the geographic pole at low latitudes; several in the Southern Hemisphere. Some measurements from the 2.8 m - 3.8 m interval also approach equatorial latitudes. Such large displacements from the north geographic pole over these intervals are likely to reflect unreliable declination, as a direct result of rotation during core penetration.

The upper 2 m of core yields VGPs that are proximal to the geographic pole, but somewhat far-sided with respect to the core site; as are all VGPs for this core. The fact that the mean VGP does not coincide with the geographic pole may demonstrate that 30,000 years is insufficient time to average out secular variation of the dipole field. This is also suggested by the correspondence of VGP clusters to various depth intervals in the core, as illustrated in Figure 6.9. However, studies that have reported clustering of VGPs about a mean centred at the geographic pole have used data compilations from multiple regions around the globe to provide a spatial *and* temporal mean (Opdyke & Henry, 1969; Ohno & Hamano, 1992). Far sidedness of all VGPs, together with a negative inclination anomaly for core JPC95 (see section 6.4) is consistent with the proposition of an offset axial dipole; displaced to the north of the equatorial plane (Wilson, 1971).

7. CONCLUSIONS

7.1 Suitability of methods

The appropriateness of saturation ARM (sARM) as a normalising parameter for studies of relative paleointensity in marine sediments has been established through the following observations:

- Similarity in the coercivity spectra of NRM and ARM.
- Stability of the NRM/ARM ratio throughout AF demagnetisation.
- Lack of correlation between the normalised paleointensity record and magnetic parameters that are grain-size and/or concentration dependent.
- Linearity of Arai plots.
- The high degree of similarity between the RPI record from core JPC95 and numerous records compiled to produce the GLOPIS-75 global relative paleointensity stack (Laj et al., 2004).

7.2 Suitabillity of NZ marine sediments for paleomagnetism

This study, using cores collected from the Waipaoa Basin (K32, K47, K54, K70 and K87), Bay of Plenty (JPC95) and northern Chatham Rise (JPC 28), highlights the potential of New Zealand marine sediments to provide accurate and reliable records of paleosecular variation (PSV) and relative paleointensity (RPI) of the geomagnetic field. Those from the Waipaoa Basin provide high resolutions; paleosecular variation (PSV) and relative paleointensity (RPI) signals preserved in core K47 record variability on a decadal scale back to 300 yrs. B.P. Several factors allude to the suitability of New Zealand's east coast as a prime locality for future paleomagnetic investigations:

- **Tephrochronology** – the east coast of the North Island is proximal to the Taupo Volcanic Zone (TVZ). Sediments are thus likely to contain deposits of deglacial and Holocene tephras derived from various volcanic centres.

- **Magnetic mineralogy & granulometry** – sediments from the Bay of Plenty and the Waipaoa Basin contain ferrimagnetic minerals capable of retaining a remanence, and that are suited to AF demagnetisation.
- **Accumulation rates** – high rates of accumulation along the continental margin result in stratigraphic records of high resolution.

Marine sediments from the Waipaoa Basin exhibit spatial variability in their response to AF demagnetisation; the best responses were exhibited by samples from the central Waipaoa shelf and slope. The magnetic fraction of these sediments is likely to be dominated by a ferrimagnetic iron oxide such as magnetite, present in the grain size range (1-15 μm) and in sufficient concentrations to retain a stable remanence. These sediments are well suited to AF demagnetisation. Down-core magnetic homogeneity (King et al., 1983) has been established for several cores from the Waipaoa continental shelf; thus providing evidence that sediments from this region can provide accurate and reliable records of relative paleointensity.

Samples from the shelf north of Poverty Bay and near-shore, to the south of Poverty Bay, show evidence for magnetic mineralogies dominated by antiferrimagnetics such as hematite or goethite. Sediments from these areas respond poorly to AF treatments, and are better suited to thermal demagnetisation.

Cores K32 and K54, both of which are close to the shelf break, contain coarser magnetic grain sizes below 1.45 m and 0.9 m, respectively, which, in core K54, corresponds to an age of ~75 yrs B.P. based on the available sedimentation rate. The presence of magnetic grains in the multi-domain (MD) state renders such sediments less capable of retaining a primary remanence. Should granulometric variations be a characteristic of the shelf break sediments in general, they are unlikely to yield continuous and reliable paleomagnetic records.

7.3 Relative paleointensity

Two excursion events are identified in RPI and PSV records derived from core JPC95. The Laschamp excursion occurs at 3.5 m, or 42,600 ± 250 cal. yrs B.P. and the Mono Lake excursion at 2.9 m, or 35,707 ± 250 cal. yrs B.P. (based upon the available tephrochronology

alone) with durations of ≤ 2 k.y. and ~ 1 k.y., respectively. The Laschamp excursion event has been used to fine tune the chronology for core JPC95 through correlation with the GLOPIS-75 paleointensity stack Laj et al. (2004), in which the event is centred at 41 ka, and of comparable duration. The resulting attuned chronology places the Mono Lake excursion at 34,786 $\pm$ 250 cal. yrs B.P. The manifestation of these excursions in RPI records from New Zealand marine sediments attests to their global and thus dipolar nature. The longitudinal path of the dipolar field during the Laschamp excursion is constrained to lie between 87.44°E and 99.66°E; maximum agreement with paleomagnetic data is achieved using the former value. The latitudinal deviation from geographic north during the excursion is estimated to be 80° - 110° in magnitude (along the 87.44°E meridian).

Other millennial to sub-millennial scale features of the RPI signal recorded in core JPC95, including several peaks preceding the Laschamp excursion and a peak immediately post-dating the Mono Lake excursion, are also globally correlative. Identification of features with the shortest time constants thought to be associated with dipole variations (600-700 years; Hulot & Le Mouel, 1994) suggests that core JPC95 achieves the maximum possible resolution of the (globally synchronous) dipole RPI signal.

7.4 Paleosecular Variation

The Laschamp and Mono Lake excursions are manifest more prominently in paleosecular variation records from the South Pacific (core JPC95) and South Atlantic than in available Northern Hemisphere records of comparable resolution. Other millennial-scale features are also correlative between the South Atlantic and South Pacific inclination records; but not between available Northern Hemisphere and Southern Hemisphere records. The observed temporally persistent hemispheric asymmetry intimates associated asymmetry in conditions at the core-mantle boundary (over the past ~ 50 k.y.) more complex than can be explained by a wobbling geocentric dipolar field. More records of similar resolution from both hemispheres are required to test this implication.

The inclination anomaly for core JPC95, $\Delta I = -8.1°$, is greater than the previous estimate of ~ -5° for New Zealand (Elmelah et al., 2001); but is consistent with the proposition of a

negative inclination anomaly characterising the southwest Pacific. Thermal core-mantle coupling and influence of the topography of the core-mantle boundary are potential mechanisms for producing such a temporally persistent non-zonal structure.

The PSV record from core JPC95 provides little evidence for reduced secular variation in the Bay of Plenty from ~ 22 ka to 47 ka. Fluctuations are greater in amplitude than those in available records from Italy, France, Siberia and Japan with similar temporal resolution. This implies that the alleged secular variation low dominating the Pacific Region is not manifest in New Zealand over the past ~50 k.y. However, several features in the South Atlantic exhibit enhanced amplitudes with respect to New Zealand correlatives. Longer and more continuous records from the Southern Hemisphere are therefore required to test this inference.

Both the negative inclination anomaly and far-sidedness of virtual geomagnetic poles from core JPC95 support the contention of a northward-displaced axial dipole, proposed and modelled by Wilson (1971).

7.5 Future work

Given the confirmed suitability of New Zealand marine sediments for paleomagnetic studies, a logical step forward from this study is to derive more records of PSV and RPI from this region. Such records could be used to establish regional consistency (or otherwise), to bridge the gaps in the records from core JPC95, and to extend the observation window back further in time. Corroboration of multiple records will facilitate development of a PSV curve for New Zealand.

Paleomagnetic studies of more Southern Hemisphere records are required to build on the few existing RPI and PSV curves from the South Atlantic and Pacific. Comparison of more records from the Southern Hemisphere, of comparable temporal resolution, will further constrain the size of non-dipole sources and longevity of hemispheric asymmetry in millennial-scale paleosecular variation.

Core K47 records fluctuations of the paleofield at a temporal resolution shorter than the shortest time constants associated with the dipole signal (600-700 years according to Hulot & Le Mouel, 1994). More records of comparable scale and resolution to that of core K47 are required to determine the spatial extent of the non-dipole RPI and PSV signal on a decadal to centennial scale, and to constrain the maximum resolution at which these signals can be utilized as a tool for stratigraphic correlation. Aside from the Waipaoa Basin, potential targets for such studies include other continental margin regions e.g. Gulf of Papua, Papua New Guinea; or coastal areas of the East Indies and Philippines, characterised by high rates of accumulation. Should a regionally consistent signal be detected in New Zealand, it may be utilized to date records of paleoclimate on human time scales, providing un-rivalled time resolution.

8. REFERENCES

Alfven, H. 1950: Cosmic Electrodynamics. Princeton Series in Astrophysics (Oxford: Clarendon Press).

Aldredge, L.R.; Hurwitz, L. 1964: Radial dipoles as the sources of the Earth's main magnetic field, *Journal of Geophysical Research 69*: 2631-2640.

Ballance, P.F. 1993: South Pacific Sedimentary Basins. *Sedimentary Basins of the World 2.* Ed. K.H. Hsu, Elsevier Amsterdam, 413 pp.

Banerjee, S.K.; King, J.; Marvin, A. 1981: A rapid method for magnetic granulometry with applications to environmental studies. *Geophysical Research letters 8*: 333-336.

Barbetti, M.; McElhinny, M. W. 1972: Evidence of a Geomagnetic Excursion 30,000 yr B.P. *Nature (London) 239 (5371)*: 327-330.

Barbetti, M. F.; McElhinny, M.W. 1976: The Lake Mungo geomagnetic excursion. *Philosophical Transactions of the Royal Society of London, Series A: Mathematical and Physical Sciences 281 (1305):* 515-542.

Barbetti, M. 1977: Measurements of Recent geomagnetic secular variation in southeastern Australia and the question of dipole wobble. *Earth and Planetary Science Letters 36 (1):* 207-218.

Barton, C. E.; McElhinny. M. W. 1979: Detrital remanent magnetisation in five slowly redeposited long cores of sediment (*in* Sedimentology and magnetostratigraphy). *Geophysical Research Letters 6 (4):* 229-232.

Barton, C. E.; Barbetti, M. 1982: Geomagnetic secular variation from recent lake sediments, ancient fireplaces and historical measurements in southeastern Australia. *Earth and Planetary Science Letters 59 (2):* 375-387.

Benson, L.; Liddicoat, J.; Smoot, J.; Sarna-Wojcicki, A.; Negrini, R.; Lund, S. 2003: Age of the Mono Lake excursion and associated tephra. *Quaternary Science Reviews 22 (2-4):* 135-140.

Bingham, D.; Stone, D. 1972: Paleosecular variation of the geomagnetic field in the Aleutian Islands, Alaska. *Geophysical Journal of the Royal Astronomical Society 28:* 317-335.

Bloemendal, J. 1983: Paleoenvironmental implications of the magnetic characteristics of sediments from DSDP Site 514, Southeast Argentine Basin. *Initial Reports DSDP 71*: 1097-108.

Bloxham, J.; Gubbins, D. 1986: Geomagnetic field analysis; IV, Testing the frozen-flux hypothesis *Geophysical Journal of the Royal Astronomical Society 84 (1):* 139-152.

Bloxham, J. 2000: Sensitivity of the geomagnetic axial dipole to thermal core-mantle interactions *Nature (London) 405 (6781)*: 63-65.

Bonhommet, N.; Babkine, J. 1967: Sur la presence d'aimantations inverses dans la Chaine de Puys, C.R. *Academie des Sciences, Paris 264*: 92-94.

Brandt, U.; Nowaczyk, N.R.; Ramrath, A.; Brauer, A.; Mingrim, J.; Wulf, S.; Negendank, J.F.W. 1999: Paleomagnetism of Holocene and Late Pleistocene sediments from Lago di Mezzano and Lago Grande di Monticchio (Italy): initial results. *Quaternary Science Reviews 18*: 961-976.

Buffett, B.A. 2000: Earth's core and the Geodynamo. *Science 228*: 2007-2012.

Butler, R.F. 1992: *Paleomagnetism: Magnetic Domains to Geologic Terranes.* Blackwell Science Inc. Boston, MA. 319 pp.

Brown, L. 2002: Paleosecular variation from Easter Island revisited: modern demagnetisation of a 1970s data set. . *Physics of the Earth and Planetary Interiors 133:* 73-81.

Carlut, J.; Courtillot, V. 1998: How complex is the time-averaged geomagnetic field over the past 5 Myr? *Geophysical Journal International 134 (2)*: 527-544.

Carter, R.M.; Carter, L.; Johnson, D.P. 1986: Submergent shorelines in the SW Pacific: evidence for an episodic post-glacial transgression. *Sedimentology 33*: 629-649.

Carter, L.; Nelson, C.S.; Neil, H.L.; Frogatt, P.C. 1995: Correlation, dispersal and preservation of the Kawakawa Tephra and other late Quaternary tephra layers in the southwest Pacific Ocean. *New Zealand Journal of Geology & Geophysics 38*: 29-46.

Channell, J.; Stoner, J.S.; Hodell, D.; Charles, C. 2000: Geomagnetic paleointensity from late Bruhnes age piston cores from the subantarctic South Atlantic. *Earth and planetary Science Letters 175*: 145-160.

Cisowski, S. 1981: Interacting vs. non-interacting single domain behaviour in natural and synthetic samples. *Physics of the Earth and Planetary Interiors 26 (1-2)*: 56-62.

Cisowski, S.; Hall, F. 1997: An examination of the paleointensity record and geomagnetic excursions recorded in Leg 155 cores (*in* Proceedings of the Ocean Drilling Program; scientific results, Amazon Fan; covering Leg 155 of the cruises of the drilling vessel JOIDES Resolution, Bridgetown, Barbados, to Bridgetown, Barbados,

sites 930-946, 25 March-24 May 1994). *Proceedings of the Ocean Drilling Program, Scientific Results 155:* 231-243.

Coe, R.S. 1977: Source models to account for Lake Mungo paleomagnetic excursion and their implications. *Nature 269*: 49-51.

Constable, C.; Tauxe, L. 1987: Paleointensity in the pelagic realm; marine sediment data compared with archaeomagnetic and lake sediment records. *Geophysical Journal of the Royal Astronomical Society 90 (1):* 43-59.

Cook, J. 1771: Variation of the compass, as observed on board the Endeavour Bark, in a voyage round the world. *Philosophical Transactions of the Royal Society of London 61 (2)*: 422-432.

Cox, A. 1962: Analysis of present geomagnetic field for comparison with paleomagnetic results. *Journal of Geomagnetism and Geoelectricity 13*: 101.

Cox, A. 1969: A paleomagnetic study of secular variation in New Zealand. *Earth and planetary Science Letters 6*: 257-267.

Cox, A. 1971: Paleomagnetism of San Cristobal Island Galapogas. *Earth and planetary Science Letters 11:* 152-160.

Creer, K.M.; Hogg, T.E. 1977: Synthetic geomagnetic long period secular variation plots obtained from an oscillating radial dipole model. *Eos, Transactions, American Geophysical Union 58 (8)*: 709.

Creer, K.M.; Tucholka, P. 1982: Construction of type curves of geomagnetic secular variation for dating lake sediments from east central North America. *Canadian Journal of Earth Sciences = Journal Canadien des Sciences de la Terre 19 (6):* 1106-1115.

Creer, K.M. 1983: Computer synthesis of geomagnetic paleosecular variations. *Nature (London) 304 (5928)*: 695-699.

Creer, K.M.; Valencio, D. A.; Sinito, A. M.; Tucholka, P.; Vilas, J. F. A. 1983(b): Geomagnetic secular variations 0-14000 yr B.P. as recorded by lake sediments from Argentina. *Geophysical Journal of the Royal Astronomical Society 74 (1)*: 199-221.

Day, R.; Fuller, M.; Schmidt, V.A. 1977: Hysteresis properties of titanomagnetites: grain-size and compositional dependence. *Physics of the Earth and Planetary Interiors 13*: 260-267.

Dearing, J.A. 1999: Holocene environmental change from magnetic proxies in lake sediments. In: *Quaternary climates, environments and magnetism.* Ed. Maher, B. A.; Thompson, R. Cambridge University Press, Cambridge, United Kingdom, p. 231-278.

Doell, R.; Cox, A. 1972: The Pacific geomagnetic secular variation anomaly and the question of lateral uniformity in the lower mantle. In: *The nature of the solid Earth*, McGraw-Hill Book Co. [New York] p. 245-284.

Elsasser, W. M. 1946: Induction effects in terrestrial magnetism. *Physics Reviews 69:* 106-116

Elsasser, W.M. 1958: The Earth as a dynamo. *Scientific American 198:* 44-48.

Evans, M.F.; Heller, F. 2003: *Environmental magnetism. Principles and Application of environmagnetics.* International Geophysics Series v. 86. Academic Press, San Diego. 299 pp.

Farr, C.C. 1916: A magnetic survey of the Dominion of New Zealand and some outlying islands. Government Printer, Wellington, 64 pp.

Foster, G.; Carter L. 1997: Mud sedimentation on the continental shelf at an accretionary margin – Poverty Bay, *New Zealand. New Zealand Journal of Geology & Geophysics 40*: 157-173.

Fraser-Smith, A.C. 1987: Centred and eccentric geomagnetic dipoles and their poles, 1600-1985. *Reviews of Geophysics 25 (1)*: 1-16.

Froggatt, P.C.; Lowe, D.J. 1990: A review of late Quaternary silicic and some other tephra formations from New Zealand. *New Zealand Journal of Geology & Geophysics 33*: 89-109.

Gauss, C.F. 1839: Allgemeine Theorie des Erdmagnetismus. In: Gauss, C.F.; Weber, W. (Eds.) 1863: Resultate aus den Beobachtungen des magnetischen Vereins im Jahre 1838, Leipzig, Germany, pp. 1–57, 146–148. Reprinted in Werke, vol. 5. p.121–193, Dieterich, Göttingen, Germany.

Glatzmaier, G.A.; Roberts, P.H. 1995: A three-dimensional convective dynamo solution with rotating and finitely conducting inner core and mantle. *Physics of the Earth and Planetary Interiors 91*: 63-75.

Guyodo, Y.; Valet, J.P. 1999: Global changes in intensity of the earth's magnetic field during the past 800 kyr. *Nature 399:* 249-252.

Haag, M. 2000: Reliability of relative paleointensities of a sediment core with climatically-triggered strong magnetisation changes. *Earth and planetary Science Letters 180:* 49-59.

Harrison, C.G.A. 1980: Secular Variation and excursions of the earth's magnetic field. *Journal of Geophysical Research 85*: 3511-3522.

Herrero-Bervera, E.; Valet, J.P. 2002: Paleomagnetic secular variation of the Honolulu Volcanic Series (33-700 ka) O'ahu (Hawaii). *Physics of the Earth and Planetary Interiors 133*: 83-97.

Herrero-Bervera, E.; Ubango, R.; Aka, F.T.; Valet, J.P. 2004: Paleomagnetic and paleoseclar variation study of the Mt. Cameroon volcanics, (0.0-0.25 Ma), Cameroon, West Africa. *Physics of the Earth and Planetary Interiors 147:* 171-182.

Hide, R. 1966: Free hydromagnetic oscillations of the earth's core and the theory of the geomagnetic secular variation. *Philosophical Transactions of the Royal Society of London, Series A: Mathematical and Physical Sciences 259 (1107):* 615-650.

Holme, R. 2004: A fuel-efficient geodynamo. *Nature (London) 429 (6988)*: 137.

Hospers, J. 1954b: Rock magnetism and polar wandering. *Nature 173*: 1183.

Hu, S.; Appel, E.; Hoffmann, V.; Schmahl, W.W.; Wang, S. 1998: Gyromagnetic remanence acquired by Greigite (Fe2S4) during static three-axis alternating field demagnetisation. *Geophysical Journal International 134 (3):* 831-842.

Hulot, G.; Le Mouel, J.L. 1994: A Statistical approach to the earth's main magnetic field. *Physics of the Earth and Planetary interiors. 82:* 167-183.

Irving, E. 1964: Paleomagnetism and its application to geological and geophysical problems. Wiley & Sons, New York. 399 pp.

Johnson, H.P.; Lowrie, W.; Kent, D. 1975: Stability of Anhysteretic Remanent Magnetisation in Fine and Coarse Magnetite and Maghemite Particles. *Geophysical Journal of the RAS 41:* 1-10.

Johnson, H.P.; Constable, C. 1998. Persistently anomalous Pacific geomagnetic fields. *Geophysical Research Letters 25*: 1011 1014.

King, J.; Banerjee, S.; Marvin, J.; Holschuh, N. 1981: A critical evaluation of a method; the NRM/ARM ratio of lake sediments as an estimate of relative geomagnetic field intensity. In: American Geophysical Union; 1981 spring meeting, Anonymous. *Eos, Transactions, American Geophysical Union 62 (17)*: 272.

King, J.; Banerjee, S.; Marin, J., Ozdemir, O. 1982: A comparison of different magnetic methods for determining grain size of magnetite in natural materials: some results from lake sediments. *Earth and planetary Science Letters 59*: 404-419.

King, J.; Banerjee, S., Marin, J. 1983: A new rock-magnetic approach to selecting sediments for geomagnetic paleointensity studies: application to paleointensity for the last 4000 years. *Journal of Geophysical Research 88 (B7):* 5911-5921.

Kohn, B.P.; Glasby, G.P. 1978: Tephra distribution and sedimentation rates in the Bay of Plenty, New Zealand. *New Zealand Journal of Geology & Geophysics 21*: 49-79.

Krause, F.; Roberts, P. H. 1980: *Advances in Space Research 1 (231)*: 240.

Laj, C.; Kissel, C.; Mazaud, A.; Channell, J.E.T.; Berr, J. 2000: North Atlantic paleointensity stack since 75 ka (APIS-75) and the duration of the Laschamp event. *Phil. Trans. Royal Society, Series A 358:* 1009-1025.

Laj, C.; Kissel, C.; Beer, J. 2004: High-resolution paleointensity stack since 75 kyr (GLOPIS-75) calibrated to absolute values. *Geophysical Monograph Series 145*: *Timescales of the paleomagnetic field:* 255-265.

Lanza, R.; Zanella, E. 2003: Paleomagnetic secular variation at Vulcano (Aeolian Islands) during the last 135 kyr. *Earth and planetary Science Letters 213*: 321-336.

Levi, S.; Banerjee, S. 1976: On the possibility of obtaining relative paleointensities from lake sediments. *Earth and planetary Science Letters 29*: 219-226.

Levi, S.; Karlin, R. 1989: A sixty thousand year paleomagnetic record from Gulf of California sediments: secular variation, late Quaternary excursions and geomagnetic implications. *Earth and planetary Science Letters 92*: 219-233.

Levi, S.; Audunsson, H.; Duncan, R.; Kristjansson, L.; Gillot, P.; Jakobsson, S. 1990: Late Pleistocene geomagnetic excursion in Icelandic lavas; confirmation of the Laschamp Excursion. *Earth and Planetary Science Letters* 96 (3-4): 443-457.

Lewis, K.B. 1971: Growth Rate of Folds Using Tilted Wave-planed Surfaces; Coast and Continental Shelf, Hawke's Bay, New Zealand (*in* Recent Crustal Movements). *Bulletin - Royal Society of New Zealand 9*: 225-231.

Lewis, K.B. 1973: Erosion and deposition on a tilting continental shelf during Quaternary Oscillations of sea level. *New Zealand Journal of Geology & Geophysics 40*: 157-173.

Lewis, K. B. 1980: Quaternary sedimentation on the Hikurangi oblique-subduction and transform margin, New Zealand (*in* Sedimentation in oblique-slip mobile zones). *Special Publication of the International Association of Sedimentologists 4*: 171-189.

Lewis, K.B.; Pantin, H.M.1984: Intersection of a marginal basin with a continent: structure and sedimentation of the Bay of Plenty. *Geological Society of London Special Publication 16*: 121-135.

Lewis, K.B.; Pettinga, J.R. 1993: The emerging imbricate frontal wedge of the Hikurangi margin. In: Ballance, P.F. (Ed.) South Pacific Sedimentary Basins. *Sedimentary Basins of the World v. 2.* Elsevier Science publishers, Amsterdam, p. 225-250.

Lewis, K.B.; Collot, J.Y.; Lallemand, S.E. 1998: The dammed Hikurangi trough: a channel-fed trench blocked by subducting seamounts and their avalanches, New Zealand – France. *GeodyNZ Project. Basin Research 10*: 441-468.

Liddicoat, J. C.; Coe, R. S.1979: Mono Lake geomagnetic excursion. *Journal of Geophysical Research 84 (B1)*: 261-271.

Lilley, F.E.M. 1970: On kinematic dynamos. *Proceedings Royal Society London A, v. 316,* p. 153-167.
Love, J. 1999: Reversals and excursions of the geodynamo. *Astronomy & Geophysics 40 (6):* 14-19.

Lowe, D.J.; Newnham, R.M.; Ward, C.M. 1999: Stratigraphy and chronology of a 15 ka sequence of multi-sourced silicic tephras in a montane peat bog, eastern North Island. *New Zealand Journal of Geology & Geophysics 42*: 565-579.

Lowes, F.J. 1955: Secular variation and the non-dipole field. *Annals of Geophysics 11*: 91-94.

Meynadier, L., Valet, J.P.; Weeks, R.; Shackleton, N.J.; Hagee, V.L. 1992: Relative geomagnetic intensity of the field during the last 140 ka. *Earth and planetary Science Letters 114*: 39-57.

McElhinny, M.W. 1973: *Paleomagnetism and Plate Tectonics.* Cambridge, London. 356pp.

McElhinny, M. W.; Senanayake, W. E. 1980: Paleomagnetic evidence for the existence of the geomagnetic field 3.5 Ga ago. *Journal of Geophysical Research 85* (*B7*): 3523-3528.

McFadden, P. L.; McElhinny, M. W. 1997: A physical model for paleosecular variation. *Geophysical Journal of the Royal Astronomical Society v. 78 (3),* p. 809-830.

Merrill, R.T.; McElhinny, M.W. 1977: Anomalies in the time-averaged paleomagnetic field and their implications for the lower mantle. *Reviews of Geophysics and Space Physics 15 (3):* 309-323.

Merrill, R.T.; McElhinny, M.W. 1983: *The Earth's Magnetic Field.* Academic Press, London. 401 pp.

Merrill, R.T.; McElhinny, M.W.; McFadden, P. 1998: *The magnetic field of the earth - paleomagnetism of the core and deep mantle.* International Geophysics Series v. 63. Academic press, Inc., 531 pp.

Miller, K.R. 1981: *Surficial sediments and sediment transport in Poverty Bay.* Unpublished MSc thesis. Department of Earth Sciences, University of Waikato, Hamilton, 179 pp.

Ohno, M.; Hamano, Y. 1992: Geomagnetic poles over the past 10,000 years *Geophysical Research Letters 19 (16)*: 1715-1718.

Ohno, M.; Hamano, Y.; Maruyama, M.; Matsumoto, E.; Iwakura, H.; Nakamura, T.; Taira, A. 1993: Paleomagnetic record over the past 35,000 years of a sediment core from off Shikoku, southwest Japan, *Geophysical Research Letters 20:* 1395-1398.

Olson, P.; Glatzmaier, G. 1996: Magnetoconvection and thermal coupling of the earth's core and mantle. *Philosophical Transactions of the Royal Society of Society of London Series A, 354:* 1-12.

Opdyke, N.D.; Channell, J.E.T. 1996: *Magnetic Stratigraphy.* International Geophysics Series v. 64. Academic Press, Inc. 346 pp.

Orpin, A.; Carter, L.; Kuehl, S.; Trustrum, N.A.; Lewis, K.B.; Alexander, C.R.; Gomez, B. 2002a: Deposition from very high sediment yield New Zealand rivers is captured in upper margin basins. *Margins Newsletter no. 9*: 1-4.

Orpin, A.R. 2004: Holocene sediment deposition on the Poverty-slope margin by the muddy Waipaoa River, East Coast, New Zealand. *Marine Geology 209*: 69-90.

Ota, Y.; Hull, A.G.; Berryman, K.R. 1987: Coseismic uplift of Holocene marine terraces on the northeast coast of the North Island, New Zealand, and their tectonic significance. *New Zealand Journal of Geology & Geophysics 35:* 273-288.

Parry, L.G. 1965: Magnetic properties of dispersed Magnetite powders. *Philosophical Magazine 11*: 303-312.

Peck, J.A.; King, J.W.; Colman, S.M.; Cravchinsky, V.A. 1996: An 84 kyr paleomagnetic record from the sediments of Lake Baikal, Siberia. *Journal of Geophysical Research, B, Solid Earth and Planets 101 (5):* 365-11,385.

Peters, C., Thompson, R. 1998: Magnetic identification of selected natural iron oxides and sulphides. *Journal of Magnetism and Magnetic Materials 183*: 365-374.

Peters, C.; Dekkers, M.J. 2003: Selected room temperature magnetic parameters as a function of mineralogy, concentration and grain size. *Physics and Chemistry of the Earth 28*: 659-667.

Pillans, B.; Wright, I. 1990: 500,000 year paleomagnetic record from New Zealand loess. *Quaternary Research 33:* 178-187.

Pillans, B.; Wright, I. 1992: Late Quaternary tephrostratigraphy from the southern Havre Trough – Bay of Plenty, northeast New Zealand. *New Zealand Journal of Geology & Geophysics 35*: 129-143.

Prevot, M.; Mankinen, E.A.; Coe, R.S.; Gromme, C.S. 1985: The Steens mountain (Oregon) geomagnetic polarity transition, II. Field intensity variations and discussion of reversals models. *Journal of Geophysical Research 90*: 10417-10448.

Pullaiah, G.; Irving, G.; Buchan, K.; L. Dunlop, D. J. 1975: Magnetisation changes caused by burial and uplift. *Earth and Planetary Science Letters 28*: 133-143.

Quinn, 2004: *High Resolution Environmental Magnetism of short sediment cores from Lake Tekapo, New Zealand.* Unpublished PGDip. Sci. thesis, geology library, University of Otago. 61 pp.

Rees, A.I.; Woodall, W.A. 1975: The magnetic fabric of some laboratory deposited sediments. *Earth and planetary Science Letters 25*:121-130.

Robertson, D.J. 1986: A paleomagnetic study of Rangitoto Island, Auckland, *New Zealand. New Zealand Journal of Geology & Geophysics 29*: 405-411.

Robinson, S.G. 1986: The Late Pleistocene paleoclimatic record of North Atlantic deep-sea sediments revealed by mineral magnetic measurements. *Physics of the Earth and Planetary Interiors 42*: 22-46.

Roperch, P.; Taylor, G.K. 1986: The importance of gyromagnetic remanence in alternating field demagnetisation. Some new data and experiments on GRM and RRM. *Geophysical Journal of the Royal Astronomical Society 87*: 949-965.

Roperch, P.; Bonhommet, N.; Levi, S. 1988: Paleointensity of the earth's magnetic field during the Laschamp excursion and its geomagnetic implications. *Earth and planetary Science Letters 88:* 209-219.

Salis, J. S. 1987: *Variation seculaire du champ magnetique terrestre; direction et paleointensite sur la periode 7.000 - 70. 000 BP dans la chaine des Puys.* Sci. thesis, Centre Armoricain d'Etude Structurale des Socles, 190

pp.

Schneider, D.; Kent, D.V. 1990a: The time averaged paleomagnetic field. *Reviews of Geophysics 28*: 71-96.

Schramm, A.; Stein, M.; Goldstein, S. 2000: Calibration of the ^{14}C time scale to > 40 ka by ^{234} U- ^{230} Th dating of Lake Lisan sediments (last glacial Dead Sea). *Earth and Planetary Science Letters 175 (1-2)*: 27-40.

Sikes, E.L.; Samson, C.R.; Guilderson, T.P.; Howard, W.R. 2000: Old Radiocarbon ages in the southwest Pacific Ocean during the last glacial period and deglaciation. *Nature 405*: 555-559.

Stoner, J.; Channell, J.; Hillaire-Marcel, C.; Kissel, C. 2000: Geomagnetic paleointensity and environmental record from the Labrador Sea core MD95-2024: global marine sediment and ice chronostratigraphy for the last 110 kyr. *Earth and planetary Science Letters 183*: 161-177.

Stoner, J.; Laj, C.; Channell, J.E.T.; Kissel, C. 2002: South Atlantic and North Atlantic geomagnetic paleointensity stacks (0-80 ka): implications for inter-hemispheric correlation. *Quaternary Science Reviews 21*: 1141-1151.

Stuiver, M.; Reimer, P.J.; Bard, E.; Beck, J.W.; Burr, G.S.; Hughen, K.A.; Kromer, B.; McCormac, G.; van der Plicht, J.; Spurk, M. 1998: INTCAL1998 radiocarbon age calibration, 24,000-0 cal. B.P. *Radiocarbon 40*: 1041-1083.

Tanaka, H.; Otsuka, A.; Tachibana, T.; Kono, M. 1994: Paleointensities for 10-22 ka from volcanic rocks in Japan and New Zealand. *Earth and Planetary Science Letters 122 (1-2)*: 29-42.

Tarling, D.H. 1983: *Paleomagnetism; principles and applications in geology, geophysics and archaeology.* Chapman and Hall, London, United Kingdom (GBR), 379 pp.

Tauxe, L.; Wu, G. 1990: Normalised remanence in sediments of the western Equatorial Pacific; relative paleointensity of the geomagnetic field? *Journal of Geophysical Research* 95 *(B8):* 12337-12350.

Tauxe, L. 1993: Sedimentary records of relative paleointensity of the geomagnetic field: theory and practice. *Reviews of Geophysics 31 (3):* 319-354.

Tauxe, L., Pick, T., Kok, Y. 1995: Relative paleointensity in sediments: a pseudo-Thellier approach. *Geophysical Research letters 22 (21):* 2885-2888.

Tauxe, L. 2002: *Paleomagnetic Principles and Practice*. Modern Approaches in Geophysics v. 18. Kluwer Academic publishers, 312 pp.

Tauxe, L. 2005: Lectures in paleomagnetism. **http://earthref.org/MAGIC/books/Tauxe/2005/**

Thompson, R.; Oldfield, F. 1986: *Environmental magnetism.* Allen & Unwin (publishers) Ltd., 227 pp.

Thouveny, N.; Creer, K.M.; Blunk, I. 1990: Extension of the Lac du Bouchet paleomagnetic record over the last 120 000 years. *Earth and planetary Science Letters 97*: 140-161.

Tric, E.; Valet, J.P.; Tucholka, P.; Paterne, M.; Labeyre, L.; Guichard, F.; Tauxe, L.; Fontugne, M. 1992: Paleointensity of the geomagnetic field during the last 80 000 years. *Journal of Geophysical Research 97 (B6):* 9337-9351.

Tucker, P. 1980: A grain mobility model of post-depositional realignment. *Geophysical Journal of the Royal Astronomical Society 63(1)*: 149-163.
Turner, G.M.; Thompson, R. 1981: Lake Sediment record of the geomagnetic secular variation in Britain during Holocene times. *Geophysical Journal of the Royal Astronomical Society 65 (3):* 703-725.

Turner, G.M.; Lyons, R.G. 1986: A paleomagnetic secular variation record from c. 120 000 yr old New Zealand cave sediments. *Geophysical Journal of the Royal Astronomical Society 87*: 1181-1192.

Turner, G.M. 1987: A 5000 year paleosecular variation record from southern British Columbia; an example of paleomagnetic pattern matching (*in* International Union of Geodesy and Geophysics (IUGG), XIX general assembly; abstracts--Union Geodesique et Geophysique Internationale (UGGI); XIX assemblee generale; resumes, Anonymous,) *International Union of Geodesy and Geophysics, General Assembly 19, Vol. 2:* 478.

Turner, G.M.; Lillis, D.A. 1994: A paleomagnetic secular variation record for New Zealand during the past 2500 years. *Physics of the Earth and Planetary Interiors 83*: 265-282.

Verosub, K. L. 1977: Depositional and post-depositional processes in the magnetisation of sediments. *Reviews of Geophysics and Space Physics 15 (2)*: 129-143.

Verosub, K. L.; Mehringer, P.J.; Waterstraat, P. 1986: Holocene secular variation in western North America; paleomagnetic record from Fish Lake, Harney County, Oregon. *Journal of Geophysical Research 91 (B3):* 3609-3623.

Verosub, K.L.; Roberts, A.P. 1995: Environmental magnetism; past, present, and future. *Journal of Geophysical Research, B, Solid Earth and Planets 100 (2):* 2175-2192.

Walling, D.E.; Webb, B.W. 1996: Erosion and sediment yield: a global overview. In: Walling, D.E.; Webb, B.W. (Eds.) Erosion and Sediment Yield: Global and Regional Perspectives (Proceedings of the Exeter Symposium, July, 1996*). International Association of Hydrological Science Publications 236:* 3-19.

Weeks, R.J.; Laj, C.; Endignoux, L.; Mazaud, A.; Labeyrie, L.; Roberts, A.P.; Kissel, C.; Blanchard, E. 1995: Normalised natural remanent magnetisation intensity during the last 240 000 years in piston cores from the central North Atlantic Ocean: geomagnetic field intensity or environmental signal? *Physics of the Earth and Planetary Interiors 87*: 213-229.

Wilson, L. 1971: Dipole offset; the time-average paleomagnetic field over the past 25 million years. *Geophysical Journal of the Royal Astronomical Society 22 (5)*: 491-504.

Wilson, C. J. N. 2001: The 26.5 ka Oruanui eruption, New Zealand; an introduction and overview. *Journal of Volcanology and Geothermal Research 112(1-4):* 133-174.

World Data Centre for Geomagnetism, graduate school of science, Kyoto University, Kyoto. IAGA – VMOD – geomagnetic field modelling: International Geomagnetic Reference Field IGRF. Webpage: http://swdcdb.kugi.kyoto-u.ac.jp/index.html

Yamazaki, T. 1999: Paleointensity of the geomagnetic field during the Bruhnes Chron recorded in North Pacific deep-sea sediment cores: orbital influence? *Earth and planetary Science Letters v. 169*, p. 23-35.

Yamazaki, T.; Ioka, N. 1994: Long term secular variation of the geomagnetic field during the last 200 kyrs recorded in sediment cores from the western equatorial Pacific. *Earth and planetary Science Letters v. 128*, p. 527-544.

Yukutake, T. 1979: Review of the geomagnetic secular variations on the historical time scale. *Physics of the Earth and Planetary Interiors 20 (2-4):* 83-95.

Yukutake, T. 1993: The geomagnetic non-dipole field in the Pacific. *Journal of Geomagnetism and Geoelectricity 45 (11-12):* 1441-1453.

Yukutake, T.; Tachinaka, H. 1968: The non-dipole part of the earth's magnetic field. *Bulletin of the Earthquake Research Institute = Tokyo Daigaku Jishin Kenkyusho Iho 46 (*5): 1027-1062.

9. APPENDICES

9.1 2G Enterprises Cryogenic Magnetometer

All measurements of magnetic moment and susceptibility were made using a 2G Enterprises Cryogenic magnetometer in the University of Otago paleomagnetic research facility. It comprises five major components:

1. An in-line Bartington *MS2C* Susceptibility Bridge, deigned for volume susceptibility measurements, with a 47 mm aperture diameter. The relative response:
   κ rel. $= 3.45(d/D)^3 = 0.2384$ for measurements made in this study, where
   d = core material diameter
   D = *MS2C* diameter + 8 mm.

2. In-line alternating field coils (three sets: x, y, z) to facilitate demagnetisation in three-orthogonal directions. A 12-bit electronic attenuator controls the amplitude of the alternating field.

3. The magnetometer itself comprises three Superconducting Quantum Interference Devices (SQUIDS). The SQUIDS measure the current induced in the superconducting puck-up coils – two are for measurement of transverse movement (X and Y axes), whilst the other is for measuring axial motion (Z axis).

4. DC axial solenoid extending through the axial degaussing coils to ensure application of a steady dc field to the long core on either side of the degaussing coil, where the AC field is decaying to zero.

5. Automated track sample handler, controller and driver system. The handler consists of aluminium and fibreglass channels designed to support and guide the long core through a pull rope attached to a geared high-torque stepper motor.

The treatment and measurement of samples using the magnetometer is controlled by the software 'LONG CORE 3.3'. This program also provides the option to correct for the sample tray (cleaned and measured prior to each new long core sample) and for drift (linear correction between first and final background readings). LONG CORE 3.3 also contains hidden corrections whose source and nature are largely unknown. However, the accuracy and precision of data output has been verified (see Quinn, 2004).

Magnetometer Set-up

To make U-channel measurements, the long core tray was placed in the magnetometer and parameters in the Measurement Queue Editor were set as shown in Figure 9.1. Measurement type was set to continuous and measurement interval to 1 cm. The long core tray was then cleaned at 1200 Gauss and a background set of magnetic moment and susceptibility measurements made and saved. These initial measurements are used to correct all core data for background magnetisation levels.

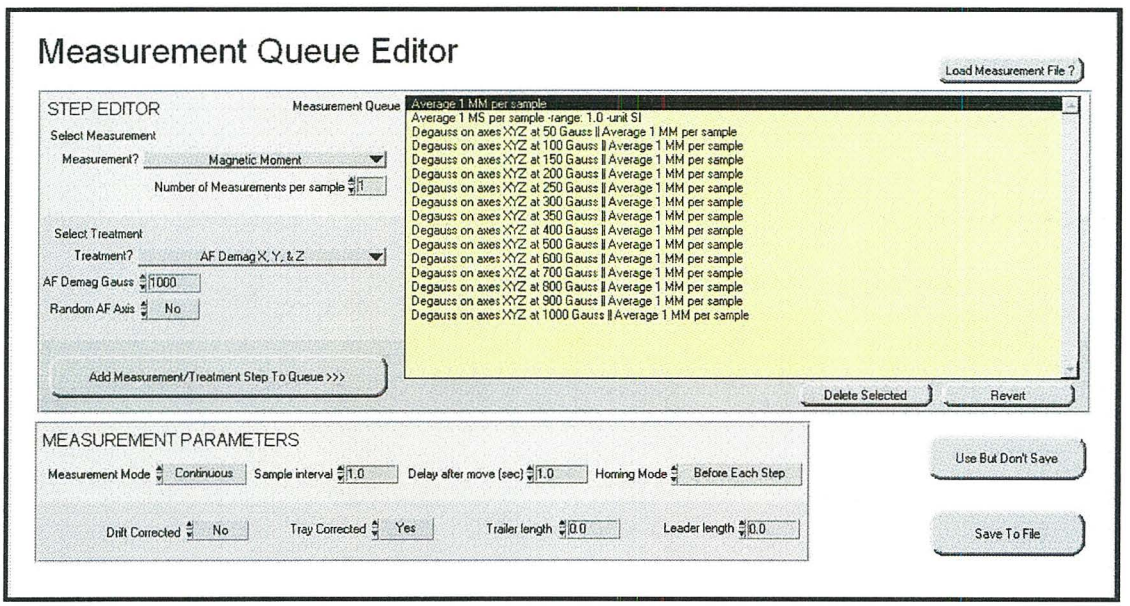

Figure 9.1: Measurement queue editor for cryogenic magnetometer showing list of alternating field demagnetisation steps and measurements that were carried out on each core sample (at 1 cm intervals).

Information specific to each U-channel including length, depth, volume (correction made) and sample numbers were then entered into the Sample Input Data Table as shown in Table 9.1. A volume correction was applied (using $4cm^2$ cross-sectional area and the response functions specific to each SQUID) as well as a correction for any lost sample. No drift correction was made, since all measurements are made in a very low-field environment and a change in background magnetisation due to a flux jump cannot be accounted for through a linear correction. Masking tape was used to adhere the u-channel to the base of the tray.

Sample ID	Pos/Length	Depth	Volume/ Area	Sample Azimuth	Sample Dip	Formation Azimuth	Formation Dip
JPC95.1	1.1	0	4				
JPC95.2	1.5	1.1	4				
JPC95.3	1.5	2.6	4				

Table 9.1: Example of inputs for the sample input data table for core JPC95. Samples are identified according to u-channel number (core section). Position/length is length of each u-channel; depth is the depth of the top of the u-channel. Volume/area refers to the cross-sectional area of the u-channel. The last four columns, which are specific to discrete samples are left blank.

9.2 Definitions

9.2.1 Natural Remanent Magnetisation (NRM)

Natural remanent magnetisation is the fossil (remanent) magnetisation preserved within the sediment prior to any laboratory treatment. It is dependant on the strength and direction of the geomagnetic field at the time of remanence acquisition, as well as on mineralogy, concentration and grain size. Geological, biological and chemical processes may also affect intensity and direction of NRM. Description of NRM requires quantification of declination, inclination and intensity. Intensity of NRM provides a crude indication of the size, type, orientation and concentration of magnetic grains, and requires a volume correction (Opdyke & Channell, 1996). This study is primarily concerned with detrital remanent magnetisation (DRM). Other types of NRM include thermoremanent magnetisation (TRM) and Chemical remanent magnetisation (CRM).

9.2.2 Detrital Remanent Magnetisation (DRM)

NRM acquired through orientation of sedimentary grains as they settle through a water column, and during subsequent lithification of sedimentary rocks is termed Detrital Remanent Magnetisation (DRM). DRM is affected by the complex processes involved in the formation of sedimentary rocks (Butler, 1992) and is hence more complex to decipher than other types of NRM. Processes of DRM acquisition may be divided into two stages: depositional, and post-depositional. The former stage involves the aligning influence of the geomagnetic field on a magnetic particle as it encounters the sediment/water interface. The substantial force controlling alignment of fine grains during deposition is termed magnetic coupling (Rees & Woodall, 1975). The latter stage of remanence acquisition can result in modification of the initial DRM, as sediments undergo processes such as bioturbation, slumping, dewatering, compaction and lithification. Chemical changes affecting ferromagnetic minerals during diagenesis may result in a secondary NRM, or CRM.

9.2.3 Characteristic Remanent Magnetisation (ChRM)

The remanent magnetisation of a sample that remains after partial demagnetisation to remove spurious, viscous, secondary components of magnetisation is termed the characteristic remanence (ChRM). The ChRM, or high-stability component of magnetisation, can be in many cases logically inferred to be *primary NRM*; though additional information is required to validate this implication. The term ChRM can be applied to results of demagnetisation experiments, without inference regarding the time of remanence acquisition, which is inherently attached to *primary NRM* (Butler, 1992).

9.2.4 Chemical Remanent Magnetisation (CRM)

Chemical changes that form ferromagnetic minerals (below their blocking temperature) in a magnetising field results in acquisition of a Chemical Remanent Magnetisation (CRM). This type of NRM is most often associated with sedimentary rocks. Reactions may involve precipitation of ferromagnetic minerals from solution or alteration of a pre-existing mineral.

9.2.5 Viscous Remanent Magnetisation (VRM)

Natural VRM is gradually acquired long after deposition during exposure to weak geomagnetic fields. In magnetite-bearing rocks, VRM is generally carried by multi-domain (MD) grains of low coercive force (B_{cr}) and low relaxation time (τ). VRM may also be imparted on a sample during coring procedures depending upon magnetisation of the core barrel. The barrel may act as a magnetic dipole, most intensely magnetised at both ends. Partial demagnetisation techniques employed in this study preferentially erase viscous components of magnetisation to reveal the primary components of paleomagnetic interest.

9.2.6 Magnetic Susceptibility (κ)

The ratio of induced magnetisation acquired by a sample to the strength of the applied field per unit volume is termed the *volume magnetic susceptibility* (κ) (Verosub & Roberts, 1995), a property controlled by electron precession. *Actual* κ is derived by dividing the measured value by the relative response κ_{REL} (see appemdix 9.1), and multiplying by 10^{-5}. Ferrimagnetic minerals magnetite and maghemite have κ is 3-4 orders of magnitude greater than that of common antiferrimagnetics such as hematite and goethite, and κ is commonly log normally distributed (Irving et al., 1966). Magnetic susceptibility (κ) is proportional to ferrimagnetic mineral concentration (Dearing, 1999) and shows least granulometric dependence of all magnetic parameters. Only as the superparamagnetic (SP) range (<0.03 μm) is entered does systematic change occur, where κ increases abruptly by an order of magnitude. Large MD magnetite grains (> 10 μm) that do not carry stable remanence also have enhanced κ (Evans & Heller, 2003). At low magnetic concentrations, interpretation may be complicated as κ responds to antiferrimagnetic (e.g. Hematite), paramagnetic (e.g. Fe Silicates), and diamagnetic ($CaCO_3$, Si) material. In paleomagnetic studies, κ is often used in conjunction with sARM or sIRM to characterise grain size or concentration variations throughout sediment cores. It thus aids in distinguishing the paleofield contribution to the NRM signal from that due to mineralogical or granulometric effects.

9.2.7 Alternating Field (AF) Demagnetisation

Alternating Field Demagnetisation is a technique used to isolate the components of NRM. This is achieved through exposing a sample to an oscillating direct field with a sinusoidal waveform, which decreases in magnitude with time. Through incrementally increasing the strength of this field, the NRM of a sample is progressively randomised by forcing the magnetic moments of grains with coercivities ≤ peak AF strength to realign in a zero direct field (with no aligning influence). This demagnetisation is performed along three orthogonal axes. As the peak demagnetising field is progressively raised, a larger proportion of the total of magnetic grains become demagnetised and therefore cease to contribute to the remanence of the sample (Opdyke & Channell, 1996). This creates a coercivity spectrum, which serves

as an indication of how the intensity of a sample changes under magnetic fields of different intensities, which is dependant on the sum of all magnetic grains in the sample.

9.2.8 Median Destructive Field (MDF)

The median destructive field (MDF) is the demagnetisation level at which 50% of the NRM in a sample has been erased/randomised by AF demagnetisation. This parameter provides a proxy for coercivity (B_{cr}), which in turn is grain-size and mineralogy dependent. Coarse-grained samples have generally lower coercivities, and hence are likely to demonstrate soft demagnetisation behaviour with attendant low MDF values. Antiferrimagnetic minerals of high coercivity e.g. Hematite yield higher MDF values than ferromagnetic minerals e.g. Magnetite

9.2.9 Magnetic activity

The magnetic activity of a sample is dependent on such factors as concentration of magnetic material, magnetic mineralogy, and grain size. Variation in these between sampling intervals results in differing responses to an applied field of particular strength. Estimation of magnetic activity through the bulk parameters sARM, sIRM and κ enables derivation of a normalised DRM, which at least reflects the relative intensity of the applied field.

9.2.10 Gyroremanent Magnetisation (GRM)

GRM is a spurious magnetisation, acquired during alternating field demagnetisation using the three-axis stationary method. GRM is linked to high field anisotropy of a sample (Roperch & Taylor, 1986), and is commonly recognized through a decrease and subsequent increase in intensity at higher fields. In orthogonal component plots, a GRM is typically manifest as a change in direction of inclination and declination away from the origin at higher peak alternating fields.

9.2.11 Virtual Geomagnetic Pole (VGP)

A VGP is the pole of a geocentric dipole that can account for the observed magnetic field direction at a single location at a single point in time. The orientation of the best fitting geocentric dipole to a single measurement of the field at Earth's surface is calculated using the dipole formula (equation 1.1). VGPs calculated from globally distributed measurements of the present magnetic field cluster about the present geomagnetic pole (Butler, 1992). A compendium of VGPs that represent a period of time sufficient to average out geomagnetic secular variation of both non-dipole and dipole fields are expected to cluster about the geographic pole, as demonstrated for the past 10 k.y. by Ohno & Hamano (1992).

9.3 Ship-board core descriptions

K32

Mostly clay rich silt with some fine sand interspersed throughout.

0-3 cm: Greyish olive (10Y4/2), silty clay; soupy; upper 15 cm poorly consolidated.

3-28 cm: Grades between 12 and 20 cm from olive brown to dark olive grey (5GY4/1) silty clay with distinctive black streaks; heavily mottled and bioturbated.

28-150 cm: Dark olive grey silty clay (5GY4/1); becomes darker grey at 90 cm.

150-235 cm: Dark olive grey silty clay; slightly coarse relative to above with higher silt content. Colour darkens again at base.

K47

Upper 23 cm questionable; top 2 cm lost.

0 - 6 cm: yellow-green (5GY5/2) slushy fine clay-rich mud to 6 cm.

6-14 cm: dark greenish grey (5GY4/1) fine grained mud; mottled; black layer at 14 cm; no black streaks.

14 - 82 cm: dark greenish grey fine grained mud with black streaks; mottled.

82 - 245 cm: dark greenish grey fine grained mud with minor black specs.

K54

0-3 cm: Greyish olive (10Y4/2), clayey silt, soupy.

3-195 cm: Dark greenish grey (5GY4/1) clayey silt with vague black streaks.

195-229 cm: Dark greenish grey clayey silt; black specs 1 cm long near base; tephra interspersed.

K70

Overall thinly bedded to laminated

0-9 cm: greyish olive (10Y4/2), silty clay; slightly disturbed; soupy; bioturbated.

Remainder of core consists of laminae of 3 distinct colours:

(1) Dark greenish grey (5GY4/1)

(2) Greenish black (5GY2/1), generally mottled

(3) Greenish grey (5GY6/1)

In addition to these, distinct black lamiae < 1 cm in thickness occur at 15 cm, 27 cm, 59 cm, 100 cm, 104 cm, and 109 cm. More soupy light grey silt layers (contrasting to consolidated surrounding material) occur at 46 - 50 cm, 61 cm, 89 cm, 94 cm, 107 cm, and 110 cm.

112-120 cm: Cross laminated brown-grey silt, less bioturbated than material above.

K87

Upper 5 cm lost. Overall green-brown to olive grey clayey silt

0-6 cm: greyish olive (10Y4/2) silty clay

6-7 cm: Layer of silt and fine sand; soupy relative to bounding material.

7-52 cm: Dark greenish grey (5GY4/2); well consolidated towards the base.

JPC 28

0-20 cm: greenish grey (10Y6/1) silty clay with some oxidised material in upper 5 cm, where the top of the core is unconsolidated and soupy.

20-22 cm: disseminated tephra

22-90 cm: homogeneous greenish grey (10Y6/1) clay rich mud containing black streaks; mottled and bioturbated horizontally.

90-105 cm: Homogeneous olive grey (5Y 5/2 –4/2) clayey mud with black streaks; slight angle to bioturbation.

105-160 cm: Homogeneous olive grey-olive (5Y5/3 – 5/2) clayey mud with horizontal black streaks; mottled.

160-187 cm: grey (10YR5/1) tephra - normally graded (over 27 cm) from coarse – medium sandy tephra to medium-fine sand, and then to fine sandy tephra interspersed with clayey mud at the upper contact; gradational contact to overlying unit; sharp basal contact to underlying mud.

192-200 cm: Patch of isolated coarse tephra may represent a coring artefact.

200-255: Homogeneous greenish grey (5GY6/1) silt, containing horizontal black streaks.

JPC95

0-16 cm: Not recovered. Well-sorted, fine-medium grained, massive, tephric sand.

16-40 cm: Predominantly homogeneous sandy silt with occasional black streaks; mottled; interrupted by Dark brown-grey very fine sandy silt layers of 1-1.5 cm thickness at 40-45 cm and by tephra horizons at the following intervals:

27-31 cm: patches of white-grey tephra, with brown oxidized silt layers immediately above and below.

64-68 cm: patches of white-grey tephra, with brown oxidized silt layers immediately above and below.

45-240 cm: Homogeneous green-grey silt (10Y5/1) with occasional black streaks; medium-coarse sand-filled oval shaped burrows (0.5-1 cm diameter). Interrupted by several tephra horizons:

191-195 cm: Tephra – grades from medium to very fine sand and silt.

195-200 cm: Tephra – fines upwards from medium-coarse to fine sand.

200-209 cm: Tephra – normally graded from medium-coarse sand to medium-fine sand, moderately well sorted.

240-258 cm: Colour transition at ca. 240 cm from a green-grey mud to darker grey (5Y4/1) silty mud, with no black streaks.

258-320 cm: Homogeneous grey silt interspersed with fine sandy mud layers ~ 1 cm thick. Graded bedding is evident throughout this interval.

320-408.5 cm: Sediment becomes progressively more massive fine sandy mud, though sandy layers are less distinct from muddy ones than in the above interval.

9.4 Deconvolution of intensity

The SQUID sensor takes intensity readings over a span of ca. 10 cm according to a response function, such that no measurement is completely independent of the next. Towards each end of a U-channel, where that 10 cm range includes sample plus air, a deconvolution adjustment is required to account for the decrease in volume and consequent decrease in remanence intensity that is measured.

Correction factors were initially calculated using the parabolic response curves for directions x, y, and z by employing the formula:

$$\text{correction factor} = \left\{ \frac{\text{total response area}}{\text{actual response area}} \right\} \qquad [9.1]$$

The mean result for x, y, and z response curves was then used to multiply the measured intensity. Unfortunately this method failed to adequately compensate for attenuation of intensity for any type of remanence.

A more accurate adjustment was obtained using IRM data from K47. Intensity data was collected initially using continuous measurements of 1.5 m long core sections. U-channels for this core were later dissected into 2 cm lengths for IRM pulse magnetising, and IRM measured continuously by reassembling the pieces of U-channel adjacently. Upon completion of all IRM experiments, all pieces of this core were pulse magnetised at 1T (to saturation) and measured as discrete samples (rather than continuous), to provide volume corrected sIRM data (SIRMd). Comparison of the volume corrected sIRMd with the continuous (sIRMc) intensities reveals the extent to which intensity is attenuated at section ends (Fig. 9.2).

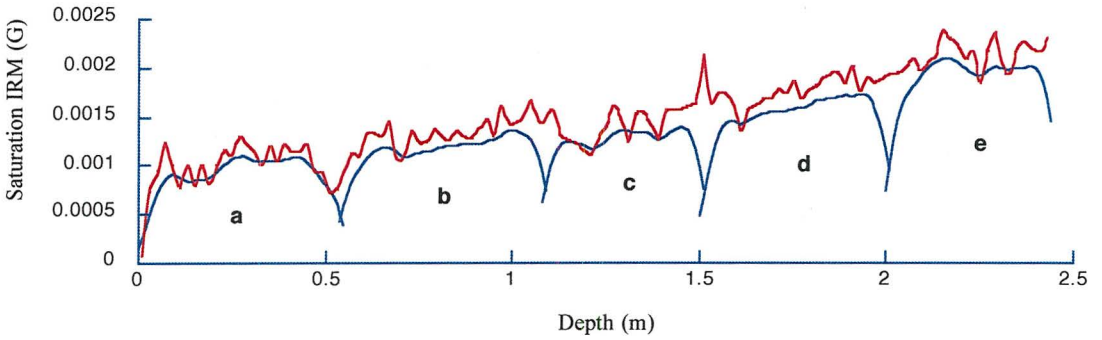

Figure 9.2: Saturation IRM measured for K47. Red (upper) line = volume corrected sIRM measured using discrete (2 cm) lengths. Blue (lower) line = sIRM measured continuously in 5 sections (labelled a to e). The lowered intensities recorded at section boundaries using continuous measurements occur due to the response function of the SQUID sensor, and thus require deconvolution.

The normalised difference between the two data sets (= (sIRMd – sIRMc) / sIRMd) was then calculated and plotted against the measurement profile. Normalised differences for the first and last 10 cm of sections a-e (all sections) were then combined into a single data set and plotted versus distance from section end. The best-fitting power function to describe the entire suite of data points was then calculated (Fig. 9.3). The ability of the function to transform intensities from a continuous data set into volume corrected intensities was then tested as follows:

sIRMv = sIRMc / (1-normalised difference function) [9.2]

Where sIRMv = volume corrected sIRM approximated from function; sIRMc = sIRM measured continuously. SIRMv is compared to SIRMd in figure 9.4. The volume corrected sIRMv (derived through equation 9.2) does not satisfactorily reproduce the SIRMd for all sections; under- or over-compensating at several boundaries. This is attributable to the variation in normalised difference profiles between sections, which is expected given that sIRM is also influenced by grain properties (shape anisotropy) and orientation. Hence no single function can accurately approximate data from all sections; but that shown in Figure 9.3 can provide rough estimates with only a few outliers (Fig. 9.4).

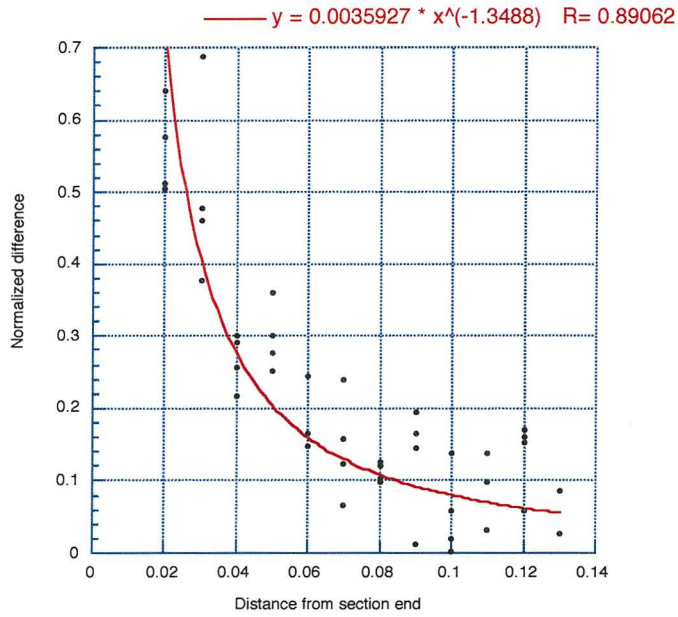

Figure 9.3: plot of normalised difference (sIRMd – sIRMc) / sIRMd versus distance from the end/start of a section for K47. Points represent combined data from 5 sections (a-e) for which both continuous and volume corrected (discrete) values of SIRM were measured. Data from the start of section a and end of section e are omitted owing to potential disturbance of sediment.

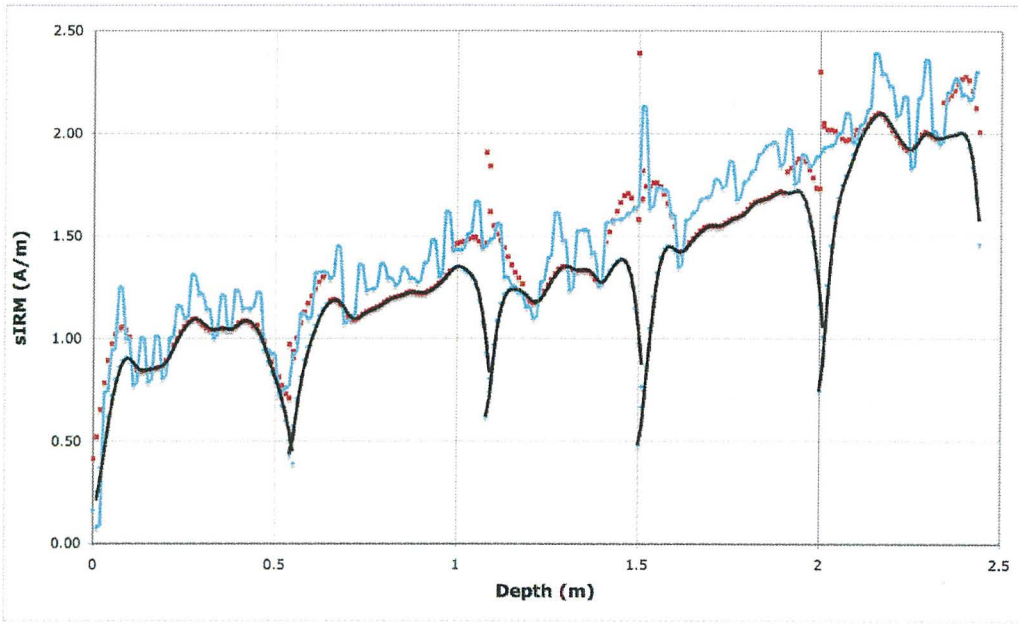

Figure 9.4: Volume corrected sIRM, measured using discrete samples (blue/upper line); volume uncorrected sIRM measured using continuous samples (black/lower line); and sIRM predicted from continuous measurements using function shown in Figure 9.3 at section ends (red dots). The function produces values that do not always approximate sIRMd; the discrepancy differing for each section.

For the purpose of estimating volume-corrected intensities for other IRM steps (between 0 and 1T), a separate function was calculated for each section end in order to minimize erroneous estimates that arise from incorporating all data into the same function. However,

the power function in figure 9.3 provides the best generalized approximation of volume-corrected sIRM (sIRMd). Intensities from all mid-sections were linearly corrected through multiplying by a factor of 1.1.

9.5 Calculation of Virtual Geomagnetic Poles

Each reliable measurement of paleofield direction in core JPC95 was used to calculate a VGP using the sequence of calculations shown below. The initial step requires determination of magnetic *colatitude* p, which represents the distance along a great circle from site to pole:

$$p = \tan^{-1}\left[\frac{2}{\tan I}\right] \qquad [9.3]$$

where I is the inclination value measured. Since p is a distance and cannot be negative, 180° was added to account for the negative sign introduced from Southern Hemisphere inclinations. Pole latitude λp is then given by:

$$\lambda p = \left(\sin\lambda s \cos p + \cos\lambda s \sin p \cos D\right) \qquad [9.4]$$

where λs is site latitude; and D is the declination measured. The longitudinal difference between site and pole is denoted by β (positive to the east):

$$\beta = \sin^{-1}\left[\frac{\sin p \sin D}{\cos\lambda p}\right] \qquad [9.5]$$

Longitude of the pole ϕ_p is then calculated through one of two equations:

If $\cos p \geq \sin\lambda s \sin\lambda p$, (always the case for JPC95 measurements) then $\phi p = \phi s + \beta$ [9.6]

If $\cos p \leq \sin\lambda s \sin\lambda p$, then $\phi p = \phi s + 180° - \beta$ [9.7]

where ϕ_s is the site longitude.